Unraveling structural features of flavodiiron proteins

A detailed structural insight for oxygen or nitric oxide reduction

Patrícia Alexandra Teixeira Borges

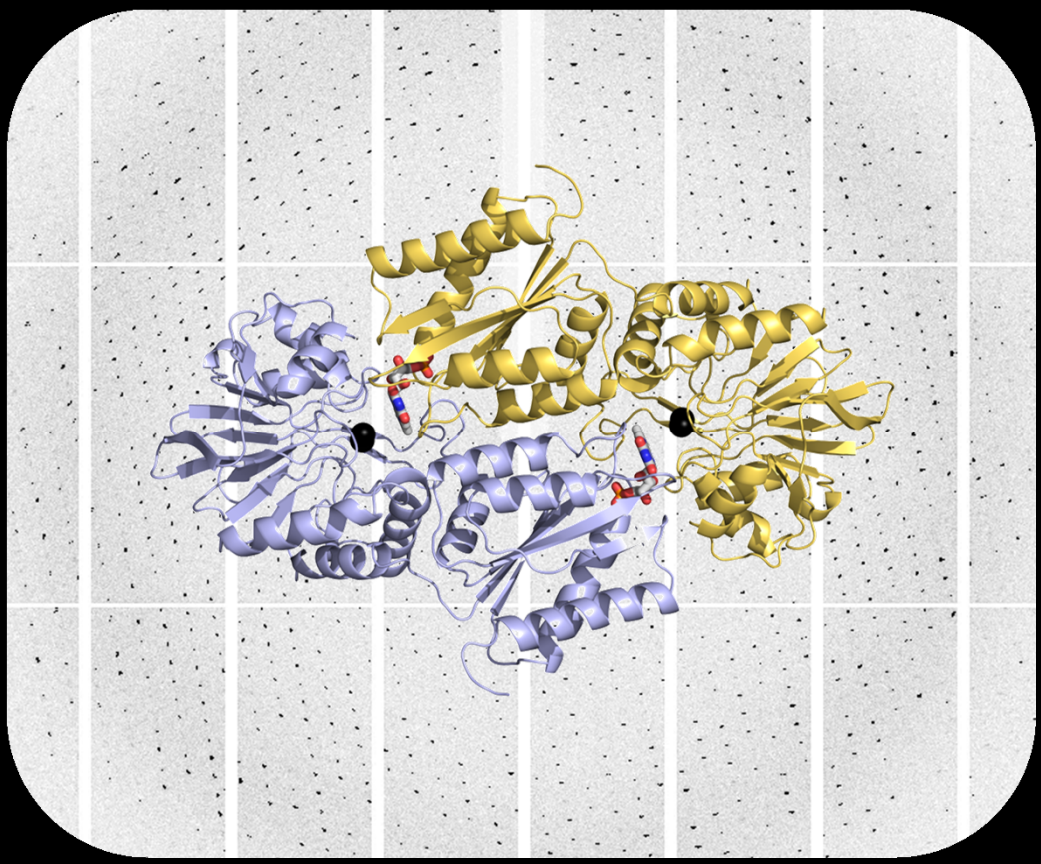

Dissertation presented to obtain the Ph.D degree in Biochemistry

Instituto de Tecnologia Química e Biológica António Xavier | Universidade Nova de Lisboa

Oeiras,
May, 2019

UNIVERSIDADE NOVA DE LISBOA

ITQB-UNL | Av. da República, 2780-157 Oeiras, Portugal
Tel (+351) 214 469 100 | Fax (+351) 214 411 277

www.itqb.unl.pt

Unraveling structural features of flavodiiron proteins: a detailed structural insight for oxygen or nitric oxide reduction

Patrícia Alexandra Teixeira Borges

Dissertation presented to obtain the Ph.D degree in Biochemistry

Instituto de Tecnologia Química e Biológica António Xavier |
Universidade Nova de Lisboa

Supervisor: Dr. Célia V. Romão

Co-Supervisor: Dr. Carlos Frazão

FCT Fundação para a Ciência e a Tecnologia
MINISTÉRIO DA CIÊNCIA, TECNOLOGIA E ENSINO SUPERIOR

Apoio financeiro da Fundação para a Ciência e Tecnologia do Programa Operacional Potential Humano do Fundo Social Europeu POPH/FSE no âmbito do quadro comunitário de apoio (Bolsa de Doutoramento SFRH/BD/85106/2012). Este trabalho foi financiado pela Fundação para a Ciência e Tecnologia (FCT) através do projecto PTDC/BBB-BQB/3135/2014 e do Programa Horizon 2020 de investigação e inovação da União Europeia com o contrato No 810856. Este trabalho foi ainda financiado pela MOSTMICRO (LISBOA-01-0145-FEDER-007660).

From left to right: Fernando Antunes, Bruno Victor, Célia Romão, Patrícia Borges, Carlos Frazão, Sandra Ribeiro, Ana Maria Gonçalves and Pedro Matias.

Second Edition, May 2019

Cover: X-ray diffraction image of *E. coli* FDP-ΔRd S262Y crystal and its “head-to-tail” dimer.

Structural Genomics Laboratory - Macromolecular Crystallography Unit

Instituto de Tecnologia Química e Biológica António Xavier

Universidade Nova de Lisboa

Av. da República (EAN)

2780-157 Oeiras

Portugal

Thesis Outline

This dissertation entitled “Unraveling structural features of flavodiiron proteins: a detailed structural insight for oxygen or nitric oxide reduction” is the result of the research work done in the Structural Genomics Laboratory, Macromolecular Crystallography Unit at the Instituto de Tecnologia Química e Biológica António Xavier from Universidade Nova de Lisboa, under the supervision of Dr. Célia Valente Romão and Dr. Carlos Frazão.

The work here described focus on the studies of flavodiiron proteins from the prokaryote *Escherichia coli* and the cyanobacterium *Synechocystis* sp. PCC 6803. This dissertation is divided in five parts: Part I, comprising a general introduction. Part II, contains the analysis of the crystal structure from *E. coli* FDP-ΔRd S262Y mutant truncated in its rubredoxin domain (Rd) in the as-isolated (oxidized) state. Part III, concerns the structural analysis from *E. coli* FDP-ΔRd single and double mutants, D52K, S262Y and D52K/S262Y, in the as-isolated (oxidized) and chemically reduced states. Part IV, reports the structural analysis from *Synechocystis* sp. PCC 6803 Flv1-ΔFlR truncated from its NAD(P)H:flavin oxidoreductase-like domain (FlR). Part V comprises a general discussion and concluding remarks that integrates all results obtained in this work.

Acknowledgements

I am deeply thankful to **Dr. Célia Romão**, my supervisor, for the inspiration she has given as being an enthusiastic and devoted scientist. For supporting my research with a great encouragement and guidance. Her dedication, critical sense and persistence were an important lesson to me. This thesis was not possible without her support both in and out of science. Forever grateful for that!

Dr. Carlos Frazão, my co-supervisor, for his fruitful discussions and guiding me throughout my PhD thesis. For providing me precious knowledge and experience in the field of X-ray crystallography.

Professor Maria Arménia Carrondo, head of the Macromolecular Crystallography Unit, for her incondicional support and for the opportunity to work in the Structural Genomics Laboratory.

Professor Miguel Teixeira, for many helpful discussions as part of my PhD thesis commission. For providing important insights into the FDPs project. I also thank him the helpful revisions and comments about my thesis.

Dr. João Vicente, for all helpful advices and useful discussions as part of my PhD thesis commission. I also thank him the helpful revisions and comments about my thesis.

Dr. Filipe Folgosa, for sharing his knowledge and for the helpful discussions and suggestions.

Dr. Pedro Matias, for passing his knowledge in X-ray crystallography and also for his support during synchrotron trips.

Dr. José Brito, for sharing his knowledge in protein crystallization and crystallography. I also thank his support in synchrotron trips.

Dr. Colin McVey, for his help during synchrotron trips and for revision of my thesis.

Dr. Tiago Bandeiras, for providing knowledge and useful sugestions in Thermofluor assays.

Dr. Elin Moe, for the opportunity to work in her group and for supporting me in many challenging moments, especially during the writting of the PhD thesis.

I thank to my **Macromolecular Crystallography Unit** coleagues: Ana Teresa Gonçalves, Andreia Fernandes, Bruno Correia, Bruno Salgueiro, Carolina Gonçalves, Catarina Silva, Catarina Tomé, Cristiana Sousa, Dalila Fernandes, Denise Pinel,

Diana Silva, Filipe Rollo, Joana Pedroso, José Silva, Kelly Frade, Margarida Acher, Margarida Rocha, Micael Freitas, Paulo Espirito Santo, Rute Chitas, Sandra Santos, Sara Silva, where I have spent almost 5 years performing the research for this thesis. We created all together an amazing working space where everybody can get guidance and help, and find great friends.

I also thank to all the past and present members of the **Macromolecular Crystallography Unit**, namely from the groups; Structural Genomics, Structural Biology, Membrane Protein Crystallography, Structural Virology and Industry and Medicine Applied Crystallography.

A special thanks to **Sandra Santos**, for being an amazing listener and for always being there in good and less good moments. For the helpful discussions and for the fun moments we shared inside and outside ITQB.

To **Dalila Fernandes**, **José Silva** and **Sandra Santos**, I express my gratitude for their unconditional friendship, support and patience throughout these years.

Finally, I thank my parents for all their love and support over the years, without which I would not be who I am today.

To all my friends outside ITQB who supported and encouraged me during this time.

I would also like to thank **Paulo** for his love, care and encouragement throughout my PhD. For always showing how proud you are of me and making me feel good about my accomplishments and myself.

A special thanks to Joaninha for being by my side while I was writting the thesis.

Lastly, I also acknowledge Fundação para a Ciência e Tecnologia do Programa Operacional Potential Humano do Fundo Social Europeu POPH/FSE for financial support in the frame of the Quadro Comunitário de Apoio through the PhD grant SFRH/BD/85106/2012. This work was financed by the Portuguese Fundação para a

Ciência e Tecnologia (FCT) through grant PTDC/BBB-BQB/3135/2014. This work was further financially supported by MOSTMICRO (LISBOA-01-0145-FEDER-007660) Research Unit cofunded by FCT. This work has received funding from the European Union's Horizon 2020 research and innovation programme under grant agreement No 810856.

Thesis publications

- **Borges, P. T.,** Romão, C. V., Saraiva, L. M., Gonçalves V. L., Carrondo, M. A., Teixeira, M., Frazão, C., "Analysis of a new flavodiiron core structural arrangement in Flv1-ΔFlR protein from *Synechocystis* sp. PCC 6803", Journal of Structural Biology, 2019, 205:91-102.

- Martins, M. C., Folgosa, F., Romão, C. V., **Borges, P. T.**, Frazão, C., Teixeira, M., "How Superoxide Reductases and Flavodiiron Proteins combat oxidative stress in anaerobes", Free Rad. Biol. Med., 2019, *in press*.

Two manuscripts are in preparation, based on the studies presented in Chapters II and III

- **Borges, P. T.,** Romão, C. V., Folgosa, F., Martins, M. C., Gotthard, G., Royant, A., Carrondo, M. A., Teixeira, M., Frazão, C., "A S262Y mutation in *Escherichia coli* flavodiiron protein increases radiation damage sensitivity in the crystal structure", manuscript under preparation.

- **Borges, P. T.,** Romão, C. V., Folgosa, F., Martins, M. C., van der Linden, P., Carrondo, M. A., Teixeira, M., Frazão, C., "Structure of mutants from *Escherichia coli* Flavodiiron-type nitric oxide reductase reveals changes in the diiron site", manuscript under preparation.

Other publications not included in this thesis

- Romão C.V., Vicente J.B., **Borges P.T.,** Victor B., Lamosa P., Silva E., Pereira L., Bandeiras T.M., Soares C.M., Carrondo M.A., Turner D., Teixeira M., Frazão C., "Structure of *Escherichia coli* Flavodiiron Nitric Oxide Reductase", Journal of Molecular Biology, 2016, 428: 4686–4707.

- Romão C.V., Vicente J.B., **Borges P.T.,** Frazão C., Teixeira M., “The dual function of flavodiiron proteins: oxygen and/or nitric oxide reductases”, Journal of Biological Inorganic Chemistry, 2016, 21:39-52.

- **Borges, P.T.,** Frazão, C., Miranda, C.S., Carrondo, M.A., Romão, C.V., "Structure of the monofunctional heme catalase DR1998 from *Deinococcus radiodurans*", FEBS Journal, 2014, 281:4138-4150.

- **Borges, P.T.,** Miranda, C.S., Santos, S.P., Carita, J.N., Frazão, C., Romão, C.V., "Purification, crystallization and phase determination of the DR1998 haem b catalase from *Deinococcus radiodurans*", Acta Cryst., 2014, F70:659-662.

Dissertation abstract

The work presented in this dissertation focuses on Flavodiiron Proteins (FDPs), a family of enzymes able to reduce oxygen and/or nitric oxide into water or non-toxic nitrous oxide. FDPs are widespread in prokaryotes and unicellular eukaryotes as well as in phototrophs, from cyanobacteria and unicellular algae to higher plants.

The FDP minimal structural unit is composed of two domains: a metallo-β-lactamase-like domain at the N-terminal harbouring a diiron catalytic center and a flavodoxin-like domain at the C-terminal containing a non-covalently bound flavin mononucleotide (FMN). The diiron site is where the substrate reduction occurs while the FMN cofactor shuttles the electrons to this catalytic center. The two redox centers within the same monomer are too far away (~40 Å) to allow an efficient electron transfer between them. Therefore, the minimal functional unit of FDPs, consists of a homodimer with a "head-to-tail" arrangement, which brings close together (~6 Å) the diiron center of one monomer and the FMN cofactor of the neighbouring monomer.

FDPs are classified according to the composition and distribution of their structural domains, and currently eight classes (A-H) have been identified. The Class A family is the simplest one, since it contains only the flavodiiron core (metallo-β-lactamase and flavodoxin-like domains). The Classes B and C have extra domains at the C-terminal: rubredoxin (Rd) and flavin reductases (FlR), respectively. The other classes (D-H) have other modular structures and are less studied.

This thesis focuses on the study of the flavodiiron core from FDPs, in particular the single (D52K and S262Y) and double mutants (D52K/S262Y) of the Class B *E. coli* FDP. Our aim is to understand the structural determinants that affect the substrate selectivity (O_2 or NO) in this family of proteins. Additionally, in this work it is also reported for the first time, the crystal structure of a Class C flavodiiron core from a cyanobacterium, *Synechocystis* sp. PCC 6803 Flv1, which is essential to understand the function of Class C FDPs in photosynthetic organisms.

In order to unravel the structural determinants that define FDPs substrate selectivity, a comparison of the crystal structures from FDPs with different substrate affinities was performed. Differences were observed at the two positions mentioned above (D52 and S262, NO-reducing *E. coli* FDP numbering), located in the diiron second coordination sphere. Kinetic studies previously performed with the O_2-reducing *Entamoeba histolytica* FDP aimed at showing the role played by the two equivalent residues (K53

and Y271) in the modulation of FDP substrate selectivity. Single and double variants (K53D and Y271S and K53D/Y271S) were then generated and showed that Y271 residue was important for the modulation of substrate specificity (O_2 vs NO) in FDPs.

In the work performed for this PhD, we attempt to convert the NO reductase *E. coli* FDP into an O_2 reductase. With this purpose, the D52K, S262Y and D52K/S262Y site-directed mutants were produced, crystallized and their crystal structures determined. The *E. coli* FDP mutants were produced omitting the Rd domain (FDP-ΔRd) so as to allow a comparison with *E. histolytica* FDP mutants. The structures of these mutants share a similar overall fold with that of the native *E. coli* FDP. However, the FDP-ΔRd S262Y mutant revealed some structural anomalies in the diiron active site region. These inconsistencies comprise longer iron coordination distances, negative Fourier difference densities in some metal ligands and lack of electron density at the side chains of some metal ligands. Despite the low calculated absorbed dose (1.07 MGy), the S262Y mutation induced a significant X-ray radiation crystal sensitivity contrary to the *E. coli* FDP-ΔRd D52K and D52K/S262Y mutations. This instability is not due to the absence of the Rd domain since the native *E. coli* FDP-ΔRd shows an active site region with electron density comparable to that of native FDP, despite its high calculated absorbed dose (27.26 MGy). These results suggest that the presence of a tyrosine residue in the diiron second coordination sphere induced an increased sensitivity to X-ray radiation. However, this feature was not observed in the double mutant probably resulting from the effect of the other mutation, D52K.

The genome sequences of cyanobacteria and other oxygenic photosynthetic organisms contain genes encoding Class C FDPs, and form a distinct clade from the other classes of FDPs. Each sequenced organism has at least two FDP encoding genes. While one of the FDPs has the canonical Type 1 metal ligands, namely carboxylate and histidine ligands, the other one shows different residues as putative ligands (Types 2-17).

The cyanobacterium *Synechocystis* sp. PCC 6803 genome comprises four FDP genes: Flv1 (sll1521), Flv2 (sll0219), Flv3 (sll0550); and Flv4 (sll0217). Flv3 and Flv4 contain conserved residues matching the canonical ones known to be involved in iron coordination (Type 1), while in Flv1 and Flv2 these residues are replaced by neutral and basic ones (Type 2).

In this PhD work, the *Synechocystis* sp. PCC 6803 Flv1 truncated from its NAD(P)H:flavin oxidoreductase-like domain (FlR), Flv1-ΔFlR, was produced, crystallized and its crystal structure determined. This protein contains the second most common arrangement of non-canonical basic and neutral residues (Type 2) in the pseudo diiron site, H108-x-N110-x-N112-R113-x64-H178-x18-K197-x56-H254. However, a metal site was absent even after several attempts of metal incorporation. Instead, anionic species were located in the pseudo diiron cavity, which could be due to the non-canonical basic residues as well as to an excess of basic vs acidic residues in its neighborhood.

As mentioned above, the minimal functional unit in FDPs is composed of a “head-to-tail” dimer, essential for an efficient electron transfer between the two redox centers. However, the Flv1-ΔFlR crystal structure shows one monomer in the asymmetric unit, and no oligomerization was suggested by the crystal packing. Nevertheless, we cannot rule out that the truncated NAD(P)H:flavin oxidoreductase could have a determinant role in the protein oligomerization.

The present work addresses structural studies in the flavodiiron core of two FDPs that belong to different classes (B and C) and highlight different oligomerization arrangements as well as canonical and non-canonical putative metal ligands.

Resumo da dissertação

O trabalho apresentado nesta dissertação foca-se no estudo de proteínas flavodiférricas (FDPs), uma família de enzimas capazes de reduzir o oxigénio e/ou o óxido nítrico a água e/ou óxido nitroso não-tóxico. As FDPs estão presentes em procariontes e eucariontes unicelulares, assim como em organismos fotossintéticos produtores de oxigénio, desde cianobactérias e algas unicelulares até plantas superiores.

A unidade mínima estrutural das FDPs é composta por dois domínios: um domínio tipo metalo-β-lactamase no N-terminal, contendo um centro catalítico diférrico, e um domínio tipo flavodoxina no C-terminal, contendo um mononucleótido de flavina não covalentemente ligado (FMN). O centro diférrico é onde ocorre a redução dos substratos enquanto o cofactor FMN transfere os electrões para este centro catalítico. No mesmo monómero, os dois centros redox estão a uma distância demasiado elevada (~40 Å) para permitir uma transferência electrónica eficiente. Assim, a unidade mínima funcional das FDPs consiste num homodímero com uma conformação "*head-to-tail*", que aproxima (~6 Å) o centro diférrico de um monómero ao cofactor FMN do monómero vizinho.

As sequências de aminoácidos das FDPs foram analisadas e classificadas de acordo com a composição e distribuição dos domínios estruturais, e até ao momento oito classes (A-H) foram identificadas. A classe A é a mais simples, uma vez que contém apenas o dominío flavodiférrico (domínios tipo metalo-β-lactamase e flavodoxina). As classes B e C têm domínios extras no C-terminal: rubredoxina (Rd) e flavina redutase (FlR), respectivamente. As outras classes (D-H) têm outros módulos estruturais e são menos estudadas.

Esta tese tem como foco o estudo do dominío flavodiférrico de FDPs, em particular os mutantes simples e duplos da FDP de *E. coli* (D52K , S262Y and D52K/S262Y). O nosso objectivo é compreender os determinantes estruturais que afectam a selectividade de substratos (O_2 ou NO) nesta família de proteínas. Além disso, neste trabalho também é relatada pela primeira vez, uma estrutura cristalográfica do domínio flavodiférrico de uma FDP da classe C de uma cianobactéria, Flv1 de *Synechocystis* sp. PCC 6803, que é essencial para compreender a função das FDPs desta classe em organismos fotossintéticos.

De modo a elucidar os determinantes estruturais que afectam a selectividade de substratos nas FDPs, foi realizada uma comparação de estruturas cristalográficas de FDPs com diferentes afinidades para substratos. Foram observadas diferenças em duas posições (D52 e S262, *E. coli* FDP selectiva para NO) localizadas na segunda esfera de coordenação do centro diférrico. Existem reportados estudos cinéticos para a FDP selectiva para oxigénio de *Entamoeba histolytica* com o objectivo de mostrar o papel desempenhado pelos dois resíduos equivalentes (K53 and Y271) na modelação de selectividade de substratos. Foram assim gerados os mutantes simples K53D, Y271S e duplo K53D/Y271S, que mostraram que o residuo Y271 é importante na modelação de especificidade de substrato (O_2 vs NO) nas FDPs.

Neste trabalho, tentámos converter a redutase de NO de *E. coli* numa redutase de O_2. Deste modo, as proteínas com as seguintes mutações pontuais D52K, S262Y e D52K/S262Y foram produzidas, cristalizadas e as suas estruturas cristalográficas determinadas. Os mutantes de FDP de *E. coli* foram gerados omitindo o domínio Rd (FDP-ΔRd) de modo a serem comparados com os mutantes de FDP de *E. histolytica*.

A estrutura destes mutantes é semelhante à estrutura nativa de FDP. No entanto, o mutante FDP-ΔRd S262Y revelou algumas anomalias estruturais na região do centro diférrico. Essas inconsistências incluem distâncias mais longas de coordenação ao ferro, densidades negativas de diferenças de Fourier em alguns ligandos e falta de densidade electrónica nas cadeias laterais de alguns ligandos do metal.

Apesar da baixa dose absorvida calculada (1.07 MGy), a mutação S262Y induziu uma sensibilidade significativa à radiação de raios-X nos cristais, contrariamente às mutações FDP-ΔRd D52K e D52K/S262Y de *E. coli*. Esta instabilidade não é devida à ausência do domínio Rd, pois a FDP-ΔRd nativa de *E. coli* mostra que a região do centro activo tem densidade electrónica semelhante à da FDP nativa, apesar da elevada dose absorvida calculada (27.26 MGy). Estes resultados sugerem que a presença de uma tirosina na segunda esfera de coordenação do centro diférrico induziu um aumento da sensibilidade da proteína à radiação dos raios-X. No entanto, esta característica não foi observada no duplo mutante devido provavelmente à mutação D52K.

As sequências do genoma de cianobactérias e de outros organismos fotossintéticos oxigénicos contêm genes que codificam as FDPs de classe C, formando um grupo distinto das outras classes de FDPs. Todas as FDPs de cianobactérias e de

organismos fotossintéticos pertencem à classe C e cada organismo sequenciado possui pelo menos dois genes que codificam FDPs. Enquanto uma dessas FDPs possui os ligandos do metal canónicos de Tipo 1, nomeadamente carboxilatos e histidinas, a outra FDP apresenta diferentes residuos como possíveis ligandos (Tipos 2-17).

O genoma da cianobactéria *Synechocystis* sp. PCC 6803 contém quatro genes que codificam FDPs: Flv1 (sll1521), Flv2 (sll0219), Flv3 (sll0550); e Flv4 (sll0217). A Flv3 e Flv4 contêm resíduos canónicos envolvidos na coordenação do ferro (Tipo 1), enquanto na Flv1 e Flv2 esses resíduos são substituídos por resíduos neutros e básicos (Tipo 2).

Nesta dissertação, a Flv1 de *Synechocystis* sp. PCC6803 truncada do seu domínio NAD(P)H:flavina oxidoredutase (FlR), Flv1-ΔFlR, foi produzida, cristalizada e a sua estrutura cristalográfica determinada. Esta proteína contém a segunda combinação mais comum de resíduos básicos e neutros não canónicos (Tipo 2) no possível centro diférrico, H108-x-N110-x-N112-R113-x_{64}-H178-x_{18}-K197-x_{56}-H254. No entanto, este centro não contém qualquer metal mesmo após várias tentativas de incorporação de metais. Pelo contrário, espécies aniónicas foram localizadas nesta cavidade, o que poderá ser devido aos resíduos básicos não canónicos, bem como a um excesso de resíduos básicos *vs* ácidos na vizinhança do possível centro diférrico.

Como acima mencionado, a unidade mínima funcional nas FDPs é composta por um dimero "*head-to-tail*", essencial para uma transferência eficiente de electrões entre os dois centros redox. No entanto, a estrutura cristalográfica de Flv1-ΔFlR apresenta um monómero na unidade assimétrica e o empacotamento no cristal não sugere nenhuma oligomerização. No entanto, não se pode excluir a hipótese de que o domínio truncado NAD(P)H:flavina oxidoredutase possa ter um papel determinante na oligomerização da proteína.

Este trabalho foca-se em estudos estruturais do domínio flavodiférrico de duas FDPs que pertencem a diferentes classes (B e C) e evidencia diferentes arranjos oligoméricos bem como possíveis ligandos de metal, canónicos e não-canónicos.

Abbreviations

Å	Angstrom
a.d.p.	Atomic displacement parameter
ATP	Adenosine triphosphate
a.u.	Asymmetric unit
Da	Dalton
DSF	Differential scanning fluorimetry
DWD	Diffraction-weighted dose metric
EPR	Electron Paramagnetic Resonance
F_{420}	7,8-Dimethyl-8-hydroxy-5-deazariboflavin
$F_{420}H_2$	Reduced 7,8-dimethyl-8-hydroxy-5-deazariboflavin
Fc	Calculated structure factors
Fo	Observed structure factors
FAD	Flavin adenine dinucleotide
FDP	Flavodiiron protein
Fe_d	Distal iron
Fe_p	Proximal iron
FlR	NAD(P)H:flavin oxidoreductase
FMN	Flavin mononucleotide
g	EPR *g*-factor
GSH	Glutathione
GSNO	S-nitrosoglutathione
Hmp	Flavohaemoglobin
Hrb	High molecular weight rubredoxin
iNOS	Inducible nitric oxide synthase
IPTG	Isopropyl-β-D-thiogalactopyranoside
LB	Luria Bertani
lcNOR	Long-chain NOR
MGy	Mega gray
MOPS	3-(N-morpholino) propansulfonic acid
MR	Molecular replacement
NADH	Reduced nicotinamide adenine dinucleotide
NADPH	Reduced nicotinamide adenine dinucleotide phosphate

NOR	Nitric oxide reductase
O_2R	Oxygen reductase
PDB	Protein Data Bank
PEG	Polyethylene glycol
PSI	Photosystem I
PSII	Photosystem II
Rbr	Rubrerythrin
Rd	Rubredoxin
r.m.s.d.	Root-mean-square distance
RNS	Reactive nitrogen species
ROO	Rubredoxin:oxygen oxidoreductase
ROS	Reactive oxygen species
SAXS	Small angle X-ray scattering
scNOR	Short-chain NOR
SDS-PAGE	Sodium dodecyl sulfate-polyacrylamide gel electrophoresis
SOD	Superoxide dismutase
SOR	Superoxide reductase
TFZ	Translation-function Z-score
TPTZ	2,4,6-Tripyridil-1,3,5-triazine
Tris-HCl	Tris(hydroxymethyl)aminomethane hydrochloride

Table of Contents

Chapter I – General Introduction

Chapter II – Structure of *Escherichia coli* flavodiiron protein S262Y mutation

Chapter III – Structure of mutants from *Escherichia coli* Flavodiiron-type nitric oxide reductase

Chapter IV – Structural analysis of Flv1-ΔFlR protein from *Synechocystis*

Chapter V – General discussion and concluding remarks

Part I

General Introduction

Chapter I

General Introduction

1.1 Enzymatic systems involved in oxygen and reactive oxygen species detoxification

Molecular oxygen (O_2) is converted into water by a four electrons reduction. However, the sequential one electron reduction may lead to the formation of highly reactive oxygen species (ROS), namely superoxide anion ($O_2^{\bullet-}$), hydrogen peroxide (H_2O_2) and the hydroxyl radical ($^{\bullet}OH$) (Fig. 1.1). High intracellular concentration of ROS can oxidize and damage biologically important macromolecules, such as proteins, lipids and DNA. Therefore, when the intracellular level of ROS increases, the organism is in an “oxidative stress” state. In addition to their harmful effect, ROS at lower concentrations play an important role as regulators of immune responses and cell signaling (Hancock et al., 2001; Rhee, 1999).

To avoid ROS accumulation and consequent cell damage it is important to remove these highly reactive species. Therefore, organisms contain antioxidant systems to protect themselves from cellular damage and death caused by these species. These systems include enzymatic and non-enzymatic antioxidant mechanisms that have the function to detoxify ROS by its conversion into nontoxic species.

The non-enzymatic antioxidant systems are low-molecular-mass compounds that can neutralize ROS by reducing them directly. These systems include α-tocopherol (vitamin E), β-carotene (vitamin A), ascorbic acid (vitamin C), xanthophylls (yellow pigments related with carotene), flavonoids (aromatic oxygen heterocyclic compounds found in higher plants), glutathione (GSH) and small Mn complexes (Culotta and Daly, 2013; Frei, 1994; Lee, 1999; Valentine et al., 1998).

The enzymatic antioxidant systems include superoxide dismutases (SODs), superoxide reductases (SORs), catalases, peroxidases and flavodiiron proteins (FDPs) (Fig. 1.1).

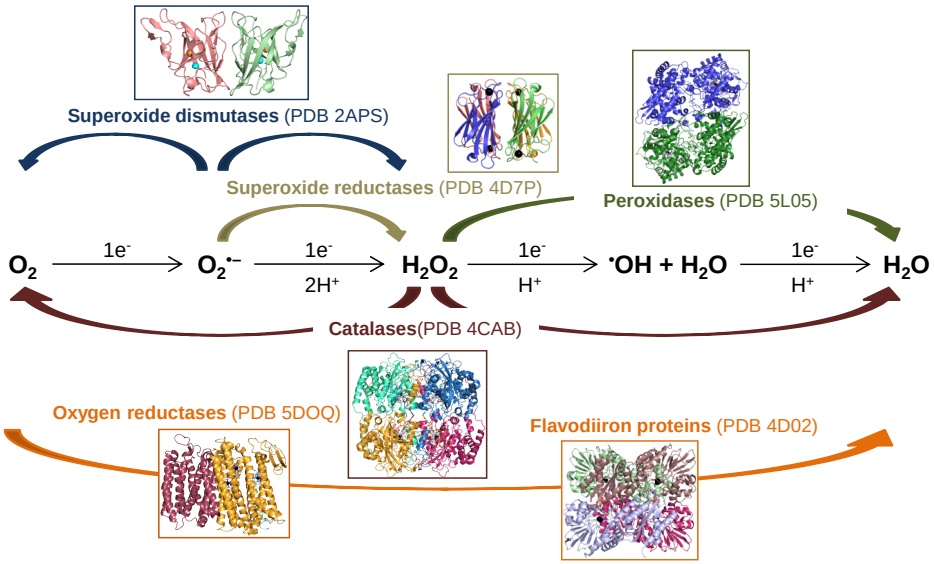

Figure 1.1- Representation of different steps for the reduction of oxygen to water and the different ROS enzymatic defence systems. Examples of proteins involved in the different steps are represented in different panels.The crystallographic structure for each protein is showed in cartoon, with the corresponding PDB code. Figures of structures, were prepared with PyMOL (DeLano, 2002; Schrodinger, 2010).

Superoxide dismutase (SOD) catalyzes by dismutation the conversion of two superoxide anions into H_2O_2 and O_2. There are five known types of SODs according to their metal cofactors: Cu-SOD, Cu/Zn-SOD, Fe-SOD, Mn-SOD and Ni-SOD (Abreu and Cabelli, 2010; Culotta et al., 2006; Miller, 2012; Sheng et al., 2014). The Cu/Zn-SOD, Mn-SOD and Fe-SOD are found in Archaea, Bacteria and Eukarya while the Ni-SODs are present in Bacteria and Eukarya (Sheng et al., 2014). The Cu-SOD are present so far, in Bacteria and Eukarya (Robinett et al., 2018). The active site residues are highly conserved in all Mn- and Fe-SODs, where the metals are coordinated by three histidines and an aspartate residue (Abreu and Cabelli, 2010; Sheng et al., 2014). The same type of coordination for the zinc center in Cu/Zn-SOD is observed, whereas the copper is coordinated by three histidines (Fig. 1.2 A). A complete different metal coordination occurs in Ni-SODs in which the metal is coordinated by two cysteines and one histidine. The Cu-SOD retains the same copper coordination site of Cu/Zn-SODs.

Superoxide reductases (SORs) are nonhaem iron-containing enzymes which catalyze the one electron reduction of $O_2^{\bullet-}$ to produce H_2O_2 without the formation of O_2, as

occurs in SODs (Abreu and Cabelli, 2010; Auchere and Rusnak, 2002; Kurtz, 2004; Niviere and Fontecave, 2004; Pinto et al., 2010; Sheng et al., 2014). SORs have been identified in organisms from the three life domains, but so far mostly are anaerobic and microaerophilic prokaryotes. SORs can be generally classified according to their number of irons, namely 1Fe-SOR and 2Fe-SOR. Both classes have in common the catalytic domain, initially named neelaredoxin (Nlr), which contains the catalytic Fe center. The iron is coordinated by four histidines and one cysteine in the reduced form (Fig. 1.2 B), and can have a sixth glutamate ligand in the oxidized state. The 2Fe-SOR, contains an extra domain at the N-terminal, named desulforedoxin (Dx), harboring a second iron site.

Catalases and peroxidases catalyze the decomposition of hydrogen peroxide (Chelikani et al., 2004; Rhee et al., 2005; Veal et al., 2007). Catalases dismutate hydrogen peroxide into water and oxygen, whereas the peroxidases, use several electron donors, such as glutathione, to transfer electrons to reduce hydrogen peroxide or organic peroxides to water molecules (Diaz et al., 2012). Haem-containing catalases and peroxidases are the most abundant group and are spread among Bacteria, Archaea and Eukarya (Bernroitner et al., 2009; Zamocky et al., 2008). In catalases, the haem is coordinated by a proximal tyrosine ligand, while in most peroxidases, this position is occupied by a histidine (Fig. 1.2 C) (Zamocky et al., 1997; Zamocky and Koller, 1999).

Respiratory oxygen reductases (terminal oxidases) are enzymes part of the end of the respiratory chains of organisms, reducing O_2 to water (Borisov et al., 2011). There are three families of oxygen reductases: haem-copper oxygen reductases, cytochromes *bd* and alternative oxidases

FDPs are widespread in the three life domains (Bacteria, Archaea and Eukarya), and present in both aerobic and anaerobic organisms. This family of proteins is involved in the reduction of oxygen into water without production of reactive oxygen species. Recently, it was reported a new function in the FDPs field (Folgosa et al., 2018b), since a *Clostridium difficile* FDP, has the ability to also fully reduce H_2O_2 to water.

FDPs will be discussed in more detail in section 1.3.

A

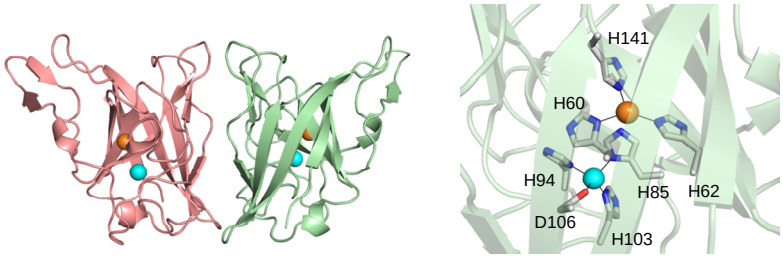
H141
H60
H94
H85
H62
D106
H103

B

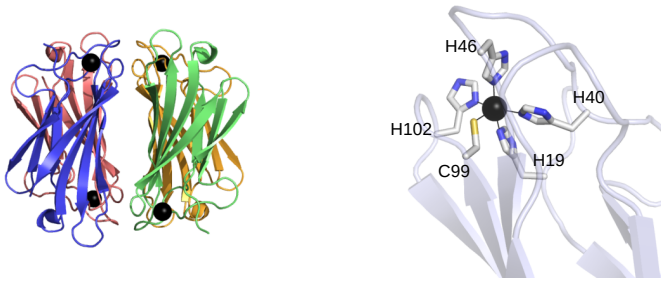
H46
H40
H102
C99
H19

C

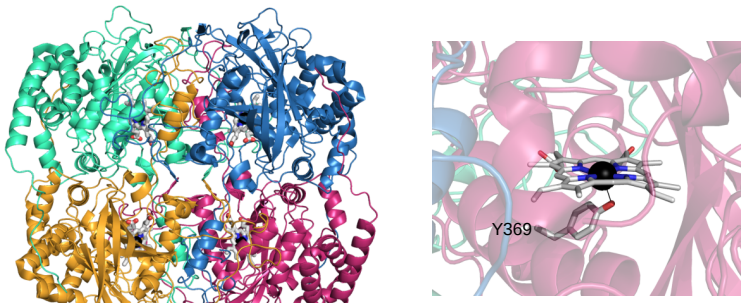
Y369

D

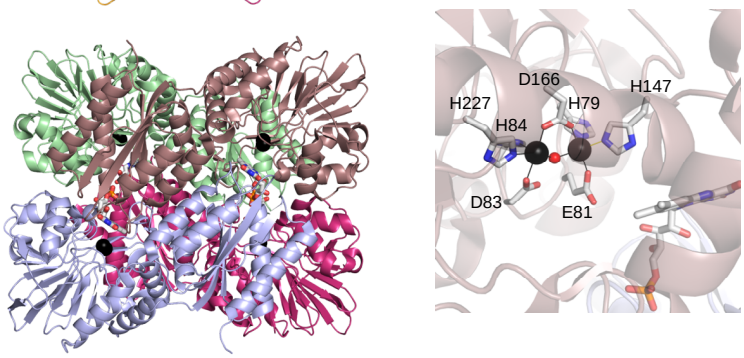
D166
H147
H227
H79
H84
D83
E81

Figure 1.2- Enzymatic defence systems against ROS and their metal catalytic centers. **A)** Cu/Zn Superoxide dismutase (PDB 2APS) from *Actinobacillus pleuropneumoniae*, **B)** Superoxide reductase (PDB 4D7P) from *Giardia intestinalis*, **C)** Haem catalase (PDB 4CAB) from *Deinococcus radiodurans*, **D)** Flavorubredoxin (PDB 4D02) from *Escherichia coli*. Cartoon representation of the overall structure of Cu/Zn SOD, SOR, catalase and FDP are presented in the left panel; and the corresponding catalytic metal center in the right panel. Bonds are represented as sticks. The μ-hydroxo-bridging oxygen, zinc, iron and copper are represented as spheres in red, cyan, black and orange, respectively. Ligands and FMN are shown as sticks with carbon atoms in grey, nitrogen in blue, oxygen in red and phosphorous in orange.

1.2 Enzymatic systems involved in nitric oxide and reactive nitrogen species detoxification

Nitric oxide (NO) was among the first gases to be discovered, by Joseph Priestley in 1772, two years before he discovered oxygen (O_2) (Neville, 1974; Severinghaus, 2003; Smith, 1972). For more than two centuries this colorless and odorless gas was considered to be highly toxic. However, in the last fourty years, several studies about the crucial biological role of NO have been reported.

NO can have a harmful biological effect or a protective role, depending on its intracellular concentration. At lower concentrations (nanomolar range), NO plays a key role in a wide range of physiological and pathological processes, such as vasodilation, cellular signaling and immune response (Garthwaite, 1991; Langrehr et al., 1993; Moncada et al., 1989). However, at higher concentrations (micromolar range), NO can react with other radicals, such as superoxide, to form highly reactive nitrogen species (RNS), as well as with metal centers. One of those RNS is peroxynitrite, $ONOO^-$, a strong oxidant that reacts with most biological molecules (e.g. tyrosine nitration) (Beckman et al., 1990). Nitrogenous products such as nitroxyl (HNO), nitrosonium cation (NO^+), and oxides of nitrogen derived from the reaction of NO with $O_2^{\bullet -}$ and O_2, are examples of other RNS (Fang, 2004; Nathan and Shiloh, 2000). Each of these species has different properties in terms of reactivity, half-life and lipid solubility, leading to several harmful effects on biological systems, such as oxidation, nitrosation and nitration (Fig. 1.3) (Wink et al., 1996; Wink and Mitchell, 1998).

The nitrosation involves the addition of NO^+ from dinitrogen trioxide (N_2O_3) to an amine generating a nitrosamine or S-nitrosothiol in case of thiol. Nitration is associated with the addition of a NO_2 group to an aromatic residue.

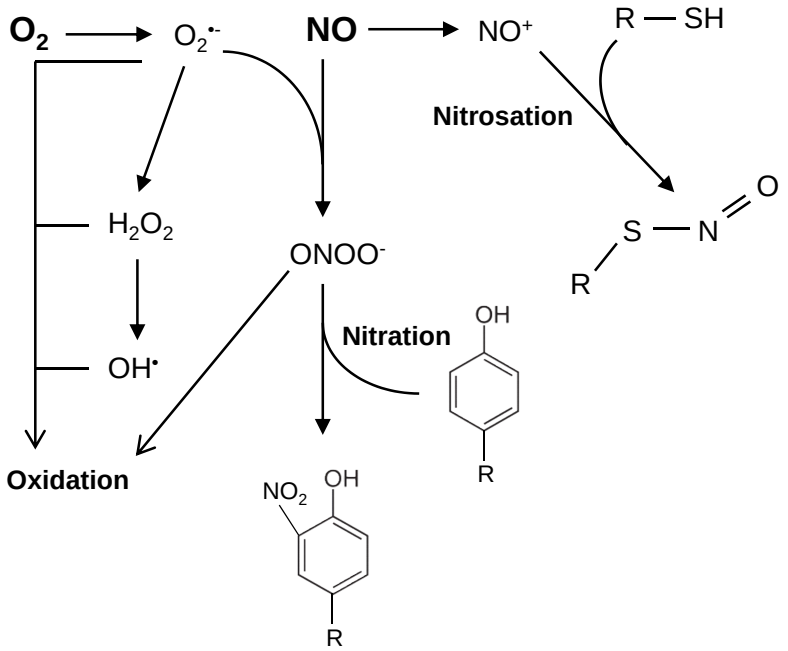

Figure 1.3- Nitric oxide dependent reactions (oxidation, nitrosation and nitration) involved in reactive nitrogen species (RNS) formation. The reduction of molecular oxygen (O_2) produces superoxide (O_2•−) which is the precursor of other reactive oxygen species (hydrogen peroxide (H_2O_2), hydroxyl (•OH)).

Biologically, NO can be produced by non-enzymatic or enzymatic systems. Abiotic mild acidification of nitrite is a non-enzymatic system for NO production which have potent antimicrobial effects against a broad range of potential pathogens (Dykhuizen et al., 1998; Lundberg et al., 2004; Lundberg et al., 2008; Zweier et al., 1999).

An enzyme was identified in mammals, as part of the immune response against microbial infection, namely the inducible nitric oxide synthase (iNOS). This enzyme synthesizes NO and L-citrulline from L-arginine in the presence of O_2 and NADPH (Bredt et al., 1991; Griffith and Stuehr, 1995; Marletta, 1994; Marsden et al., 1992; White and Marletta, 1992). Therefore, host infecting bacteria are challenged by the presence of NO and RNS, produced by the immune response to control microbial propagation. Alternative enzymatic systems for NO generation are known, such as

nitrite reductases that catalyze the nitrite reduction to NO (Meyer, 1973; Payne et al., 1997; Walters and Taylor, 1965).

In order to detoxify NO and consequently survive to the nitrosative stress, microbes acquired throughout evolution enzymatic systems, such as, globins, NO reductases (NORs) and FDPs (Almeida et al., 2006; Figueiredo et al., 2013; Gardner et al., 2002; Gomes et al., 2002b; Poock et al., 2002; Poole and Hughes, 2000; Wu et al., 2003). All these proteins are able to reduce NO to nontoxic compounds protecting biological targets from the cytotoxic effects of NO.

Globins are a family of cytoplasmatic proteins that can be classified in three main classes: *i)* single-domain globins, *ii)* truncated globins and *iii)* flavohaemoglobins (Frey and Kallio, 2003). The first bacterial single-domain globin to be identified and sequenced was the haemoglobin from *Vitreoscilla* (VHb) (Wakabayashi et al., 1986; Webster and Hackett, 1966). Nowadays these proteins can be found in bacteria and protozoa. This single-domain haemoglobin comprises a globin-like domain, with a three-on-three α-helical fold with a haem *b* group (Fig. 1.4 A) (Tarricone et al., 1997). Several functions have been attributed to these proteins beyond its role on NO detoxification (conversion to nitrate), such as oxygen binding at low concentrations, as occurs in the VHb (Park et al., 2002; Wu et al., 2003). The single-domain globin from *Campylobacter jejuni*, Cjb, was proposed to afford protection against nitrosative stress, since the *cjb* knockout mutant was sensitive to nitrosating agents (GSNO) and a NO-releasing compound (spermine NONOate) (Elvers et al., 2004; Lu et al., 2007b).

The truncated globins are 20-40 amino acid residues smaller than single-domain globins, being widely distributed in bacteria, cyanobacteria, protozoa and plants (Jokipii-Lukkari et al., 2009; Wittenberg et al., 2002). The function of truncated haemoglobins include oxygen scavenging and detoxification of NO by its conversion to nitrate (Lu et al., 2007a; Milani et al., 2005; Ouellet et al., 2002; Vuletich and Lecomte, 2006). Flavohaemoglobins, found in many bacterial and lower eukaryotic species, comprise a globin domain homologous to VHb single-domain globin, fused to a flavin reductase-like domain that contains an FAD cofactor and oxidises NADH (Ilari et al., 2002; Membrillo-Hernandez et al., 1998; Nobre et al., 2008; Poole and Hughes, 2000; Vasudevan et al., 1991). These proteins confer resistance to nitrosative stress by converting NO into nitrate under aerobic or microaerobic conditions while in anaerobic conditions, these proteins reduce NO to N_2O (Gardner, 2005; Gardner et al., 1998; Hausladen et al., 2001; Justino et al., 2005; Kim et al., 1999). The first

flavohaemoglobin to be identified was from *E. coli* (Vasudevan et al., 1991). This protein together with FDP is able to protect *E. coli* against NO in anaerobic conditions (Justino et al., 2005).

The globin domain is conserved among the different families mentioned above. Until today, all globins structurally characterized revealed the presence of a highly conserved histidine residue involved in haem-iron coordination.

As mentioned above, respiratory NO-reductases are another family of proteins able to reduce NO. NORs are typically found in denitrifying organisms and some can also be present in pathogenic bacteria, where they may protect against toxic NO produced by macrophages in the host immune system. These proteins are membrane-bound and reduce NO to dinitrogen oxide (N_2O). They are classified as short-chain group (scNOR) with ~ 450 amino acids and long-chain group (lcNOR) with ~ 760 amino acids (Hino et al., 2010).

The scNOR is composed of two subunits, NorB with ~53 kDa and NorC with ~17 kDa. The subunit NorC is a membrane-bound cytochrome *c* and its haem-containing region is oriented to the periplasmic space allowing this protein to interact with a soluble and/or membrane-associated cytochrome or (pseudo)azurin to provide electrons to the catalytic subunit, NorB (Thorndycroft et al., 2007; Zumft et al., 1994). This subunit is transmembranar (Arai et al., 1995; Cramm et al., 1997; de Boer et al., 1996; Zumft et al., 1994) and its binuclear active site contains a haem *b* and a nonhaem iron center (Hendriks et al., 1998). NorB contains another haem *b*, involved in the reduction of the active site. This subunit has six conserved histidines and one glutamate coordinating the two haem groups and the nonhaem iron (Fig. 1.4 B) (Hino et al., 2010).

The lcNOR is a membrane-bound subunit that lacks the cytochrome *c* subunit, accepting then electrons from quinol. Its active site comprises one haem *b,* in addition to the same binuclear center present in NorB (Hino et al., 2010; Zumft, 2005).

FDPs are also a family of proteins involved in the detoxification of nitric oxide. FDPs reduce NO to nontoxic nitrous oxide, and will be described in detailed in Section 1.3, since it is the scope of this thesis.

Overall, the overproduction of ROS/RNS and/or the failure of biological detoxification systems lead to an increase of oxidative/nitrosative stress. Moreover, both ROS and RNS are closely related leading to reactive species that can damage key cellular components, such as amino acids, lipids, metal centers and nucleic acids, thereby affecting the cellular processes.

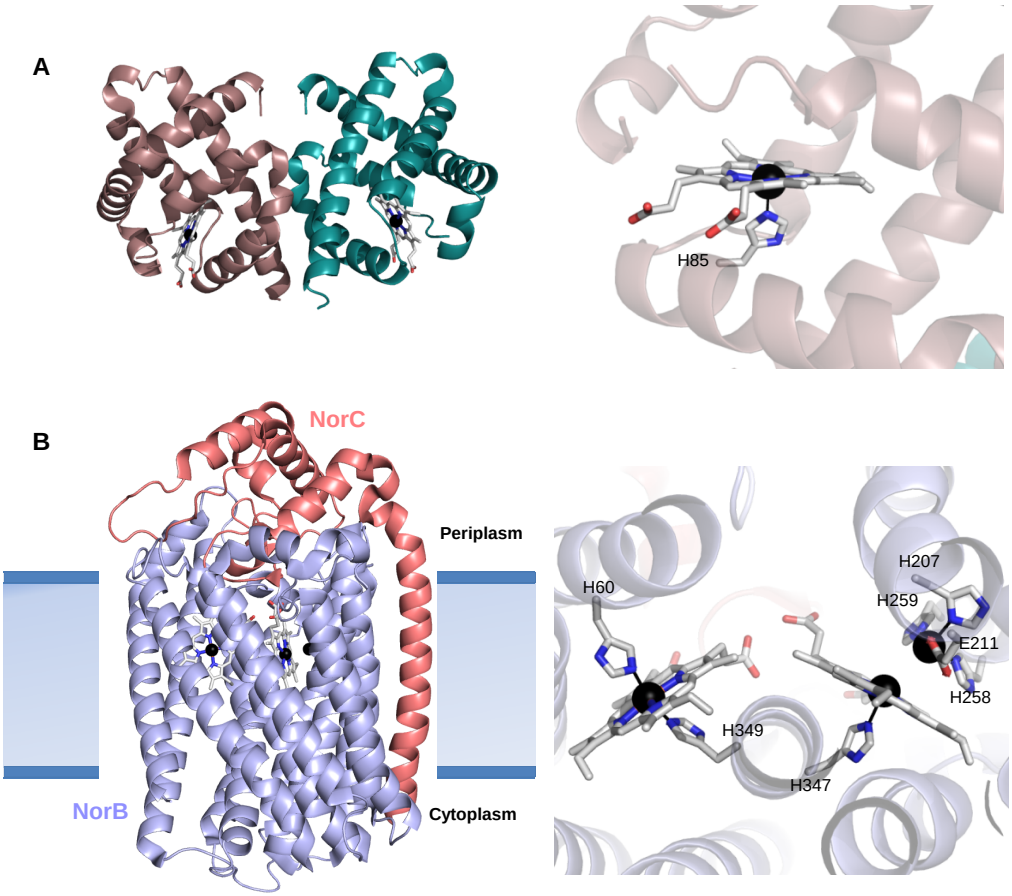

Figure 1.4- Enzymatic defence systems against RNS and their metal catalytic centers. **A)** Single-domain globin (PDB 1VHB) from *Vitreoscilla stercoraria*. **B)** Nitric oxide reductase (PDB 3O0R) from *Pseudomonas aeruginosa*. Cartoon representation of the single-domain globin and nitric oxide reductase is presented in the left panel, and its corresponding metal catalytic center in the right panel. Bonds are represented as sticks. Iron atoms are represented as black spheres and ligands are shown as sticks with carbon atoms in grey, nitrogen in blue and oxygen in red.

1.3 Flavodiiron proteins

FDPs have a key role in oxygen and/or nitric oxide detoxification. This family of proteins was firstly mentioned as A-type flavoproteins (FprA) (Wasserfallen et al., 1998) based on its amino acid sequence analysis. This allowed to identify a new family of flavo(metallo)enzymes, and for the first time, a classification based on their different domains was proposed (see below) (Wasserfallen et al., 1998). A few years

latter, these proteins were renamed as flavodiiron proteins (FDPs), which is their current designation (Silaghi-Dumitrescu et al., 2003).

Nowadays, FDPs can be found in strict or facultative anaerobes among Bacteria, Archaea as well as in some protozoan pathogens (e.g. (Di Matteo et al., 2008; Gomes et al., 2002b; Saraiva et al., 2004; Vicente et al., 2012; Wasserfallen et al., 1998)). FDPs have also been identified in some oxygenic photosynthetic bacteria and eukaryotes (Chaux et al., 2017; Gerotto et al., 2016; Gonçalves et al., 2011a; Shimakawa et al., 2017; Vicente et al., 2002; Yamamoto et al., 2016; Zhang et al., 2009).

In the last twenty years, the increasing knowledge in this family of proteins has been relevant for a better understanding of their function.

1.3.1 Biochemical characterization

In 1993, it was reported for the first time the characterization of a FDP from *Desulfovibrio gigas*, initially named as rubredoxin:oxygen oxidoreductase (ROO) (Chen et al., 1993b). The *D. gigas* ROO revealed the ability to reduce oxygen directly to water without formation of ROS, using electrons donated by a rubredoxin (Rd), which is reduced by an NADH:rubredoxin oxidoreductase (Chen et al., 1993a; Gomes et al., 1997).

Based on amino acid sequence analysis, Wasserfallen *et al.* in 1998 identified forteen FDPs and performed a characterization in three of them, namely from *E. coli*, *Rhodobacter capsulatus* and *Synechocystis* (Wasserfallen et al., 1998). Sequence analysis of *E. coli* C-terminal extension revealed that it encoded a putative rubredoxin, with a CxxC-x_{29}-CxxC motif. In *Synechocystis* sp. PCC 6803 were identified two flavins cofactors, namely FAD and FMN in an approximate 1:1 ratio (Wasserfallen et al., 1998). A flavodoxin-like domain could be involved in FMN binding, however the presence of FAD was unexpected since there is no clear evidence from the protein sequence analysis that the C-terminal extension might have a FAD-binding site. Nevertheless, a few years latter was identified for the first time in *Synechocystis* sp. PCC 6803, a NADH:flavin oxidoreductase C-terminal extension that harbors one FMN or FAD cofactor (Vicente et al., 2002).

In 2000, the determination of the first FDP crystal structure (PDB 1E5D), ROO from *D. gigas* (Frazao et al., 2000), allowed to identify a β-lactamase-like fold harbouring a

non-haem diiron center and a flavodoxin-like domain containing a FMN cofactor non-covalently bound.

The monomer molecular mass (Mm) of FDPs characterized so far, was determined by SDS-PAGE, being in accordance with the calculated protein sequence Mm (Table 1.1). Class A enzymes composed only by the flavodiiron core (Class A, see Section 1.3.2) have approximately 43-48 kDa. FDPs composed of the flavodiiron core in addition to the rubredoxin domain have approximately 54 kDa (Class B, see section 1.3.2), and those with the flavodiiron core plus a NADH:flavin oxidoreductase domain have approximately 63 kDa (Class C, see section 1.3.2) (Table 1.1). The largest FDP thus far studied has 845 amino acids (Class F, see section 1.3.2), with Mm of 90 KDa.

As can been seen in Table 1.1, the Mm of *Thermotoga maritima* and *Treponema denticola* FDPs has not been experimentally determined. However, from the protein sequence it can be inferred to be as 45 kDa and 46 kDa, respectively.

The oligomeric state of these proteins (homotetramers or homodimers), has been determined by native gel electrophoresis or size exclusion chromatography (Table 1.1).

The FDPs cofactors, namely iron and flavin, have been determined by different experimental methods, such as, the 2,4,6-tripyridyl-1,3,5-triazine method (TPTZ) (Fischer and Price, 1964) for iron quantification, and acid extraction for flavin quantification (Susin et al., 1993). The iron content on FDPs has been determined as approximately two iron atoms per monomer, with the exception of the *E. coli* and *Clostridium difficile* Class F FDPs, that additionally to the flavodiiron core, contain one more iron atom belonging to the rubredoxin domain (Rd) with a [Fe-Cys_4] center. Therefore, the presence of two or more iron atoms by monomer, is dependent of the presence of extra C-terminal domains (Classes B, D, F-H, see below).

Currently, several proteins that belong to the FDP family have been characterized (Table 1.1). These proteins are from several organisms and although the biochemical properties are quite similar between them, they present different reductase activities as will be explained in Section 1.3.4.

Table 1.1- Biochemical properties of FDPs.

	Organism	Oligomeric state	Mm (kDa)	Fe by monomer		Flavin by monomer		Reference
				Exp.	Pred.	Exp.	Pred.	
1993	*Desulfovibrio gigas*	Dimer	43	n.d	2.0	FMN	FMN	(Chen et al., 1993b)
1995	*Methanothermobacter thermoautotrophicum*	Dimer	45	n.d.	2.0	1.3	1.0	(Nolling et al., 1995)
1995	*Methanothermobacter marburgensis*	Tetramer	43	n.d.	2.0	0.7	1.0	(Wasserfallen et al., 1995)
1998	*Rhodobacter capsulatus*	Dimer	48	n.d.	2.0	0.9	1.0	(Wasserfallen et al., 1998)
1998	*Escherichia coli*	Tetramer	54	2.0	3.0	0.6	1.0	(Wasserfallen et al., 1998)
1998	*Synechocystis* sp. PCC 6803	Dimer	64	n.d.	2.0	FMN FAD	2.0	(Wasserfallen et al., 1998)
2002	*Synechocystis* sp. PCC 6803	Dimer	63	1.9	2.0	FMN FAD	2.0	(Vicente et al., 2002)
2003	*Moorella thermoacetica*	Dimer	45	1.9	2.0	0.9	1.0	(Silaghi-Dumitrescu et al., 2003)
2004	*Methanobrevibacter arboriphilus*	n.d.	45	2.0	2.0	1.1	1.0	(Seedorf et al., 2004)
2005	*Desulfovibrio vulgaris*	Dimer	45	1.8	2.0	0.8	1.0	(Silaghi-Dumitrescu et al., 2005b)
2008	*Giardia intestinalis*	Tetramer	45	1.5	2.0	0.5	1.0	(Di Matteo et al., 2008)
2008	*Thermotoga maritima*	n.d.	n.d.	1.7	2.0	0.6	1.0	(Le Fourn et al., 2008)
2009	*Clostridium acetobutylicum* FDP_1	Dimer	45	2.0	2.0	1.0	1.0	(Hillmann et al., 2009)
2009	*Clostridium acetobutylicum* FDP_2	Tetramer	45	2.0	2.0	1.0	1.0	(Hillmann et al., 2009)
2009	*Trichomonas vaginalis*	Dimer	45	1.5	2.0	0.5	1.0	(Smutna et al., 2009)
2012	*Entamoeba histolytica*	Dimer	45	1.6	2.0	0.9	1.0	(Vicente et al., 2012)
2015	*Treponema denticola*	n.d.	n.d.	2.0	2.0	1.0	1.0	(Frederick et al., 2015)
2018	*Clostridium difficile 630*	Dimer	90	1.4	3.0	1.8	2.0	(Folgosa et al., 2018b)

n.d- not determined.

1.3.2 Modular classification

The FDP minimal structural unit is composed of two domains: metallo-β-lactamase-like domain and flavodoxin-like domain, in the N-terminal and C-terminal, respectively. The N-terminal domain harbors a diiron site, where the substrate (O_2 and/or NO) reduction occurs, and the C-terminal domain contains a non-covalently bound FMN cofactor, that donates electrons to the metal center. Therefore, these two domains constitute the common denominator of this protein family (FDPs). Additionally to the metallo-β-lactamase and the flavodoxin-like domains, FDPs can have more extra modular structures, due to the presence of C-terminal extensions. Therefore, as recently reported, FDPs can be classified into eight different classes, accordingly to the composition and distribution of the extra domains (Fig. 1.5 A) (Folgosa et al., 2018a; Saraiva et al., 2004).

Class A FDPs (approx. 400 residues) are the simplest structural arrangement since it comprehends only the flavodiiron core, being most widespread in Bacteria, although can also be found in Archaea and Protozoa. This Class A includes the largest number of FDPs so far studied (Table 1.1 and 1.2) (Di Matteo et al., 2008; Rodrigues et al., 2006; Seedorf et al., 2004; Silaghi-Dumitrescu et al., 2003; Silaghi-Dumitrescu et al., 2005b; Smutna et al., 2009; Vicente et al., 2012).

Class B FDPs (approx. 480 residues) have a rubredoxin domain (Rd) in the C-terminal, with the [Fe-Cys_4] binding motif CxxC-x_{29}-CxxC, being therefore named as flavorubredoxins (Fig. 1.5 A). The proteins belonging to this class have been found only in the Proteobacteria phylum (gamma, delta and beta classes). The *E. coli* FDP is the only protein from this class that has been characterized (Table 1.1 and 1.2), with NO reductase activity, and a very low O_2 reductase activity. This is the only studied example of an FDP with a clear substrate preference for NO (Gardner et al., 2002; Gomes et al., 2002b). The Rd domain is the electron entry point of FDPs belonging to this class, transferring electrons to the diiron center through a kinetically stable flavin semiquinone (Vicente et al., 2007b; Vicente and Teixeira, 2005).

Class C FDPs (approx. 600 residues) are constituted by an extra C-terminal with a NAD(P)H:flavin oxidoreductase domain, containing flavin cofactors. The proteins from this class, can be found in cyanobacteria but also in oxygenic photosynthetic eukaryotes (Allahverdiyeva et al., 2015a; Chaux et al., 2017; Gerotto et al., 2016; Gonçalves et al., 2011a; Helman et al., 2003; Yamamoto et al., 2016; Zhang et al., 2009). *Synechocystis* sp. PCC 6803 encodes four flavodiiron proteins (Flv1, Flv2,

Flv3, and Flv4) all belonging to this Class. Flv3 was the only FDP from this class so far characterized, and presents oxygen reductase activity (Vicente et al., 2002) (Table 1.1 and 1.2).

The modular properties of the new putative Classes D, E, G and H were deduced from their respective amino acid sequences (Fig. 1.5 A) (Folgosa et al., 2018a; Saraiva et al., 2004).

The Class D FDPs (approx. 440 residues) was predicted to have one extra domain in the C-terminal extension, Rd_{Rbr}, similar to the rubredoxin domain from rubrerythrins (Rbr), with a CxxC-x_{12-14}-CxxC metal binding motif. Rubrerythrins, have a non-catalytic domain with a [Fe-Cys_4] center, with an overall fold similar to rubredoxins, although in these latter proteins, the two CxxC motifs are separated by 29 amino acids. These proteins have been found so far only in the *Firmicutes* phylum (*Clostridiales* order).

The Class E FDPs (approx. 500 residues) contains in addition to the flavodiiron core, an extra domain, known as “Divergent 4Fe-4S mono-cluster protein”, that may contain an [3Fe-4S] or [4Fe-4S] cluster, with a CxHxxxC-x_{33}-CP binding motif. This class has only been found in *Firmicutes* phylum (*Clostridiales* order).

The Class F FDPs (approx. 850 residues) contain two domains in the C-terminal extension, namely a Rd_{Rbr} and a NADH:rubredoxin oxidoreductase-like domains. FDPs from this class can be found mainly in *Firmicutes* phylum (*Clostridiales* order), but also in some eukaryotic protozoa, such as *Trichomonas vaginalis*. Recently, the *Clostridium difficile* FDP that belongs to this class was characterized, being so far the most complex FDP studied (Folgosa et al., 2018b).

The Class G FDPs (approx. 600 residues) contain two domains additionally to the FDP core, a Rd_{Rbr} and a NAD(P)H:flavin oxidoreductase-like domains. These proteins are present in the *Firmicutes* phylum (*Clostridiales, Erysipelotrichiales* and *Lactobacillales* orders).

The Class H FDPs (approx. 870 residues) besides the flavodiiron core, have three domains, a Rd_{Rbr}, a NAD(P)H:flavin oxidoreductase and a second Rd_{Rbr}-like domains.

While writing this thesis, a new class (Class I) of FDPs was identified, containing besides the FDP core, a desulforedoxin-like domain (Dx) and a neelaredoxin-like domain (Nlr) in the C-terminal extension (Martins et al., 2019).

Most Class A FDPs require the contribution of two redox partners (Fig. 1.5 B), as for *D. gigas* ROO, that is reduced by a Rd which in turn receives electrons from a NADH:rubredoxin oxidoreductase (Chen et al., 1993a). Another case, is the *M.*

thermoacetica FDP also from Class A, which uses a high molecular weight rubredoxin (Hrb) that consists in a rubredoxin domain (CxxC-x_{29}-CxxC binding motif), fused to a NAD(P)H:flavin oxidoreductase domain. This domain was suggested to accept electrons from NADH, transferring them to the Rd-domain to finally reduce the flavodiiron protein (Silaghi-Dumitrescu et al., 2003). Moreover, was proposed that the presence of a NADH:rubredoxin oxidoreductase protein is essential to donate electrons to a Rd (CxxC-x_{29}-CxxC binding motif), which thereafter will reduce the *T. maritima* FDP (Hayashi et al., 2010). In contrast, the Class A enzymes from *M. marburgensis* and *M. arboriphilus* only require an external redox cofactor, $F_{420}H_2$ (abundant in methanogenic organisms) that is used to directly reduce FDPs from these organisms abolishing the need of other redox proteins (Fig. 1.5 B) (Seedorf et al., 2004; Seedorf et al., 2007).

The *E. coli* FDP, belonging to Class B, is dependent on an external redox partner to be reduced, receiving therefore electrons from an NADH:rubredoxin oxidoreductase containing a FAD cofactor (Vicente et al., 2007b; Vicente and Teixeira, 2005).

Class C FDPs have an extra C-terminal NAD(P)H:flavin oxidoreductase domain that directly accepts electrons from NAD(P)H, thus the electron transfer chain is condensed into a single polypeptide. So far, only the Class C Flv3 from *Synechocystis* sp. PCC 6803 has been characterized, being reduced directly by NADH (Vicente et al., 2002).

Although the physiological extra redox partners of FDPs from Class A and B of many organisms remain to be identified, their simple structural arrangement does not allow them to be independent from extra redox partners. The similar domains in Class D and B FDPs, suggests that similar redox partners may be involved in both classes. The more complex modular nature of Class C FDPs abolishes the need of an external redox protein. The presence of an iron-sulfur cluster in Class E FDPs suggests a different redox partner that needs to be further investigated.

The “standalone” proteins biochemically characterized so far, are the Class C Flv3 from *Synechocystis*, and the Class F FDP from *C. difficile* since they can be directly reduced by NADH without the need for extra electron transfer partners (Folgosa et al., 2018b; Vicente et al., 2002). Nevertheless, knowledge on the FDPs putative redox partners is still very limited.

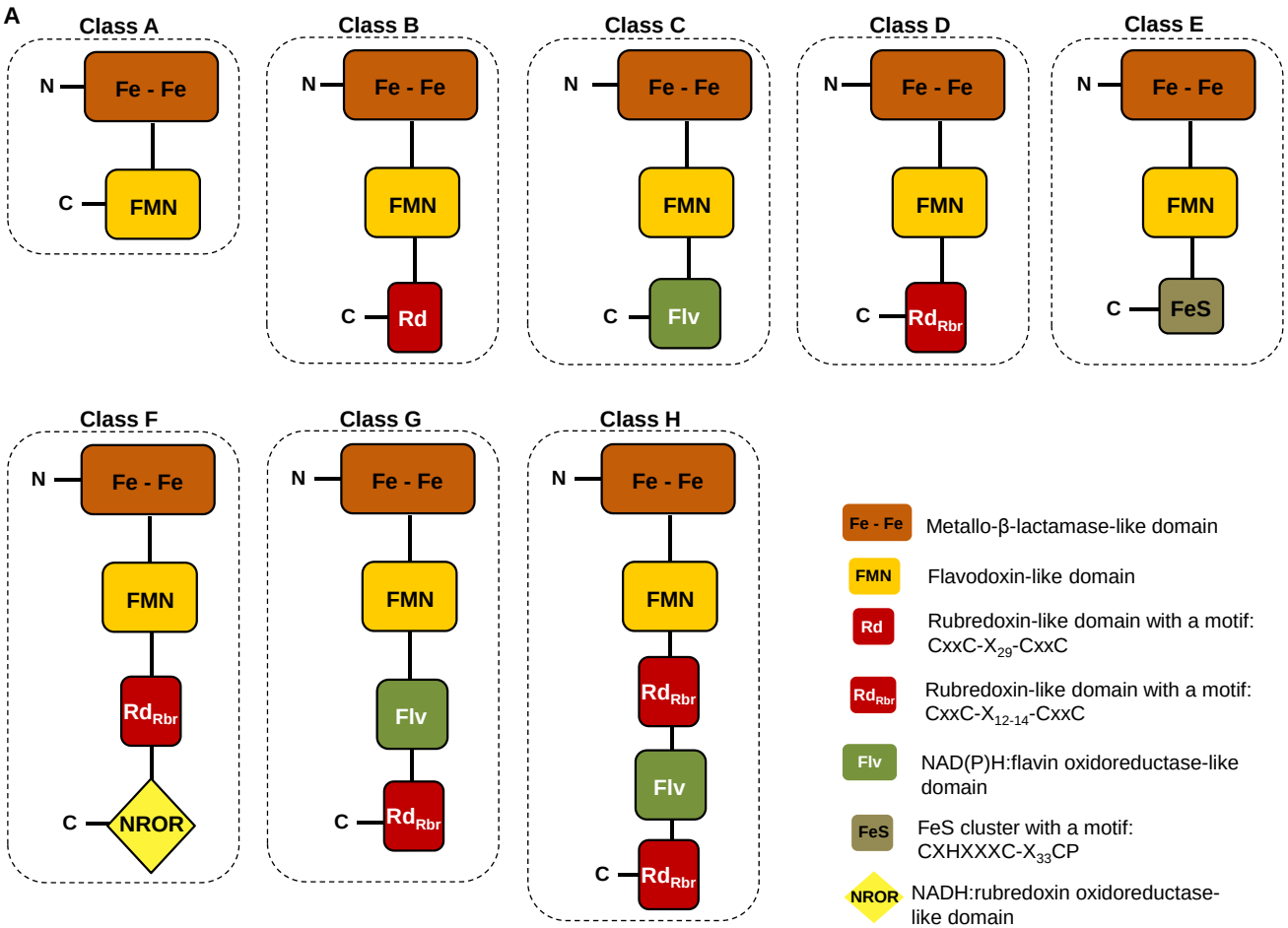
A
Class A
N
Fe - Fe
C
FMN
Class B
N
Fe - Fe
FMN
C
Rd
Class C
N
Fe - Fe
FMN
C
Flv
Class D
N
Fe - Fe
FMN
C
Rd Rbr
Class E
N
Fe - Fe
FMN
C
FeS
Class F
N
Fe - Fe
FMN
Rd Rbr
C
NROR
Class G
N
Fe - Fe
FMN
Flv
C
Rd Rbr
Class H
N
Fe - Fe
FMN
Rd Rbr
Flv
C
Rd Rbr
Fe - Fe
Metallo-β-lactamase-like domain
FMN
Flavodoxin-like domain
Rd
Rubredoxin-like domain with a motif: CxxC-X29-CxxC
Rd Rbr
Rubredoxin-like domain with a motif: CxxC-X12-14-CxxC
Flv
NAD(P)H:flavin oxidoreductase-like domain
FeS
FeS cluster with a motif: CXHXXXC-X33CP
NROR
NADH:rubredoxin oxidoreductase-like domain

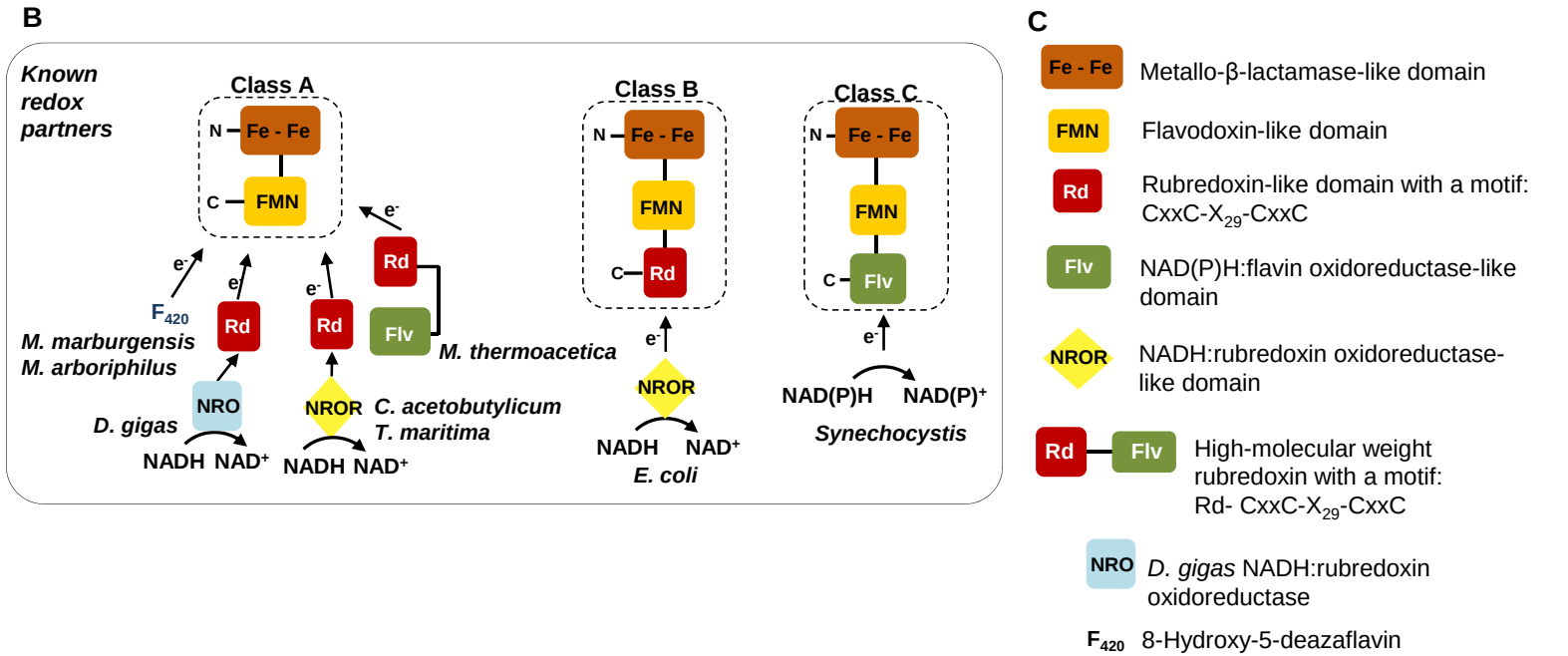

Figure 1.5- The modular organization of the flavodiiron protein family.
A) FDP classification according to the modular organization based on the proposed domain structure.
B) Scheme of the electron transfer chains comprising the known FDPs redox partners. **C)** Legend for the different domains. Adapted from (Folgosa et al., 2018a; Saraiva et al., 2004).

1.3.3 Spectroscopic properties

Spectroscopic methods such as UV-visible and Electron Paramagnetic Resonance (EPR) are commonly used to characterize the flavodiiron proteins redox centers.

The visible and near-UV region spectroscopy can be used to characterize flavins, contrary to the diiron center, since the absorptivity of this center is considerably lower (~ $3x10^3$ $M^{-1}cm^{-1}$ at 300 nm), relatively to the flavin cofactor (~ $12.5x10^3$ $M^{-1}cm^{-1}$ at 450 nm) (Saraiva et al., 2004).

The typical flavin UV-visible fingerprint of FDPs from Class A is very similar, namely the band shape and their absorption maxima at approximately 375 nm and 455 nm (Gomes et al., 2000; Silaghi-Dumitrescu et al., 2003). It was proposed that the presence of a tryptophan residue, W348 (*E. coli* FDP numbering), that is coplanar to the isoaloxazine ring of FMN cofactor, could be responsible for the the lack of resolution of the absorption band at 455 nm (Saraiva et al., 2004). In FDPs where this residue is absent (*e.g. M. marburgensis* FDP, that presents instead a glycine residue), the band at 455 nm has two shoulders (Wasserfallen et al., 1995).

In Class B FDPs, due to the existence of a rubredoxin domain in the C-terminal extension, the band at 455 nm is shifted to *ca.* 470 nm and an extra band appears at approximately 570 nm due to the [Fe-Cys_4] center (Gomes et al., 2000). Therefore, the spectra of *E. coli* flavorubredoxin results from the overlap of the spectral contributions of the flavin and rubredoxin center [Fe-Cys_4].

Also the spectra from Class C FDPs, which contain an FMN cofactor in the flavodoxin-like domain and a FAD cofactor in the NAD(P)H:flavin oxidoreductase domain, is dominated by the combination of both flavins (Vicente et al., 2002).

Since the diiron center has a low extinction coefficient, and the UV-visible spectroscopic features of the flavin are in the same spectral region, it is not possible to use this method to analyse the diiron center. EPR spectroscopy provides spectral evidence for the diiron center in FDPs (Vicente et al., 2007a). The first report of FDPs characterized by EPR was for *E. coli,* and later for enzymes from other organisms (Frederick et al., 2015; Smutna et al., 2009; Vicente and Teixeira, 2005; Vicente et al., 2012). In EPR, the FDP diiron center is silent in the oxidized state, since the two iron ions are coupled antiferromagnetically (S=0) (Silaghi-Dumitrescu et al., 2003). The diiron center is only easily detected by perpendicular mode EPR in a mixed-valence state, *i.e*, one electron reduced, displaying resonances below *g*=2.0 (Smutna et al., 2009; Solomon et al., 2000; Vicente and Teixeira, 2005; Vicente et al., 2012).

1.3.4 Physiological functions of flavodiiron proteins

The first function reported for a FDP was as oxygen reductase for the strict anaerobic sulfate reducing bacterium *D. gigas*, as a defence mechanism against O_2 deleterious effects (Eq. 1.1) (Chen et al., 1993a; Chen et al., 1993b). A few years later, a new function in FDPs was reported, namely NO reductase activity, based on *in vivo* (Gardner et al., 2002) and *in vitro* studies in *E. coli* (Eq. 1.2) (Gomes et al., 2002b). In *Salmonella* enterica serovar Typhimurium, deletion mutants of the FDP gene resulted in an impaired growth of the cell cultures exposed to NO (Mills et al., 2008).

$O_2 + 4e^- + 4H^+ \rightarrow 2H_2O$ (Eq. 1.1)

$2NO + 2e^- + 2H^+ \rightarrow N_2O + H_2O$ (Eq. 1.2)

Following this finding, in 2003 it was reported the first bifunctional FDP with both O_2 and NO reductase activity from *M. thermoacetica* (Silaghi-Dumitrescu et al., 2003). In 2006 it was also identified that *D. gigas* ROO, has *in vivo* protection against NO stress, although *in vitro* it has a lower NO reductase activity comparing with its O_2 reductase activity (Rodrigues et al., 2006).

Since 1998 until now, FDPs involved in photoprotection of oxygenic photosynthesis have been explored. The first FDP from a phototrophic organism, namely the cyanobacterial *Synechocystis* sp. PCC 6803 Flv3, was characterized by *in vitro* studies (Vicente et al., 2002; Wasserfallen et al., 1998). Biochemical and kinetic studies of Flv3 and its truncated form (NAD(P)H:flavin-reductase-like domain) showed that this protein is an NAD(P)H:oxygen oxidoreductase, being capable to reduce O_2 to H_2O, without the production of ROS (Vicente et al., 2002; Wasserfallen et al., 1998). However, only in 2003 *in vivo* studies revealed that its function together with Flv1, is associated with photoprotection of photosystem I (PSI), under specific environmental conditions through the Mehler reaction (Helman et al., 2003) as referred in Section 1.8.

The FDPs from the methanogenic *M. marburgensis* and *M. arboriphilus* have been described as exclusively O_2 reductases. These proteins accept electrons from the coenzyme $F_{420}H_2$, which is present in relatively high concentrations in methanogenic

archaea (Seedorf et al., 2004; Seedorf et al., 2007). Also FDPs from some pathogenic protozoa organisms such as *G. intestinalis*, *T. vaginalis* and *E. histolytica* are reported to have oxygen selective reductase activity (Di Matteo et al., 2008; Smutna et al., 2009; Vicente et al., 2012) (Table 1.2).

Overall, FDPs can be classified as exclusively oxygen reductases (O_2R), or nitric oxide reductases (NOR); or as bifunctional enzymes having the two reductase activities, although with different efficiencies. However, recently has been reported a Class F FDP from *C. difficile* with a high selectivity for oxygen as substrate, but also showed affinity for hydrogen peroxide, being so far, the first FDP to be characterized with peroxidase activity (Folgosa et al., 2018b).

Table 1.2- General properties of FDPs (*n.d.* not determined, (*a*) absent).

Organism	Class	Group	Quaternary Structure	Reductase Activities		Redox potential (mV)				Reference
				O_2	NO	E^{FMN}	$E^{Fe\text{-}Fe}$	E^{Rd}	E^{FAD}	
D. gigas	A	Anaerobic	Dimer	Yes	Yes	0/-130	n.d	(a)	(a)	(Chen et al., 1993b; Gomes et al., 1997; Rodrigues et al., 2006)
D. vulgaris	A	Anaerobic	Dimer	Yes	Yes	-	-	(a)	(a)	(Silaghi-Dumitrescu et al., 2005b)
M. thermoacetica	A	Anaerobic	Dimer	Yes	Yes	-117/-220	n.d	(a)	(a)	(Silaghi-Dumitrescu et al., 2003)
C. acetobutylicum FDP_2	A	Anaerobic	Tetramer	Yes	Yes	-	-	(a)	(a)	(Hillmann et al., 2009; Kawasaki et al., 2004; Kawasaki et al., 2005)
T. denticola	A	Anaerobic	n.d.	Yes	Yes	-	-	(a)	(a)	(Frederick et al., 2015)
G. intestinalis	A	Anaerobic	Tetramer	Yes	No	-66/-83	+2/+163	(a)	(a)	(Di Matteo et al., 2008; Vicente et al., 2009)
T. vaginalis	A	Anaerobic	Dimer	Yes	No	+25/+25	+50/+190	(a)	(a)	(Smutna et al., 2009)
E. histolytica	A	Anaerobic	Dimer	Yes	No	-55/-140	+170/+132	(a)	(a)	(Vicente et al., 2012)
C. acetobutylicum FDP_1	A	Anaerobic	Dimer	Yes	No	-	-	(a)	(a)	(Hillmann et al., 2009; Kawasaki et al., 2004; Kawasaki et al., 2005)
M. marburgensis	A	Anaerobic	Tetramer	Yes	No	-	-	(a)	(a)	(Seedorf et al., 2007)
M. arboriphilus	A	Anaerobic	n.d.	Yes	No	-	-	(a)	(a)	(Seedorf et al., 2004)
T. maritima	A	Anaerobic	Dimer	Yes	No	-	-	(a)	(a)	(Hayashi et al., 2010)
R. capsulatus	A	Anaerobic	Dimer	Yes	No	+20	-	(a)	(a)	(Jouanneau et al., 2000; Wasserfallen et al., 1998)
Synechocystis sp. PCC 6803	C	Aerobic	Dimer	Yes	No	-	-	(a)	-	(Vicente et al., 2002; Wasserfallen et al., 1998)
E. coli	B	Facultative anaerobic	Tetramer	No	Yes	-40/-130	-20/-90	-123	(a)	(Gomes et al., 2002b; Vicente and Teixeira, 2005; Wasserfallen et al., 1998)
C. difficile	F	Anaerobic	Dimer	Yes	No	−170/−170	-	-110	-250/-250	(Folgosa et al., 2018b)

1.4 Three-dimensional structure of flavodiiron proteins

1.4.1 Deposited FDPs crystal structures

Currently there are a total of fourteen crystallographic structures of FDPs from different organisms deposited in the Protein Data Bank (Table 1.3). The first FDP structure (ROO) was reported in 2000, from the sulfate-reducing bacteria *D. gigas* (PDB 1E5D) (Frazao et al., 2000), and the most recent one was the *E. coli* FDP (PDB 4D02) (Romao et al., 2016b).

Table 1.3- Crystallographic structures of FDPs.

Class	Reductase activity	Organism	PDB code	Oxidation state	Resolution (Å)	References
FDP domain						
A	O_2R	*T. maritima*	1VME	Oxidized	1.80	Joint Center Structural Genomics, (Fang et al., 2012)
			4DIK	Oxidized	1.75	
			4DIL	Oxidized	2.00	
A	O_2R	*M. marburgensis*	2OHH	Oxidized	1.70	(Seedorf et al., 2007)
			2OHI	Reduced	2.30	
			2OHJ	Inactive oxidized	2.26	
A	O_2R	*G. intestinalis*	2Q9U	Oxidized	1.90	(Di Matteo et al., 2008)
A	O_2R/NOR	*M. thermoacetica*	1YCF	Oxidized	3.00	(Silaghi-Dumitrescu et al., 2005a)
			1YCG	Reduced	2.80	
			1YCH	NO reacted	2.80	
A	O_2R/NOR	*D. gigas*	1E5D	Oxidized	2.50	(Frazao et al., 2000)
B	NOR	*E. coli*	4D02	Oxidized	1.75	(Romao et al., 2016b)
			5LLD	Reduced	2.65	
			5LMC	Oxidized with [Fe-4S^{G}]cluster	1.90	
β-lactamase-like domain						
C	O_2R	*Anabaena*	4FEK	Oxidized	2.00	Joint Center Structural Genomics
flavodoxin-like domain						
C	O_2R	*Anabaena*	3FNI	Oxidized	2.30	Joint Center Structural Genomics

The available FDPs structures show similar three-dimensional arrangements with overall Cα *r.m.s.d.*'s within 1.2-2.1 Å (Table 1.4).

These proteins are oxidoreductases, so it is extremely relevant to determine their structures in different oxidation states (Tabel 1.3). The majority of these structurally characterized FDPs is oxygen selective or bi-functional and belongs to Class A.

The *M. thermoacetica* FDP was crystallized in the as-isolated (oxidized) form (PDB 1YCF) and then crystals were reduced (PDB 1YCG) and reoxidized with an NO releaser (PDB 1YCH) (Silaghi-Dumitrescu et al., 2005a).

The *M. marburgensis* FDP was crystallized anaerobically in the reduced state (PDB 2OHI), and then air-exposed resulting in the active oxidized state (PDB 2OHH) and in an inactive oxidized form (PDB 2OHJ) (Seedorf et al., 2007).

The crystallographic structure of *E. coli* FDP was obtained in the as-isolated (oxidized) state (PDB 4D02), including the [Fe-4S^{G}] atoms from its Rd domain (PDB 5LMC) and in the reduced form (PDB 5LLD) (Romao et al., 2016b).

In *M. thermoacetica* FDP, the structural variations in the different oxidation states are subtle, with a distance between the two irons of 3.3-3.4 Å. The major difference between the structures is related with the presence of one ethylene glycol molecule located in the substrate binding site of the diiron site in the reduced form (PDB 1YCG), while an oxygen or water molecule was found in the as isolated state (PDB 1YCF) and NO-reoxidized state (PDB 1YCH), respectively.

In the *M. marburgensis* FDP crystal structures, higher differences among the different crystal forms were observed. These structural changes are related with the diiron center and with a "switch-loop" that comprises the region P148-P153 (Seedorf et al., 2007). In the reduced state (PDB 2OHI), the diiron site retains its metal ligands and the "switch-loop" is in a closed conformation. However, in the inactive oxidized state (PDB 2OHJ), while the distal iron (iron far from FMN cofactor, Fe_d) maintains its ligands coordination, the proximal iron (iron close to the FMN cofactor, Fe_p) is displaced away from its original location (~ 7 Å from Fe_d), disrupting then the diiron center. Moreover, a third iron center appears close to the solvent exposed molecular surface although far from Fe_d (~ 20 Å). Here, the "switch-loop" is in an open conformation. Finally, in the active oxidized state (PDB 2OHH), the diiron site is maintained but the "switch-loop" is in a mixed conformation with an occupancy of 0.6 in a closed conformation (as in reduced state) and an occupancy of 0.4 in an open conformation (as in inactive oxidized state).

Table 1.4- Comparison of FDPs overall fold. The Cα *r.m.s.d*.'s (Å) for *E. coli* FDP (PDB 4D02, 5LLD and 5LMC), *T. maritima* FDP (PDB 1VME, 4DIK, 4DIL), *M. thermoacetica* FDP (PDB 1YCF. 1YCG, 1YCH), *M. marburgensis* FDP (PDB 2OHH, 2OHI, 2OHJ), *D. gigas* ROO (PDB 1E5D) and *G. intestinalis* FDP (PDB 2Q9U) are presented above the diagonal (grey region). In the cases where more than one crystallographic structure is known, a range of Cα *r.m.s.d*.'s (Å) is represented. Sequence identities percentages (%) are shown in the rows below the diagonal. For each crystal structure is presented the corresponding resolution (Å).

	E. coli FDP oxidized (1.75 Å); reduced (2.65 Å); oxidized with [Fe-4S^{G}] cluster (1.90 Å)	*T. maritima* FDP oxidized (1.80 Å); H90A (1.75 Å); H90N (2.00 Å)	*M. thermoacetica* FDP oxidized (3.00 Å); reduced (2.80 Å); NO reacted (2.80 Å)	*M. marburgensis* FDP oxidized (1.70 Å); reduced (2.30 Å); inactive oxidized (2.26 Å)	*D. gigas* ROO (2.50 Å)	*G. intestinalis* FDP (1.90 Å)
E. coli	**0.14-0.27**	1.94-2.06	1.46-1.51	1.56-1.69	1.39-1.42	1.61-1.65
T. maritima	23.8	**0.52-0.61**	1.94-2.09	1.96-2.05	1.74-1.81	2.01-2.06
M. thermoacetica	41.9	26.5	**0.09-0.24**	1.35-1.44	1.16-1.18	1.46-1.53
M. marburgensis	37.8	29.5	41.6	**0.52-0.69**	1.38-1.41	1.29-1.33
D. gigas	34.9	25.9	41.4	31.9	--	1.41
G. intestinalis	31.6	24.1	37.8	31.1	31.8	--

Recently, it was reported by the first time the structure of a FDP with exclusive nitric oxide reductase activity and belonging to Class B, thus composed of an extra C-terminal Rd domain, namely *E. coli* FDP (Romao et al., 2016b). The crystallographic structures were obtained for the as-isolated (oxidized) form (PDB 4D02, 5LMC) and upon chemical reduction (PDB 5LLD). The major differences between these two forms consist in: *i)* a loss upon reduction of the μ-OH^- moiety bridging the two irons in the catalytic center, *ii)* a shorter Fe_p-Fe_d distance in the reduced form and *iii)* the presence of a phosphate anion in the active site pocket in the as-isolated (oxidized) form, while in the reduced form it is present an oxygen molecule.

The *E. coli* FDP as-isolated (oxidized) form (PDB 5LMC) showed in its solvent region a well-defined tetrahedral electron density with *ca.* 3.9 Å long edges, suggesting that could correspond to the Fe-S4 center from the rubredoxin domain. This indicates a disordered localization of the C-terminal Rd domain that is connected to the flavodiiron core by a flexible coil with ~ 20 amino acids. This is in agreement with previous reported Small-angle X-ray scattering (SAXS) studies of this protein in solution (Petoukhov et al., 2008). A representative model of the *E. coli* FDP Rd domain structure obtained by NMR (PDB 2MS3) was tentatively positioned in the asymmetric unit (*a.u.*) by fitting its [Fe–$4S^G$] moiety into the tetrahedron shaped electron density found in the solvent region of *E. coli* FDP. This approach allowed to relate the extra density of the heavier atoms from its [Fe-Cys_4] center, with the highly disordered Rd domain (Fig. 1.6).

The crystal structure of a Class C FDP, composed of the flavodiiron core plus the extra C-terminal NAD(P)H:flavin oxidoreductase, remains to be determined. However, structures of the truncated β-lactamase and flavodoxin-like domains are available. One of these structures is the metallo-β-lactamase-like domain of *Anabaena* sp. PCC 7120 (PDB 4FEK), although revealing the absence of a diiron center. The flavodoxin-like domain structure of *Anabaena* sp. PCC 7120 (PDB 3FNI) was also determined, being however deflavinated. The FDP core domain (β-lactamase and flavodoxin-like domains) of Flv1 from *Synechocystis* sp. PCC 6803, was determined in the scope of this thesis (Chapter IV).

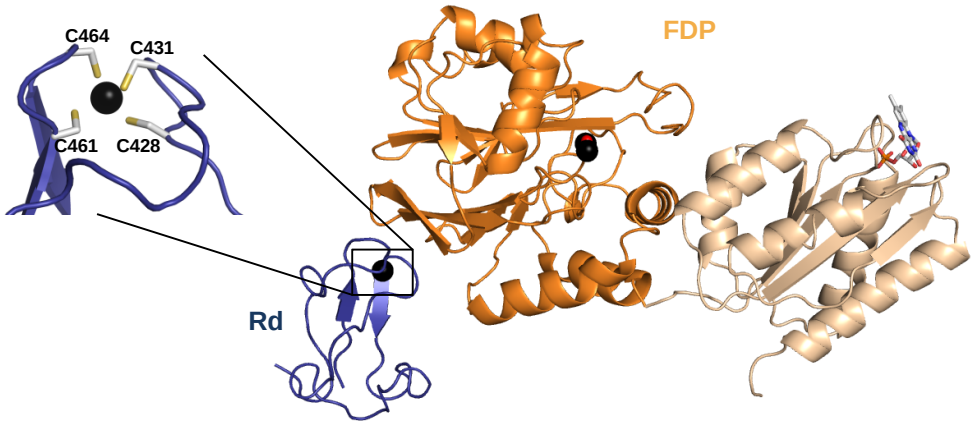

Figure 1.6- Monomeric structure of *E. coli* FDP and its rubredoxin domain. Cartoon representation of the crystallographic structure of *E. coli* FDP (PDB 4D02) monomer (β-lactamase and flavodoxin-like domains are colored as orange and light brown, respectively), and localization of the Rd domain (blue) determined by NMR (PDB 2MS3) in one of the possible orientations. Iron atoms are represented as black spheres, and FMN and residues as sticks. Carbon is colored as grey, nitrogen in blue, sulfur in yellow, oxygen in red and phosphorous in orange.

1.4.2 Minimal functional unit

The FDP core is defined by two structural domains: a metallo-β-lactamase and a flavodoxin-like folds (Section 1.3.2) (Fig. 1.7 A).

The first three dimensional structure of an FDP (Frazao et al., 2000), revealed the presence of a minimal functional unit that results from a “head-to-tail” arrangement of two monomers (Fig. 1.7 B). This dimeric arrangement has been observed in other FDPs structurally characterized so far (Table 1.3). Since the iron atoms and the FMN cofactor of the same monomer are located at *ca*. 40 Å apart, the “head-to-tail” dimerization will allow an efficient electron transport from the FMN cofactor of one monomer to the diiron center of the opposing monomer since it brings these two cofactors to a shorter distance (~6 Å) (Frazao et al., 2000; Romao et al., 2016a; Seedorf et al., 2007).

Flavodiiron proteins have been isolated as functional homodimers or homotetramers (dimer of dimers) (Di Matteo et al., 2008; Frazao et al., 2000; Romao et al., 2016b; Seedorf et al., 2007; Silaghi-Dumitrescu et al., 2005a) (Table 1.1 and Fig. 1.7 C, D).

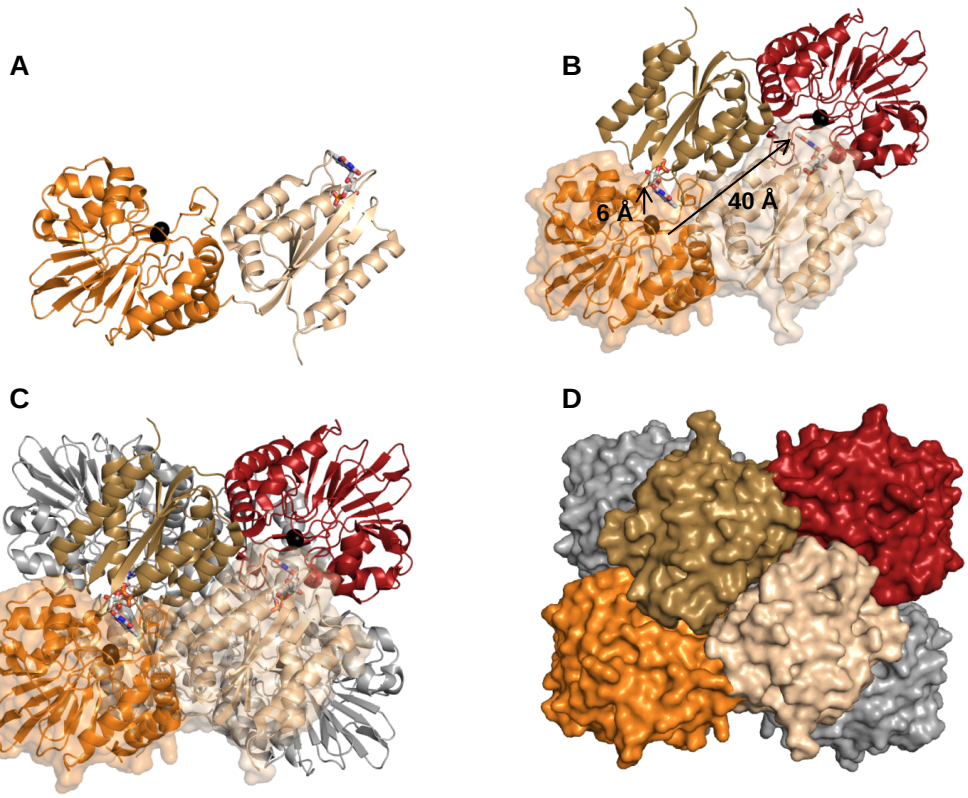

Figure 1.7- Overall structure of *E. coli* FDP. **A)** Cartoon representation of the crystallographic structure of *E. coli* FDP (PDB 4D02) monomer, with the N-terminal metallo β-lactamase-like domain colored in orange and the C-terminal flavodoxin-like domain in light brown. **B)** Cartoon representation of the dimeric "head-to-tail" configuration with molecular surface of one of the monomers colored as referred in A) while the other monomer has the β-lactamase-like domain colored as red and the flavodoxin-like domain as brown. Distances between the diiron and the FMN cofactor from the same monomer or by the "head-to-tail" related monomer are represented. **C)** Cartoon representation of the tetramer conformation with molecular surface of one of the monomers. The "head-to-tail" dimer in the back view is colored as grey. **D)** Molecular surface representation of the tetramer conformation colored as in C). Iron atoms are represented as black spheres and FMN as sticks with carbon in grey, nitrogen in blue, and oxygen in red.

1.4.3 Metallo-β-lactamase-like domain

FDPs monomers contain a metallo-β-lactamase-like domain (~250 residues) in the N-terminal. In spite of the low amino acid sequence identity (11-20%) between the β-lactamase-like domain of FDPs and other metallo-β-lactamase proteins, they have a very similar fold, a *αββα* sandwich fold where the two inner β-sheets are surrounded

by two sets of solvent exposed α-helices (Fig. 1.8 A and B) (Cameron et al., 1999; Carfi et al., 1995; Garau et al., 2005; Gomes et al., 2002a; Romao et al., 2016b). The structural comparison of metallo-β-lactamases and metallo-β-lactamase-like domain in FDPs, shows Cα *r.m.s.d.*'s within 2.1-2.7 Å for 3.5 Å Cα distances cutoff (Table 1.5).

The β-lactamases-like proteins catalyze redox or hydrolytic reactions, and may harbour mononuclear or binuclear metal centers with single or mixed metals such as iron, zinc or manganese (Fig. 1.8 C) (Bebrone, 2007; Liu et al., 2005; Paul-Soto et al., 1998; Schilling et al., 2005; Sharma et al., 2006; Yu et al., 2009). Persulfide dioxygenases and FDPs are proteins involved in redox reactions. While persulfide dioxygenases catalyses the oxidation of glutathione persulfide (GSSH) to glutathione and persulfite, the FDPs are involved in the direct reduction of dioxygen and/or nitric oxide to water and nitrous oxide. The hydrolytic reactions are performed by methyl parathion hydrolase, glyoxalase II, metallo-β-lactamases, N-acyl homoserine lactone hydrolase and alkylsulfatase (Bebrone, 2007; Cameron et al., 1999; Carfi et al., 1995; Dong et al., 2005; Garau et al., 2005; Garces et al., 2010; Hagelueken et al., 2006; Kabil and Banerjee, 2012; Liu et al., 2005). For example, the glyoxalase II is part of a glyoxalase system that catalyzes the conversion of toxic 2-oxoaldehydes to the corresponding 2-hydroxycarboxylic acids using glutathione as a coenzyme. The metallo-β-lactamases hydrolyze β-lactams, while alkylsulfatases have the ability to hydrolyze long-chain alkyl esters such as the detergent sodium dodecyl sulfate (SDS).

Table 1.5- Comparison of FDPs N-terminal domain with the β-lactamases proteins. The Cα *r.m.s.d*.'s (Å) are presented above the diagonal (grey region). FDP codes: *E. coli* FDP (PDB 4D02), *T. maritima* FDP (PDB 1VME), *M. thermoacetica* FDP (PDB 1YCF), *M. marburgensis* FDP (PDB 2OHH), *D. gigas* ROO (PDB 1E5D), *G. intestinalis* FDP (PDB 2Q9U). The β-lactamases proteins codes: *H. sapiens* glyoxalase II (PDB 1QH5), *H. sapiens* persulfide dioxygenase (PDB 4CHL) and *P. aeruginosa* alkylsulfatase (PDB 2CFU). Sequence identities percentages (%) are shown in the rows below the diagonal.

	E. coli	*T. maritima*	*M. thermoacetica*	*M. marburgensis*	*D. gigas*	*G. intestinalis*	*H. sapiens* glyoxalase	*H. sapiens* persulfide dioxygenase	*P. aeruginosa* alkylsulfatase
E. coli	--	1.28	1.07	1.30	1.23	1.45	2.50	2.38	2.15
T. maritima	34.2	--	1.42	1.64	1.25	1.54	2.61	2.47	2.07
M. thermoacetica	41.1	32.9	--	1.03	1.30	1.41	2.57	2.38	2.31
M. marburgensis	38.3	35.6	42.6	--	1.03	1.47	2.51	2.57	2.19
D. gigas	43.6	32.9	45.6	36.9	--	1.33	2.56	2.54	2.14
G. intestinalis	39.6	30.2	43.0	36.2	38.3	--	2.67	2.64	2.25
H. sapiens glyoxalase	12.1	11.4	13.5	17.4	13.9	18.1	--	1.95	2.40
H. sapiens persulfide dioxygenase	20.1	12.8	14.4	19.5	16.8	14.3	25.5	--	2.48
P. aeruginosa alkylsulfatase	19.5	18.8	18.1	19.5	20.1	13.1	16.1	16.8	--

The enzymes within the metallo-β-lactamase superfamily require several different metals. The glyoxalase II enzymes contain a binuclear metal center that can bind zinc, iron, or even mixed metals (Wenzel et al., 2004; Zang et al., 2001). Metallo-β-lactamases are zinc-dependent enzymes, containing a mono- or di-zinc center, and alkylsulfatases have a binuclear zinc center (Fig. 1.8 C) (Hagelueken et al., 2006). Persulfide dioxygenases have the ability to bind an iron (Pettinati et al., 2015) and FDPs contain a diiron center as referred on Section 1.4.3.1. The main ligands involved in metal coordination in these enzymes are the imidazole groups of histidine, and the acidic side chains of aspartate and glutamate residues.

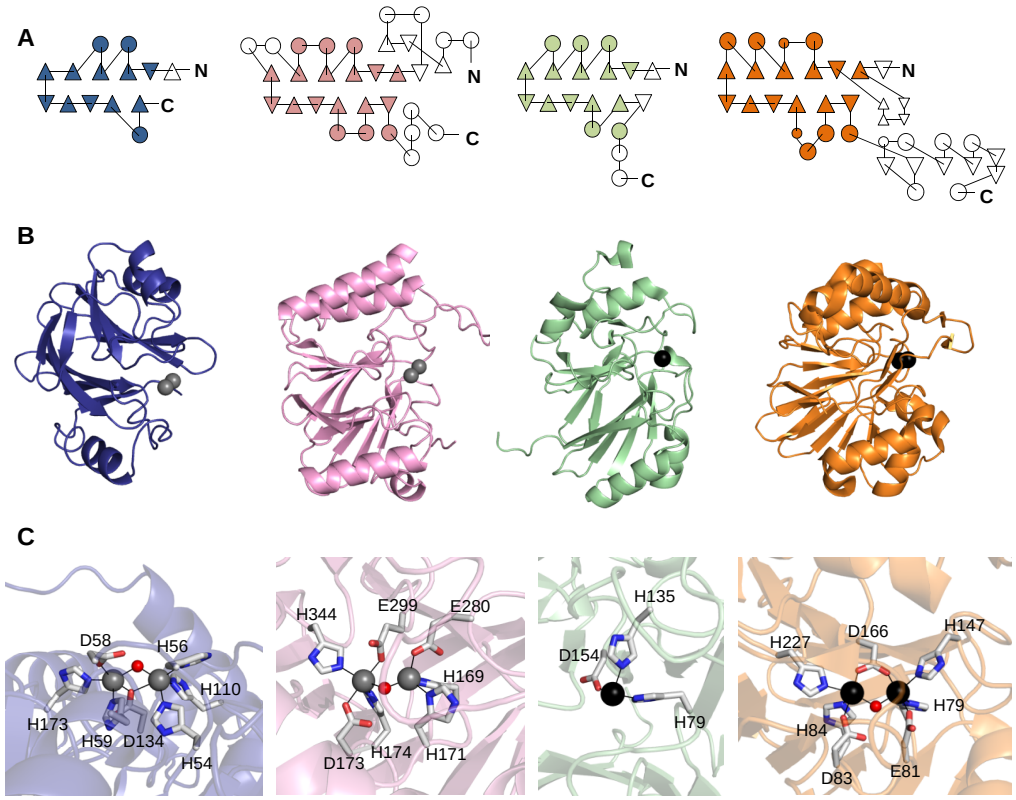

Figure 1.8- Structural comparison of the metallo-β-lactamase-like domains. **A)** Topology diagram of the monomers with the αββα lactamase-like fold for the *H. sapiens* glyoxalase II (PDB 1QH5, coloured in blue), *P. aeruginosa* alkylsulfatase (PDB 2CFU, pink), *H. sapiens* persulfide dioxygenase (PDB 4CHL, green) and *E .coli* FDP (PDB 4D02, orange). Circles and triangles represent α-helices and β-chains, respectively. **B)** Cartoon representation of the monomers color coded as in A). **C)** Stick representation of the metals active site for the same proteins as referred in A). The oxygen, zinc and iron ions are represented as red, grey and

black spheres, respectively. Ligands are shown as sticks with carbon atoms in grey, nitrogen in blue and oxygen in red.

1.4.3.1 Diiron center

The catalytic center of FDPs is a diiron site, where reduction of O_2 (to H_2O) and/or NO (to N_2O) occurs (Kurtz, 2007; Romao et al., 2016a). This center is located within a groove at the interface between the two inner β-sheets of the β-lactamase-like fold. It is surrounded by αβ loops and β-hairpins, being in the vicinity and limited by the C-terminal domain of the opposing monomer. In the metallo-β-lactamases superfamily, there is a large pocket for the bulky substrates binding, while in FDPs the metal site is covered by a unique two-stranded β-sheet which hinders the access of large substrates, namely β-lactams, to be hydrolyzed. Neverthless, it allows the acess of small molecules, such as oxygen and nitric oxide to the active active center (Fig. 1.9) (Romao et al., 2016a).

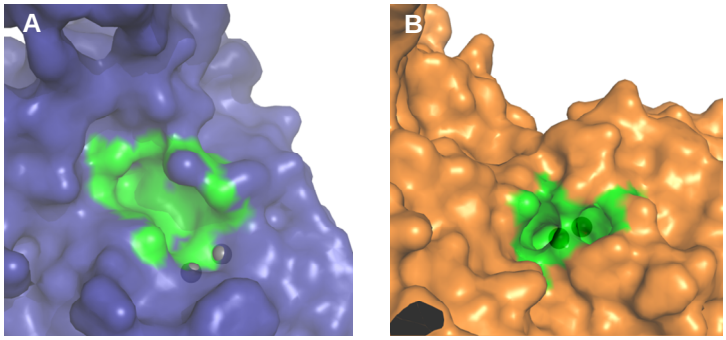

Figure 1.9- Molecular-surface comparasion of the cavity adjacent to the catalytic metal center in glyoxalase and FDPs. **A)** Molecular surface for glyoxalase II (PDB 1QH5) from *Homo sapiens*. **B)** Molecular surface for FDP (PDB 4D02) from *E. coli*. The molecular-surface representations in panels A and B are in the same orientation. The cavity is coloured in green and its calculation was performed using the *CASTp* server (Dundas et al., 2006).

The ligands that coordinate FDPs diiron center, are almost strictly conserved (canonical FDPs) with the exception of some FDPs from oxygenic photosynthetic organisms that contains a high variety of possible metal ligands (non-canonical FDPs), namely positively charged or neutral residues. This led to the classification of 17 different subtypes of Class C FDPs as explained in the Discussion section.

The conserved ligands present in canonical FDPs are composed of four histidines, two aspartates and one glutamate residues, from a highly conserved motif: H79-x-E81-x-D83-H84-x_{62}-H147-x_{18}-D166-x_{60}-H227 (*E. coli* FDP numbering).

The proximal iron (Fe_p), which is the iron closest to the FMN, is coordinated by $H147^{NE2}$, $H79^{NE2}$ and $E81^{OE1}$, whereas the distal iron (Fe_d), which is the iron further to the FMN, is coordinated by $D83^{OD2}$, $H84^{NE2}$, $H227^{NE2}$ and $D166^{OD1,OD2}$ bridges the two irons (Fig. 1.10 and 1.11 A). Additionally, one μ-hydroxo bridge can coordinate both irons.

In *D. gigas* ROO (PDB 1E5D), the H84 side chain is displaced from the diiron center being replaced by a water molecule (Fig. 1.11 B). This residue establishes hydrogen bonds with $D225^{OD1,OD2}$, $D49^{OD1}$ and $Q78^{N}$ (*D. gigas* ROO numbering). While D49 is conserved among all FDPs with known structures, the residue D225 is substituted by a serine in *M. marburgensis, E. coli* and *M. thermoacetica* FDPs, or by an alanine in *G. intestinalis* FDP, and Q78 is substituted by an asparagine residue in all others FDPs (Fig. 1.10). Therefore, the unique H84 conformation observed in *D. gigas* ROO, could be related with the presence of D225 and Q78. In order to understand the role of this H84 (*D. gigas* ROO), the corresponding histidine residue from *T. maritima* FDP was mutated to an alanine (H90A) or an asparagine (H90N) (Fang et al., 2012). While in the crystal structure of *T. maritima* FDP H90N (PDB 4DIL), the mutated asparagine is coordinating Fe_d, in H90A (PDB 4DIK), a solvent molecule coordinates this iron. However, steady-state activities and pre-steady-state kinetics were not significantly affected by these mutations, remaining the oxygen reductase activity higher than the nitric oxide reductase one, as verified in wild-type *T. maritima* FDP. This suggests that H84 (*D. gigas* ROO numbering) is not related with substrate specificity (Fang et al., 2012) (Section 1.5).

β-lactamase-like domain
A Tm_FDP MGSDKIHHHHHHMPKIWTERIFDDPEIYVLRIDDDRIRYFEAVWEIPEGISYNAYLVKLNGANVLID GWKGNYAKEFIDALS 82
Eh_FDP MKALEVVKDLYWVGVFDKELR.VFDIIMTTPYGTSYNSFLLKSEKGNVLFE TCKENFAGECLERIE 65
Mm_FDP MKAAAKRISDGVYWTGVLDWDLRNYHG...YTLQGTTYNAYLVCGDEGVALIDNSYPGTFDELMAR..VEDAL 68
Mt_FDP MSQPVA.ITDGIYWVGAVDWNIRYFHGPAFSTHRGTTYNAYLIV.DDKTALVD TVYEPFKEELIAKLK 66
Dg_FDP MQATKIIDGFHLVGAIDWNSRDFHG.YTLSPMGTTYNAYLVE.DEKTTLFD TVKAEYKGELLCGIA 64
Gi_FDP MSSKPKYVQDQEMIPGVYWVGIVDWMVRIFHG..YHTDEGSSYNSYFID.DECPTVID SVKYPFAEEWLSRIA 70
B Ec_FlRd MSIVVK...NNIHWVGQRDWEVRDFHGTEYKTLRGSSYNSYLIR.EEKNVLID TVDHKFSREFVQNLR 64
C Flv1 MGIHAKLETVQLPLLVSCLFPPLTMPAKDVQICPIAVDTTVFRSRTWDRL.KFEIEYGLQRGTTANSYLIS.ADKIALFD PPGESFTDNFVGTLI 93
Flv2 ..MISPIGGLSQALHSPSDSIFVASLPRDIQVAEIAPQTKVLRSRLWDRL.KFEVEYGRRRGTTSNSYLIQ.ADHTALID PPGESFCDLYLAELP 91
Flv3 MFTTPLPP.....QKRLSTQTEAIAKNITAIRSLDWDRD.RFDIEFGLQNGTTYNSYLIQ.ADKVALVD SSHEKFRQLYLDLLQ 77
Flv4 MVTLIDSPTSAAVQPRLTLQTADIAAHTTAIRCLDWDRD.RFDIEFELRHGTTYNSFLIR.GEKTALID TSHRKFEAVYLQLLQ 82
D Ck_FDP MNALEIKKDIYWVGALDPDLR.IFDIIMNTPYGTTYNSYVIKGSEKTAVFE TAKERFFDEFLERLN 65
E Sw_FDP1 MQSVKIKENIYWVGVQDPDLR.VFDIIMRTEKGSSYNAYLIKGSEKTALVE TVKDEFFEEYIEKLQ 65
F Pd_FDP MSLKSLKIKENLYWVGSLDPDLR.VFDIIMYTPYGTTYNSYVLKGTEKTVLFE TVKDKHFDNYIERLN 67
G E_FDP MNDKITDSIVYVGVNDYDID.LFEGHYVVPEGMAYNSYVIL.DQKVAVMD TVDQRKTSEWLQNVY 63
H Sw_FDP2 MAENYSKGGMLVKALEIKENVFYVGVQDYDLR.VFDIVMRTEYGTSYNAYLVKGREKTVLVE TVKDKFFDEYIKDLQ 76
β-lactamase-like domain
A Tm_FDP KI.VDPKEITHIIVNHTEPDHSGSLPATLKTIGHDVEIIASNFGKRLLEGFYGIK...DVTVVKDG..EEREIG.GKKFKFVMTPWLHWPDTMVTYLDG. 174
Eh_FDP DVIGKEGKLDYIVLNHTEPDHSGSLVHILEKY.PEATVIGTMAALNNIKYIGHIK..ENTKTLNSGKIKTLDLG.NYHLKFLIQPFLHWPDTMMTVIEEM 161
Mm_FDP QQ.VGMERVDYIIQNHVEKDHSGVLVELHRRF.PEAPIYCTEVAVKGLLKHYPSLREAEFMTVKTG..DVLDLG.GKTLTFLETPLLHWPDSMFTLLDED 163
Mt_FDP QI.KDPVKLDYLVVNHTESDHAGAFPAIMELC.PDAHVLCTQRAFDSLKAHYSHI.DFNYTIVKTG..TSVSLG.KRSLTFIEAPMLHWPDSMFTYVPEE 160
Dg_FDP SV.IDPKKIDYLVIQHLELDHAGALPALIEAC.QPEKIFTSSLGQKAMESHFHYK.DWPVQVVKHG..ETLSLG.KRTVTFYETRMLHWPDSMVSWFADE 158
Gi_FDP AC.CPLDKIKYVVMNHAEGDHASSLKDHYHKF.TNATFVCTKKCQEHLKILYGME.KATWLIVDDK..YTLKIG.KRTLKFIPVPLLHWPDSTFTYCPED 164
B Ec_FlRd NE.IDLADIDYIVINHAEEDHAGALTELMAQI.PDTPIYCTANAIDSINGHHHHP.EWNFNVVVKTG..DTLDIGNGKQLIFVETPMLHWPDSMMTYLTGD 159
C Flv1 QR.LDLNSLDYVILGHVNANRAHTLKLLLSLA.PQATIICSNPAAQNLEKLLADAEVNNPIQVMKGN.DHLDLGRGHELTFIPTPSPRYPGQLCTYDPRT 190
Flv2 KY.LDLAQLDYIVASHVNPNRMVTLEQLLRRA.TKAKLICSRPAAKVLKATFPHWEER..FQTVRSQ.DMLDLGRGHKLQLMTLPTPRWPDGLCAYDAGS 186
Flv3 GL.IDPQRIDYLIVSHTEPDHSGLVKDILQLN.PRITVVATKVALQFLDNFVHQPFER...IQVKSG.DRLDLGQGHDLEFVSAPNLHWPDTMLTYDPAT 171
Flv4 DL.VDLRSLDYLIVNHTEPDHSGLIPDLLELA.PQVTVVGSKVAIQFLEKLVHRPFES...QIVKSG.HSLDLGQGHELQFISAPNLHWPDTILTYDSGT 176
D Ck_FDP SANVDIKNIDYIVVDHTEPDHSGSIAKLLDLS.PNAKLVGSAAAIRFMKAISNKK..FDSIVVKDG..DTLDLG.NKTLQFISAPFLHWPDSIYTYVPED 159
E Sw_FDP1 EI.IKLEDIDYLIMNHTEPDHSGSIARLLEKA.PGITVVGSSNTIEFLREIINKD..FDARIVGQG..SNLNLG.DKSLHFIGATLLHWPDSIYSYLPED 158
F Pd_FDP DLNIDFEKIDYIVVSHTEPDHAGSVEKLLDLA.KNAKVVASETAIKYLKEIVNKD..FEYVAVTDG..DTLSIG.DKTLEFFSVPMLHWPDTIYTYIKED 161
G E_FDP CV.LQGRRPDYLVVQHMEPDHSASIQAFLNTY.PETTVVGNSKIFQMIHQFFPELTLKNKLEVGDG..DTLRLG.THELTFVFAPMVHWPEVMVTYDAAD 158
H Sw_FDP2 EI.VKLSEIDYLIMNHTEPDHSGSVEKLLELI.PGLTILGSQTAIRFLKEISNKN..FSSRELNHG..DELDLG.GKTLRFISAPFLHWPDSMYSYLPED 169
* * * * *

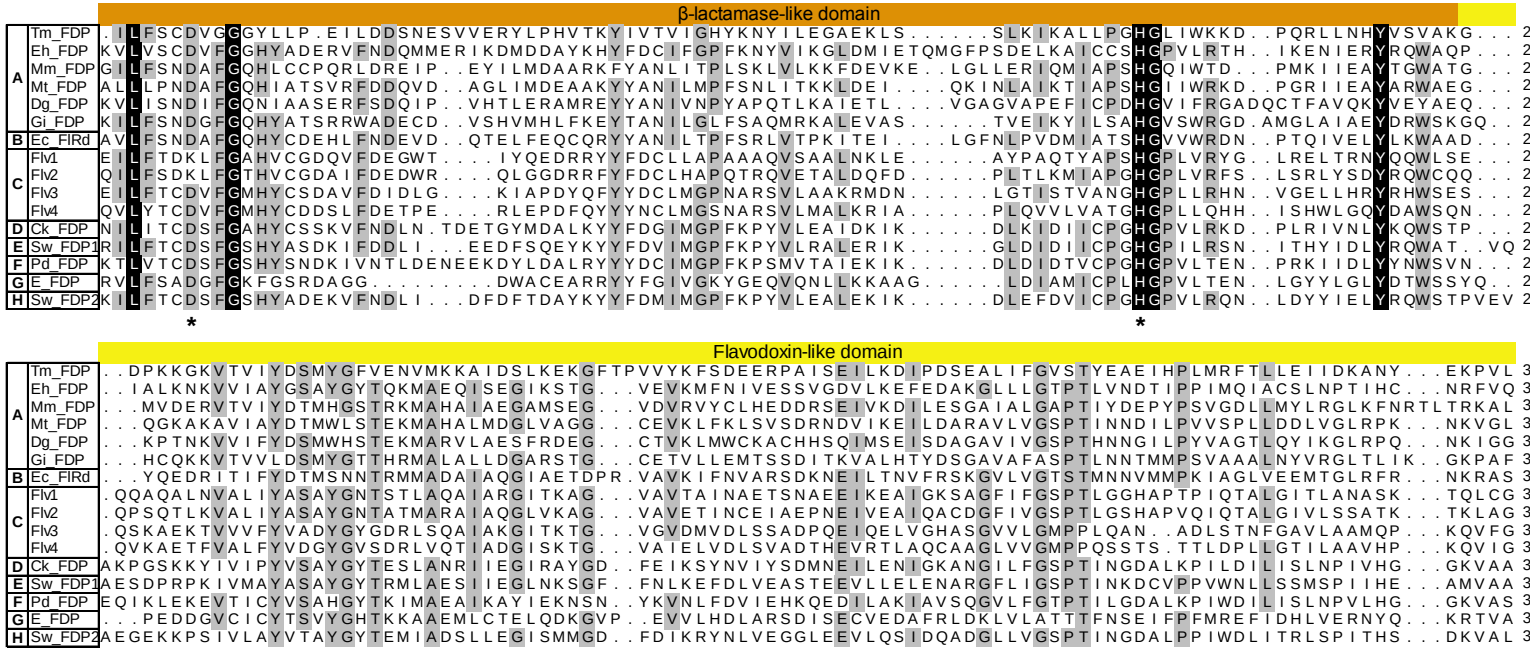
β-lactamase-like domain
Flavodoxin-like domain
A Tm_FDP
Eh_FDP
Mm_FDP
Mt_FDP
Dg_FDP
Gi_FDP
B Ec_FlRd
C Flv1
Flv2
Flv3
Flv4
D Ck_FDP
E Sw_FDP1
F Pd_FDP
G E_FDP
H Sw_FDP2

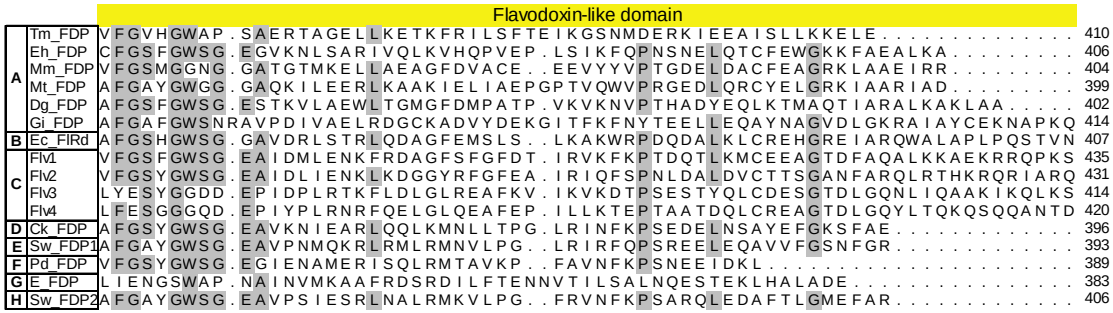

Figure 1.10- Amino acid sequence alignment of FDPs from classes A-H. The sequence alignment was obtained with ClustalX (Larkin et al., 2007) using *Thermotoga maritima* FDP (Tm_FDP), *Entamoeba histolytica* FDP (Eh_FDP), *Methanothermobacter marburgensis* FDP (Mm_FDP), *Moorella thermoacetica* FDP (Mt_FDP), *Desulfovibrio gigas* ROO (Dg_FDP), *Giardia intestinalis* FDP (Gi_FDP), *Escherichia coli* FDP (Ec_FDP), *Synechocystis* FDPs (Flv1, Flv2, Flv3 and Flv4), *Clostridium kluyveri* FDP (Ck_FDP), *Syntrophomonas wolfei* FDP (Sw_FDP1), *Peptoclostridium difficile* FDP (Pd_FDP), *Eubacterium* FDP (E_FDP), *Syntrophomonas wolfei* FDP (Sw_FDP2). The C-terminal extensions from classes B-H were not included. Black boxes correspond to strictly conserved residues and the grey boxes represent the mostly conserved residues. The metal ligands that coordinate the catalytic iron atoms are highlighted with *.

In almost all the FDPs structures was identified the presence of a solvent bridge coordinating both irons, with the exception of *M. marburgensis* FDP in the reduced and oxidized states (PDB 2OHI and 2OHH, respectively); in this last one, only in chain E was observed this bridge. Also, in reduced *E. coli* FDP (PDB 5LLD), this solvent bridge is absent. Moreover, in *M. thermoacetica* FDP, it was detected a solvent bridge based on Mössbauer spectroscopy, which was corroborated by theoretical calculations (Silaghi-Dumitrescu et al., 2003; Weitz et al., 2017). Nevertheless, it has not been possible to establish the exact chemical nature of this bridge, as being hydroxyl, aquo or oxo, since the resolution of the 3D structures (1.80-3.00 Å) is not high enough to determine its protonation state. However, it was possible to assign this solvent bridge as a μ-hydroxo specie, due to the oxygen sp2 configuration, hydrogen bonded with the free carboxylic oxygen of the ligand D83, as recently proposed for the crystallographic structure of the nitric oxide reductase from *E. coli* FDP (Romao et al., 2016b).

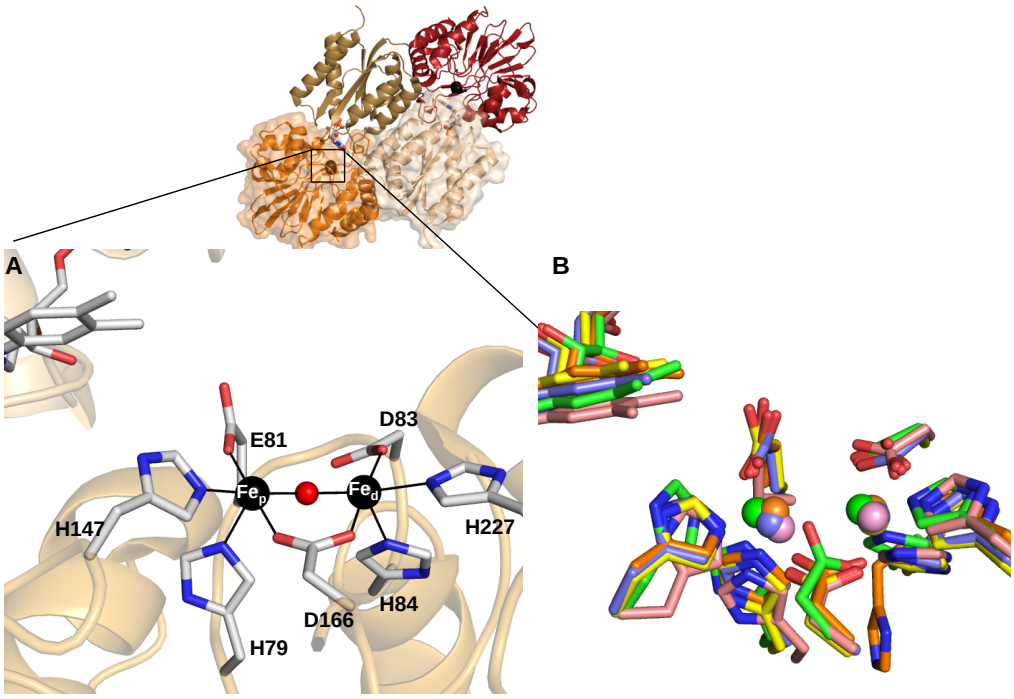

Figure 1.11- Structure of the diiron active site in flavodiiron proteins. **A)** Zoomed view of *E. coli* FDP (PDB 4D02) diiron center, with iron atoms represented as black spheres labelled as Fe_p and Fe_d. Bonds of iron ligands are represented as full lines. Metal ligands and FMN are shown as sticks with carbon atoms in grey, nitrogen in blue, oxygen in red and phosphorous in orange. The μ-solvent moiety which is bridging the two iron atoms is shown as a red sphere. **B)**

Representation of the active sites superposition from the available FDPs structures: *E. coli* in yellow (PDB 4D02), *D. gigas* in orange (PDB 1E5D), *M. thermoacetica* in pink (PDB 1YCF), *M. marburgensis* in green (PDB 2OHH) and *G. intestinalis* in blue (PDB 2Q9U). In *D. gigas* ROO, a water molecule (not shown), replaces the H84 coordination. Panel B) has the same orientation as A).

The overall diiron center geometry is conserved in different oxidation states among the FDPs structurally characterized. However, as referred on Section 1.4.1, the *M. marburgensis* FDP is an exception, since its diiron center varies significantly in different oxidation states.

Three different FDPs were crystallized in both redox states so far, namely *M. thermoacetica*, *M. marburgensis* and *E. coli* FDPs (Table 1.3). The *M .thermoacetica* and *M. marburgensis* FDPs, show distances between the irons of 3.4 Å to 3.3 Å and 3.6 Å to 3.7 Å in the oxidized and reduced states, respectively (Table 1.6).

In *E. coli* FDP, the distance between the two iron atoms in the oxidized form is 3.5 Å while in the reduced one is 3.2 Å. While in other non-haem diiron proteins with histidine and carboxylate ligands, such as ruberythrin and ribonucleotide reductase (Jin et al., 2002; Voegtli et al., 2003) there is an increase of Fe-Fe distance up to 0.7 Å upon reduction, in FDPs this trend is not verified.

Table 1.6- Iron-ligand and iron-iron interatomic distances (Å) for FDPs structures (*E. coli* FDP numbering). Individual distances are shown for two molecules or averaged distances with the corresponding distances interval within brackets. Interatomic distances (Å) may be compared with Cambridge Structural Database distances for Fe coordination to carboxylic oxygen [2.01(5), range 1.90-2.09 Å] and imidazole nitrogen atoms [2.08(9), range 1.95-2.22 Å] (Harding, 1999).

Organism		PDB code	Resolution (Å)	Fe_p –Fe_d	Fe_p–H79^{NE2}	Fe_p–E81^{OE1}	Fe_p–H147^{NE2}	Fe_p–D166^{OD2}	Fe_p–μOH	Fe_p–X[a]
D. gigas	Oxidized	1E5D	2.50	3.4, 3.4	2.1, 2.1	2.0, 2.0	2.1, 2.1	1.9, 1.9	2.3, 2.3	2.7, 3.1
T. maritima	Oxidized	1VME	1.80	3.4, 3.6	2.3, 2.3	2.2, 2.0	2.3, 2.4	2.2, 2.3	1.9, 1.9	3.2, 3.2
	Oxidized	4DIK	1.75	3.3, 3.3	2.4, 2.4	2.2, 2.1	2.3, 2.3	2.1, 2.2	1.8, 1.8	2.6, 2.6
	Oxidized	4DIL	2.00	3.3, 3.2	2.5, 2.6	2.3, 2.2	2.3, 2.4	2.2, 2.3	1.8, 1.8	2.3, 2.6
M. thermoacetica	Oxidized	1YCF	3.00	3.4 (3.3-3.5)	2.5 (2.4-2.7)	2.3 (1.9-2.7)	2.2 (2.1-2.3)	2.1 (2.0-2.2)	2.0 (2.0-2.0)	3.1 (2.9-3.3)
	Reduced	1YCG	2.80	3.3 (3.3-3.4)	2.0 (1.9-2.0)	2.1 (2.0-2.1)	1.9 (1.9-1.9)	2.0 (2.0-2.1)	1.9 (1.9-1.9)	3.2 (3.0-3.3)
	NO-reacted	1YCH	2.80	3.4 (3.2-3.6)	2.3 (2.2-2.4)	2.1 (1.8-2.3)	2.4 (2.3-2.5)	2.2 (2.1-2.3)	2.0 (2.0-2.0)	3.4 (3.2-3.5)
M. marburgensis	Oxidized	2OHH	1.70	3.6 (3.5-3.7)	2.2 (2.1-2.3)	2.1 (1.9-2.2)	2.3 (1.9-2.7)	2.2 (2.1-2.3)	1.8	3.3 (2.7-3.8)
	Reduced	2OHI	2.30	3.7 (3.4-4.0)	2.7 (2.2-3.2)	2.8 (2.0-4.6)	2.8 (2.0-3.5)	2.3 (2.1-2.5)	-	3.6, 3.2
G. intestinalis	Oxidized	2Q9U	1.90	3.5, 3.6	2.3, 2.3	2.1, 2.1	2.2, 2.1	2.1, 2.1	2.1, 1.9	2.3, 2.2
E. coli	Oxidized	4D02	1.75	3.5	2.2	2.1	2.1	2.1	2.0	2.3
	Reduced	5LLD	2.65	3.2	2.5	2.5	2.0	2.2	-	3.4
	Oxidized [Fe-Cys_4]	5LMC	1.90	3.5	2.2	2.2	2.2	2.1	1.9	2.7

Organism		PDB code	Resolution (Å)	Fe_d– D83^{OD2}	Fe_d– H84^{NE2}	Fe_d–D166^{OD1}	Fe_d–H227^{NE2}	Fe_d–μOH	Fe_d–X[a]
D. gigas	Oxidized	1E5D	2.50	2.3, 2.3	2.4, 2.6[b]	2.1, 2.1	2.0, 2.0	1.8, 1.8	2.6, 2.6
T. maritima	Oxidized	1VME	1.80	2.1, 2.1	2.1, 2.1	2.1, 2.1	2.2, 2.1	2.0, 1.9	2.2, 2.2
	Oxidized	4DIK	1.75	2.2, 2.2	2.3, 2.4[b]	2.2, 2.2	2.4, 2.4	1.8, 1.8	2.3, 2.3
	Oxidized	4DIL	2.00	2.3, 2.3	2.4, 2.4[c]	2.3, 2.2	2.4, 2.4	1.8, 1.8	2.1, 2.5
M. thermoacetica	Oxidized	1YCF	3.00	2.2 (2.1- 2.2)	2.2 (2.1-2.3)	2.1 (2.0-2.2)	2.1 (2.0-2.1)	2.0 (2.0-2.0)	2.8 (2.4-3.2)
	Reduced	1YCG	2.80	2.1 (2.1-2.1)	1.9 (1.9-1.9)	2.1 (2.1-2.1)	1.9 (1.9-1.9)	1.9 (1.9-1.9)	3.9 (3.7-4.1)
	NO-reacted	1YCH	2.80	2.1 (2.0-2.3)	2.2 (2.1-2.4)	2.3 (2.2-2.4)	2.1 (2.0-2.2)	2.0 (2.0-2.0)	3.2 (3.1-3.2)
M. marburgensis	Oxidized	2OHH	1.70	2.6 (2.3-2.9)	1.9 (1.8-2.0)	2.0 (1.8-2.1)	2.1 (2.0-2.1)	2.2	2.8 (1.9-3.3)
	Reduced	2OHI	2.30	2.8 (2.4-3.2)	2.1 (2.0-2.2)	2.2 (2.1-2.4)	2.3 (2.1-2.6)	-	2.5, 2.8
G. intestinalis	Oxidized	2Q9U	1.90	2.1, 2.1	2.2, 2.1	2.0, 2.1	2.1, 2.2	1.9, 2.0	2.1, 2.0
E. coli	Oxidized	4D02	1.75	2.3	2.1	2.1	2.2	2.1	1.9
	Reduced	5LLD	2.65	2.3	2.0	2.2	2.3	-	2.6
	Oxidized [Fe-Cys_4]	5LMC	1.90	2.3	2.1	2.1	2.2	2.0	2.1

[a] Distance to the closest atom of the exogenous ligand (X), e.g. phosphate anion (see text). [b] Coordinating water distance for substituting H84 (*E. coli* FDP numbering). [c] Coordinating distance for substituting H84 ligand (*E. coli* FDP numbering).

Each iron is coordinated by five ligands, thus there is a sixth available position (above the Fe-O(H)-Fe plane) for binding the substrate. FDPs structures show different molecules within this position, namely, oxygen, water, sulfate, nitrate and phosphate. These molecules are equidistant to both iron atoms or located closer to the Fe_d, and are located in an active site pocket that is delimited by the metal ligands. In some FDPs, this pocket is crossed by a long tunnel that reaches the protein external surface (see Section 1.6).

1.4.4 Flavodoxin-like domain

The FDPs core presents at the C-terminal a flavodoxin-like domain (~ 150 residues), with a αβα fold similar to short-chain flavodoxins, where the inner β-sheet is surrounded by two sets of α-helices (Fig. 1.12 A and B) (Romao et al., 2016a).
Both the flavodoxin-like domain in FDPs and the flavodoxin-like proteins, have a non-covalently bound FMN cofactor that assures the electron transfer. The overall fold between these flavodoxin domains presents Cα *r.m.s.d*.'s values within 1.9-2.3 Å for 3.5 Å Cα distances cutoff (sequences identities of 16-26 %) (Table 1.7). One of the major differences between them, is related with the reduction potential of the FMN cofactor, that is higher for FDPs relatively to flavodoxin-like proteins. The reduction potential of the flavin cofactors of several FDPs range from 0 to -117 mV for the FMN_{ox}/FMN_{sq} and -130 to -220 mV for FMN_{sq}/FMN_{red} (Table 1.2), while in canonical flavodoxins the redox potential of this cofactor range from +121 to -244 mV for the FMN_{ox}/FMN_{sq} and -370 to -522 mV for FMN_{sq}/FMN_{red} (Hoover et al., 1999; Paulsen et al., 1990). This difference could be related with a higher predominance of basic residues *vs* acidic residues surrounding the FMN isoalloxazine ring in FDPs (Frazao et al., 2000).

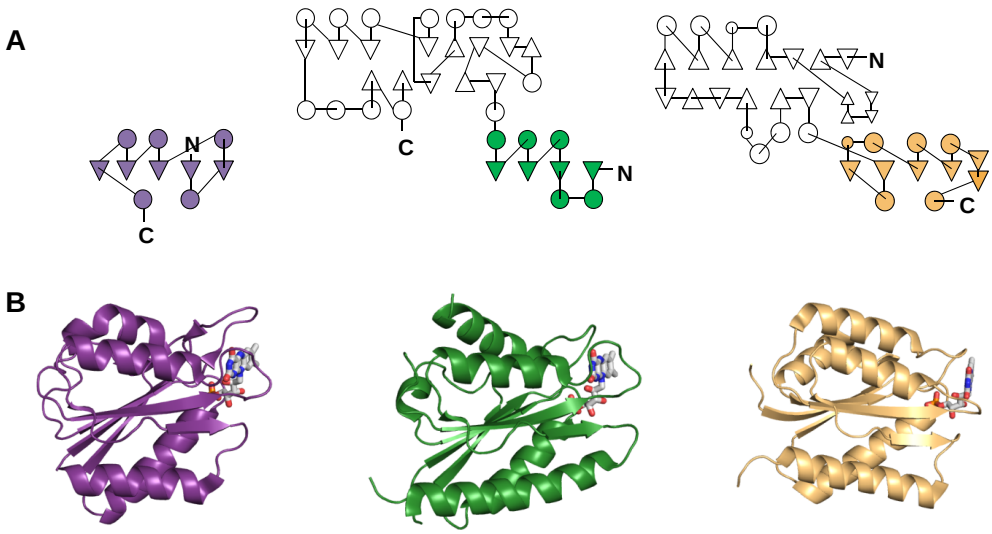

Figure 1.12- Structural comparison of the flavodoxin-like domains. **A)** Topology diagram of the monomers with the αβα flavodoxin-like fold for the *D. gigas* flavodoxin (PDB 4HEQ, in purple), *R. norvegicus* nitric oxide synthase (PDB 1TLL, in green) and for *E .coli* FDP (PDB 4D02, in light brown). Circles and triangles represent α-helices and β-chains, respectively. **B)** Cartoon representation of the monomers color coded as in A). FMN is shown as sticks with carbon atoms in grey, nitrogen in blue, oxygen in red and phosphorous in orange.

Table 1.7- Comparison of FDPs C-terminal domain with flavodoxins. The Cα *r.m.s.d.*'s (Å) are presented above the diagonal (grey region). FDP codes: *E. coli* FDP (PDB 4D02), *T. maritima* FDP (PDB 1VME), *M. thermoacetica* FDP (PDB 1YCF), *M. marburgensis* FDP (PDB 2OHH), *D. gigas* ROO (PDB 1E5D), *G. intestinalis* FDP (PDB 2Q9U). Flavodoxins codes: *R. norvegicus* nitric oxide synthase (PDB 1TLL) and *D. gigas* flavodoxin (PDB 4HEQ). Sequence identities percentages (%) are shown in the rows below the diagonal.

	E. coli	*T. maritima*	*M. thermoacetica*	*M. marburgensis*	*D. gigas*	*G. intestinalis*	*R. norvegicus* nitric oxide synthase	*D. gigas* flavodoxin
E. coli	--	2.22	1..31	0.99	1.32	1.43	2.14	1.95
T. maritima	13.4	--	2.19	2.22	2.00	2.26	2.23	2.25
M. thermoacetica	38.6	19.7	--	1.14	1.11	1.06	2.02	2.06
M. marburgensis	34.6	27.6	39.4	--	1.22	1.28	2.12	2.03
D. gigas	32.3	22.0	44.1	29.9	--	1.25	1.96	1.86
G. intestinalis	26.8	21.3	33.1	32.3	30.7	--	2.28	2.15
R. norvegicus nitric oxide synthase	22.1	24.4	23.8	24.0	25.7	24.4	--	2.40
D. gigas flavodoxin	23.6	18.1	22.8	21.3	17.3	15.7	24.6	--

1.4.4.1 FMN cofactor

The FMN cofactor is localized in the edge of the flavodoxin-like domain, at the monomer interface, covered by the “head-to-tail” dimer, and thus is not solvent exposed (Fig. 1.13 A). The FMN conformation allows an efficient electron transfer with the diiron center, through the methyl group C8M of the isoalloxazine ring that is at a van der Waals distance from the metal ligand $E81^{OE2}$ (*E. coli* FDP numbering) of the monomer mate (Fig. 1.14).

The side chains of W148 and W348 residues are nearby the FMN isoalloxazine ring while W375 is vicinal to the FMN phosphate group (Fig. 1.14). The W148 residue is conserved among FDPs, with exception of *Synechocystis* Flv1 that instead contains a tyrosine residue (Fig. 1.10). Although W348 and W375 residues are not conserved among all the FDPs, they are conserved in all flavorubredoxins sequences (Romao et al., 2016b). As referred in Section 1.3.3, the W348 residue has been proposed to modulate the visible spectral features of FDPs through interaction with the flavin isoalloxazine ring (Saraiva et al., 2004; Vicente et al., 2007a). The *M. marburgensis* FDP lacks W348 and W375 (*E. coli* FDP numbering) that are replaced by a glycine and a tyrosine residue, respectively (Fig. 1.10). The presence of a glycine instead of a tryptophan residue could facilitate the access of coenzyme F_{420} to the FMN site, binding at an equivalent position to W348, allowing the cofactor to receive electrons directly from this redox partner (Seedorf et al., 2007). This tryptophan residue is exclusively replaced by a glycine in FDPs from methanogens (Vicente et al., 2008a).

The binding site of FMN includes interactions between residues and its isoalloxazine ring, ribitol and phosphate groups (Fig. 1.13 A). Several FMN interactions with different amino acid residues are summarized in Table 1.8. Three regions contribute to the formation of the FMN binding pocket, namely T260-T265 that interact with the phosphate group- *Region I*, T314 and S345 residues that interact with the ribitol group- *Region II* and N316-N317 and G347-G350 residues that stabilize the isoalloxazine ring- *Region III*.

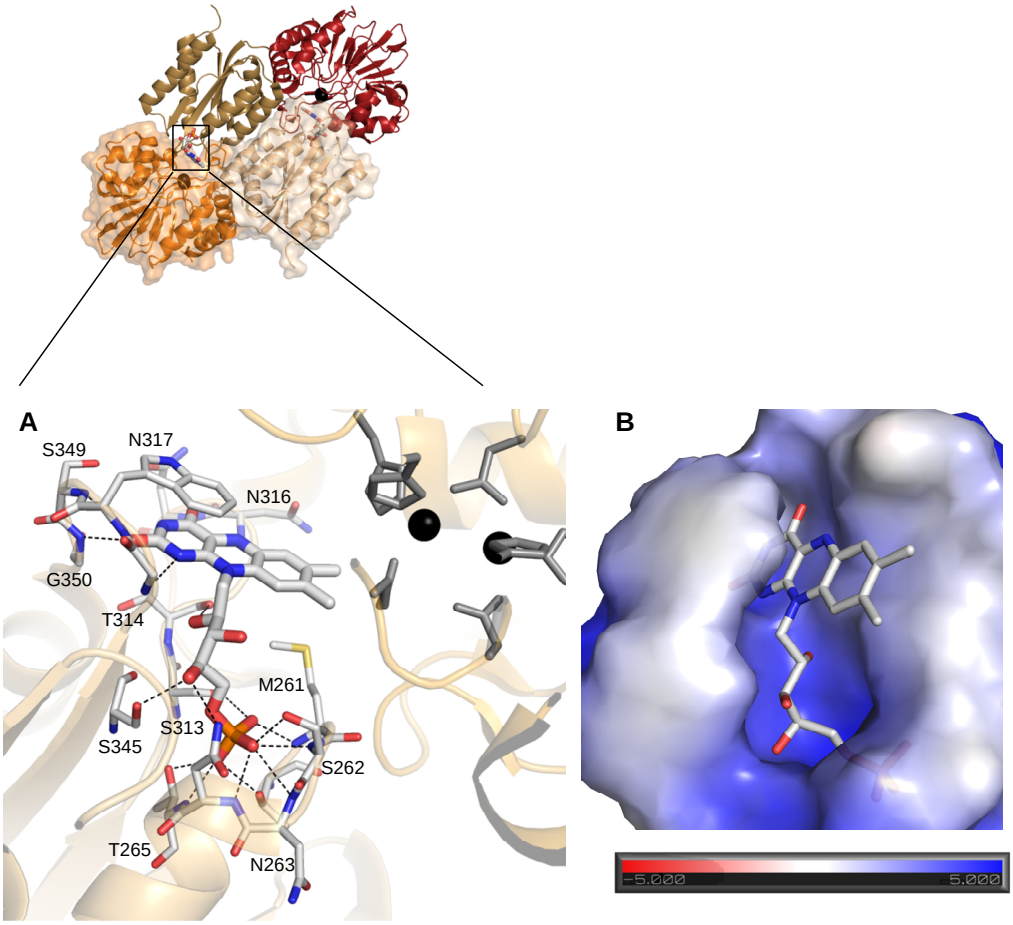

Figure 1.13- Representation of FMN moiety in flavodiiron proteins. **A)** Zoomed view of the FMN site from *E. coli* FDP (PDB code 4D02). The interactions between residues and the FMN are labeled with dash lines (black). Residues and FMN are shown as sticks with carbon atoms in grey, nitrogen in blue, oxygen in red and phosphorous in orange. Metal ligands are shown as grey sticks. Iron atoms are represented as black spheres. **B)** Electrostatic surface shows the charge distribution of the FMN-binding site with the displayed potentials ranging from -5.0 (red) to 5.0 (blue) kTe^{-1}.

The interaction occurring with N316 in the Region III, induced a different effect on the nature of the flavin semiquinone, between FDPs and short-chain flavodoxins. In FDPs, the main chain amino group of the N316 residue (*E. coli* FDP numbering) is hydrogen bonded with the FMN isoalloxazine N5 atom, preventing the FMN protonation and stabilizing the red anionic radical (Vicente and Teixeira, 2005). In short-chain flavodoxins, the FMN N5 atom is accessible for protonation which stabilizes the neutral blue semiquinone. Both types of semiquinones have different absorption bands in the UV-visible spectrum. The red anionic radical (FDPs), absorbs at 380 nm

with a sharp peak at 400 nm and a broader peak at 490 nm, while the neutral blue semiquinone (short-chain flavodoxins), has maxima absorption bands at 400 nm, 500 nm and between 580 and 620 nm (Choong and Massey, 1980; Muller et al., 1972). The *T. maritima* FDP (PDB 1VME) and flavodoxin-like domain from *Anabaena* sp. PCC 7120 (PDB 3FNI) are the only FDPs structures that lack the FMN cofactor.

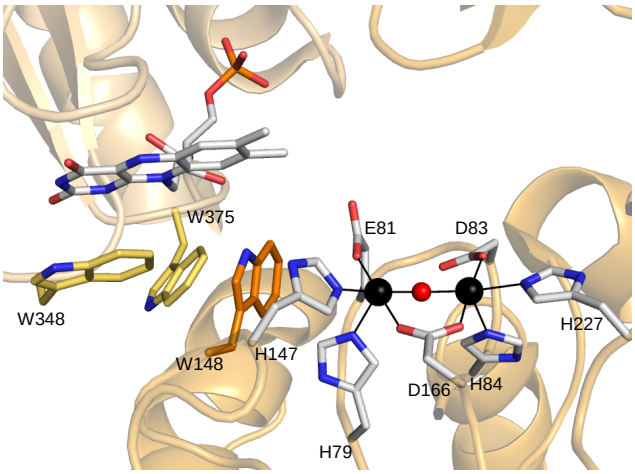

Figure 1.14- Diiron catalytic center of *E. coli* FDP within the "head-to-tail" dimer. The interface of this "head-to tail" dimer is represented as cartoon, in which the β-lactamase-like domain from one subunit is colored as orange and the flavodoxin-like domain of the opposing subunit as light brown. Iron atoms and μ-OH^- are represented as black and red spheres, respectively. Metal ligands and FMN are represented as sticks with carbon, nitrogen, oxygen, and phosphorus atoms in white, blue, red, and orange, respectively. The tryptophan residues, W148, W348 and W375, are highlighted with carbon atoms in orange and light brown colors, accordingly to the subunit color.

Table 1.8- Interactions between FMN and the surrounding residues.

	***E. coli* FDP**		***D. gigas* ROO**		***M. thermoacetica* FDP**		***M. marburgensis* FDP**		***G. intestinalis* FDP**	
FMN atom	Residue atom	Distance (Å)	Residue atom	Distance (Å)	Residue atom	Distance (Å)	Residue atom	Distance (Å)	Residue atom	Distance (Å)
O1P	$T260^{OG1}$	2.7	$S261^{OG}$	2.7 (2.7-2.7)	$T261^{OG1}$	2.7 (2.7-2.8)	$T265^{OG1}$	2.7 (2.7-2.8)	$S265^{OG}$	2.7 (2.7-2.8)
	$T265^{N}$	2.7	$T266^{N}$	2.5 (2.5-2.6)	$T266^{N}$	2.8 (2.8-2.9)	$T270^{N}$	2.7 (2.7-2.8)	$T270^{N}$	2.9 (2.9-2.9)
	$T265^{OG1}$	2.6	$T266^{OG1}$	2.6 (2.6-2.7)	$T266^{OG1}$	2.6 (2.5-2.7)	$T270^{OG1}$	2.6 (2.6-2.7)	$T270^{OG1}$	2.7 (2.7-2.7)
O3P	$S262^{OG}$	2.6	-	-	-	-	-	-	-	-
	$S262^{N}$	2.8	-	-	-	-	-	-	-	-
	$N263^{N}$	3.0	$H264^{N}$	3.0 (3.0-3.1)	-	-	-	-	$G268^{N}$	3.1 (3.1-3.2)
	$N264^{N}$	2.9	$S265^{N}$	2.5 (2.5-2.6)	$S265^{N}$	3.0 (3.0-3.1)	$S269^{N}$	2.8 (2.7-2.9)	$T269^{N}$	2.9 (2.9-2.9)
O2P	$M261^{N}$	2.6	$M262^{N}$	2.8 (2.8-2.8)	$M262^{N}$	2.6 (2.6-2.7)	$M266^{N}$	2.7 (2.7-2.7)	$M266^{N}$	2.6 (2.6-2.7)
	-	-	$W263^{N}$	2.7 (2.6-2.8)	$W263^{N}$	2.8 (2.7-2.9)	$H267^{N}$	2.7 (2.7-2.8)	$Y267^{N}$	2.7 (2.6-2.8)
	$S313^{OG}$	2.8	-	-	-	-	-	-	-	-
O4'	$N264^{ND2}$	2.8	-	-	-	-	-	-	-	-
	$S345^{OG}$	2.7	$S344^{OG}$	2.8 (2.6-3.0)	-	-	$S351^{OG}$	2.6 (2.6-2.7)	-	-
O2'	$T314^{O}$	3.0	$T313^{O}$	3.0 (3.0-3.0)	$T313^{O}$	2.7 (2.6-2.8)	$T317^{O}$	2.6 (2.5-2.7)	$T317^{O}$	2.8 (2.8-2.9)
N5	$N316^{N}$	3.0	$N315^{N}$	3.0 (3.0-3.0)	$N315^{N}$	3.1 (3.0-3.2)	$Y319^{N}$	2.8 (2.8-2.9)	-	
O4	$N317^{N}$	2.8	$N316^{N}$	2.8 (2.8-2.8)	$N316^{N}$	2.9 (2.8-3.0)	$D320^{N}$	2.8 (2.8-2.9)	$N320^{N}$	2.8 (2.8-2.9)
N1	$G347^{N}$	3.1	$G346^{N}$	3.0 (3.0-3.0)	-	-	$G353^{N}$	3.0 (3.0-3.0)	$G351^{N}$	3.1 (3.1-3.2)
O2	-	-	$G346^{N}$	3.0 (3.0-3.0)	-	-	$G353^{N}$	3.1 (3.0-3.2)	$G351^{N}$	3.1 (3.1-3.2)
	$W348^{N}$	2.7	$W347^{N}$	2.6 (2.5-2.7)	$W347^{N}$	3.0 (2.9-3.1)	$G354^{N}$	2.7 (2.6-2.8)	$W352^{N}$	2.9 (2.9-2.9)
	$S349^{N}$	3.2	$S348^{N}$	2.7 (2.7-2.8)	$G348^{N}$	3.0 (3.0-3.0)	-	-	$S353^{N}$	2.8 (2.8-2.8)
	$G350^{N}$	2.8	-	-	$G349^{N}$	2.9 (2.9-3.0)	$G356^{N}$	2.8 (2.8-2.8)	-	-

1.5 Substrate selectivity

Despite the several physiological and structural studies on FDPs, it remains to be elucidated the structural determinants that affects the substrate selectivity, in this family of proteins.

No structural differences are observed in the first coordination sphere of their diiron centers, since the metal ligands (H79-x-E81-x-D83-H84-x_{62}-H147-x_{18}-D166-x_{60}-H227, *E. coli* FDP numbering) present in FDPs, with different substrate selectivities are almost strictly conserved. As mentioned in Section 1.4.3.1, H84 is not related with substrate selectivity, since site-directed mutations made in this position in *T. maritima* FDP, did not change its higher affinity for oxygen (Fang et al., 2012).

In order to unravel the key features that modulates the activity in FDPs, a comparison between a structural model and crystal structures of FDPs with different substrate affinities was performed. For this analysis, it was used the model of the O_2-selective FDP from *Entamoeba histolytica* (EhFDP), the crystal structures of the *G. intestinalis* and *T. maritima* O_2-selective FDPs, the *D. gigas* and *M. thermoacetica* bifunctional FDPs and the NO-reducing *E. coli* FDP (Fig. 1.15) (Gonçalves et al., 2014). In the diiron second coordination sphere, were observed differences at two positions, namely a lysine and a tyrosine residues present in O_2-selective FDPs that are replaced by an aspartate and a serine residues in the NO-selective *E. coli* FDP, respectively (Fig. 1.10 and Table 1.9). The bifunctional *D. gigas* and *M. thermoacetica* FDPs have different combinations of residues in these two positions (Fig. 1.15A).

Table 1.9- Residues from the diiron second coordination sphere from FDPs with different substrate selectivities.

Organism	Aminoacids		Reductase activity
E. histolytica FDP	**K53**	**Y271**	O_2R
G. intestinalis FDP	K58	Y267	O_2R
T. maritima FDP	K58	Y264	O_2R
M. thermoacetica FDP	Y54	W263	O_2R>NOR
D. gigas ROO	K52	W263	O_2R>NOR
E. coli FDP	**D52**	**S262**	NOR

Therefore, to try to clarify the substrate selectivity in FDPs, were designed single and double mutations of the O_2-selective EhFDP, replacing the K53 and Y271 residues by the equivalent D52 and S262 residues from the NO-selective *E. coli* FDP. These EhFDP mutations, K53D, Y271S and K53D/Y271S, were then aimed to convert the O_2-selective EhFDP into a NO-selective FDP.

The reported kinetic and thermodynamic properties of single and double mutations of EhFDP, Y271S and K53D/Y271S, resulted in an increased selectivity towards NO, when compared with the wild-type protein. Remarkably, these two mutations appear to be more reactive towards O_2, although they are inactivated under multiple turnover conditions. Therefore, the Y271 residue appears to be crucial in the reaction with oxygen and contributes to stabilize the protein by preventing its inactivation in multiple turnovers (Gonçalves et al., 2014).

For the first time, were presented evidences for the determination of the specificity for substrates (O_2 *vs* NO) in *E. histolytica,* but the key molecular determinants that are responsible for these results need to be better explored.

The same approach was performed for the NO-reducing *E. coli* FDP, but in this case the single and double mutations, D52K, S262Y and D52K/S262Y, are an attempt to convert this NO-selective FDP into a protein with substrate preference for O_2. The structural studies of these protein targets are the scope of this thesis, and the crystal

structure determination and analyses of *E. coli* FDP single and double mutations (D52K, S262Y and D52K/S262Y) are discussed in Chapters II and III.

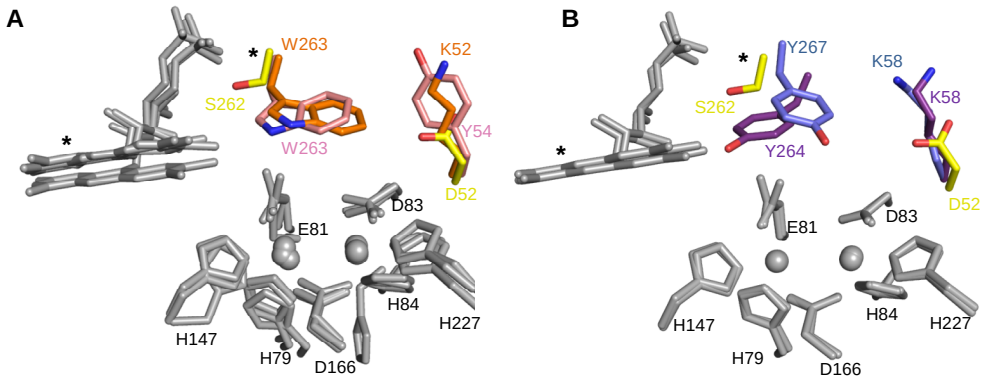

Figure 1.15- Structural superimposition of the second coordination sphere of the diiron site from FDPs with different substrate selectivities. **A)** O_2 /NO-selective FDPs, *D. gigas* FDP (PDB 1E5D, orange) and *M. thermoacetica* FDP (PDB 1YCF, pink), and NO-selective *E. coli* FDP (PDB 4D02, yellow). **B)** O_2-selective *G. intestinalis* FDP (PDB 2Q9U, blue) and *T. maritima* FDP (PDB 1VME, purple), and NO-selective *E. coli* FDP (PDB 4D02, yellow). The mutated residues and FMN marked with * are from the opposing monomer. The metal ligands, FMN and iron atoms are represented as light grey sticks and spheres, respectively.

1.6 Molecular tunnels

In order to understand the possible substrates routes present in these proteins, molecular dynamics simulations in *D. gigas* ROO (O_2/NO reductase), *E. coli* FDP (NO reductase) and *G. intestinalis* FDP (O_2 reductase) were made, using O_2 and NO molecules as substrates (Romao et al., 2016b; Victor et al., 2009).

These studies allowed the identification of two diffusion pathways between the catalytic site and the protein external surface, which differed particularly in their lengths and in their affinities to substrates, with the shorter pathway revealing lower affinity to O_2 or NO molecules than the longer pathway. Although these FDPs have different substrate selectivities, these studies showed a similar stability for both substrates in the diiron site pocket as well as similar diffusion profiles for both O_2 and NO molecules (Fig. 1.16). The solvent accessible surface (produced using a 1.4 Å rolling probe) of *E. coli* FDP structure, revealed a tunnel along these diffusion

pathways (Romao et al., 2016b). The residues delimiting these two pathways in FDPs are shown in Table 1.10 and 1.11.

Table 1.10- Amino acid residues that delimit the long pathway in FDPs.

Organism	Long pathway	Apolar atoms (%)
D. gigas ROO	T142, R143, L145, H146, S150, L161, I166, F167, Y193, I197, V198, T205, A208, I209, L212, V213, V217, A218, P219, I222, L332, T237, V240, Y243	77
E. coli FDP	T126, I139, V141, T143, L146, S151, M152, Y155, L162, A167, F168, Y194, Y195, I198, L199, L205, V206, K209, I210, I213, L214, L218, P219, V220, I223, S226, T236, V239, Y242	81
M. thermoacetica FDP	F57, L147, L163, F154, D167, A168, F169, Y195, I199, L200, I207, T208, K210, L211, D212, I214, Q215, L219, I221, I240, E241, Y243, A244, P370	83
T. maritima FDP	T147, L150, M156, L164, V169, Y197, I198, V201, I202, N207, Y208, I209, G212, A213, L216, S217, L219, K220, I221, L224, Q237, L240, Y243, V244	75
G. intestinalis FDP	V148, L151, F158, L167, D171, G172, F173, Y199, L204, M211, A214, L215, A218, S219, V221, E222, I223, I226, M239, I243, Y246, S250	78
M. marburgensis FDP	L150, F157, L166, D170, A171, F172, N169, F198, L202, I203, L206, L209, V210, K213, F214, V217, K218, L222, L223, I226, I229, P240, M241, I244, Y247	74

The tunnel crosses the active site pocket and includes the two paths in opposed directions. The longer tunnel section measures *ca.* 20 Å in length, and display cross-sections within 2.9-13.0 Å. The shorter tunnel section has *ca.* 10 Å in length and

cross-sections within 3.1-6.4 Å (Fig. 1.16 and 1.17). The atoms lining the longer tunel section are more apolar than those lining the shorter section (Table 1.10 and 1.11). Additionnaly, for the above referred FDPs structures, the molecular dynamics simulations revealed that the longer pathway was more populated with oxygen and nitric oxide molecules than the shorter path. Therefore, the longer section was suggested to be the substrates entrance, while the shorter section could be the reaction products exit route (Romao et al., 2016b; Victor et al., 2009).

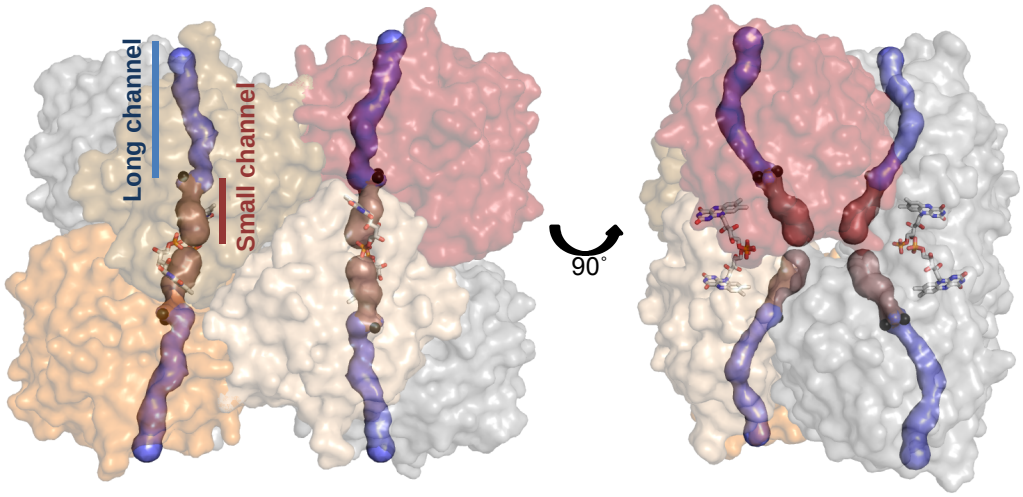

Figure 1.16- *E. coli* FDP molecular tunnels. Representation of FDP tetramer with transparent molecular surface. The β-lactamase-like domain of one monomer of the "head-to-tail" dimer in the front view, is colored as orange, while the flavodoxin-like domain is colored as light brown. The β-lactamase-like domain and flavodoxin-like domain of the other monomer is colored as dark red and the flavodoxin-like domain as brown. The other dimer is colored as grey, in the back view. Iron and oxygen atoms are represented as black and red spheres, respectively. FMN is shown as sticks with carbon in grey, nitrogen in blue, phosphorous in orange and oxygen in red. The long and short pathways are shown as blue and brown surfaces, respectively.

Interestingly, two *E. coli* FDP structures, the reduced (PDB 5LLD) and the one with the visible [Fe-Cys_4] center (PDB 5LMC), showed a constriction in the longer tunnel section, due to a slight displacement of their Y194 side chain tyrosine (Romao et al., 2016b).

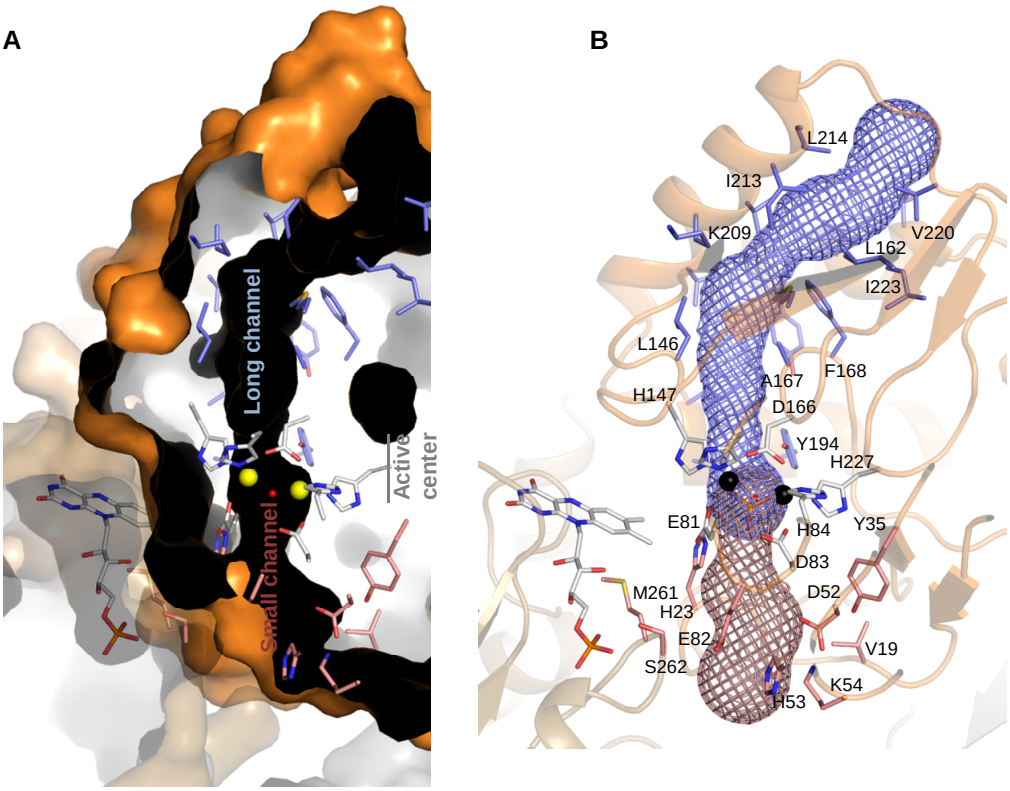

Figure 1.17- *E. coli* FDP molecular tunnels. **A)** Tunnels defined by a rolling sphere of 1.4 Å that connects the protein external surface with the diiron catalytic site. Two sections are highlighted, a long tunnel path, 20 Å, (blue) and a short tunnel path, 10 Å (dark red). The metal ligands and amino acids lining the long and short paths, are represented as sticks with carbon atoms colored in grey, blue and pink respectively. **B)** Tunnels representation as defined by MOLE highlighting the long path (blue mesh) and a short path (pink mesh). Iron and oxygen atoms are represented as black and red spheres, respectively. FMN is shown as sticks with carbon in grey, nitrogen in blue, phosphorous in orange and oxygen in red.

Although the long and short pathways are also found in others FDPs, none of these proteins has a tunnel crossing the active site pocket, like the one found in *E. coli* FDP.

Table 1.11- Amino acid residues that delimit the short pathway in FDPs.

Organism	Short pathway	Apolar atoms (%)
D. gigas ROO	D22, F23, H24, Y35, K52, D83, W263*, M262*, H264	58
E. coli FDP	V19, F22, H23, Y35, D52, H53, K54, E82, H113, H171, H227, S262*, M261*	62
M. thermoacetica FDP	I21, Y23, F24, H25, G26, Y37, Y54, D85, W263*, M262*	55
T. maritima FDP	D22, I25, R26, F28, E29, Y40, W57, K58, E87, D89, M263*, Y264*, D292	68
G. intestinalis FDP	V27, F30, H31, Y41, K58, E87, D89, H176, M266*, Y267*	59
M. marburgensis FDP	H26, L202, M266*, Y319*, Y323*, P324*, Y332, L336	65

Overall, these analyses suggest that these tunnel sections probably do not have a role in the substrate preference of FDPs. Therefore, the structural molecular determinants that affect the substrate specificity in FDP family remain to be understood.

1.7 *E. coli* flavodiiron protein

Over the last years, the *E. coli* FDP has been extensively studied (Baptista et al., 2012; Gardner et al., 2002; Gomes et al., 2002b; Gomes et al., 2000; Justino et al., 2005; Romao et al., 2016b; Vicente et al., 2008c; Vicente et al., 2007b; Vicente and Teixeira, 2005; Wasserfallen et al., 1998). Its first characterization (Table 1.1) allowed to identify its oligomerization state as a tetramer (54 kDa) with ~1 FMN and 2 Fe by monomer (Wasserfallen et al., 1998). As mentioned in Section 1.3.1, *E. coli* FDP contains a Rd domain at the C-terminal of the flavodiiron core, with a CxxC-x_{29}-CxxC motif with an [Fe-Cys_4] center, being therefore named as flavorubredoxin (Wasserfallen et al., 1998). Therefore, the number of irons per monomer was later corrected to three (Gomes et al., 2002b).

The gene coding for *E. coli* FDP (*norV*) and its redox partner, NADH:rubredoxin oxidoreductase (*norW*), form a single dicistronic transcriptional unit (da Costa et al., 2003). The *norV* promoter is activated by NO and reactive nitrogen intermediates in aerobic and anaerobic conditions (Gardner et al., 2002; Hutchings et al., 2002). The *E. coli* genome encodes other proteins besides FDPs that provide protection against reactive oxygen and nitrogen species (Table 1.12).

Table 1.12- Enzymes involved in protection of *E. coli* against oxidative and nitrosative stress.

System	Protection	Cofactor	Reference
Alkyl hydroperoxide reductase subunit C (*ahpC*)	ROS	(Cys-Cys)	(Chen et al., 1998; Smillie et al., 1992; Storz et al., 1989)
Superoxide dismutase (*sodA*)	ROS	Mn	(Takeda and Avila, 1986; Touati, 1983)
Superoxide dismutase (*sodB*)	ROS	Fe	(Carlioz et al., 1988; Fee, 1991)
Superoxide dismutase (*sodC*)	ROS	Cu, Zn	(Imlay and Imlay, 1996)
Glutathione peroxidase (*btuE*)	ROS	GSH	(Friedrich et al., 1986; Rioux and Kadner, 1989)
Catalase (*katE*)	ROS	Haem *d*	(Schellhorn, 1995; von Ossowski et al., 1991)
Catalase peroxidase (*katG*)	ROS	Haem *b*	(Loewen et al., 1985; Triggs-Raine et al., 1988)
Hybrid-cluster protein (*hcp*)	NO	FeS clusters	(Wang et al., 2016)
Cytochrome *c* (*nrf*)	RNS	Haem *c*	(Darwin et al., 1993; Hussain et al., 1994)
Cytochrome *bd*-I (*cydAB*)	ROS/RNS	Haem *b* and *d*	(Borisov et al., 2015; Cotter et al., 1997; Giuffre et al., 2014; Green et al., 1984)
Cytochrome *bd*-II (*appBC*)	ROS/RNS	Haem *b* and *d*	(Dassa et al., 1991)
Flavorubredoxin (*norVW*)	NO	FMN and Fe-Fe	(Justino et al., 2005; Mukhopadhyay et al., 2004)
Flavohaemoglobin (*hmp*)	RNS	FAD and haem *b*	(Membrillo-Hernandez et al., 1999; Vasudevan et al., 1991)

The role of *E. coli* FDP in NO detoxification was proposed based *in vivo* (Gardner et al., 2002) and *in vitro* kinetic studies (Gomes et al., 2002b) revealing that this protein can reduce NO to nontoxic N_2O under anaerobic conditions, being therefore crucial for the cell survival under nitrosative stress conditions. Transcriptional studies also showed that *norV* is one of the most upregulated *E. coli* genes in cell growth in the presence of NO, under aerobic and anaerobic conditions (Gardner et al., 2002; Justino et al., 2005; Mukhopadhyay et al., 2004).

Based on the redox potentials determined for *E. coli* FDP and NADH:rubredoxin oxidoreductase, the electrons are donated to FDP from NADH (primary electron donor) by a FAD-binding protein of the NADH:rubredoxin oxidoreductase family (Fig. 1.18) (Gomes et al., 2000; Vicente et al., 2007b; Vicente and Teixeira, 2005). Afterwards, the electrons flow to the [Fe-Cys_4] cluster in the C-terminal rubredoxin domain of FDP, being then transferred to the FMN cofactor that finally reduces the diiron center, where the substrate reduction occurs.

E. coli FDP is an example of a FDP selective for NO, although it displays a very low O_2-reductase activity (Gardner et al., 2002; Gomes et al., 2002b). Thus, the *E. coli* FDP is considered a crucial NO-detoxifying protein in this organism, additionally to the flavohaemoglobin as referred in Section 1.2 and in Table 1.12. Moreover, the *E. coli* FDP was the first FDP with an exclusive preference for NO, to be structurally characterized (Romao et al., 2016b). Due to the high flexibility of the extra functional domain, Rd, as confirmed by SAXS studies (Petoukhov et al., 2008), it was not possible to assign electron density to this full domain in the *E. coli* FDP crystal structure. Nevertheless, the presence for this domain in the crystal structure was confirmed by observing a density map assigned only to its tetrahedral mononuclear [Fe-Cys_4] center.

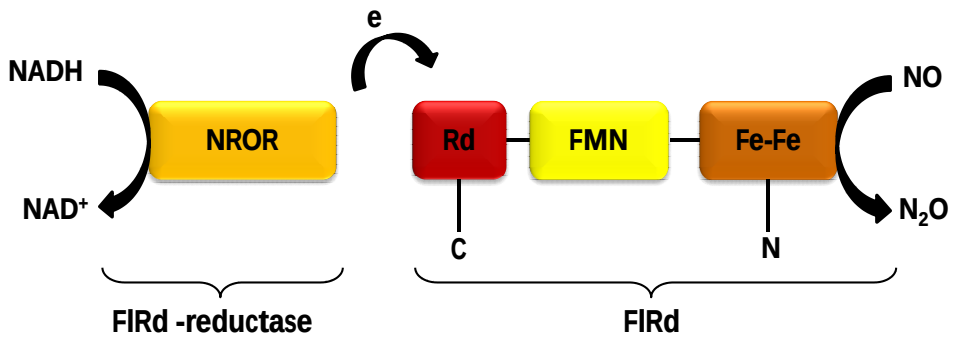

Figure 1.18- Schematic representation of electron transfer from NADH to NO, performed by *Escherichia coli* NADH:rubredoxin oxidoreductase-like and flavorubredoxin.

1.8 *Synechocystis* sp. PCC 6803 flavodiiron proteins

The first appearance of oxygenic photosynthesis started around 3.5 billion years ago when cyanobacteria were able to capture and convert light into energy. Therefore, the CO_2 reduction into carbohydrates, which are then used to store energy is only possible due to electrons released from water oxidation (Blankenship, 2010; Buick, 2008; Hohmann-Marriott and Blankenship, 2011). In this process, the simultaneous oxygen release by cyanobacteria and accumulation, in the Earth atmosphere, allowed to create aerobic conditions for development and sustainability of aerobic metabolism.

Additionally, many cyanobacteria are nitrogen-fixing microorganisms capable of transforming atmospheric nitrogen into fixed nitrogen (ammonia, nitrates, nitrites) contributing significantly to the nitrogen cycle (Bothe et al., 2010; Zehr, 2011).

Cyanobacteria are one of the largest and versatile group of prokaryotes with high biological importance, since are the only prokaryotic organisms able to perform oxygenic photosynthesis. This mechanism in cyanobacteria resembles the same of oxygenic eukaryotes (algae, mosses and higher plants). Similar to all photosynthetic eukaryotic organisms, cyanobacteria also uses photosystem I (PSI) and photosystem II (PSII) to extract electrons from water and the resulting light-driven electron transport, allow $NADP^+$ reduction to NADPH and phosphorylation of ADP to ATP for energy conservation (Fig. 1.19).

The oxygenic photosynthesis takes place in the thylakoid membranes of cyanobacteria that are within the cytoplasm, while in algae and plants are located in chloroplasts (Gantt, 2011; Stanier and Cohen-Bazire, 1977; Vothknecht and Westhoff,

2001). The PSII uses light energy to induce water splitting through the manganese-containing oxygen-evolving complex (OEC) with formation of one oxygen molecule. The resulting four electrons will reduce the mobile plastoquinone pool (PQ). Electrons from the reduced PQ (PQH_2) are then transferred to the cytochrome b_6f complex, which reduce the mobile electron carrier plastocyanin (PC) or a cytochrome c_6 in some cyanobacteria (Nugent, 1996; Rochaix, 2011). These soluble electron carriers will reduce the oxidized PSI reaction center. Direct photon absorption in PSI allows an electron transfer between the electron donor plastocyanin or cytochrome c_6 located in the lumen and the acceptor mobile electron carrier, ferredoxin (Fd), located in the cytoplasm. Finally, reduction of $NADP^+$ to NADPH is performed by a ferredoxin-$NADP^+$ oxidoreductase (FNR) (Fig. 1.19). This protein contains a FAD cofactor, which accepts electrons from Fd (Aliverti et al., 2008; Medina, 2009).

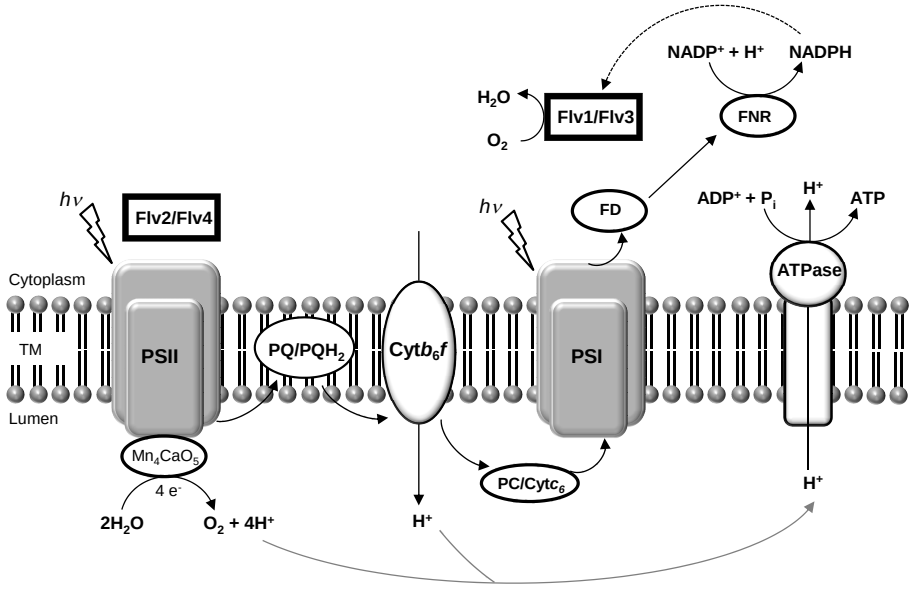

Figure 1.19- Simplified scheme of the photosynthetic process in the thylakoid membrane (TM) of cyanobacteria. Black and grey arrows represent electron and proton transfer process, respectively. Photosystem I (PSI), photosystem II (PSII), oxygen-evolving complex, OEC (Mn_4CaO_5), oxidized plastoquinone (PQ), reduced plastoquinone (PQH_2), plastocyanin (PC), ferredoxin (Fd), ferredoxin-$NADP^+$ oxidoreductase (FNR), $Cytc_6$ – cytochrome c_6. The photon energy absorbed by PSII and PSI, is represented by hν. Adapted from (Allahverdiyeva et al., 2015b). Flavodiiron proteins are represented as Flv1, Flv2, Flv3 and Flv4.

The protons released by PSII due to water splitting as well as the protons formed by the cytochrome b_6f complex, are released into the lumen. This light-induced proton flow, generates a proton gradient across the thylakoid membrane that is used by ATP synthase for ATP synthesis (Fig. 1.19).

Under particular environmental conditions, the oxygenic photosynthesis can induce negative consequences of photodamage, due to the energetic unbalance that occurs when absorbed light exceeds the photosynthesis capacity. Consequently, this leads to an over reduction of the photosynthetic electron transfer chain (Allahverdiyeva et al., 2015a). The excess of electrons can be delivered to O_2, resulting in the production of ROS that can damage the photosynthetic apparatus and affect cell viability. In order to prevent an over reduction of the photosynthetic redox centers, it becomes extremely important a diversified range of photoprotection mechanisms that dissipate the excess of electrons in a safe way.

Cyanobacteria and some oxygenic photosynthetic Eukarya, such as algae, mosses, lycophytes and some gymnosperms (Allahverdiyeva et al., 2015a; Chaux et al., 2017; Dang et al., 2014; Gerotto et al., 2016; Helman et al., 2003; Jokel et al., 2015; Peltier et al., 2010; Yamamoto et al., 2016; Zhang et al., 2009) have genes encoding FDPs in their genomes. Therefore, cyanobacteria have enzymatic mechanisms to perform the light-induced reduction of O_2 avoiding the production of ROS (Table 1.13).

The genome of the cyanobacterium *Synechocystis* sp. PCC 6803*,* contains four genes encoding FDPs: sll1521 (*flv1*), sll0219 (*flv2*), sll0550 (*flv3*), and sll0217 (*flv4*) (Helman et al., 2003). As mentioned in Section 1.3.2, all FDPs found in cyanobacteria and oxygenic phototrophic organisms belong to Class C. These proteins have an extra C-terminal NAD(P)H:flavin oxidoreductase domain (Allahverdiyeva et al., 2015a; Romao et al., 2016a; Saraiva et al., 2004).

The Synechocystis Flv3 is an NAD(P)H:oxygen oxidoreductase capable of reducing O_2 to H_2O (Helman et al., 2003; Vicente et al., 2002). Further, *in vivo* studies proposed that both *Synechocystis* Flv1 and Flv3 proteins are responsible for the O_2 photoreduction, where the source of electrons for O_2 reduction is PSI (Helman et al., 2005; Helman et al., 2003). Flv2 and Flv4 are proposed to be important for the protection of PSII centers against photoinhibition (Bersanini et al., 2014; Eisenhut et al., 2012; Hakkila et al., 2013; Zhang et al., 2009) (Fig. 1.19).

The FDPs role against nitrosative stress in *Synechocystis*, is still poorly addressed. The only fact reported is that *flv1* gene is induced in cells exposed to nitrosative stress (Gonçalves et al., 2011a).

Table 1.13- Enzymes involved in protection of *Synechocystis* against oxidative and nitrosative stress.

System	Protection	Cofactor	Reference
Superoxide dismutase (*sodB*)	ROS	Fe	(Nefedova et al., 2003)
Glutathione peroxidase (*gpx*)	ROS	GSH	(Gaber et al., 2001)
Catalase peroxidase (*katG*)	ROS	Haem *b*	(Regelsberger et al., 1999; Tichy and Vermaas, 1999)
NO reductase- cytochrome *b* subunit (*norB*)	NO	Haem *b*	(Busch et al., 2002)
Flv1 (*flv1*)	ROS/RNS	FMN and Fe-Fe	(Gonçalves et al., 2011a; Helman et al., 2003)
Flv2 (*flv2*), Flv3 (*flv3*), Flv4 (*flv4*)	ROS	FMN and Fe-Fe	(Helman et al., 2003)

The Flv3 is the only FDP from *Synechocystis* characterized *in vitro* (Vicente et al., 2002; Wasserfallen et al., 1998). Beyond the flavodiiron core, analysis of its sequence established that there is an extra NAD(P)H:flavin oxidoreductase domain. This module receives electrons directly fom NADH abolishing then the need of an external redox partners. Flv3 revealed the presence of two iron ions and two flavins per molecule, where the extra domain appears to bind FMN and FAD with equivalent affinities.

As mentioned in Section 1.4.3.1 , FDPs of oxygenic photosynthetic organisms contain a high number of different combinations of putative metal ligands (Gonçalves et al., 2011a). While Flv3 and Flv4 contain canonical iron ligand residues, Flv1 and Flv2 have non-canonical putative ligands at the diiron center, as better explained in the Discussion section. Moreover, for the first time, the crystal structure of a flavodiiron core of a Class C FDP, Flv1-ΔFlR, was determined as reported in Chapter IV.

Part II

Experimental Results

Chapter II

Structure of *Escherichia coli* flavodiiron protein S262Y mutation

This chapter is to be published in:

Patrícia T. Borges, Célia V. Romão, Filipe Folgosa, Maria C. Martins, Guillaume Gotthard, Antoine Royant, Maria Arménia Carrondo, Miguel Teixeira and Carlos Frazão, "A S262Y mutation in *Escherichia coli* flavodiiron protein increases radiation damage sensitivity in the crystal structure", manuscript under preparation.

The construction of the plasmids was performed by João B. Vicente. Patricia T. Borges performed the expression, purification, crystallization and X-ray structural characterization. The UV-visible absorption spectra of the crystals were acquired by P.T Borges with the help of Guillaume Gotthard and Antoine Royant.

2.1 Summary

Flavodiiron proteins (FDPs) safely reduce oxygen (O_2) and/or nitric oxide (NO), contributing to the organism's protection against reactive oxygen and nitrogen species. Although some FDPs show comparable affinities to both substrates, others have a marked preference for either O_2 or NO. The *Escherichia coli* FDP presents a high selectivity towards NO. Its crystal structure was recently determined, showing that the C-terminal rubredoxin-like domain (Rd) is delocalised. In order to address FDP substrate selectivity, an *E. coli* FDP-ΔRd S262Y mutation, was produced in a construct that it lacks the C-terminal domain (ΔRd). Mesh scans of the cryo-cooled crystals were vital for the success of diffraction data acquisition. As its space group, *I2*, differed from that of native *E. coli* FDP crystals, the structure was obtained by molecular replacement and refined at 1.90 Å resolution.

UV-visible microspectrophotometric measurements at 100K of the FDP-ΔRd S262Y crystals, allowed us to observe a decrease of the typical absorption bands of the flavin cofactor after the data collection. Additionally, one observes absence of electron density in some ligands side chains of the active site and also in some neighbouring residues, which led to alteration of inter-atomic distances and increase in <*a.d.p.*>'s values, when compared with the native *E. coli* FDP structure. These data suggest that the presence of the Y262 residue induced an increase of the protein sensitivity to X-ray radiation.

2.2 Introduction

The FDPs, firstly denoted as A-type flavoproteins (Wasserfallen et al., 1998) are widespread in Bacteria, Archaea and Eukarya (Allahverdiyeva et al., 2015a; Andersson et al., 2003; Chaux et al., 2017; Gerotto et al., 2016; Peltier et al., 2010; Saraiva et al., 2004; Seedorf et al., 2007; Shimakawa et al., 2017; Vicente et al., 2008b; Vicente et al., 2009; Yamamoto et al., 2016). These proteins are involved in the protection of organisms against oxidative and/or nitrosative stress by converting oxygen into water and nitric oxide into nontoxic nitrous oxide (Gardner et al., 2002; Saraiva et al., 2004).

FDPs are important for organisms that need to safely reduce the NO produced for example, by the host defence system, namely by nitric oxide synthase (iNOS) in macrophages (Fang, 1997; Figueiredo et al., 2013).

FDPs have been also described as being critical for the survival of cyanobacteria, as well as higher plants, protecting the photosystems under several conditions, such as fluctuating light intensity (reviewed in (Allahverdiyeva et al., 2015a)).

Several FDPs crystal structures were already determined, namely from the bacteria *Desulfovibrio gigas* (Frazao et al., 2000), *Thermotoga maritima* (PDB entry 1VME, 2004), *Moorella thermoacetica* (Silaghi-Dumitrescu et al., 2005a) and *Escherichia coli* (Romao et al., 2016b), from the methanogenic archaeon *Methanothermobacter marburgensis* (Seedorf et al., 2007) and from an eukaryotic protozoan, *Giardia intestinalis* (Di Matteo et al., 2008). Some of these FDPs are described as exclusively O_2 reducers (*T. maritima, M. marburgensis* and *G. intestinalis*), or exclusively NO reducers (*E. coli*) while others reduce both oxygen and nitric oxide (*D. gigas* and *M. thermoacetica*) although with different efficiency.

The enzymes mentioned above (except *E. coli*) belonging to Class A FDPs, are composed of two consecutive structural core domains: a N-terminal β-lactamase-like domain harbouring two iron atoms at the catalytic site, where the substrates reduction occurs, and a C-terminal flavodoxin-like domain containing a non-covalently bound flavin mononucleotide (FMN) cofactor that shuttles electrons to the diiron center (Romao et al., 2016a; Vicente et al., 2008a). The β-lactamase-like domain is composed of a αββα sandwich fold, differing however from metallo-β-lactamases by including two additional β-sheets that cover the diiron center, hindering the access to large substrates. The flavodoxin-like domain shows a αβα fold, characteristic of short-chain flavodoxins. The FMN cofactor is at a long distance from the diiron center (~ 40 Å), which hampers an efficient electron transfer. Interestingly, FDPs form “head-to-tail” dimers as a minimal functional unit, that bring the two cofactors close together (~ 6 Å distance), thus ensuring an efficient electron flow between the two centers.

The most recently determined FDP structure (Romao et al., 2016b), *E. coli* flavorubredoxin , was both the first example of an FDP with clear preference for nitric oxide as substrate, and the first Class B FDP family member, which includes a third domain at the C-terminal, an rubredoxin-like domain (Rd) (Gardner et al., 2002; Gomes et al., 2002b; Gomes et al., 2000; Vicente et al., 2008c; Vicente et al., 2007b; Vicente and Teixeira, 2005; Wasserfallen et al., 1998). However, both previous SAXS studies and the recent crystal structure showed that the additional third domain at the C-terminal is disordered, which was attributed to the 23 amino acids residues long

linker that connects the flavodoxin-like domain with the Rd one (Petoukhov et al., 2008; Romao et al., 2016b).

The substrate reduction in this family of proteins occurs in the β-lactamase-like domain, at a diiron site coordinated by conserved ligands, where the iron proximal to FMN cofactor, Fe_p, is coordinated by $H79^{NE2}$, $E81^{OE1}$ and $H147^{NE2}$ atoms, and the iron distal from FMN, Fe_d, is coordinated by $D83^{OD2}$, $H84^{NE2}$ and $H227^{NE2}$ atoms (*E. coli* FDP numbering). Additionally, D166 bridges both Fe_p and Fe_d through $D166^{OD2}$ and $D166^{OD1}$ atoms, respectively. Furthermore, the majority of available FDP structures also present a μ-hydroxo bridge coordinating both irons (Romao et al., 2016a).

However, the key structural determinants defining FDPs substrates specificity still remain to be clarified. A structural comparison of FDPs with different substrate affinities was performed, such as, the O_2-selective FDP from *Entamoeba histolytica* (whose structure was modelled on the basis of the very close homologue O_2-selective *G. intestinalis*) and the NO-reducing *E. coli* FDP (Gonçalves et al., 2014). In their diiron second coordination sphere were observed differences at two positions. In *E. histolytica* FDP (O_2-selective), one of the positions contains a lysine residue (K53) and the other one a tyrosine (Y271), that are replaced by an aspartate (D52) and a serine (S262) residues in *E. coli* FDP (NO-selective), respectively. The kinetic properties of *E. histolytica* Y271S and K53D/Y271S mutants, showed an increased sensitivity to O_2, since they became inactive after successive turnovers, while showing a higher affinity towards NO, when compared with the wild-type protein (Gonçalves et al., 2014). Therefore, for the first time there were experimental data suggesting that residue Y271 was a determinant in the specificity for the substrate. In this context and in order to probe the effect of such a tyrosine residue in the nitric oxide reductase *E. coli* FDP, the S262Y mutation was designed. In order to compare with *E. histolytica* FDP, that is composed only by the flavodiiron core, the mutant was produced omitting the third Rd domain and its linker, and was named *E. coli* FDP-ΔRd S262Y. Here it is reported its expression, crystallization, structure determination and analysis at 1.90 Å resolution.

2.3 Materials and Methods

Protein expression and purification

The genes coding for the *E. coli* FDP-ΔRd and FDP-ΔRd S262Y mutants (from residue 1 up to 412) were generated at GenScript. Direct sequencing was used to confirm the inserted mutation. Afterwards, *E. coli* BL21(DE3) Gold cells were transformed with the plasmid and plated at 37 ºC into LB plates containing kanamycin (30 µg/ml). These cells were used to inoculate a pre-inoculum grown in LB at 37ºC, overnight. A 2L growth (in 2L flasks) in minimal medium (M9) supplemented with 100 µM $FeSO_4.7H_2O$ at 37 ºC and 140 rpm was inoculated with 5% of the pre-inoculum. The growth was induced at an optical density (600 nm) of 0.4 with 100 µM isopropyl-β-D-thiogalactopyranoside (IPTG) at 30 ºC. After 7 h of induction, cells were harvested by centrifugation at 10,000g for 10 minutes at 4 ºC. Cells were then ressuspended in 20 mM Tris-HCl pH 7.5, disrupted in a French press at 1000 p.s.i. and ultracentrifuged at 100,000g, 4 °C for 1 h. The soluble fraction was dialysed at 4 ºC overnight against 20 mM Tris-HCl pH 7.5 with 2.5% (*v/v*) glycerol.

Purification of both proteins, *E. coli* FDP-ΔRd and FDP-ΔRd S262Y, was performed in two consecutive steps, using an ÄKTAprime system (GE Healthcare) at 4 ºC, as previously described (Vicente and Teixeira, 2005). The soluble fraction was firstly loaded on an anionic Q-Sepharose Fast Flow column equilibrated with 20 mM Tris-HCl pH 7.5, 5% (*v/v*) glycerol and eluted using a linear gradient from 0 to 1 M NaCl. Fractions containing the flavin UV-visible fingerprint (peak at 375 nm and 455 nm) (Fig. 2.1A), and a low Abs (280 nm)/Abs (455 nm) ratio, were eluted at *ca* 250 mM NaCl and were pooled together. The second purification step consisted on a size exclusion chromatography on a Superdex-200 column equilibrated with 20 mM Tris-HCl pH 7.5, 250 mM NaCl and 5% (*v/v*) glycerol. Protein purity was confirmed by SDS-PAGE (Fig. 2.1B) and the fractions were pooled and concentrated up to 15 mg/mL.

Crystallization and cryoprotection

Crystallization conditions were screened with a nanodrop crystallization robot (Cartesian, Genomic Solutions) using the sitting drop vapour diffusion method with round-bottom Greiner 96-well CrystalQuick^{TM} plates (Greiner Bio-One). The Structure Screen I and II (Molecular Dimensions) at 20 ºC led to crystals formation within two days in condition A9 consisting of 0.1 M sodium citrate pH 5.6, 20% (*w/v*) PEG 4000

and 20% (*v/v*) 2-propanol, in a drop of 0.1 µl protein solution (15 mg/mL) plus 0.2 µl reservoir solution. Following this crystallization hit, microliter scale optimization proceeded using the hanging drop vapour-diffusion method in XRL 24-well crystallization plates (Molecular Dimensions). In these scale-up experiments different ranges of conditions were tested, namely PEG 4000 (15-28%) and 2-propanol (15-25%) concentrations and also the pH of sodium citrate (4.5-8.0). After 2-3 days, orange thin plate crystals reached 0.1-0.2 mm maximal length dimensions in 0.1 M sodium citrate pH 5.6, 20-23% (*w/v*) PEG 4000 and 23-25% (*v/v*) 2-propanol, when using 1 µL of protein (15 mg/mL) and 2 µL of reservoir solution (Fig. 2.1C).

E. coli FDP-ΔRd S262Y crystals were cryo-protected using the reservoir solution supplemented with 10% (*v/v*) glycerol prior to flash-cooling in liquid nitrogen. *E. coli* FDP-ΔRd crystals were prepared and cryo-protected as previously described (Romao et al., 2016b).

Data collection and processing

Diffraction was measured at 100 K in the European Synchrotron Radiation Facility (ESRF, Grenoble, France). Crystals appeared as stacks of thin plates and did not produce useful diffraction data, because, although spots were visible, they could not be indexed. Introduction of mesh scans at beamline ID29 (Svensson et al., 2015) allowed us to improve data collection by centring the beam on their best diffraction spots, by screening them with a 20 µm diameter X-ray beam section over an 18 µm spaced grid. X-rays images were taken at each grid position and their diffraction strengths evaluated, combining an analysis of Bragg peaks with their intensity distribution as a function of resolution. The best diffracting position of the crystal was then aligned with the X-ray beam, the loop rotated by 90˚ degrees and new set of diffraction images collected to find the crystal best diffraction spot. Diffraction images were obtained in a PILATUS 6M detector, using 1.0000 Å wavelength radiation, with a crystal-to-detector distance of 372 mm, and 0.15º oscillations widths in a total of 120º rotation during 29.60 s. Diffraction spots were indexed, integrated, scaled and the final amplitudes calculated using XDS (Kabsch, 2010). POINTLESS (Evans, 2011) suggested re-indexing the data in space group number 5 from the initial setting *C*2 into *I*2, in order to obtain the *beta* angle closer to 90˚, as recommended by the IUCr convention (Mighell, 2002), which was accomplished with XPREP (Bruker).

UV-visible absorption spectra of the crystals were measured offline before and after X-ray irradiation at 100 K using a microspectrophotometer setup (QE65 Pro from Ocean Optics, 10 micron slits, HC-1 grating) with 1.68 nm of optical resolution at ID29S Cryo-Bench beamline in order to monitor changes in the oxidation state of the protein crystals after the data collection (Royant et al., 2007).

Data collection details and processing statistics are listed in Table 2.1.

Structure determination and refinement

Estimation of the unit cell contents was obtained with the Matthews Probability Calculator which estimated two molecules in the asymmetric unit (Kantardjieff and Rupp, 2003; Matthews, 1968). The phase problem was solved by molecular replacement with PHASER (McCoy et al., 2007a) within the PHENIX suite (Adams et al., 2010b), and using the coordinates of the native *E. coli* FDP structure (PDB 4D02) (Romao et al., 2016b) as the search model. For cross validation purposes, 2% of reflections in thin-resolution shells were excluded from refinement. The TLSMD server (http://skuld.bmsc.washington.edu/~tlsmd) (Painter and Merritt, 2006) was used to define polypeptide chain regions for translation, libration and screw refinement of anisotropic atomic displacement parameters (<*a.d.p.*>). Iterative refinement cycles were produced with PHENIX.REFINE (Adams et al., 2010a) followed by $sigma_A$ Fourier maps examination and model optimization with COOT (Emsley et al., 2010). Standard stereochemical dictionary (Engh and Huber, 1991) was used in refinement except for iron ligations that were refined without target restraints. Water solvent molecules were initially located automatically in difference Fourier maps at peaks with hydrogen bonding distances within 2.45-3.40 Å. Some atoms were modelled with partial occupancies, eventually in discretely alternating occupancies, when hinted by the difference Fourier maps and neighbouring <*a.d.p*> values.

Refinement and model edition iterations were performed until R_{work} and R_{free} values converge, before calculation of the final R_{factor} using all available diffraction data.

The quality of the model was checked with MOLPROBITY (Chen et al., 2010). Models structural superpositions were performed with MODELLER (Webb and Sali, 2014). All figures were prepared with PyMOL (DeLano, 2002). For sake of simplicity, structural comparisons of the mutation structure involve only its chain A, which showed lower <*a.d.p*.>. The refinement statistics are presented in Table 2.1.

Calculation of absorbed X-ray doses

X-ray absorbed doses by *E. coli* FDP-ΔRd and FDP-ΔRd S262Y crystals were determined with RADDOSE-3D (Zeldin et al., 2013) using the diffraction-weighted dose metric (DWD). The input parameters used for each crystal are reported in Table 2.4.

Table 2.1- Crystallographic parameters, diffraction data and refinement statistics of *E. coli* FDP-ΔRd S262Y mutant. Values in parentheses correspond to the highest resolution shell.

Data collection statistics	
Beamline	ESRF ID29
Detector	PILATUS 6M
Wavelength (Å)	1.0000
Space Group	*I*2
Unit cell parameters (Å)	a = 89.4, b = 64.4, c = 147.3, β = 91.09°
Resolution (Å)	75.83-1.90 (2.00-1.90)
No. of observations	129422 (18166)
Unique reflections	57099 (8802)
Completeness (%)	96.8 (88.5)
Multiplicity	2.3 (2.1)
Mosaicity (º)	0.6
$CC_{1/2}$ (%)[a]	99.4 (52.4)
R_{sym} (%)[b]	10.9 (58.8)
R_{meas} (%)[c]	11.7 (70.3)
$R_{p.i.m.}$(%)[d]	7.5 (49.5)
unmerged data $<I/\sigma(I)>$	3.7
merged data $<I/\sigma(I)>$	5.2 (1.3)
Wilson B factor (Å^2)	21
No. of molecules in asymmetric unit	2
V_M (Å^3 Da^{-1})	2.28
Estimated crystal solvent content (%)	45.9
Refnement statistics	
R_{factor} (%)[e]	19.9
R_{work} (%)[f]	20.7
R_{free} (%)[f]	23.5
r.m.s.d. for bond lengths (Å)	0.018
r.m.s.d. for bond angles (°)	0.560
Average chain B-factor (Å^2)	25
Number of residues	400
Number of solvent waters	783
Ramachandran plot	
Residues in favored regions (%)	96.5
Residues in allowed regions (%)	3.5
Residues in disallowed regions (%)	0

[a] $CC_{1/2}$ = Percentage of correlation between intensities from random half-datasets (Karplus and Diederichs, 2012).

b $R_{sym} = \Sigma_{hkl} \Sigma_i |I_i(hkl) - \langle I(hkl)\rangle| / \Sigma_{hkl} \Sigma_i I_i(hkl)$, where $I_i(hkl)$ is the observed intensity and $\langle I(hkl)\rangle$ is the average intensity of multiple observations from symmetry-related reflections (Arndt et al., 1968).

c $R_{meas} = \Sigma_{hkl} [N/(N(hkl) -1)]^{1/2} \Sigma_i |I_i(hkl) - \langle I(hkl)\rangle| / \Sigma_{hkl} \Sigma_i I_i(hkl)$, where N(hkl) is the data multiplicity, $I_i(hkl)$ is the observed intensity and $\langle I(hkl)\rangle$ is the average intensity of multiple observations from symmetry-related reflections. It is an indicator of the agreement between symmetry related observations (Diederichs and Karplus, 1997).

d $R_{p.i.m.} = \Sigma_{hkl} [1/(N(hkl) -1)]^{1/2} \Sigma_i |I_i(hkl) - \langle I(hkl)\rangle| / \Sigma_{hkl} \Sigma_i I_i(hkl)$, where N(hkl) is the data multiplicity, $I_i(hkl)$ is the observed intensity and $\langle I(hkl)\rangle$ is the average intensity of multiple observations from symmetry-related reflections. It is an indicator of the precision of the final merged and averaged data set (Weiss, 2001).

e $R_{factor} = \Sigma |F_{obs} - F_{calc}| / \Sigma F_{obs}$, where F_{obs} and F_{calc} are the amplitudes of the observed and the model calculated structure factors, respectively. It is a measure of the agreement between the experimental X-ray diffraction data and the crystallographic model.

f R_{work} refers to the actual working data set used in refinement, while R_{free} refers to a cross validation set that is not directly used in refinement and is therefore free from refinement bias.

2.4 Results and Discussion

Crystal structure of the FDP-ΔRd S262Y and its comparison with native FDP

In order to address the role of a tyrosine residue in the second coordination sphere of the active site of FDPs, a FDP-ΔRd S262Y mutation was designed omitting the C-terminal Rd domain and its linker. Crystallization experiments led to orange coloured crystals, distinctive of the presence of oxidized FMN (Fig. 2.1C). Crystals appeared as stacked thin plates that were very difficult to separate individually. However, the mesh scan system available at the synchrotron beamline ID29, allowed selection of good diffraction crystals and the accurate localization of their most favourable diffraction regions (Fig. 2.1D) (Svensson et al., 2015). The best crystal, centred at its optimal position, diffracted up to 1.90 Å resolution. The mesh scan analysis of the crystal was crucial to yield this high resolution diffraction data (see Table 2.1 for diffraction data and refinement statistics).

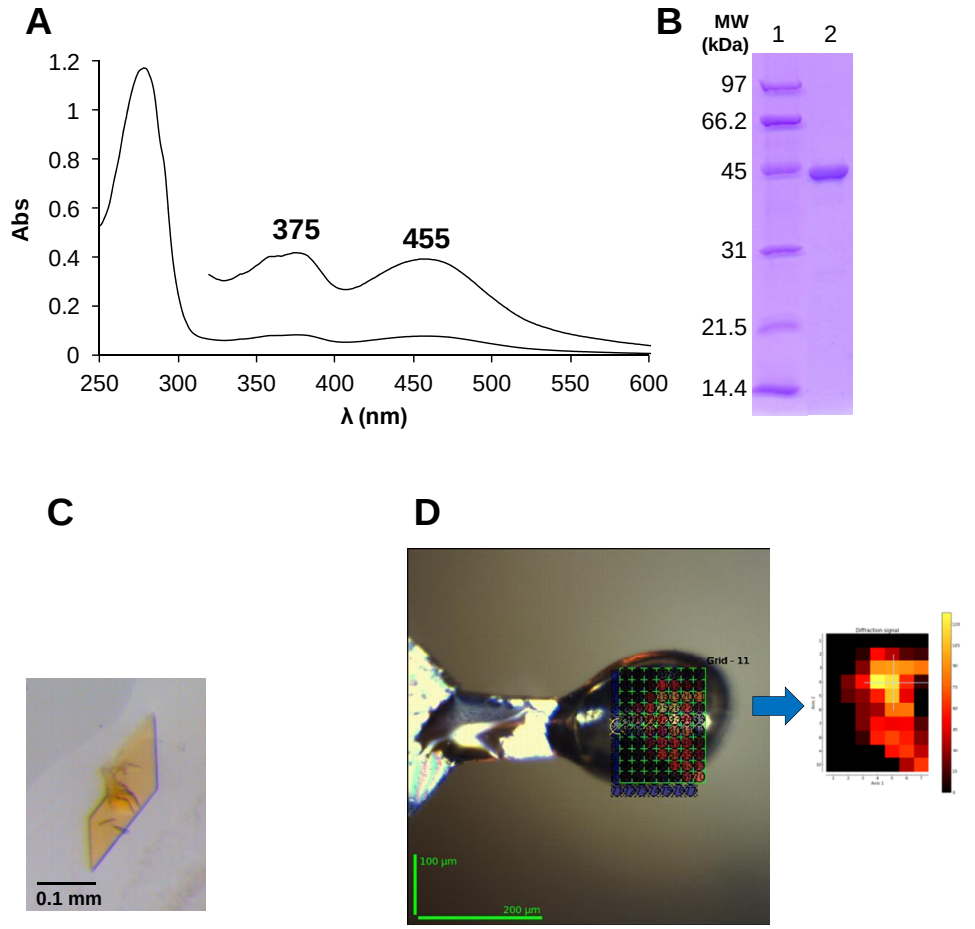

Figure 2.1- Spectral, purity and crystal features of *E. coli* FDP-ΔRd S262Y **A)** UV–vis absorption spectrum. The spectral region characteristic of the flavin cofactor is amplified six times, showing the typical peaks at 375 and 455 nm. **B)** SDS–PAGE. Lane 1, low-molecular mass markers (kDa). Lane 2, protein eluted from Superdex-200 column. **C)** Crystals grew as orange thin-plates, with dimensions 0.20, 0.10 and 0.05 mm, in 0.1 *M* sodium citrate pH 5.6, 23% (*w/v*) PEG 4000 and 20% (*v/v*) 2-propanol. **D)** Crystal mesh scan. The crystal holding loop (left) is shown superposed with the grid of positions for diffraction scan. The crystal heat map (right) shows the grid positions colour coded (black to yellow) with the rank of diffraction strengths. The heat map reveals the size and shape of the actual diffracting crystal, and highlights the best diffraction region (yellow colour).

The mutated protein, FDP-ΔRd S262Y, crystallized in a space-group different from the native FDP, and thus the structure was determined by molecular replacement. Although the crystal asymmetric unit included two independent monomers, the characteristic FDPs “head-to-tail” homodimer was not formed. However, this dimeric

arrangement, as well as the homotetrameric one, became evident when applying the crystal symmetry (Fig. 2.2), similar to the native FDP (Romao et al., 2016b).

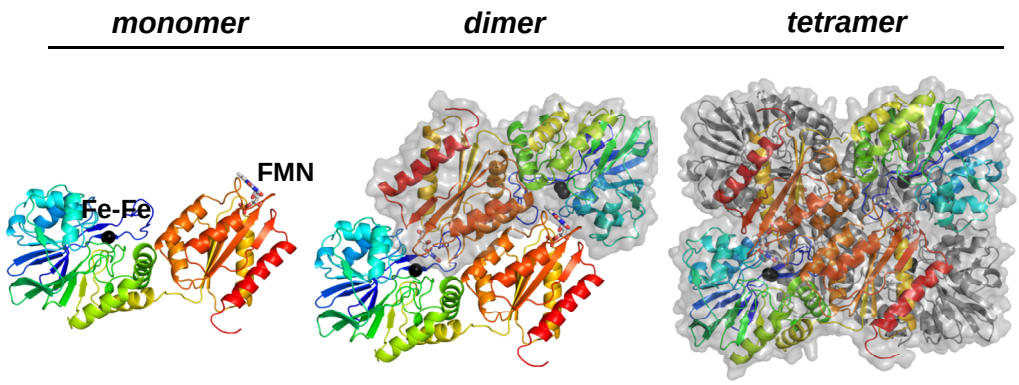

Figure 2.2- Overall structure of *E. coli* FDP-ΔRd S262Y mutant. Cartoon representation of the monomer rainbow-colored, composed of two structural domains, metallo β-lactamase-like domain (blue to green) and flavodoxin-like domain (yellow to red). Cartoon representation of the "head-to-tail" dimer and transparent solvent accessible surface for one monomer. Cartoon representation and transparent solvent accessible surface of the homotetramer where the front "head-to-tail" dimer is rainbow-colored and the symmetry related homodimer is grey colored. Iron atoms are represented as black spheres and FMN is shown as sticks with carbon atoms in grey, nitrogen in blue, oxygen in red and phosphorous atoms in orange.

The structure was refined to R_{work}/R_{free} 0.207/0.235 and a final R_{factor} 0.199, when using all available diffraction data. Both monomers show electron density in the main-chain for 2-401 residues. Additionally, each monomer shows one FMN cofactor, two iron atoms linked by a μ-hydroxo (OH^-) bridge in the active site, and a dioxygen molecule occupying the active site pocket.

The two monomers in the asymmetric unit show between them root-mean-square distances (*r.m.s.d.*s) of 0.12 Å. A structural superposition with the native FDP led to 0.40 Å *r.m.s.d.*s (Fig. 2.3A) for their residues main-chain atoms, while the comparison with the available FDPs gives *r.m.s.d.*s within 1.39-2.15 Å. Figure 2.3A shows main and side chains *r.m.s.d.*s between *E. coli* FDP and FDP-ΔRd S262Y.

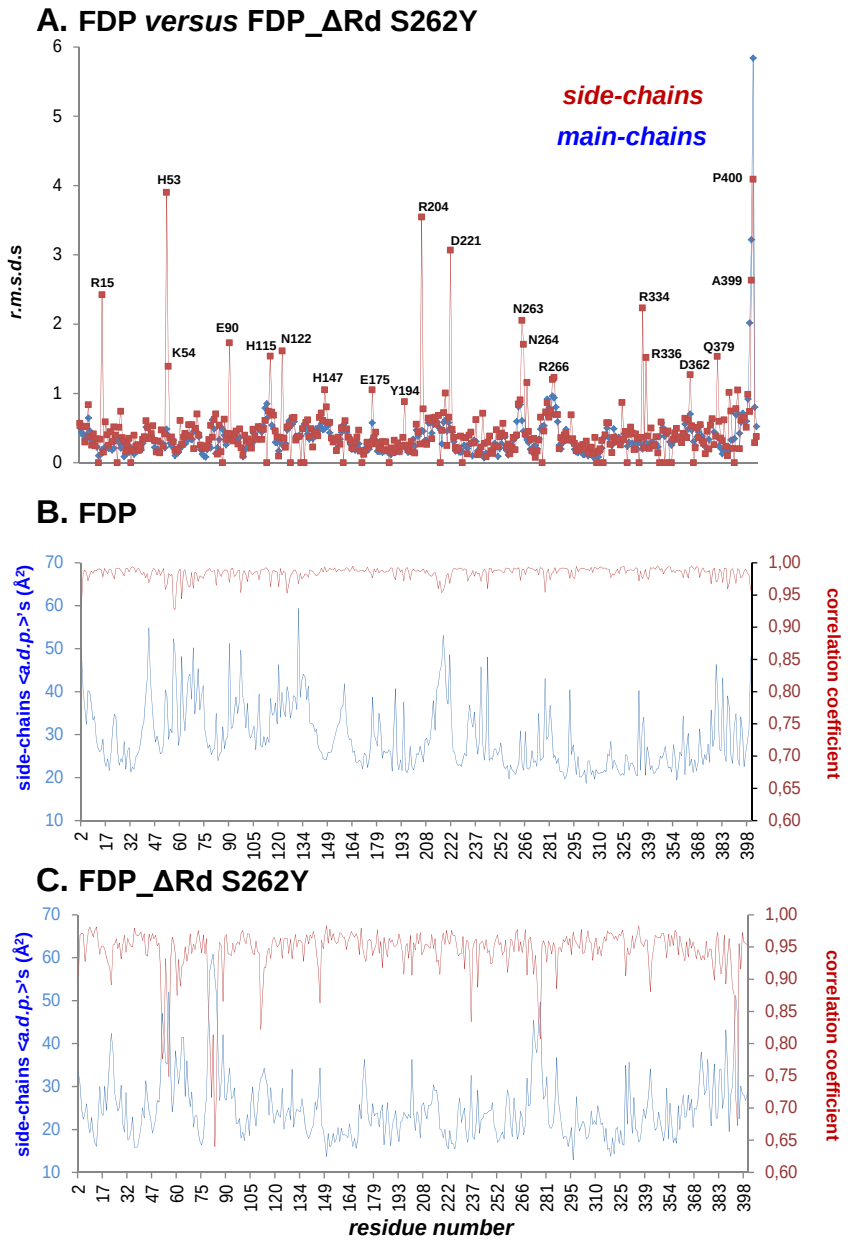

Figure 2.3- Structure comparison between native FDP and FDP-ΔRd S262Y proteins. **A)** Plot of main chains (blue colour) and side chains (red colour) *r.m.s.d.*s between native and mutant structures. **B)** Plots of real space electron density correlation coefficients (red colour) and <*a.d.p.*>'s (blue colour) for the residues side chains of native FDP structure. **C)** Plots of real space electron density correlation coefficients (red colour) and <*a.d.p.*>'s (blue colour) for the residues side chains of the FDP-ΔRd S262Y structure.

As expected, solvent exposed hydrophilic side chains display low local electron density correlation coefficients and high <*a.d.p.*> s (Fig. 2.3B, C). However, this comparison also pin points a set of internal residues, E81-G86, belonging to the diiron site and to its vicinity, that show significantly lower side chain electron density and higher <*a.d.p.*> values in the FDP-ΔRd S262Y structure relative to the native FDP (Figs. 2.3B, C, 2.4 and Table 2.2). Noticeably, residues E81, D83 and H84 are iron ligands, while E82, A85 and G86 are in the neighborhood of the diiron active site. Additionally, the iron atoms <*a.d.p.*> values of the FDP-ΔRd S262Y structure are significantly higher (~43 $Å^2$) comparatively with the *E. coli* FDP structure (~28 $Å^2$).

Table 2.2- <*a.d.p.*> values ($Å^2$) of residues main chain (MC) and side chain (SC) from *E. coli* FDP-ΔRd S262Y.

Residue	MC (A, B)	SC (A, B)
E81	42.5, 40.7	47.0, 48.5
E82	53.5, 49.9	59.7, 54.4
D83	58.3, 56.5	60.0, 58.2
H84	59.4, 62.4	61.8, 57.3
A85	55.7, 65.8	54.4, 62.5
G86	51.5, 56.7	---

Interestingly, the FDP-ΔRd S262Y refinement of the μ-hydroxo bridge indicated a sub-stoichiometric occupancy (~0.6) and an increased hydrogen bond distance to D83 free carboxylic oxygen (Table 2.3), in contrast to the native FDP structure. Although, the distance between the two iron atoms is similar in both structures, some of the iron ligands in FDP-ΔRd S262Y structure, show markedly longer coordination distances reaching non-coordination distances, namely between Fe_p and $H79^{NE2}$ or $H147^{NE2}$, and between Fe_d and $D166^{OD1}$ (Table 2.3).

Table 2.3- FDP active site inter-atomic distances (Å) may be compared with Cambridge Structural Database distances for Fe coordination to carboxylic oxygen [2.01(5), range 1.90-2.09 Å] and imidazole nitrogen atoms [2.08(9), range 1.95-2.22 Å] as extracted from (Harding, 1999).

	E. coli FDP	*E. coli* FDP-ΔRd S262Y
Fe_p –Fe_d	3.5	3.6, 3.6
Fe_p–$H79^{NE2}$	2.2	2.9, 2.7
Fe_p–$E81^{OE1}$	2.1	1.9, 1.9
Fe_p–$H147^{NE2}$	2.1	2.8, 2.6
Fe_p–$D166^{OD2}$	2.1	2.2, 2.1
Fe_p–μOH	2.0	2.1, 2.1
Fe_p–O_2^{O1}	---	3.1, 3.1
Fe_p–O^{PO4}	2.3	---
Fe_d– $D83^{OD2}$	2.3	2.3, 2.3
Fe_d– $H84^{NE2}$	2.1	2.2, 2.2
Fe_d–$D166^{OD1}$	2.1	2.7, 2.5
Fe_d–$H227^{NE2}$	2.2	2.2, 2.2
Fe_d–μOH	2.1	1.7, 1.7
Fe_d–O^{O2}	---	2.5, 2.7
Fe_p–O^{PO4}	1.9	---
μOH-$D83^{OD1}$	2.6	3.3, 3.2
PDB entry	4D02	---

Another noteworthy difference between the two structures concerns the electron density blob found in the vicinity of Fe_d. In the native FDP structure, this was assigned as a phosphate, in accordance to its size and contact distances (Fig. 2.4 *a2, a3*), whereas the smaller density blob found in an equivalent region in FDP-ΔRd S262Y, hinted for a dioxygen molecule (Fig. 2.4 *b2, b3*). Its refinement led to reasonable <*a.d.p.*>'s values and contact distances, similar to those found in the chemically reduced FDP crystal (Romao et al., 2016b), as well as in aerobically produced *D. gigas* or *M. thermoacetica* FDP structures (Frazao et al., 2000; Silaghi-Dumitrescu et al., 2005a).

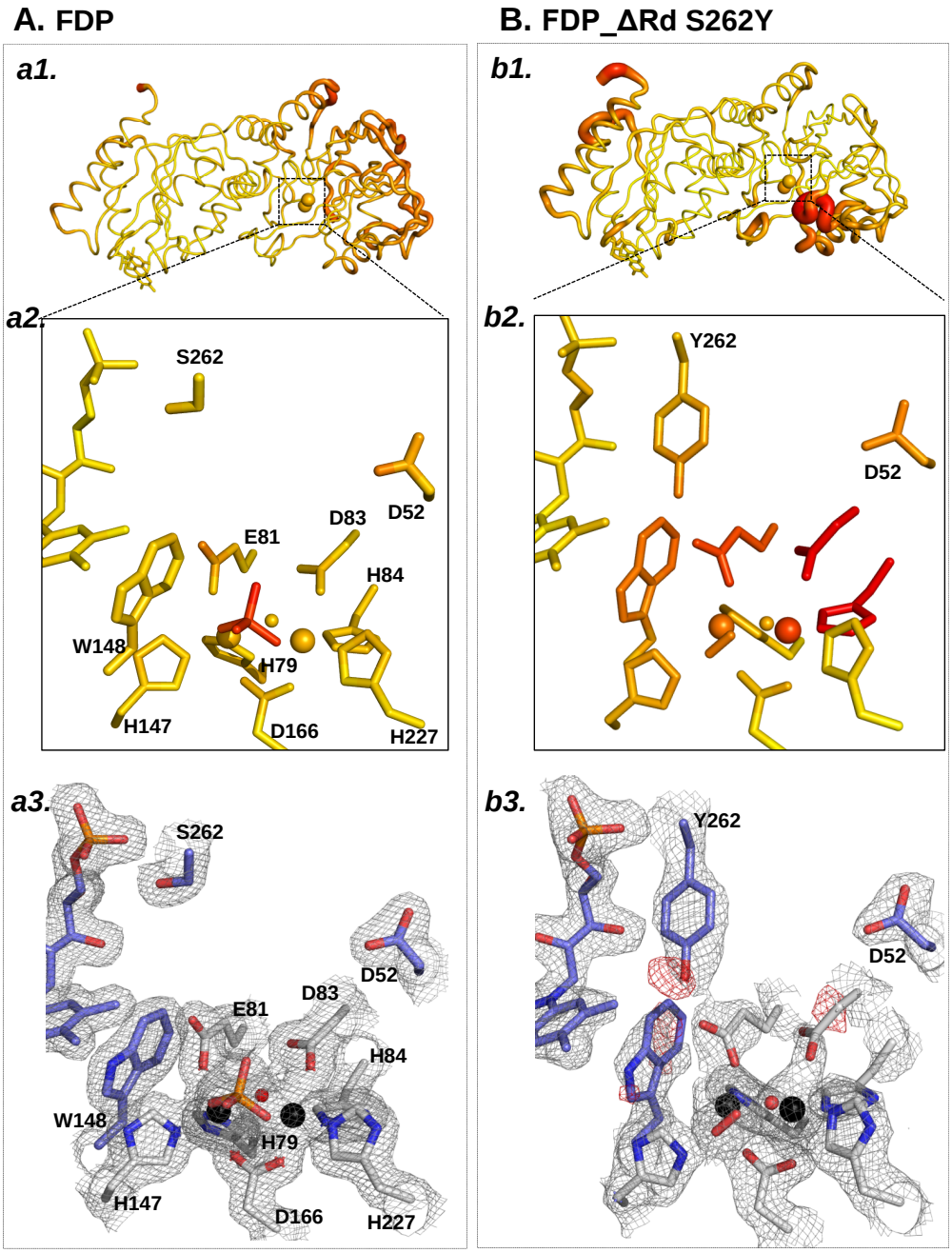

Figure 2.4- Representation of structures and electron density of native FDP and FDP-ΔRd S262Y. A) Native FDP structure and B) FDP-ΔRd S262Y mutant structure in the same orientation. (*a1* and *b1*) Cartoon representation of the main-chain structures with thickness

proportional to <*a.d.p.*> values, colour coded from yellow (15 $Å^2$) to red (60 $Å^2$). (*a2* and *b2*) Zoomed view of the active site accordingly the same colour coded for <*a.d.p.*> values as in *a1* and *b1*. (*a3* and *b3*) Grey mesh represents $2m|F_o|-D|F_c|$ maps at 1σ contour, and green/red mesh represents $m|F_o|-D|F_c|$ maps at +3σ/-3σ contour, respectively, in the active site region. Iron atoms and μ-hydroxo bridge are represented as black and red spheres, respectively. Residues are shown as sticks with nitrogen in blue and oxygen in red. Carbon is coloured in grey for active site ligands or in blue for other residues. FMN is shown as sticks with carbon atoms in blue, nitrogen in blue, oxygen in red and phosphorous atoms in orange.

Radiation damage

As mentioned above, the FDP-ΔRd S262Y structure shows poorly defined electron density in some of its iron ligands and neighbouring residues side chains (Fig. 2.4 *b2*, *b3*). Difference Fourier maps showed negative densities in the metal ligand $D83^{C\beta}$ and near $Y262^{OH}$, the latter being the residue from the diiron center's second coordination sphere which belongs to the symmetry related monomer (Fig. 2.4 *b3*).

We hypothesize that these altered densities in the active site and its neighborhood might have resulted from X-ray radiation damaging effects. In fact, X-rays water photolysis is known to produce extremely reactive free-radical species in macromolecular protein crystals (Southworth-Davies and Garman, 2007). Therefore, even at cryogenic temperatures, radiation damage can occur due to the high beam intensity available at synchrotron beamlines (Burmeister, 2000; Garman, 2003).

The calculated absorbed X-ray doses for both native FDP and FDP-ΔRd S262Y crystals, 1.30 and 1.07 MGy, respectively, did not vary significantly for the two protein structures (Table 2.4). Additionally, the calculated doses are significantly below the experimental accepted dose limit of 30 MGy in macromolecular crystallography (Owen et al., 2006), although there are reports of damaged proteins with doses of 1.0-1.5 MGy (Adam et al., 2004; Corbett et al., 2007).

Table 2.4- Calculated X-rays diffraction-weighted absorbed doses (Zeldin et al., 2013).

	E. coli FDP	*E. coli* FDP-ΔRd S262Y	*E. coli* FDP-ΔRd
Dimensions (μm)	100, 100, 100	200, 100, 50	100, 100, 100
Gaussian beam type with full width and half maximum (μm)	30, 50	30, 50	30, 50
Beam flux (photons/s)	$7.4x10^{11}$	$6.3x10^{11}$	$7.3x10^{12}$
Energy (keV)	12.6	12.4	12.6
Exposure time (s)	41.8	29.6	88.8
Dose (MGy)	1.30	1.07	27.26

Moreover, to exclude the possibility that the observed electron density anomalies have derived from fortuitous protein mishandling, a new batch of the FDP-ΔRd S262Y protein was produced, purified and crystallized. Crystals were obtained under the same conditions, diffraction data sets were collected and the corresponding structures refined with similar resolutions, 1.90-2.20 Å (data not shown). All crystals structures showed similarly altered electron density by the active site and neighbouring residues. Additionally, it was relevant to rule out the role of the labile Rd domain in these structural anomalies, since this domain was absent in the FDP-ΔRd S262Y crystals. Therefore, we produced and crystallized a truncated form of FDP that lacked the rubredoxin domain and its linker, FDP-ΔRd. The resulting crystal was isomorphous with those of native FDP and diffracted up to 1.82 Å resolution (data not shown). The crystal was severely irradiated, up to a calculated absorbed dose of 27.26 MGy, during diffraction data collection. However, its final electron density was comparable to that of native FDP, in particular at the active site region. This indicated that the labile Rd domain was not the responsible for the quenching of free radicals in FDP. These results, suggest that the Y262 residue has an important role on the sensitivity of the mutated protein to X-rays radiation, even at low absorbed doses.

Photo-reduction

The visible spectra of FDP-ΔRd S262Y crystals was measured before and after exposure to X-rays (von Stetten et al., 2015). A total of five crystals were tested and in all of them a similar result was obtained. Before data collection it is present the typical FMN absorption band with two maxima at 375 and 455 nm, identical to the spectrum

of pure protein (Fig. 2.1, 2.5). However, after collecting a 180º dataset (corresponding to a dose that ranged from 0.56 MGy to 1.49 MGy, depending on the crystal), a decrease in the typical FMN absorption band at 455 nm was observed as well as a slight shift of the band at 375 nm (Fig. 2.5A). Subtracting the crystal spectrum before being exposed to the X-rays to the one that was irradiated, the obtained spectrum is similar to a typical FDP semiquinone spectrum (Fig. 2.5B).

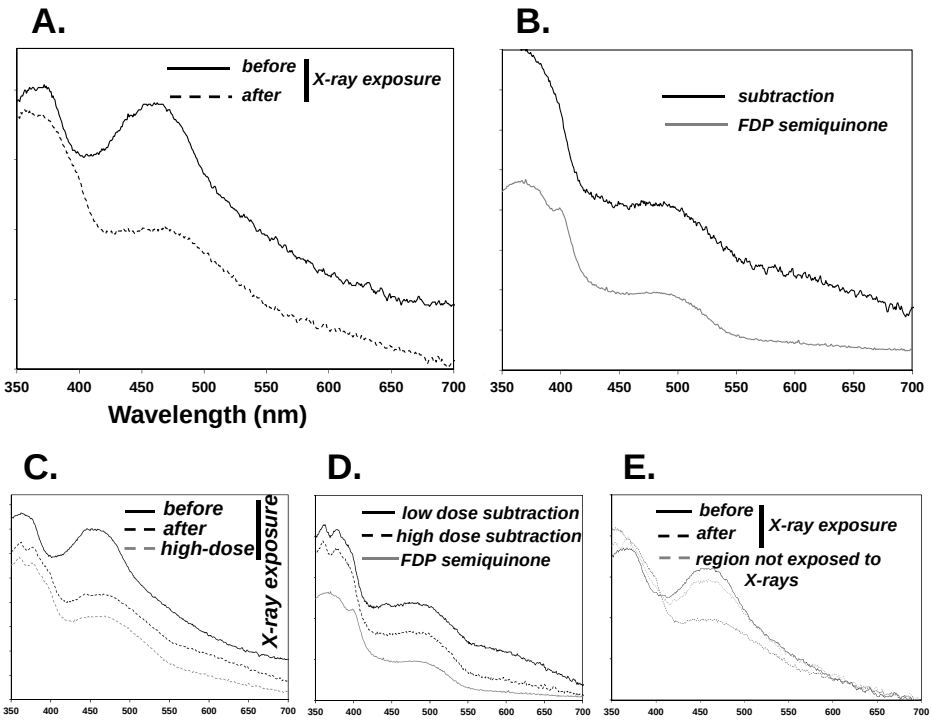

Figure 2.5- Visible spectra of the protein crystals from *E. coli* FDP-ΔRd S262Y. **A)** Visible spectra before (black full line) and after (black dash line) X-ray diffraction data set collection (dose 1.22 MGy). **B)** Subtraction of the visible spectra (black full line) presented in panel A compared with a spectrum of a FDP seminiquinone state (grey full line). A 30% contribution of the before X-ray exposure spectrum was subtracted to the spectrum obtained after X-ray exposure presented in panel A. **C)** Visible spectra before (black full line), after X-ray diffraction data set collection (black dash line, dose 1.49 MGy) and after a high-dose of X-ray exposure (grey dash line, dose 2.92 MGy). **D)** Subtraction of the visible spectra (black full and dash lines) presented in panel C compared with a spectrum of a FDP seminiquinone state (grey full line). A 30% contribution of the before spectrum was subtracted to both spectra obtained after X-ray exposure. **E)** Visible spectra before (black full line), after X-ray diffraction data set collection (black dash line, dose 0.65 MGy) and in a crystal region that was not exposed to X-rays (grey dash line).

The only difference is the broad band around 650 nm, that is not observed in the semiquinone spectrum and which origin is presently unknown. It is interesting to observe that, a further data collection in the same position in the crystal, with more 180º (corresponding to further dose of 2.92 MGy), shows that this broad band is no longer present in the subtracted spectrum (Fig. 2.5C, D). This indicates that exposure of crystals to the X-ray beam generated the semiquinone state in the protein, (Fig. 2.5B, D). The observed change affected only the region that was irradiated by X-rays

(Fig. 2.5E). In the native FDP, the reduction potentials of the FMN are -40 and -130mV and the ones for the diiron are -20 and -90mV (Vicente and Teixeira, 2005). This suggests that under those conditions the diiron site may be partially reduced, probably in the mixed-valence state.

Aromatic residues chains

Tyrosine and tryptophan side chains have been considered key players in the protection of oxidoreductases from radicals damage. They promote the transfer of oxidizing equivalents from the redox active site to the exterior of the protein, where they can be scavenged by cellular reductants (Gray and Winkler, 2015; Winkler and Gray, 2015). The native *E. coli* FDP structure present two chains of tyrosine and tryptophan side chains, which were proposed to function as exit routes, namely *via* Y249 and W348 residues, located at the protein surface (Romao et al., 2016b).

The *E. coli* FDP-ΔRd S262Y crystal structure show that the C^{α} of Y262 residue is in a similar structural position as the corresponding residue in the *G. intestinalis* FDP. However, its side chain is closer to the FMN ($Y262^{OH}$... FMN^{C8M} - 3.3 Å) in FDP-ΔRd S262Y when compared with *G. intestinalis* FDP ($Y267^{OH}$... FMN^{C8M} - 5.1 Å) (Fig. 2.6).

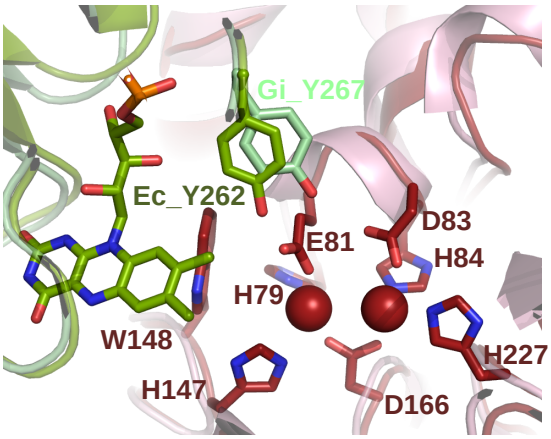

Figure 2.6- Structural superposition of *E. coli* FDP-ΔRd S262Y and *G. intestinalis* FDP. The diiron center is from *E. coli* FDP-ΔRd S262Y structure. The residue Y262 from *E. coli* FDP-ΔRd S262Y is represented in dark green and Y267 from *G. intestinalis* FDP is represented in light green.

In the case of the present FDP-ΔRd S262Y crystal structure, the Y262 side chain is not only located at the surface but also near the active site, at 4.8 and 5.4 Å from Fe_p

and Fe_d, respectively. Additionally, it may also indirectly communicate with Fe_p *via* W148, at 5.2 Å distance (Fig. 2.7A). The structural damage observed at the FDP-ΔRd S262Y active site still remains intriguing, since with the mutation an additional putative exit route was created.

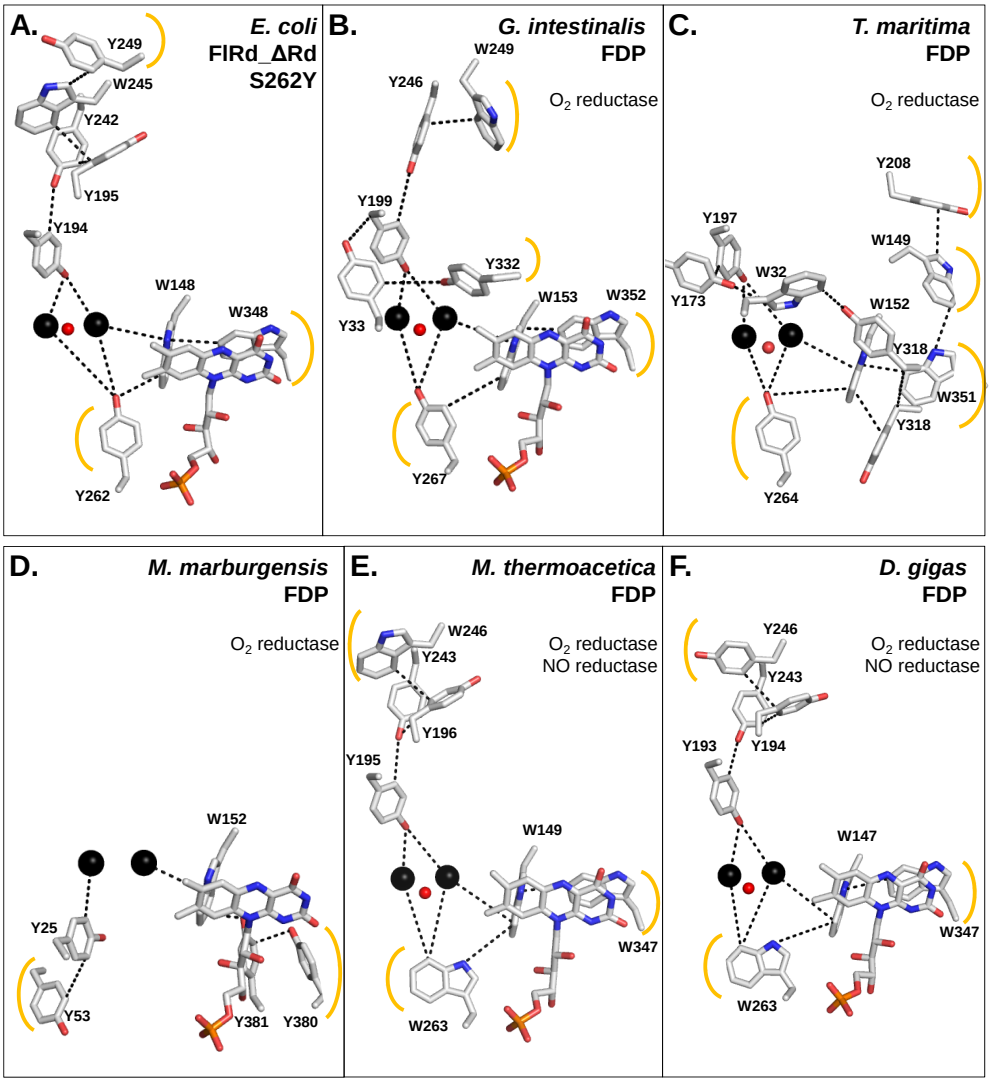

Figure 2.7- Distribution of tyrosine and tryptophan residues, from available FDPs structures (*G. intestinalis*, PBD entry 2Q9U, *T. maritima*, 1VME, *M. marburgensis*, 2OHH, *M. thermoacetica*, 1YCF and *D. gigas*, 1E5D), with the shortest edge-to-edge distance (dash line), between aromatic residues from the active site to the solvent accessible surface. *E. coli* FDP-ΔRd S262Y protein structure in panel A, FDPs with only O_2 reductase activity in panels B-D, and FDPs with both O_2 and NO reductase activities in panels E and F. The tyrosine/tryptophan chains are represented as sticks with carbons colored in grey, nitrogen in blue and oxygen in red. The residues that contact with the external surface of the protein are highlighted with a yellow line. The iron atoms and μ-hydroxo bridge are represented as black and red spheres, respectively. FMN is shown as sticks with carbon atoms in grey, nitrogen in blue, oxygen in red and phosphorous atoms in orange.

A comparison between the FDP-ΔRd S262Y and available FDPs structures shows that only W148 (*E. coli* FDP numbering) is conserved in these chains, with Y194 and W348 residues being replaced by a phenylalanine and a glycine residues, respectively, only in *M. marburgensis* FDP.

The subset of O_2-selective *G. intestinalis* and *T. maritima* FDPs structures, present four oxidizing equivalent exit routes, although only two are conserved, namely Y262 and W348 (*E. coli* FDP numbering) (Fig. 2.7B, C). The O_2-selective *M. marburgensis* FDP shows only two exit routes (Fig. 2.7D), although, none of these are conserved in the others O_2-selective FDPs.

Interestingly, in the FDP-ΔRd S262Y structure, the distance between Y262 and W148 is shorter than in the oxygen selective FDPs from *G. intestinalis* and *T. maritima* (4.1 *versus* 5.1 and 5.3 Å, respectively). Relatively to the bi-functional FDPs, three possible Tyr/Trp chains connect the diiron site with the protein surface, although only one is conserved, W348 (Fig. 2.7 E, F). Noteworthy, the oxygen reducing FDPs (except *M. marburgensis* FDP) show a higher number of putative escaping routes.

2.5 Conclusions

Flavodiiron proteins are responsible for the direct reduction of oxygen and/or nitric oxide to water and nitrous oxide, respectively. Although FDPs have been biochemically studied since 1993, the structural determinants affecting its substrate (NO or O_2) selectivity, still remain to be determined. Studies on an FDP with oxygen preference (EhFDP) highlighted the importance of a tyrosine residue in the second coordination sphere of the diiron site, as being relevant for its substrate selectivity (Gonçalves et al., 2014).

Here, it is reported a 1.90 Å resolution crystal structure from *E.coli* FDP, with the Rd domain omitted and including the S262Y mutation, FDP-ΔRd S262Y. As crystals formed piled plates, diffraction data were only obtained upon a mesh scan of the crystals. Although the overall fold of the FDP-ΔRd S262Y structure compares well with that of native FDP, it revealed some structural anomalies in the diiron active site region. They included longer iron coordination distances, negative Fourier difference densities in some metal ligands and lack of electron density at the side chains of some metal ligands. In order to try to rationalize the observed structural inconsistencies, absorbed X-ray doses were determined for the native *E. coli* FDP as well as for its

structure depleted of the Rd domain, and also for the FDP-ΔRd S262Y structure. Noticeably, the S262Y mutation induced significant crystals X-rays radiation sensitivity in spite of the low calculated absorbed dose. Putative oxidizing equivalents exit routes were mapped for available FDPs structures, but further studies are still necessary in order to fully understand FDPs radicals scavenging mechanisms.

2.6 Acknowledgments

This work was financed by the Portuguese Fundação para a Ciência e Tecnologia (FCT) through grant PTDC/BBB-BQB/3135/2014 (MT). CVR and PB acknowledge the FCT grants SFRH/BPD/94050/2013 and SFRH/BD/85106/2012, respectively. This work was further financially supported by MOSTMICRO (LISBOA-01-0145-FEDER-007660) and by iNOVA4Health (LISBOA-01-0145-FEDER-007344) Research Units funded by FCT, through national funds, and by FEDER under the PT2020 Partnership Agreement. We acknowledge the beamline staff (ID29 and ID29S) at ESRF (Grenoble, France) for the support during the synchrotron data collections.

Chapter III

Structure of mutants from *Escherichia coli* Flavodiiron-type nitric oxide reductase

This chapter is to be published in:

Patrícia T. Borges, Célia V. Romão, Filipe Folgosa, Maria C. Martins, Peter van der Linden, Maria Arménia Carrondo, Miguel Teixeira and Carlos Frazão, “Structure of mutants from *Escherichia coli* Flavodiiron-type nitric oxide reductase reveals changes in the diiron site”, manuscript under preparation.

The construction of the plasmids was performed by João B. Vicente. Patricia T. Borges performed the expression, purification, crystallization and X-ray structural characterization.

3.1 Summary

Escherichia coli flavorubredoxin catalyzes the two-electron reduction of NO to nontoxic N_2O protecting the organism from reactive nitrogen species. Recently, based on kinetic studies, it was explored the possible role for K53 and Y271 residues in modulation of substrate selectivity in *Entamoeba histolytica* FDP (O_2 reductase). Therefore, to understand the structural effects of these residues, located in the diiron second coordination sphere, crystal structures of *E. coli* FDP-ΔRd mutants were determined, namely the single mutants D52K and S262Y, as well as the double mutant D52K/S262Y, in both oxidized and reduced states.

Like in other FDPs, the minimal functional unit of *E. coli* FDP-ΔRd mutants is composed of a "head-to-tail" dimer bringing the diiron site close to the FMN cofactor from the opposing monomer. The two irons are coordinated by conserved residues, namely, a bridging aspartate, four histidines, one aspartate and one glutamate. However, some structural differences were observed in the diiron site of FDP-ΔRd S262Y in the reduced state, similarly to the oxidized state (Chapter II), probably due to a high sensitivity of this mutant to radiation damage.

For the first time, molecular tunnels were identified in this family of proteins, using krypton pressurization experiments. Both side chains of residues in positions 52 and 262 from *E. coli* FDP-ΔRd mutants are in the vicinity of the shorter pathway, however their function in substrate selectivity still needs to be further investigated.

3.2 Introduction

Flavodiiron proteins (FDPs) are widespread in the three-life domains, however they have been identified mostly in anaerobic organisms (Andersson et al., 2003; Di Matteo et al., 2008; Gonçalves et al., 2011a; Loftus et al., 2005; Peltier et al., 2010; Sarti et al., 2004; Smutna et al., 2009; Vicente et al., 2002; Vicente et al., 2008b; Vicente et al., 2012; Wasserfallen et al., 1998; Zhang et al., 2009). These proteins play an important role in the protection mechanisms against oxidative and/or nitrosative stress since they have the ability to reduce oxygen to water and/or nitric oxide to non-toxic nitrous oxide (Gardner et al., 2002; Kurtz, 2007; Romao et al., 2016a; Saraiva et al., 2004). A classification into eight classes has been proposed for this family of proteins based on the different structural domains that composed each protein (Folgosa et al.,

2018a; Saraiva et al., 2004). Besides the different classes, the flavodiiron core is shared to all FDPs, and is divided into an N-terminal metallo-β-lactamase-like domain and a C-terminal flavodoxin-like domain (Frazao et al., 2000; Vicente et al., 2008a). The first domain contains the catalytic site, a non-heme Fe-Fe center, in which the reduction of substrates occurs, while the second domain harbors a non-covalently bound FMN cofactor, which is responsible for donating electrons to the diiron site. The FDPs minimal arrangement ("head-to-tail" dimer) allows a short distance (~6 Å) between the diiron center of each monomer and the FMN moiety of the opposing monomer, thus permitting an efficient electron transfer. Moreover, two possible quaternary conformations have been identified both in solution and in crystal structures, namely homodimers or homotetramers (dimer of dimers).

The FDPs catalytic site contains iron atoms coordinated by conserved residues among different organisms, namely four histidines, two aspartates and one glutamate. A solvent bridge coordinating the two irons was assigned as a μ-hydroxo (μ-OH^-) in *E. coli* FDP structure (PDB 4D02) (Romao et al., 2016b). Most of the structural characterized FDPs show higher affinity for oxygen (Di Matteo et al., 2008; Frazao et al., 2000; Seedorf et al., 2007; Silaghi-Dumitrescu et al., 2005a), being the flavorubredoxin from *E. coli* (*Ec*FDP) the only exclusive for nitric oxide (Romao et al., 2016b). With the high conservation of the diiron first coordination sphere among FDPs, it remains to clarify the structural determinants for the different substrate specificities, oxygen *versus* nitric oxide. A comparison among model and crystal structures from FDPs with different substrate selectivities was performed. The O_2-selective FDP from *Entamoeba histolytica* (*Eh*FDP) that has homology with the O_2-selective *Giardia intestinalis* FDP (PDB 2Q9U), was compared with the NO-reducing *Ec*FDP (PDB 4D02) (Fig. 3.1). Differences were observed at two positions within the diiron second coordination sphere: K53 and Y271 in *Eh*FDP are replaced by D52 and S262 in *Ec*FDP, respectively.

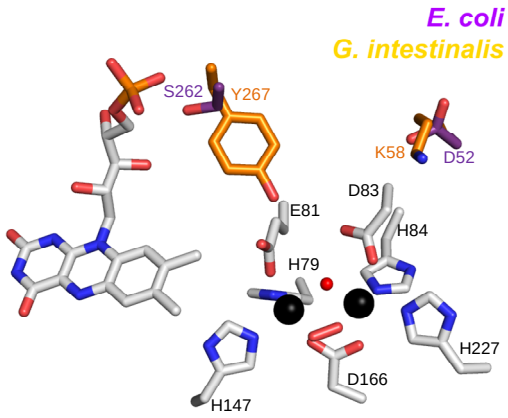

Figure 3.1- Structural comparison of residues from the second coordination sphere of the diiron center of *E. coli* FDP (NO reductase) (PDB 4D02) in purple, with *G. intestinalis* FDP (O_2 reductase) (PDB 2Q9U) in orange. The Fe atoms are shown as black spheres and the μ-hydroxo bridge as red sphere. The amino acid residues and FMN are shown with carbon, oxygen, nitrogen and phosphorous atoms as grey, red, blue and orange sticks, respectively.

In order to try to convert the EhFDP oxygen reductase into a nitric oxide reductase, single mutants K53D, Y271S and double mutant K53D/Y271S were constructed. The kinetic properties of mutants Y271S and K53D/Y271S, showed an increased affinity towards NO, and a higher sensitivity to O_2 since they became inactive after multiple turnovers conditions, relatively to the wild-type protein (Gonçalves et al., 2014). Therefore, these evidences at molecular detail suggests a possible role for Y271 residue (*Eh*FDP numbering) in modulation of substrate specificity (O_2 *vs* NO) in FDPs. On the other hand, in order to convert the NO reductase *E. coli* FDP into an O_2 reductase, its FDP-ΔRd D52K, S262Y and D52K/S262Y mutants, were produced, crystallized and their crystal structures determination pursued. Hereby, we report the 3D structures of these mutants, in order to try to elucidate the molecular mechanism behind FDPs substrate specificity.

3.3 Material and methods

Protein expression, purification and crystallization

E. coli FDP belongs to Class B but the FDP mutants are composed only by the flavodiiron core, *i.e.,* the C-terminal rubredoxin domain was deleted (FDP-ΔRd) in order to be comparable with the Class A *E. histolytica* FDP.

E. coli FDP-ΔRd mutants were generated by site-directed mutagenesis (Genscript, USA) and direct sequencing was used to ensure that the mutations were correctly inserted in the nucleotide sequence. The expression and purification conditions for all protein mutants are the same as previously described (Chapter II).

The crystallization experiment was performed as reported in Chapter II. Briefly, the crystals from the *E. coli* FDP-ΔRd mutants were obtained at 20 ºC after 2-3 days with the hanging-drop vapor diffusion method upon mixing 1 µL of protein (15 mg/mL) with 2 µL of reservoir solution containing 0.1 *M* sodium citrate pH 5.6, 20-23% w/v PEG 4000 and 23-25% v/v 2-propanol. Crystals were cryoprotected with the reservoir solution supplemented with 10% glycerol prior to flash-cooling in liquid nitrogen.

In order to obtain the crystal structures in the reduced state, an excess of sodium dithionite powder was added into a drop with cryoprotected crystals. A change in the color of the crystal from orange to colorless allows us to confirm that the protein was chemically reduced, and it was immediately flash cryo-cooled in liquid nitrogen. Crystals in the as-isolated state were considered to be oxidized, and labeled as *oxi,* while those that were chemically reduced, were labeled as *red*.

Crystal high pressurization with krypton

Krypton pressurization of *E. coli* FDP-ΔRd D52K crystals was performed in order to localize protein hydrophobic tunnels. Crystals were harvested with a specific pluggable sample support and transferred into a recently developed high-pressure cooling system at ESRF (van der Linden et al., 2014). After 5 min of pressurization under krypton gas at 100 bar, the krypton-containing crystals were directly flash cooled, depressurized and transferred into cryocaps under liquid nitrogen for data collection. The crystal pressurized with krypton from *E. coli* FDP-ΔRd D52K was labelled as *Kr.*

X-ray diffraction, crystal structure determination and refinement

Diffraction data of *E. coli* FDP-ΔRd mutants were measured at 100 K at synchrotron beamlines (Table 3.1). As previously described (Chapter II), mesh scan analysis was essential to obtain good quality diffracting data of *E. coli* FDP-ΔRd mutants since although spots were visible they could not be properly indexed, probably due to the multiple stacked crystals as thin plates.

Diffraction spots were indexed, integrated, scaled and the final amplitudes calculated using XDS (Kabsch, 2010). XPREP (Bruker) was used to re-index the data in space group number 5 from the initial *C2* setting into *I2*, in order to obtain the beta angle closer to 90˚, as recommended by the IUCr convention (Mighell, 2002). Data collection details and processing statistics are listed in Table 3.1.

The distribution of the Matthews coefficient (Kantardjieff and Rupp, 2003; Matthews, 1968) indicated a high probability of two *E. coli* FDP-ΔRd molecules in the asymmetric unit. As all the present *E. coli* FDP-ΔRd mutants were isomorphous with the S262Y$_{oxi}$ crystal (Chapter II), in each mutant, the two monomers in the asymmetric unit were refined with PHENIX.REFINE (Adams et al., 2010a; Afonine et al., 2012; Terwilliger et al., 2008) using an initial rigid-body refinement followed by refinement of atomic positions, isotropic atomic displacement parameters (*a.d.p.*s) and domains of translation, libration and screw refinement of anisotropic *a.d.p.s* (TLS), which had been previously defined with the TLSMD server (http://skuld.bmsc.washington.edu/~tlsmd) (Painter and Merritt, 2006). Cycles of iterative models inspection and edition against σ_A electron density maps with COOT (Emsley and Cowtan, 2004) were alternated with model refinement. Although refinement included standard stereochemistry libraries (Engh and Huber, 1991) the inter-atomic distances involving iron centers were refined without target restraints. Approximately 2% of reflections, in bins of thin-resolution shells, were randomly chosen for R_{free} monitoring. Solvent water molecules were automatically assigned from σ_A difference maps peaks neighboring hydrogen bonding acceptors/donors within 2.45-3.40 Å distances. Other solvent molecules were identified through comparison of their shapes against electron density blobs, as well as by comparing their refined *a.d.p.*s with those of neighboring atoms.

Refinement and model edition iterations were performed until R_{work} and R_{free} values converge, before calculation of the final R_{factor} using all available diffraction data.

In the last refinement cycle containing all experimental data, the weighting factors for stereochemical and atomic displacement parameters were manually set in order to obtain bonds and angles root-mean-square distances (*r.m.s.d*) similar to the ones in the previous cycle, when R_{free} was used to set the refinement strategy.
The stereochemistry of the refined structures was analyzed with MOLPROBITY (Chen et al., 2010). Refinement statistics are presented in Table 3.1. The analysis of molecular tunnels was performed with MOLE 2.0 (Sehnal et al., 2013) and PyMOL (DeLano, 2002; Schrodinger, 2010). Figures of structural models were prepared with PyMOL (DeLano, 2002; Schrodinger, 2010).

Table 3.1- Crystallographic parameters, diffraction data and refinement statistics of *E. coli* FDP-ΔRd mutants.

	D52K$_{oxi}$	**D52K$_{red}$**	**S262Y$_{red}$**	**D52K/S262Y$_{oxi}$**	**D52K/S262Y$_{red}$**	**D52K$_{Kr}$**
Data collection statistics						
Beamline	ESRF ID-29	PETRA III P14	ESRF ID-29	ESRF ID-23.2	ESRF ID-23.2	ESRF ID-23.1
Wavelength (Å)	0.9762	0.9763	0.9762	0.8726	0.8726	0.9724
Space group	*I2*	*I2*	*I2*	*I2*	*I2*	*I2*
Unit cell parameters (Å)	*a* = 89.1, *b* = 64.1, *c* = 146.7, *β* = 91.16°	*a* = 88.9, *b* = 64.9, *c* = 146.7, *β* = 91.53°	*a* = 89.2, *b* = 64.2, *c* = 146.6, *β* = 91.04°	*a* = 89.1, *b* = 64.9, *c* = 147.3, *β* = 91.60°	*a* = 89.6, *b* = 64.7, *c* = 147.9, *β* = 91.42°	*a* = 89.1, *b* = 64.1, *c* = 146.7, *β* = 91.16°
Resolution (Å)	76.81-1.98 (2.07-1.98)	75.18-1.95 (2.05-1.95)	76.80-1.90 (2.00-1.90)	75.39-2.54 (2.64-2.54)	77.44-2.20 (2.29-2.20)	52.33-2.20 (2.30-2.20)
Number of observations	193300 (29494)	137447 (20721)	221835 (35709)	114331 (16785)	217362 (32264)	107641 (17131)
Unique reflections	56529 (8571)	60345 (8881)	65086 (10367)	27589 (4039)	42726 (6547)	41495 (6564)
Completeness (%)	95.9 (90.5)	98.2 (89.3)	98.7 (97.9)	97.8 (89.3)	98.7 (94.1)	96.2 (94.5)
Multiplicity	3.4 (3.4)	2.3 (2.3)	3.4 (3.4)	4.1 (4.1)	5.1 (4.9)	2.6 (2.6)
Mosaicity (°)	0.2	0.2	0.2	0.4	0.2	0.3
$CC_{1/2}$ (%)[a]	98.7 (67.0)	96.9 (69.2)	99.1 (63.8)	97.9 (52.8)	98.4 (58.5)	98.7 (74.5)
R_{sym} (%)[b]	13.8 (53.5)	12.5 (53.6)	12.9 (48.6)	20.0 (67.3)	19.5 (67.5)	12.9 (43.5)
R_{meas} (%)[c]	18.3 (96.7)	17.1 (70.5)	16.1 (68.8)	26.3 (129.1)	25.0 (119.2)	18.0 (72.6)
R_{pim} (%)[d]	8.8 (33.6)	8.3 (35.7)	8.2 (30.5)	11.1 (37.2)	9.5 (32.6)	9.3 (30.5)
<I/σ(I)>	5.8 (1.7)	5.5 (1.4)	6.9 (1.9)	5.2 (1.2)	6.3 (1.3)	5.7 (1.8)
Wilson B-factor (Å^2)	24	19	19	35	24	22
V_M (Å^3 Da^{-1})	2.28	2.30	2.28	2.31	2.33	2.28
Estimated solvent content (%)	45.9	46.5	46.1	46.8	47.2	45.9
Refinement statistics						
R_{factor} (%)[e]	20.5	18.7	18.5	20.7	19.2	23.7
R_{work} (%)[f]	21.4	20.1	19.6	22.0	20.9	25.4
R_{free} (%)[f]	24.0	24.0	22.4	23.7	26.2	29.5
rmsd for bond lengths (Å)	0.010	0.009	0.013	0.012	0.008	0.013
rmsd for bond angles (°)	0.580	0.650	0.695	0.405	0.561	0.572
Average chain B-factor (Å^2)	27, 29	20, 23	21, 23	35, 36	27, 29	26, 28
Number of residues	401	400	400	400	400	400
Number of solvent waters	518	725	791	122	365	381
Ramachandran plot						
Residues in favored regions (%)	96.2	97.8	96.4	96.7	97.5	97.9
Residues in allowed regions (%)	3.8	2.2	3.6	3.3	2.5	2.1
Residues in disallowed regions (%)	0	0	0	0	0	0

[a] $CC_{1/2}$ = Percentage of correlation between intensities from random half-datasets (Karplus and Diederichs, 2012).
[b] $R_{sym} = \Sigma_{hkl} \Sigma_i |I_i(hkl) - \langle I(hkl)\rangle| / \Sigma_{hkl} \Sigma_i I_i(hkl)$, where $I_i(hkl)$ is the observed intensity and $\langle I(hkl)\rangle$ is the average intensity of multiple observations from symmetry-related reflections (Arndt et al., 1968).
[c] $R_{meas} = \Sigma_{hkl} [N/(N(hkl) -1)]^{1/2} \Sigma_i |I_i(hkl) - \langle I(hkl)\rangle| / \Sigma_{hkl} \Sigma_i I_i(hkl)$, where N(hkl) is the data multiplicity, $I_i(hkl)$ is the observed intensity and $\langle I(hkl)\rangle$ is the average intensity of multiple observations from symmetry-related reflections. It is an indicator of the agreement between symmetry related observations (Diederichs and Karplus, 1997).
[d] $R_{p.i.m.} = \Sigma_{hkl} [1/(N(hkl) -1)]^{1/2} \Sigma_i |I_i(hkl) - \langle I(hkl)\rangle| / \Sigma_{hkl} \Sigma_i I_i(hkl)$, where N(hkl) is the data multiplicity, $I_i(hkl)$ is the observed intensity and $\langle I(hkl)\rangle$ is the average intensity of multiple observations from symmetry-related reflections. It is an indicator of the precision of the final merged and averaged data set (Weiss, 2001).
[e] $R_{factor} = \Sigma |F_{obs} - F_{calc}| / \Sigma F_{obs}$, where F_{obs} and F_{calc} are the amplitudes of the observed and the model calculated structure factors, respectively. It is a measure of the agreement between the experimental X-ray diffraction data and the crystallographic model.
[f] R_{work} refers to the actual working data set used in refinement, while R_{free} refers to a cross validation set that is not directly used in refinement and is therefore free from refinement bias.

Calculation of absorbed X-ray doses

RADDOSE-3D (Zeldin et al., 2013) was used in order to calculate the absorbed X-ray dose by crystals using the parameter diffraction-weighted dose (DWD). The input parameters used for each crystal are reported in Table 3.2.

Table 3.2- Calculated X-rays diffraction-weighted absorbed doses for cuboid-shaped crystals (Zeldin et al., 2013).

	D52K$_{oxi}$	D52K$_{red}$	S262Y$_{red}$	D52K/S262Y$_{oxi}$	D52K/S262Y$_{red}$
Gaussian beam type with full width and half maximum (µm)	10, 10	10, 10	20, 20	10, 10	10, 10
Beam flux (photons/s)	$1.4x10^{11}$	$1.3x10^{11}$	$1.7x10^{11}$	$1.1x10^{11}$	$1.2x10^{11}$
Energy (keV)	14.2	12.7	12.7	14.2	14.2
Exposure time (s)	125.3	129.6	24.0	118.9	136.5
Dose (MGy)	7.50	6.20	0.81	6.87	9.25

3.4 Results

Structure determination and quality

Based on previous studies, it was proposed that residues located in the diiron 2nd coordination sphere would be involved in substrates selection (Gonçalves et al., 2014) (Table 3.3). Therefore, the following site-directed mutants were produced, *E. coli* FDP-ΔRd D52K, S262Y and double mutant D52K/S262Y. All mutant proteins were submitted to crystallization experiments in the as-isolated state (oxidized state), and in the chemically reduced state.

Table 3.3- Residues from the diiron second coordination sphere, that have been proposed to be involved in the substrate selectivity of FDPs.

Protein (organism)	Aminoacids		Reductase Activity
FDP (*E. histolytica*)	K53	Y271	O_2R
FDP (*G. intestinalis*)	K58	Y267	O_2R
FDP (*T. maritima*)	K58	Y264	O_2R
FDP (*M. thermoacetica*)	Y54	W263	O_2R > NOR
FDP (*D. gigas*)	K52	W263	O_2R > NOR
FDP (*E. coli*)	D52	S262	NOR

The *E. coli* FDP-ΔRd mutants crystal structures were refined at resolutions ranging from 1.9 to 2.5 Å, as presented in Table 3.1. The side chains of the mutated residues were truncated to alanine, and the refined electron density confirmed the success of the respective mutation. Each mutant polypeptide chain could be traced in the electron density within residues ranges 1-401 for FDP-ΔRd D52K$_{oxi}$, and 2-401 for the remaining mutants. The electron density enabled the localization of two Fe atoms in the crystallographic structures. The μ-hydroxo bridge was refined with full occupancy, except for the FDP-ΔRd S262Y$_{red}$ and FDP-ΔRd S262Y$_{oxi}$ (Chapter II), which was refined with occupancies within 0.42-0.53. Most of the residues are within the most favored region of the Ramachandran plot (Table 3.1).

Final models include one FMN cofactor, two iron atoms, one μ-hydroxo bridge and one dioxygen molecule. An isopropanol molecule (IPA) was found in chain B of *E. coli*

FDP-ΔRd D52K$_{red}$. The krypton pressurization experiment led to the presence of three krypton atoms in each chain of *E. coli* FDP-ΔRd D52K$_{Kr}$ mutant.

Overall structure of *E. coli* FDP-ΔRd mutants

The overall fold of the several *E. coli* FDP-ΔRd mutants in different oxidation states did not show significant differences. Although the asymmetric units of the crystals include two independent monomers, the characteristic FDPs "head-to-tail" dimer is not visible in the asymmetric unit. Nevertheless, the FDP dimer become apparent if one applies the two-fold rotation crystal symmetry, which produces for each monomer the corresponding "head-to-tail" opposing partner (Fig. 3.2A). The final set of four chains corresponds to a dimer of dimers with pseudo *222* point group symmetry (Fig. 3.2B), similar to the native FDP.

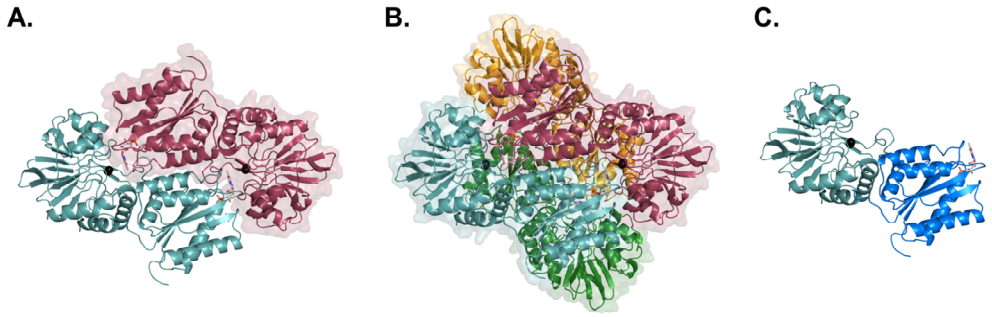

Figure 3.2- Overall structure of *E. coli* FDP-ΔRd D52K. **A**- Cartoon representation of the "head-to-tail" dimer and transparent solvent accessible surface of one of the monomers, with one chain represented as dark red and the other as cyan. **B-** Cartoon representation and transparent solvent accessible surface of the tetramer, where the chains are colored as dark red, cyan, green and orange. **C-** Cartoon representation of the monomer composed of two structural domains, a N-terminal metallo-β-lactamase-like domain (cyan) and a C-terminal flavodoxin-like domain (blue). Iron atoms are represented as black spheres and FMN is shown with carbon, oxygen, nitrogen and phosphorous atoms as grey, red, blue and orange sticks.

All *E. coli* FDP-ΔRd mutants are homotetramers in solution, as being observed by size exclusion chromatography (Fig. 3.3).

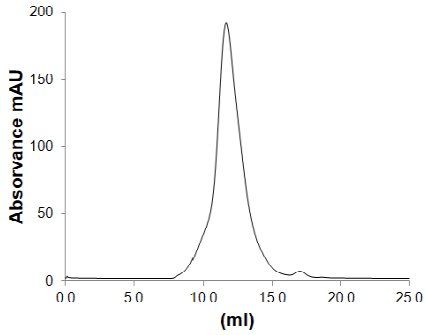

Figure 3.3- Gel filtration chromatogram showing the tetramer peak from the *E. coli* FDP D52K mutant eluted from a Superdex 200 10/300 GL column.

Superimposition of the independent molecules from *E. coli* FDP-ΔRd mutants showed low *r.m.s.d.*s between Cα atoms (0.11-0.23 Å). Their superposition with others FDPs structures (*G. intestinalis*, *T. maritima*, *M. marburgensis*, *M. thermoacetica* and *D. gigas*) showed similar three-dimensional arrangements with overall C*α r.m.s.d.*'s within 1.38-1.93 Å. Smallest *r.m.s.d.*'s values were obtained, as expected, among the *E. coli* FDP structures.

Each monomer of the *E. coli* FDP-ΔRd mutants (Fig. 3.2C) as in others FDPs, contains two structural domains: a metallo-β-lactamase-like domain, located on the N-terminal region (residues 1-246) and a flavodoxin-like domain in the C-terminal region (residues 247-401). The β-lactamase-like domain shows the αββα topology characteristic of metallo-β-lactamase-like folds, and contains a diiron site, where the reduction of O_2 or NO occurs. The flavodoxin-like domain has the αβα topology of short chain flavodoxins, and contains a non-covalently bound flavin mononucleotide (FMN), which acts as electron donor to the diiron site. Similarly to *E. coli* FDP, the binuclear site in *E. coli* FDP-ΔRd mutants, is covered by a two stranded β-sheet that blocks the access to larger substrates (such as β-lactams).

Structural features in the diiron site

The metal ligands in the *E. coli* FDP-ΔRd mutants are composed by four imidazole nitrogens and three oxygens from carboxylate residues. For the *E. coli* FDP-ΔRd mutants, Fe_p (Fe proximal to FMN), is coordinated by $E81^{OE1}$, $D166^{OD2}$, $H147^{NE2}$, $H79^{NE2}$ and Fe_d (Fe distal to FMN) is coordinated by $D83^{OD2}$, $D166^{OD1}$, $H84^{NE2}$ and

H227^{NE2} (Fig. 3.4A). This coordination is similar to the diiron coordination previously described for the *E. coli* FDP as well as others FDPs (Fig. 3.4B).

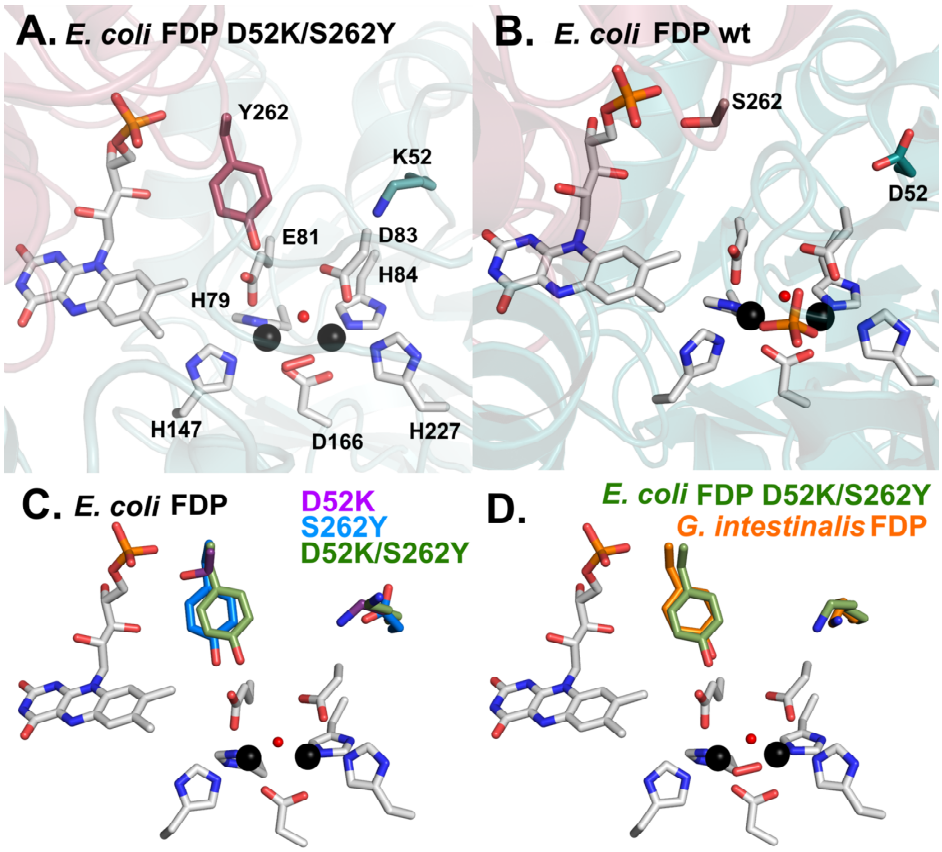

Figure 3.4- Diiron catalytic site of FDPs. **A**- Representation of the K52 and Y262 residues from the diiron second coordination sphere of *E. coli* FDP-ΔRd D52K/S262Y. Cartoon representation of the monomers, colored in dark red and in cyan. **B**- Representation of the D52 and S262 residues from the diiron second coordination sphere of *E. coli* FDP (PDB 4D02). Cartoon representation of the monomers, colored in dark red and in cyan. **C**- Superposition of the diiron second coordination sphere from *E. coli* FDP-ΔRd D52K (purple), S262Y (blue) and D52K/S262Y (green). **D**- Superposition of the diiron second coordination sphere from *E. coli* FDP-ΔRd D52K/S262Y (green) with *G. intestinalis* FDP (PDB 2Q9U) (orange). Iron atoms are represented as black spheres. The amino acid residues and FMN are shown as sticks with carbon atoms in grey, nitrogen in blue, oxygen in red and phosphorous atoms in orange. The μ-hydroxo bridge is shown as red sphere.

The inter-atomic distances that iron atoms stabilishes with metal ligands and other species are listed in Table 3.4.

Table 3.4- Distances (Å) between iron atoms and to metal ligands and neighboring oxygen molecule. Individual distances are given for the two chains.

Distance (Å)	D52K$_{oxi}$	D52K$_{red}$	S262Y$_{oxi}$	S262Y$_{red}$	D52K/S262Y $_{oxi}$	D52K/S262Y $_{red}$	D52K$_{Kr}$
Fe_p–H79^{NE2}	2.4, 2.5	2.4, 2.4	2.7, 2.9	2.4, 2.5	2.5, 2.5	2.4, 2.4	2.4, 2.4
Fe_p–E81^{OE1}	2.0, 2.0	2.1, 2.1	1.9, 1.9	1.7, 1.8	2.0, 2.0	1.9, 2.0	1.9, 1.9
Fe_p–H147^{NE2}	2.2, 2.3	2.2, 2.3	2.6, 2.8	2.4, 2.5	2.4, 2.4	2.4, 2.3	2.3, 2.4
Fe_p–D166^{OD2}	2.1, 2.1	2.0, 2.1	2.1, 2.2	2.1, 2.1	2.1, 2.2	2.0, 2.2	2.1, 2.2
Fe_p–μOH	1.8, 1.9	1.9, 2.1	2.1, 2.1	2.2, 2.4	2.0, 2.0	2.0, 2.2	1.9, 2.0
Fe_p–O_2	2.8, 3.0	3.0, [a]	3.1, 3.2	3.2, 3.3	3.0, 3.1	2.9, 3.2	3.2, [b]
Fe_d– D83^{OD2}	2.4, 2.5	2.4, 2.4	2.3, 2.3	2.4, 2.4	2.5, 2.6	2.3, 2.4	2.4, 2.5
Fe_d– H84^{NE2}	2.0, 2.1	2.0, 2.1	2.2, 2.2	2.1, 2.1	2.1, 2.2	2.0, 2.1	2.1, 2.1
Fe_d–D166^{OD1}	2.3, 2.3	2.2, 2.3	2.5, 2.7	2.3, 2.4	2.3, 2.3	2.4, 2.4	2.4, 2.5
Fe_d–H227^{NE2}	2.2, 2.2	2.1, 2.2	2.2, 2.2	2.2, 2.3	2.2, 2.1	2.1, 2.2	2.2, 2.1
Fe_d–μOH	1.9, 1.9	2.0, 2.2	1.7, 1.7	1.8, 1.8	1.7, 1.8	2.0, 2.1	1.9, 2.0
Fe_d–O_2	3.0, 3.0	2.7, [a]	2.5, 2.7	2.6, 2.9	2.8, 2.9	2.4, 2.4	3.2, [b]
Fe_p –Fe_d	3.3, 3.4	3.7, 3.7	3.6, 3.6	3.6, 3.7	3.4, 3.4	3.6, 3.6	3.4, 3.4

[a] D52K$_{red}$ chain B shows a IPA instead of O_2; [b] D52K$_{Kr}$ chain B shows a water molecule instead of O_2.

As mentioned above, two residues of the diiron site second coordination sphere, D52 and S262, were mutated into lysine and tyrosine, respectively (Fig. 3.4C). However, while D52 is located at ~8 Å from Fe_d in the same monomer, the closest S262 residue is at ~10 Å from Fe_p and belongs to the "head-to-tail" opposing monomer. The K52

and Y262 residues are in the same structural position as K58 and Y267, respectively from *G. intestinalis* (Fig. 3.4D).

Although keeping the wild type fold, both redox states from *E. coli* FDP-ΔRd S262Y crystals show electron density alterations at the diiron center and in its second coordination sphere. Thus, they present a lower electron density in residues E81-G86, which led to significantly higher *a.d.p*. values when compared with the neighbouring residues (Fig. 3.5A). Some of these residues, E81, D83 and H84, are diiron ligands, while the others, E82, A85 and G86 are located at the diiron site neighbourhood. Moreover, one observes negative m|Fo|-DFc| electron density in D83 and near Y262, in contrast to the native and all other mutant structures (Fig. 3.5B and C).

Additionally, FDP-ΔRd S262Y$_{oxi}$ mutant shows three (H79, H147 and D166) out of the seven iron ligands with significantly longer coordination distances, within 2.5-2.9 Å (Table 3.4). These longer inter-atomic distances, high *a.d.p.*s and low electron density maps were attributed to plausible radiation damage (Chapter II). Similar crystallographic inconsistences were also observed in the reduced FDP-ΔRd S262Y crystal structure, although with slightly lower significance.

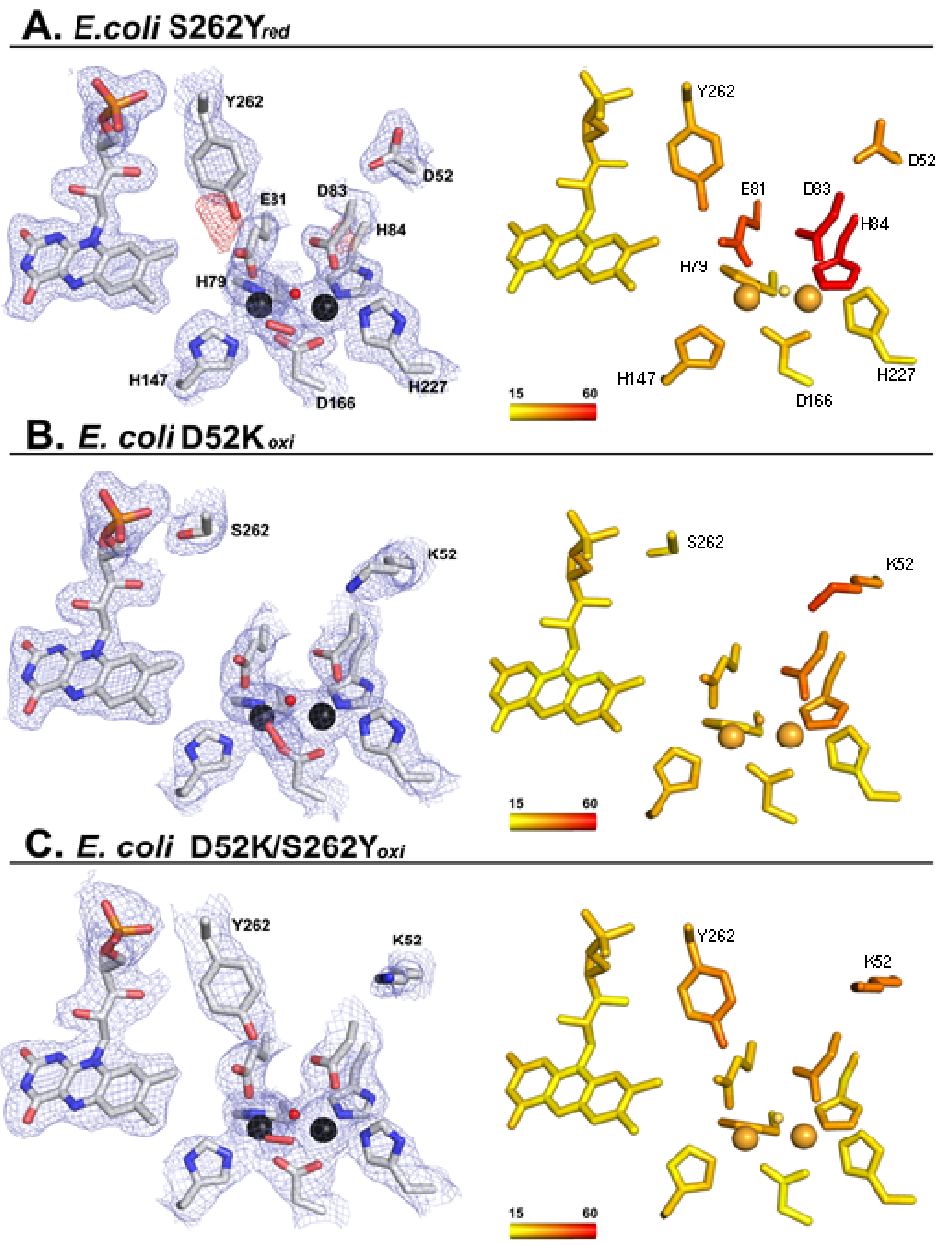

Figure 3.5- *E. coli* FDP-ΔRd mutants active site. **A, B and C left panel-** Structure representation of the diiron site and mutated residues of *E. coli* FDP-ΔRd S262Y$_{red}$, D52K$_{oxi}$ and D52K/S262Y$_{oxi}$, respectively, with map electron density 2m|Fo|-D|Fc| in blue and m|Fo|-D|Fc| in red. Iron ligands and FMN are shown as sticks with carbon atoms in grey, nitrogen in blue, oxygen in red and phosphorous atoms in orange. **A, B and C right panel** – The amino acid residues, iron atoms, solvent bridge and FMN are colored ramping from yellow to red for <*a.d.p.*>s ranging from 15 Å^2 to 60 Å^2.

In order to understand the nature of these structural changes, we estimated the absorbed dose in the several datasets. Diffraction-weighted dose (DWD) values were calculated for all crystals datasets (Table 3.2), and were clearly below the usually accepted crystallographic experimental dose limit, 30 MGy (Owen et al., 2006). Although, both D52K and D52K/S262Y crystals contain a higher absorbed dose relative to both redox states of S262Y crystals, their active site and surrounding neighborhood did not show any relevant structural changes, which suggests that the observed crystallographic anomalies may be related with the replacement of a serine by a tyrosine residue in position 262.

The FDP-ΔDP S262Y and D52K/S262Y mutants allows the introduction of a third aromatic residue (Y262) in contact with the protein exterior surface relative to the native *E. coli* FDP (Fig. 3.6). An inspection of the accessible surface area of Y262 residue in the FDP-ΔRd S262Y mutants revealed a lower value comparing with the double mutant, 9 and 25 $Å^2$, respectively. This appears to be due to a glutamate side chain (E82), located between residues at positions 52 and 262, that show different conformations in both mutants. Since, in the double mutant, the E82 side chain is more far from the Y262 side chain than in S262Y mutant, the solvent exposed area of this tyrosine is higher.

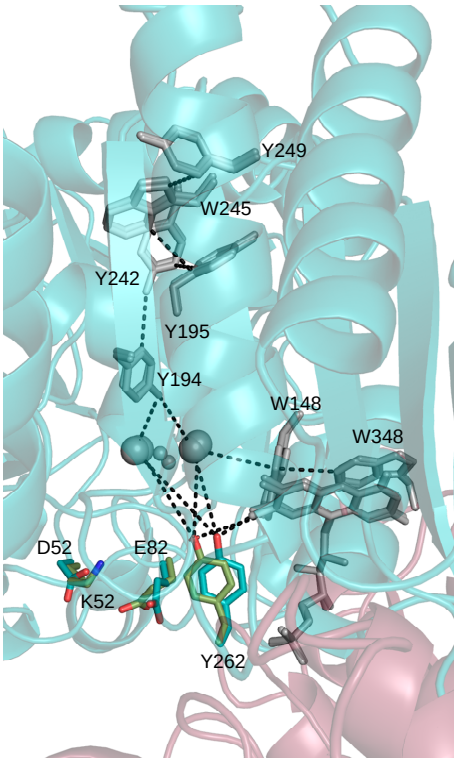

Figure 3.6- Superposition of tyrosine and tryptophan chains, from *E. coli* FDP-ΔRd S262Y and D52K/S262Y, with the shortest edge-to-edge distance (dash line) between aromatic residues from the active site to the protein solvent accessible surface. The residues in position 52, 82 and 262 are represented as sticks with carbons colored in green and blue for D52K/S262Y and S262Y mutants, respectively. One of the monomers is colored as cyan and the other opposing one as dark red. The tyrosine/tryptophan residues and FMN are represented as sticks colored in grey. The iron atoms and μ-hydroxo bridge are represented as grey spheres.

FMN binding site

As in other FDPs, the FMN cofactor in *E. coli* FDP-ΔRd mutants is located between the two monomers of the “head-to-tail” homodimer. The phosphorylated part of FMN neighbours the residues at position 262, while the tricyclic isoalloxazine ring is close to the diiron center, at van der Waals distances from the iron ligand E81. However, the FMN cofactor in both redox states of S262Y mutants structures, show a slightly longer distance to E81, when compared with the native and other mutants structures, 3.7-3.9 Å *versus* 3.4-3.5 Å, respectively.

Molecular tunnels

The molecular surface of *E. coli* FDP and its mutants, defined with a 1.4 Å rolling probe, shows one tunnel that crosses the active site pocket (Fig. 3.7). The tunnel contains the active site, where dioxygen molecules were observed in all mutant structures in oxidized and reduced forms. The active site divides the tunnel in two sections: *i)* a longer ~23 Å pathway, with diameter ~3.4-12 Å that is lined mainly by apolar atoms, and *ii)* a shorter ~9 Å pathway, with ~2.8-5.7 Å diameter that is lined with a lower fraction of apolar atoms (Fig. 3.7A). The two pathways run in opposite directions, with the longer pathway reaching the external protein surface, while the shorter pathway reaches the solvent at the hollow interior of the tetramer. In both *E. coli* FDP-ΔRd S262Y and D52K/S262Y mutants, the Y262 residue constricts an otherwise 7 Å wide side-gallery that connects the short pathway with the external surface of the protein (Fig. 3.7B).

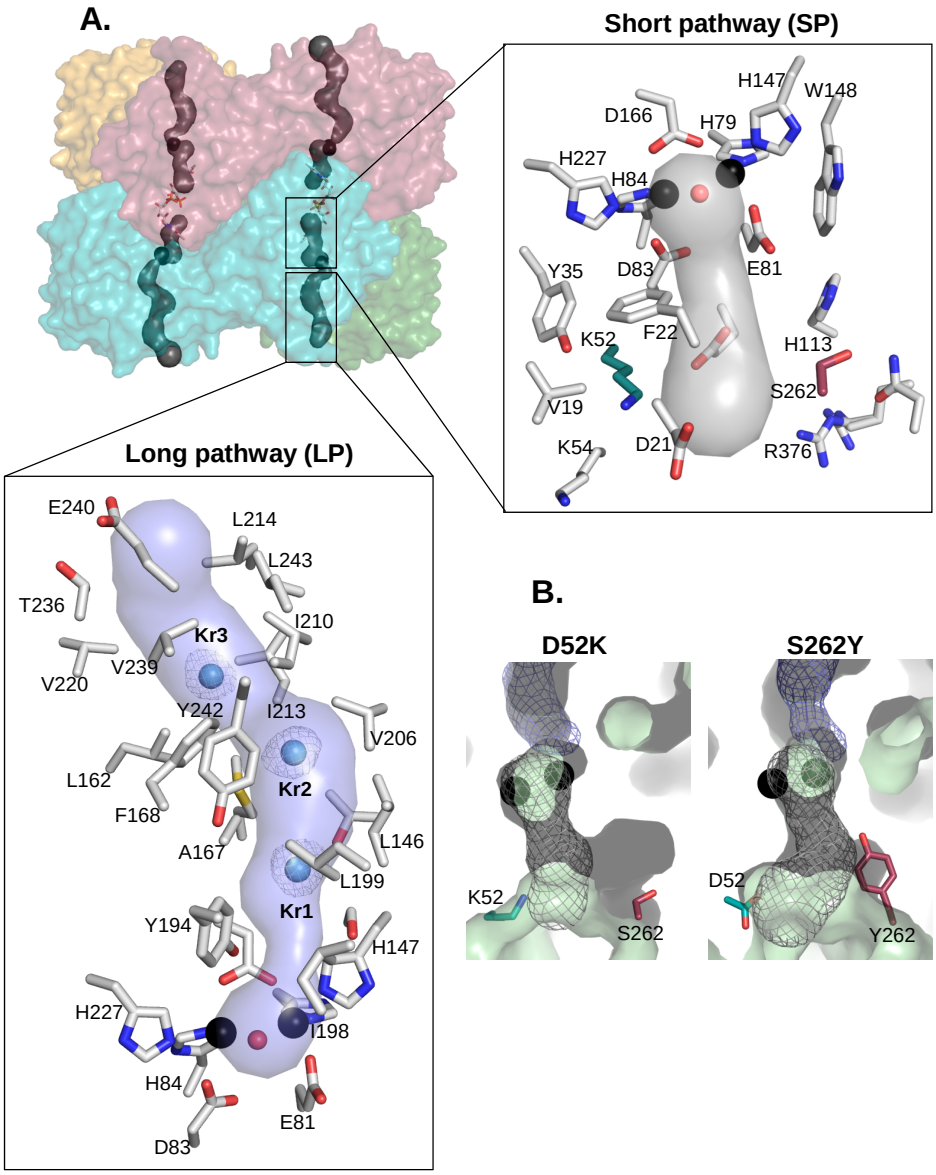

Figure 3.7- *E. coli* FDP-ΔRd D52K and S262Y molecular tunnels. **A-** *E. coli* FDP-ΔRd D52K tetramer transparent solvent accessible surface, colored as in Fig. 3.2, with both tunnel sections. The long pathway (LP), connects the external surface of the protein with the diiron catalytic site. Krypton atoms (Kr1-3) localized in LP, are shown as blue spheres and with electron density shown in grey. The short pathway (SP), is in the opposite direction of the long tunnel section, connecting the diiron site with the tetramer interior. The K52 and S262 residues are located near the SP and are shown with carbon atoms in cyan and dark red, respectively. Residues lining the SP and LP are represented by sticks with carbon atoms in grey, oxygen in red and nitrogen in blue. **B-** Long and short pathway from *E. coli* FDP-ΔRd D52K and S262Y, The residues at position 52 (cyan) and 262 (dark red) are located near the SP. The LP and SP

are shown as a blue and grey mesh, respectively.

In order to confirm the localization of the observed tunnel structures, D52K mutant crystals were pressurized with krypton gas prior to diffraction data collection. Noble gases like krypton or xenon have been used in the investigation of hydrophobic tunnels due to their hydrophobicity and high atomic numbers (Gabdulkhakov et al., 2009; Murray and Barber, 2007; Murray et al., 2008; Schiltz et al., 2003).
The similar dimensions of krypton atoms, with O_2 or NO minimal dimensions, makes this a convenient gas to locate possible O_2 and NO tunnels. In order to facilitate the diffusion of krypton gas through the crystal protein, 100 bar was used to pressurize D52K crystals, which were rapidly cryo-cooled with liquid nitrogen at 100 K ($D52K_{Kr}$). The corresponding crystal structure showed three initial putative solvent waters that were not visible in the D52K structure. These displayed significantly lower *a.d.p.*s comparing with neighbouring atoms, 3-14 $Å^2$ vs 27-46 $Å^2$, respectively, and were therefore assigned as krypton atoms (Fig. 3.7A). As the refined Kr atoms showed too high *a.d.p.* values, refinement cycles were tested by reducing successively their occupancies, until their *a.d.p.*s reached values similar to their neighboring atoms. Final Kr atoms occupancies ranged within 0.4-0.6. Atom Kr1 is located near the active site, Kr2 sits near the intermediate area of the tunnel, and Kr3 is close to the molecular outer surface.

Active site pocket

In addition to the canonical diiron metal ligands, the *E. coli* FDP active site pocket is surrounded by residues F22, H23, Y27, H171 ,Y194, I198 (Romao et al., 2016b) (Fig. 3.8). The *E. coli* FDP structures in the oxidized and reduced states differ in the presence of a phosphate or a dioxygen molecule at the sixth coordination position, respectively, while all mutant structures show a dioxygen molecule in both redox states, with exception of chain B from $D52K_{red}$, which presents an IPA molecule.

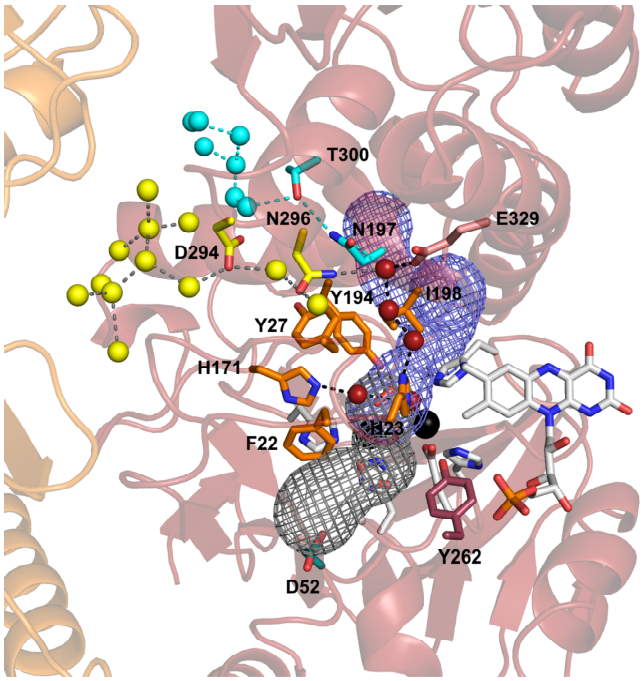

Figure 3.8- Representation of the waters chain in *E. coli* FDP-ΔRd S262Y. The residues surrounding the active site pocket are shown as sticks with carbon atoms in orange. The residues shown as sticks with carbon atoms colored in blue and yellow, represents two different waters chains. The neighbouring water molecules involved in these pathways are shown as spheres colored with the same color as the mentioned residues. The water molecules represented as red spheres represents the chain of waters from the the diiron site until the bifurcation of pathways. The D52 (green) and Y262 (dark red) residues, are located near the SP. The metal ligands and FMN are shown as sticks with carbon atoms in grey, nitrogen in blue, oxygen in red and phosphorous atoms in orange. Iron atoms are represented as black spheres. The μ-hydroxo bridge is shown as a red sphere.

The higher resolution of S262Y$_{oxi/red}$ crystal mutants allowed to identify in the active site pocket two to three water molecules, of which two of them are conserved. A chain of water molecules was observed between the active site and the protein outer surface, involving hydrogen bonds with residues H23, N296, E329 and N197, where it bifurcates either towards the tetramer interior, involving D294 residue, or towards to the outer surface with T300 residue (Fig. 3.8). These waters chains are also visible in the 1.75 Å resolution native structure and in D52K crystal mutants but not in the double mutant structures.

Conservation of histidines motif

A Blast search of flavorubredoxins (Class B FDPs), followed by their sequences alignment with the program ClustalX (Thompson et al., 1997) revealed the presence of four conserved histidines, H113-H114-H115-H116 (*E. coli* numbering), of which H113 is also conserved in *M. thermoacetica*, *D. gigas* and *M. marburgensis,* H115 is conserved in *D. gigas* and H116 is conserved in *M. thermoacetica*. A function for these four histidines has not yet been addressed. In *E. coli* FDP-ΔRd mutants, the H113 residue is located close to the short pathway, while H116 is near to the molecular surface (Fig. 3.9).

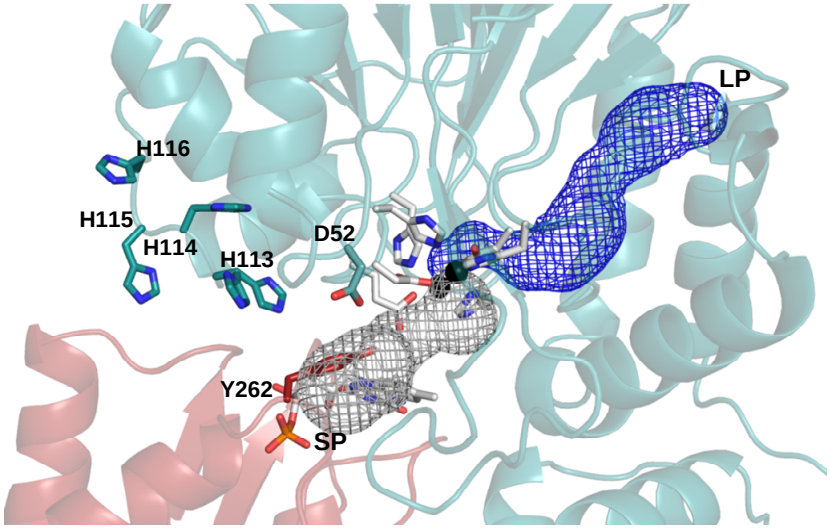

Figure 3.9- Representation of the four histidines from *E. coli* FDP-ΔRd S262Y mutant. Representation of the diiron site, D52, Y262 and H113-H116 (cyan) residues. The cartoon representation of one of the monomers is colored in dark red and the other as cyan. The long pathway (LP) and short pathway (SP) are shown as a blue and grey mesh, respectively.

3.5 Discussion

In order to try to unravel the molecular determinants that affects the *E. coli* FDP substrate selectivity, single and double mutants were produced aiming to convert this NO reductase into an O_2 reductase. The mutations rational was based on previous kinetic studies from the O_2 reductase *E. histolytica*, which had revealed that the Y271

residue from the diiron second coordination sphere had an important role in increasing the substrate preference towards nitric oxide, together with a higher sensitivity for oxygen, when compared with the wild-type protein (Gonçalves et al., 2014). Thus, crystal structures of truncated *E. coli* FDP-ΔRd single and double mutants, D52K, S262Y and D52K/S262Y (Fig. 3.4C), were determined. The residues K52 and Y262 in FDP-ΔRd double mutant, are in the same structural position when compared with the corresponding residues, K58 and Y267, of the O_2 reductase *G. intestinalis* FDP (Fig. 3.4D). All *E. coli* FDP-ΔRd mutants structures showed a homotetrameric arrangement, in agreement with the experimental results of size-exclusion chromatography. This is in agreement with the finding that, all known FDPs *in vitro* conditions were found forming homodimers or homotetramers (Di Matteo et al., 2008; Vicente et al., 2002; Wasserfallen et al., 1998).

The overall structure of the different FDP-ΔRd mutants is conserved when compared with the wild-type protein. Nevertheless some structural differences were observed in the FDP-ΔRd S262Y mutant. The most striking differences between $S262Y_{oxi/red}$ and all other structures were found in the diiron coordination region, which showed significant decreases of electron density at some residues side chains. The region within the residues E81-G86, which includes iron ligands, is highly labile and shows negative Fourier difference densities below 4σ contour level at ligand D83 and near Y262 (Fig. 3.5A). In all *E. coli* FDP-ΔRd mutants, ligands H79, H147 and D166 showed iron-coordination distances longer than those measured in the native structure, and in $S262Y_{oxi}$ these distances reached the highest values. Interestingly, a calculation of crystals diffraction-weighted dose (DWD) indicated that the $S262Y_{oxi/red}$ crystals had lower absorbed doses than the remaining mutant crystals (Table 3.2), thus suggesting that the observed structural anomalies might have resulted from a higher sensitivity of $S262Y_{oxi/red}$ to X-ray radiation. Radiation damage effects at low absorbed doses (~0.3-2 MGy) have been previously reported (Corbett et al., 2007; Holton, 2007; Olieric et al., 2007). Therefore, it seems that the single S262Y mutation has an effect on the sensitivity of the crystal to X-ray radiation, while when combined with the K52 residue (D52K/S262Y), this effect is attenuated.

As referred in Chapter II, the tyrosine/tryptophan chains are known to play a key role in protection of oxidoreductases against radicals damage, since they act as escape routes to the external protein surface (Gray and Winkler, 2015; Winkler and Gray, 2015). The *E.* coli FDP-ΔRd S262Y and D52K/S262Y mutants present a third

aromatic residue relative to native FDP that connects the diiron site with the external surface of the protein. However, the S262Y mutant shows a higher X-ray sensitivity when compared with the double mutant. This could be due to a less exposed accessible surface area of Y262 residue in the single mutant, which appears to result from the E82 residue, nearby the Y262 residue, that adopts different conformations in both mutants. The E82 residue is located between the two mutated residues present in the second coordination sphere, namely at position 52 and 262. In the S262Y mutant, E82 is closer to the Y262 residue, while in the D52K/S262Y mutant this residue becomes further apart from Y262, probably due to the presence of K52 residue. This results in a more solvent exposed tyrosine (Y262) side chain in the double mutant, which may facilitate the escape of harmful radicals.

Analysis of the wild-type protein structure in oxidized state revealed similar chains of waters between the active site and the protein outer surface (Romao et al., 2016b), as present in D52K and S262Y mutants, in both redox states. In others FDPs with known structure, it was not possible to detect equivalent water chains, even in the *M. marburgensis* FDP structure at 1.70 Å resolution.

Flavorubredoxins contain a conserved histidine-rich motif composed of four histidines (H113-H114-H115-H116, *E. coli* FDP numbering) (Fig. 3.9). Different functions have been attributed to histidine-rich regions in other proteins, *e.g.* in [NiFe] hydrogenase it was proposed to be involved in an route of protons transfer between the active center and the protein surface (Szori-Doroghazi et al., 2012). Also, the histidine-rich motif in the cactus OpsDHN1 dehydrin was proposed as a targeting element for its nuclear localization (Hernandez-Sanchez et al., 2015). However, the function of these four histidines in *E. coli* FDP has not been addressed.

The long pathway localized between the active site and the outer protein surface showed three krypton atoms upon pressurization with this gas, thus supporting previous molecular dynamic simulations that suggested this pathway to conduct the substrates to the active site (Romao et al., 2016b; Victor et al., 2009). Additionally, these studies revealed that the long pathway of *D. gigas* (O_2/NO reductase), *E. coli* (NO reductase) and *G. intestinalis* (O_2 reductase) FDPs, had similar diffusion properties and amounts of both diatomic molecules, although the set of proteins included distinct substrates selectivities (Romao et al., 2016b), which suggested that the long pathway is not involved in the selection of substrates. Additionally, a short pathway was proposed to link the active site to the tetramer interior void volume,

which showed less apolar characteristics and lower affinity to O_2 or NO molecules (Romao et al., 2016b; Victor et al., 2009). This path was proposed as a possible exit route for the reaction products. In *E. coli* FDP, the residues at positions 52 and 262 are in the vicinity of this short pathway. The Y262 residue, both in single and double mutant forms, constricts a side-gallery that connects this path with the external surface of the protein (Fig. 3.7B). Therefore, additional kinetic studies will elucidate about the possible role of this residue in *E. coli* FDP since in *E. histolytica* FDP, it was showed that apparently, this tyrosine residue has an influence in the modulation of the substrate reductase activity.

3.6 Conclusions

FDPs are a family of proteins that affords protection in Bacteria, Archaea and some Eukarya organisms, by avoiding formation of reactive oxygen and nitrogen species. Until today, the molecular determinants that affect substrate selectivity in these proteins are still unknown. However, mutations studies on the O_2-selective *E. histolytica* FDP, indicated that the Y271S mutation in the diiron second coordination sphere could have an important role in its higher preference to nitric oxide, relatively to the wild-type protein (Gonçalves et al., 2014).

In the present work, we have described several crystallographic structures of *E. coli* FDP-ΔRd mutants, both in as-isolated and in chemically reduced states. While the native *E. coli* FDP and its mutants show a similar overall fold, the S262Y mutant in particular presents significant structural differences in the diiron site region and its neighborhood. One observes a high labilization of some metal ligands side chains, longer coordination distances relative to the native *E. coli* FDP and negative Fourier difference densities in some metal ligands and neighbouring residues. These structural differences are particularly puzzling as the *E. coli* FDP-ΔRd S262Y mutation has a lower absorbed dose than either native, D52K or D52K/S262Y mutants, which suggests that the presence of K52 residue is relevant for the solvent exposed surface of Y262 and its possible role as a radicals escape route.

Krypton pressurization experiments corroborated the localization of a long pathway, previously studied by molecular dynamic simulations in other FDPs (Victor et al., 2009), which links the catalytic site with the external protein surface. The residues

lining this path are mainly hydrophobic, and it was suggested to function as a substrates entry, although the dynamic simulations studies did not related it with substrate selectivity. In the opposite side of the long pathway, a shorter and less apolar section was assigned as a probable pathway for reaction products. The mutated residue Y262 constricts a side-gallery that connects the short pathway with the external surface of the protein. Therefore, additional kinetic studies are required to unravel the influence of these diiron second coordination sphere mutations in the substrate selectivity of this family of proteins.

3.7 Acknowledgments

This work was financed by the Portuguese Fundação para a Ciência e Tecnologia (FCT) through grant PTDC/BBB-BQB/3135/2014 (MT). CVR and PB acknowledge the FCT grants SFRH/BPD/94050/2013 and SFRH/BD/85106/2012. This work was further financially supported by MOSTMICRO (LISBOA-01-0145-FEDER-007660) and by iNOVA4Health (LISBOA-01-0145-FEDER-007344) Research Units cofunded by FCT, through national funds, and by FEDER under the PT2020 Partnership Agreement. We thank the beamline staff at ESRF (Grenoble, France) and PETRA (Hamburg, Germany) for the support during the synchrotron data collections. We thank to Philipe Carpentier for being responsible by the high-throughput system for high-pressure cooling in ID-23-1 beamline from ESRF.

Chapter IV

Structural analysis of Flv1-ΔFlR protein from *Synechocystis*

This chapter is published in:

Patrícia T. Borges, Célia V. Romão, Lígia M. Saraiva, Vera L. Gonçalves, Maria A. Carrondo, Miguel Teixeira, Carlos Frazão, “Analysis of a new flavodiiron core structural arrangement in Flv1-ΔFlR protein from *Synechocystis* sp. PCC 6803”, Journal of Structural Biology, 2019, 205:91-102.

The construction of the plasmids was performed by Vera L. Gonçalves. Patricia T. Borges performed the expression, purification, crystallization and X-ray structural characterization.

4.1 Summary

Flavodiiron proteins (FDPs) play key roles in biological response mechanisms against oxygen and/or nitric oxide; in particular they are present in oxygenic phototrophs (including cyanobacteria and gymnosperms). Two conserved domains define the core of this family of proteins: a N-terminal metallo-β-lactamase-like domain followed by a C-terminal flavodoxin-like one, containing the catalytic diiron center and a FMN cofactor, respectively. Members of the FDP family may present extra modules in the C-terminus, and were classified into several classes according to their distribution and composition. The cyanobacterium Synechocystis sp. PCC 6803 contains four Class C FDPs (Flv1-4) that include at the C-terminus an additional NAD(P)H:flavin oxidoreductase (FlR) domain. Two of them (Flv3 and Flv4) have the canonical diiron ligands (Class C, Type 1), while the other two (Flv1 and Flv2) present different residues in that region (Class C, Type 2). Most phototrophs, either Bacterial or Eukaryal, contain at least two FDP genes, each encoding for one of those two types. Crystals of the Flv1 two core domains (Flv1-ΔFlR), without the C-terminal NAD(P)H:flavin oxidoreductase extension, were obtained and the structure was determined. Its pseudo diiron site contains non-canonical basic and neutral residues, and showed anion moieties, instead. The presented structure revealed for the first time the structure of the two-domain core of a Class C-Type 2 FDP.

4.2 Introduction

FDPs are a family of enzymes widespread in Bacteria, Archaea and Eukarya. These proteins provide response mechanisms to protect organisms against oxidative and nitrosative stress, reducing oxygen to water and/or nitric oxide to the non-toxic compound nitrous oxide. Some enzymes are specific for only one of the substrates, whereas others have the ability to reduce both substrates (Di Matteo et al., 2008; Gomes et al., 2002b; Hillmann et al., 2009; Kawasaki et al., 2004; Rodrigues et al., 2006; Silaghi-Dumitrescu et al., 2005a; Smutna et al., 2009; Vicente et al., 2012).

FDPs´ amino acids sequences were analysed extensively, leading to a classification according to their structural domains composition, and until now eight classes (A-H) were identified (Folgosa et al., 2018a; Romao et al., 2016a). All known FDP classes have in common the flavodiiron core (the two only domains in Class A enzymes),

which consists of a metallo-β-lactamase-like domain at the N-terminal harbouring a diiron catalytic center, linked to a flavodoxin-like domain at the C-terminal containing a non-covalently bound flavin mononucleotide (FMN). The two redox centers within the same monomer are too far away (~ 40 Å) to allow an efficient electron transfer between them. Therefore, the minimal functional unit of the FDPs that were structurally characterized until now, consists of a homodimer with a “head-to-tail” arrangement, that brings close together (~ 6 Å) the diiron center of one monomer and the FMN cofactor of the opposing neighbouring monomer (Frazao et al., 2000; Vicente et al., 2007a).

Class C FDPs have an extra C-terminal domain predicted to be similar to NAD(P)H:flavin oxidoreductases (FlR); this extra domain is able to receive electrons directly from NAD(P)H that will be transferred to the catalytic core (Vicente et al., 2002). Class C FDPs form a distinct phylogenetic cluster that includes only oxygenic photosynthetic organisms, such as cyanobacteria, green algae, lower plants (mosses and lycophytes) and higher plants (gymnosperms) (Allahverdiyeva et al., 2015b; Gerotto et al., 2016; Gonçalves et al., 2011b; Ilik et al., 2017; Peltier et al., 2010; Shimakawa et al., 2017; Zhang et al., 2009); thus far, FDPs appear to be absent in angiosperms. Moreover, Class C enzymes are the most diverse proteins of the FDP´s family, since many of them show notorious differences on the putative amino acids that are known to bind the iron ions in canonical FDPs; fifteen distinct sets of putative ligands were proposed (Gonçalves et al., 2011b). Class C-Type 1 FDPs have the canonical iron binding residues: H79-x-E81-x-D83-H84-x_{62}-H147-x_{18}-D166-x_{60}-H227 (*E. coli* FDP numbering, (Romao et al., 2016b)). Types 2-15 lack most of the canonical diiron coordination ligands, having Type 2 enzymes the second most common arrangement within Class C enzymes. In Type 2 enzymes, the following neutral and basic amino acids were proposed as putative ligands, on the basis of amino acid sequence analysis: H108-x-N110-x-N112-R113-x_{64}-H178-x_{18}-K197-x_{56}-H254 (*Synechocystis* Flv1 numbering) (Gonçalves et al., 2011b).

So far, in all cyanobacteria and photosynthetic eukaryotic organisms analysed, at least two FDP genes are present: one coding for a canonical Class C-Type 1 FDP, and a second encoding for one of the non-canonical Types identified (Gonçalves et al., 2011b). The cyanobacterium *Synechocystis* sp. PCC6803 contains four genes encoding FDPs, two Class C-Type 2, *sll1521* (Flv1) and *sll0219* (Flv2), and two Class C-Type 1, *sll0550* (Flv3), and *sll0217* (Flv4) (Helman et al., 2003). Flv1 and Flv3 were

shown to protect the photosystem I from reactive oxygen species (ROS) under fluctuating light conditions through a Mehler-like reaction (Allahverdiyeva et al., 2013; Helman et al., 2003). On the other hand, Flv2 and Flv4 were proposed to protect photosystem II against photo inhibition (Bersanini et al., 2014; Zhang et al., 2009; Zhang et al., 2012). Quite importantly, recently, expression of the moss *Physcomitrella patens* FDPs in the model plant *Arabidopsis thaliana* (Yamamoto et al., 2016) or in rice species (*Oryza sativa*) (Wada et al., 2018), which are both angiosperms and therefore lack FDPs, increased the protection of photosystem II under fluctuating light conditions. Also, expression of cyanobacterial FDPs in chloroplasts from tobacco plants (*Nicotiana tabacum*) had the same effect in photosynthesis (Gomez et al., 2018). Furthermore, FDP deletion strains of the green algae *Chlamydomonas reinhardtii* and of the moss *Physcomitrella patens* showed increased damage of photosystem I and reduced growth under fluctuating light (Chaux et al., 2017; Gerotto et al., 2016). Therefore, Class C FDPs appear as key players in photosynthetic organisms, functioning as electron sinks (safety valves) and avoiding the formation of ROS. The induction of Flv1-4 gene expression upon 12 h of exposure to S-nitrosoglutathione demonstrated that *Synechocystis* FDPs also have a role associated with nitrosative stress defences (Gonçalves et al., 2011a). So far, Flv3 from *Synechocystis* is the only Class C FDP that has been biochemically studied. The protein presents oxygen reductase activity *in vitro*, and two oligomeric forms, homotetramer or homodimer, were identified in solution (Mustila et al., 2016; Vicente et al., 2002).

Most of the FDPs whose crystallographic structures are deposited in the Protein Data Bank (PDB) belong to Class A, thus being composed of the flavodiiron core only. Additionally, the crystal structure of a Class B FDP from *E. coli,* that has an extra rubredoxin domain was also determined (Romao et al., 2016b). For Class C FDPs only two partial structures from enzymes of the cyanobacterium *Anabaena* sp. PCC7120 are available, each including only one of the two flavodiiron core structural domains: the metallo-β-lactamase-like domain from *Anabaena* FDP-Type 3 (All0177, PDB 4FEK), that was crystallized without metal ions, and the flavodoxin-like domain from *Anabaena* FDP -Type 1 (All3895, PDB 3FNI), obtained without the FMN cofactor. To fully understand the function of Class C FDPs in photosynthetic organisms, it is essential to have their three dimensional structures. Here, we took a first step towards this goal, by determining for the first time a Class C-Type 2 FDP crystal structure,

namely that of the cyanobacterium *Synechocystis* sp. PCC6803 Flv1 truncated from its NAD(P)H:flavin oxidoreductase-like domain (Flv1-ΔFlR), therefore containing only the flavodiiron core. This specific enzyme was chosen since Flv1 is a member of the most common Class C FDPs that lack the canonical diiron amino acid ligands.

4.3 Materials and methods

Protein expression and purification

Synechocystis sp. PCC6803 Flv1 was expressed with only the FDP core, designated as Flv1-ΔFlR, since the trials for the expression of the full length protein done under multiple conditions led systematically to accumulation of the protein in inclusion bodies. Additionally, the first 25 residues that constitute a putative signal peptide, were also not included in the recombinant protein. Therefore, the *Synechocystis* gene encoding Flv1-ΔFlR (residues 26-431) was cloned into pET24a+ (Novagen) to generate the recombinant plasmid pFlv1_core. *Escherichia coli* BL21-Gold (DE3) cells (Stratagene) transformed with pFlv1_core were grown in minimal medium (M9) supplemented with 30 µg/mL kanamycin and enriched with 100 µM $FeSO_4.7H_2O$, at 28ºC and 140 rpm. When cells reached an optical density at 600 nm of 0.4, 100 µM of isopropyl-β-D-thiogalactopyranoside (IPTG) was added. After 7 h of induction, cells were harvested by centrifugation at 10,000g for 10 minutes, at 4 ºC. The harvested cells were then resuspended in 20 mM Tris-HCl pH 7.5 and disrupted in a French press at 1000 psi. After ultracentrifugation at 100,000g for 1 h, at 4 °C, the soluble fraction was collected and dialysed overnight at 4 ºC against 20 mM Tris-HCl pH 7.5 and 2.5 % of glycerol.

Flv1-ΔFlR was purified in two steps using an AKTA prime system (GE Healthcare), at 4 ºC. The soluble fraction was loaded onto an anionic Q-Sepharose Fast Flow column (XK 26/40; GE Healthcare), equilibrated with 20 mM Tris-HCl pH 7.5 with 5% glycerol (buffer A). A salt gradient was applied up to 1 M NaCl in buffer A. The fraction containing Flv1-ΔFlR was eluted with 350 mM NaCl and concentrated by ultra filtration (Centricon, Vivaspin, 30 kDa cutoff). The UV-Visible spectrum of this fraction revealed the typical flavin fingerprint, with absorption bands at 375 nm and 446.5 nm. Finally, this fraction was loaded onto a Superdex 200 column (XK 26/60 GE Healthcare) previously equilibrated with buffer A with 150 mM NaCl and 5% glycerol. Fractions containing Flv1-ΔFlR, were analyzed and those judged to be pure on the basis of

SDS–PAGE were used for the further studies. The N-terminal of the pure protein was sequenced, confirming that the correct protein had been expressed and purified. The pure protein mainly eluted as a monomer, and a minor dimeric form was also detected. Nevertheless, none of the purified proteins showed the flavin UV-visible fingerprint, indicating that the protein was deflavinated in both oligomeric states. The protein concentration and total iron content were determined using the bicinchoninic acid protein assay (Pierce) (Walker, 1994) and the 2, 4, 6-tripyridyl-S-triazine method (Fischer and Price, 1964), respectively. The flavin was quantified using the acid extraction protocol (Susin et al., 1993). The final protein sample was concentrated up to 15 mg/mL, and lacked both iron and flavin. The incorporation of both cofactors was attempted by incubating anaerobically the protein with iron (ammonium iron(II) sulfate) and FMN, in a 5 molar excess, from 15 to 60 min at 37ºC. To remove the excess iron and FMN, the solution was loaded into a Superdex-200 column equilibrated with 20 mM Tris-HCl pH 7.5, 150 mM NaCl and 5% glycerol. However, despite several attempts, the incorporation of both cofactors remained unsuccessful.

Differential scanning fluorimetry assay

Differential scanning fluorimetry (DSF), also known as thermofluor (Ericsson et al., 2006; Niesen et al., 2007), was used to determine the Flv1-ΔFlR thermal stability. The thermal shift assay was performed as previously described (Santos et al., 2012), using a buffer screening with 100 mM of concentration, in the pH range 3–10, three NaCl concentrations (0, 150 and 500 mM), and 150 mM KCl. The control buffer condition was 100 mM Tris-HCl pH 7.5, 150 mM NaCl, which was the buffer used for the protein purification. The buffer condition 100 mM MOPS pH 7 and 500 mM NaCl, induced the highest melting temperature (shift from 54ºC to 58ºC). Afterwards, a buffer exchange was performed using the Superdex 200 column (XK 26/60 GE Healthcare) with the optimized buffer 50 mM MOPS pH 7, 500 mM NaCl and 5% glycerol. The purified protein has properties similar to those described above, in which the majority of the Flv1-ΔFlR in solution was a monomer, with only a minor fraction of the dimer. Dimer and monomer fractions were collected separately, concentrated up to 15 mg/ml and used for crystallization trials.

Crystallization, cofactors crystals soaking and cryoprotection

Nanolitre-scale crystallization screens were performed at 20ºC with commercial kit Structure Screen 1 and 2 (Molecular Dimensions). Drops were dispensed by a Cartesian Crystallization Robot Dispensing System (Genomics Solutions) on round-bottom Greiner 96-well CrystalQuick^{TM} plates (Greiner Bio-One). Since no crystals were obtained when using the purified protein solution, the protein in the DSF optimized buffer, 50 mM MOPS pH 7 and 500 mM NaCl plus 5% glycerol, was used instead. For the screening of the best conditions, 0.1 µl of protein (15 mg/mL) was mixed with 0.1 µl of precipitant solution and equilibrated by vapor diffusion against 40 µl of the reservoir solution. Crystals appeared within three days in 0.2 M ammonium acetate, 0.1 M tri-sodium citrate pH 5.6 and 30% (w/v) PEG 4000. Optimization trials proceeded at microliter-scale using hanging drops in vapor diffusion with 500 µL reservoir solution, using XRL 24-well crystallization plates (Molecular Dimensions). Several parameters were optimized, such as temperature, precipitant concentration and protein:reservoir proportion. The best Flv1-ΔFlR crystals were obtained by mixing 1 µl of protein (15 mg/ml in 50 mM MOPS pH 7 and 500 mM NaCl plus 5% glycerol) with 1 µl of 0.2 M ammonium acetate, 0.1 M tri-sodium citrate pH 5.6, and 23-25% (w/v) PEG 4000, at 20ºC. Incorporation of metal and FMN was also attempted by soaking crystals with a solution of iron (ammonium iron(II) sulfate), FMN, and iron and FMN, and zinc sulfate using different times of incubation. But as it happened for the solution experiments, the crystal´s soaking was also ineffective.

Finally, crystals were cryo-protected using the reservoir solution supplemented with 25% glycerol, and flash-cooled in liquid nitrogen.

Data collection and processing

All X-ray diffraction measurements were performed under a nitrogen stream at 100 K. A first *in-house* data set (named Flv1-ΔFlR$_{in\text{-}house}$) was collected using *Cu* K-alpha radiation with 1.5418 Å wavelength in a Bruker AXS Proteum Pt135 CCD detector system coupled to a Microstar-I rotating-anode X-ray generator with Montel mirrors. Images were processed with SAINT and scaled with SADABS, as part of the Bruker AXS Proteum software suite. The quality of the diffraction data was analyzed with XPREP (Bruker AXS).

Diffraction data at higher resolution were measured in ID30B (McCarthy et al., 2018) and ID30A-3 (Theveneau et al., 2013) beamlines at the European Synchrotron

Radiation Facility (ESRF, Grenoble, France) for crystals of Flv1-ΔFlR and Flv1-ΔFlR soaked with iron sulfate (named Flv1-ΔFlR$_{soaked}$), respectively. Diffraction images of Flv1-ΔFlR were obtained with a PILATUS detector, radiation wavelength 0.9762 Å, crystal-to-detector distance 292 mm and oscillations width 0.10º, in a total of 140º rotation during 28 s. The diffraction data of Flv1-ΔFlR$_{soaked}$ were obtained with an EIGER detector, radiation wavelength 0.9762 Å, crystal-to-detector distance 127 mm and oscillations width 0.10º in a total of 230º rotation during 23 s. Diffraction spots were indexed, integrated and scaled, and the final amplitudes calculated using XDS (Kabsch, 2010). Data collection details and processing statistics are listed in Table 4.1.

Structure determination, refinement and analysis

An estimation of the unit cell contents indicated one molecule in the asymmetric unit (Kantardjieff and Rupp, 2003; Matthews, 1968). Molecular replacement (MR) trials of Flv1-ΔFlR$_{in\text{-}house}$ with PHASER (Mccoy et al., 2007b) within the PHENIX suite (Adams et al., 2010a) using canonical FDP dimers or monomers as target structures, were systematically unsuccessful. However, the MR solution was readily obtained when the β-lactamase and flavodoxin-like domains were searched separately. *Anabaena* sp. PCC7120 (PDB 4FEK) β-lactamase-like domain, with 45% amino acid sequence identity with *Synechocystis* Flv1, and *Moorella thermoacetica* FDP (PDB 1YCF) flavodoxin-like domain, with 18% amino acid identity with *Synechocystis* Flv1, led to the initial MR with TFZ (lactamase-like domain) =12.5 and TFZ (flavodoxin-like domain) =12.4. The Flv1-ΔFlR$_{in\text{-}house}$ sequence was edited into the MR model followed by iterative refinement with PHENIX.REFINE (Adams et al., 2010a; Afonine et al., 2012; Terwilliger et al., 2008) and manual correction and completion of the model, upon examination of 2m|Fo|-D|Fc| and m|Fo|-D|Fc| electron density maps with COOT (Emsley and Cowtan, 2004). When the two higher resolution data sets, Flv1-ΔFlR and Flv1-ΔFlR$_{soaked}$, became available the *in-house* model was submitted to preliminary rigid-body refinement cycles followed by iterative refinement and manual model edition with each data set. Refinement included atomic positions, isotropic atomic displacement parameters (*a.d.p.*s) as well as polypeptide chain regions of translation, libration and screw refinement of anisotropic *a.d.p.*s, which were defined with the TLSMD server (http://skuld.bmsc.washington.edu/~tlsmd) (Painter and Merritt, 2006).

Standard stereochemistry libraries was used for peptides (Engh and Huber, 1991). A random set of 1.5% of the reflections were excluded from the calculations to monitor the refinement strategy. Water solvent molecules were assigned automatically from m|Fo|-D|Fc| difference maps peaks neighboring hydrogen bonding acceptors or donors within 2.45-3.40 Å distances, but only kept if their *a.d.p.*s refined to values lower than 60 $Å^2$. Other solvent anions from the protein or crystallization solutions were assigned based also on reasonable fit of their shapes to electron density blobs, polar interaction distances and a comparative analysis of their *a.d.p.*s with the neighbouring atoms. Refinement and model edition iterations proceeded until convergence of R_{free} and R_{work}, when a final cycle of refinement was produced including all available data to define the final models and their R_{factor}. In the last refinement cycle containing all experimental data, the weighting factors for stereochemical and atomic displacement parameters were manually set in order to obtain bonds and angles root-mean-square distances (*r.m.s.d*.) similar to those of the previous cycle, when R_{free} was used to set the refinement strategy. The final structures stereochemistry was analyzed with MOLPROBITY (Chen et al., 2010). The refinement statistics are presented in Table 4.1.

Three dimensional superposition of poly-peptide chains was performed with MODELLER (Webb and Sali, 2014). The domains movements were determined by the DynDom program (Hayward and Berendsen, 1998; Hayward et al., 1997). The analysis of molecular tunnels was performed with MOLE 2.0 (Sehnal et al., 2013) and PyMOL (DeLano, 2002; Schrodinger, 2010). Figures of structural models were prepared with COOT (Emsley et al., 2010) and PyMOL (DeLano, 2002; Schrodinger, 2010).

Structure factors and associated structure coordinates of *Synechocystis* Flv1-ΔFlR and Flv1-ΔFlR_{soaked} were deposited in the Protein Data Bank (www.rcsb.org) (Berman et al., 2000) with PDB codes 6H0C and 6H0D, respectively.

Table 4.1- Crystallographic parameters, diffraction data and refinement statistics of *Synechocystis* Flv1-ΔFlR and Flv1-ΔFlR$_{soaked}$. Values in parentheses correspond to the highest resolution shell.

	Flv1-ΔFlR	Flv1-ΔFlR$_{soaked}$
Data collection statistics		
Beamline	ID30B	ID30A-3
Wavelength (Å)	0.9762	0.9762
Space group	*C*2	*C*2
Unit cell parameters (Å)	*a* = 76.9, *b* = 87.8, *c* = 70.7, *β* = 100.94°	*a* = 76.8, *b* = 86.9, *c* = 72.1, *β* = 102.07°
Resolution (Å)	57.23-1.59 (1.70-1.59)	56.84-1.60 (1.70-1.60)
Number of observations	155331 (24205)	125072 (19354)
Unique reflections	58593 (9444)	58008 (9234)
Completeness (%)	95.9 (96.1)	94.7 (93.7)
Multiplicity	2.6 (2.6)	2.2 (2.1)
Mosaicity (°)	0.14	0.15
$CC_{1/2}$ (%)[a]	99.9 (65.2)	99.7 (56.7)
R_{sym} (%)[b]	3.1 (40.6)	4.1 (54.0)
R_{meas} (%)[c]	3.9 (67.5)	5.5 (75.5)
R_{pim} (%)[d]	2.2 (30.2)	3.2 (42.6)
<I/σ(I)>	15.1 (1.7)	13.4 (1.4)
Wilson B-factor (Å^2)	26	29
V_M (Å^3 Da^{-1})	2.60	2.52
Estimated solvent content (%)	52.8	51.2
Refinement statistics		
R_{factor} (%)[e]	14.8	15.9
R_{work} (%)[f]	15.3	16.5
R_{free} (%)[f]	19.8	20.6
r.m.s.d. for bond lengths (Å)	0.006	0.011
r.m.s.d. for bond angles (°)	0.923	1.296
Chain <*a.d.p.*> (Å^2)	34	39
Number of residues	405	402
Number of solvent waters	344	200
Number of solvent ions	1, 1,-	1,-,2
Residues in favored, allowed and disallowed regions of the Ramachandran plot (%)	98.8, 1.2, 0	98.0, 2.0, 0
PDB code	6H0C	6H0D

[a] $CC_{1/2}$ = Correlation coefficient between intensities from random half-datasets (Karplus and Diederichs, 2012).

[b] $R_{sym} = \Sigma_{hkl} \Sigma_i |I_i(hkl) - \langle I(hkl)\rangle| / \Sigma_{hkl} \Sigma_i I_i(hkl)$, where $I_i(hkl)$ is the observed intensity and $\langle I(hkl)\rangle$ is the average intensity of multiple observations from symmetry-related reflections (Arndt et al., 1968).

[c] $R_{meas} = \Sigma_{hkl} [N/(N(hkl) -1)]^{1/2} \Sigma_i |I_i(hkl) - \langle I(hkl)\rangle| / \Sigma_{hkl} \Sigma_i I_i(hkl)$, where N(hkl) is the data multiplicity, $I_i(hkl)$ is the observed intensity and $\langle I(hkl)\rangle$ is the average intensity of multiple observations from symmetry-related reflections. It is an indicator of the agreement between symmetry related observations (Diederichs and Karplus, 1997).

[d] $R_{p.i.m.} = \Sigma_{hkl} [1/(N(hkl) -1)]^{1/2} \Sigma_i |I_i(hkl) - \langle I(hkl)\rangle| / \Sigma_{hkl} \Sigma_i I_i(hkl)$, where N(hkl) is the data multiplicity, $I_i(hkl)$ is the observed intensity and $\langle I(hkl)\rangle$ is the average intensity of multiple observations from symmetry-related reflections. It is an indicator of the precision of the final merged and averaged data set (Weiss, 2001).

[e] $R_{factor} = \Sigma |F_{obs} - F_{calc}| / \Sigma F_{obs}$, where F_{obs} and F_{calc} are the amplitudes of the observed and the model calculated structure factors, respectively. It is a measure of the agreement between the experimental X-ray diffraction data and the crystallographic model.

[f] R_{work} refers to the actual working data set used in refinement, while R_{free} refers to a cross validation set that is not directly used in refinement and is therefore free from refinement bias.

4.4 Results

Structure determination and quality

Due to the insolubility of the full length *Synechocystis* Flv1, a truncated protein that only contained the FDP core, *i.e.*, the β-lactamase and flavodoxin-like domains, was produced. Additionally, the first 25 residues that are predicted to constitute a signal peptide sequence protein were also excluded. Therefore, the recombinant Flv1-ΔFlR contained residues 26-431, and in the purified state exhibited two oligomeric forms, namely a major monomeric and a minor dimeric forms.

Initial crystallization trials using the two different protein forms were unsuccessful. However, when using the Flv1-ΔFlR monomeric form optimized by the DSF assay, colourless polyhedric crystals were obtained within 2-3 days that reached 120, 50 and 30 µm dimensions. An initial diffraction dataset was collected *in-house* at 2.5 Å resolution (Flv1-ΔFlR$_{in\text{-}house}$) and the structure determined by molecular replacement.

In order to attempt the incorporation of the cofactors, crystals were soaked in the reservoir solution containing FMN, iron or both.

Crystal's diffraction data, from native (Flv1-ΔFlR) and soaked crystals (Flv1-ΔFlR_{soaked}), were collected with synchrotron radiation. Here, we present the highest resolution diffraction structures, from native and soaked crystals (with iron sulfate solution), Flv1-ΔFlR and Flv1-ΔFlR_{soaked} respectively. These structures were obtained at 1.59 Å and 1.60 Å resolutions and refined to final $R_{factors}$ of 0.148 and 0.159, respectively (Table 4.1).

The native structure showed lower averaged atomic displacement parameters (<*a.d.p.*>'s) when compared with the soaked protein crystal, which correlates with their overall B values from the Wilson plot (Table 4.1). Both structures contained only one molecule in the asymmetric unit. The structures were traced in 1.0 σ contour levels electron density maps for residues 26 through 431 for the Flv1-ΔFlR, and residues 26 through 428 for the Flv1-ΔFlR_{soaked}. Structural solvent analysis led to assignment of mother liquor water molecules and chloride, citrate, and sulfate anions (Table 4.1). No metals (Fe or Zn) or FMN cofactors were ever detected in any of the analysed crystals, in concordance with the chemical and spectroscopic data of the purified protein in solution. Flv1-ΔFlR was expected to contain FMN, due to the overall similarity of the flavin domain of Flv1-ΔFlR with those from canonical FDPs, namely with Flv3 from *Synechocystis* (Vicente et al., 2002; Wasserfallen et al., 1998). However, *Thermotoga maritima* FDP was isolated in an almost fully deflavinated form and crystalized without the FMN cofactor (PDB 1VME) (Hayashi et al., 2010).

Flv1-ΔFlR overall structure

The superposition of the two crystal structures, Flv1-ΔFlR and Flv1-ΔFlR_{soaked}, led to C-alpha atoms *r.m.s.d.*s of 0.35 Å. Their β-lactamase and flavodoxin-like domains showed high structural similarity with the ones in the available FDP´s structures, with the β-lactamase-like domain within 1.2-1.9 Å *r.m.s.d.*s and the flavodoxin-like domain within 1.3-2.4 Å *r.m.s.d.*s (Table 4.2).

Table 4.2- Representation of *r.m.s.d.*'s Cα superposition (Å) of the β-lactamase-like and flavodoxin-like domains of FDPs with *Synechocystis* Flv1-ΔFlR and Flv1-ΔFlR$_{soaked}$.

	Class	β-lactamase-like domain	flavodoxin-like domain	PDB
D. gigas	A	1.7	1.4	1E5D
G. intestinalis	A	1.7	1.3	2Q9U
M. marburgensis	A	1.9	1.4	2OHH
T. maritima	A	1.8	2.4	1VME
M. thermoacetica	A	1.6	1.4	1YCF
E. coli	B	1.7	1.5	4D02
Anabaena	C-Type 3	1.2	--	4FEK
Anabaena	C-Type 1	--	1.9	3FNI

The Flv1-ΔFlR metallo-β-lactamase-like domain (residues 26-278) shows the predicted αββα sandwich fold, where the first β-sheet is composed of seven strands, an anti-parallel segment with strands β_1-β_4 followed by a parallel segment with strands β_4-β_7, and the second β-sheet composed of five strands, an anti-parallel segment with strands β_8-β_{11} followed by a parallel segment with strands β_{11}-β_{12} (Fig. 4.1A and B). The two β-sheets are surrounded by eight α-helices, α_1-α_5 close to the first β-sheet and α_6-α_8 near the second β-sheet.

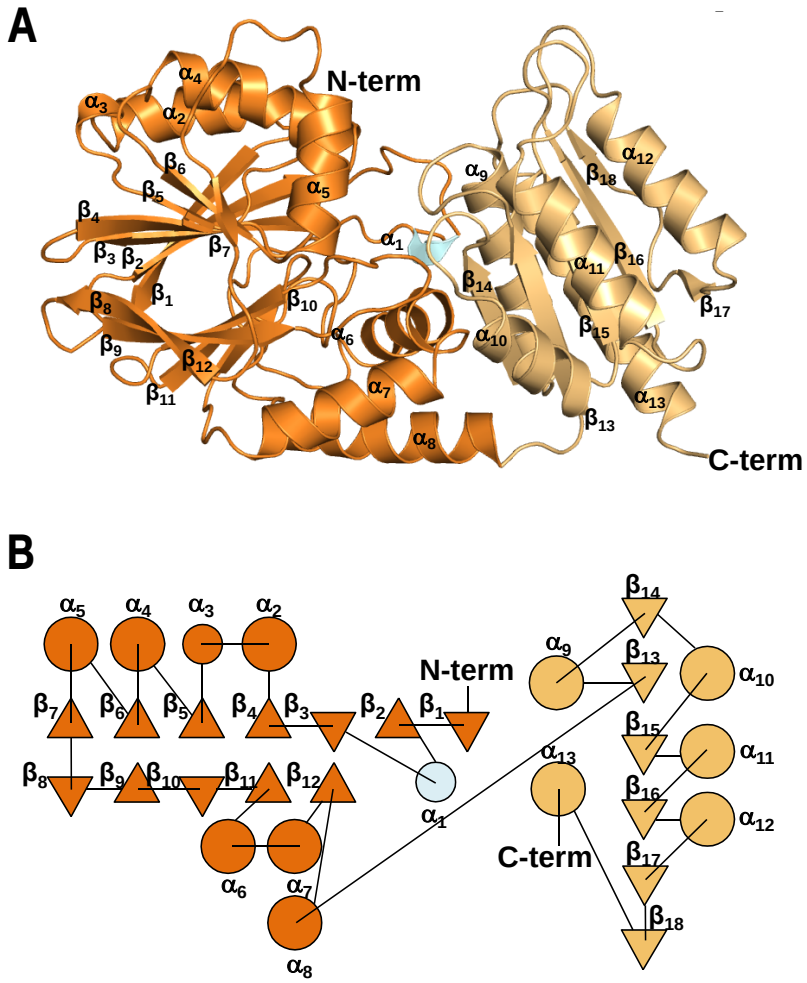

Figure 4.1- *Synechocystis* native Flv1-ΔFlR monomer. **A.** Cartoon representation of the two structural domains: β-lactamase-like domain (orange) and flavodoxin-like domain (light orange). A small α-helix (α_1) is colored in light blue. **B.** Topology diagram of the monomer, with circles and triangles representing α-helices and β-chains, respectively. The secondary structure of β-lactamase and flavodoxin-like domains are colored as in A.

All FDP structures from Classes A and B present a two stranded β-sheet covering the active site (Romao et al., 2016b). However, Flv1-ΔFlR, shows at that position a type 3_{10}-helix, α_1, instead, similarly to Class C *Anabaena* FDP (PDB 4FEK) (Fig. 4.1A and B). The two core domains are linked by a 3 residues segment, as observed in other FDPs (Fig. 4.2).

The Flv1-ΔFlR β-lactamase-like domain differs from the other available structures in its longer helix α_8, with 18 residues instead of the 10-13 residues present in Classes A

and B FDPs (Fig. 4.2). Additionally, the β-lactamase-like domains of *Synechocystis* Flv1-ΔFlR and *Anabaena* FDP (PDB 4FEK), which belong to the non-canonical Class C-Types 2 and 3, respectively, are more similar between themselves (1.2 Å *r.m.s.d.*) than Flv1-ΔFlR is with Classes A and B FDPs (1.6-1.9 Å *r.m.s.d.*s).

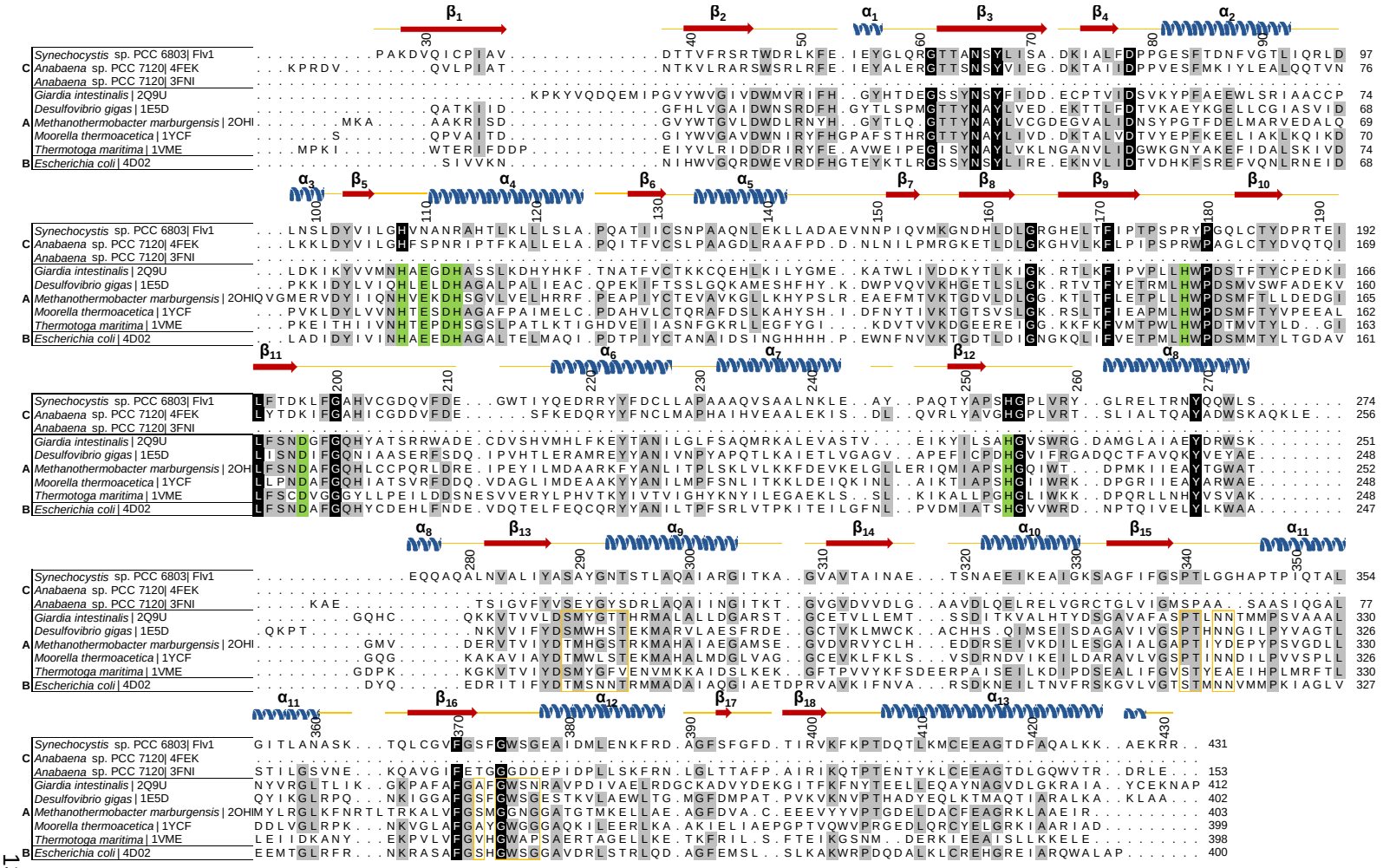
β1 β2 α1 β3 β4 α2
30 40 50 60 70 80 90
Synechocystis sp. PCC 6803| Flv1 97
C Anabaena sp. PCC 7120| 4FEK 76
Anabaena sp. PCC 7120| 3FNI
Giardia intestinalis | 2Q9U 74
Desulfovibrio gigas | 1E5D 68
A Methanothermobacter marburgensis | 2OHI 69
Moorella thermoacetica | 1YCF 70
Thermotoga maritima | 1VME 74
B Escherichia coli | 4D02 68
α3 β5 α4 β6 α5 β7 β8 β9 β10
100 110 120 130 140 150 160 170 180 190
Synechocystis sp. PCC 6803| Flv1 192
C Anabaena sp. PCC 7120| 4FEK 169
Anabaena sp. PCC 7120| 3FNI
Giardia intestinalis | 2Q9U 166
Desulfovibrio gigas | 1E5D 160
A Methanothermobacter marburgensis | 2OHI 165
Moorella thermoacetica | 1YCF 162
Thermotoga maritima | 1VME 163
B Escherichia coli | 4D02 161
β11 α6 α7 β12 α8
200 210 220 230 240 250 260 270
Synechocystis sp. PCC 6803| Flv1 274
C Anabaena sp. PCC 7120| 4FEK 256
Anabaena sp. PCC 7120| 3FNI
Giardia intestinalis | 2Q9U 251
Desulfovibrio gigas | 1E5D 248
A Methanothermobacter marburgensis | 2OH 252
Moorella thermoacetica | 1YCF 248
Thermotoga maritima | 1VME 248
B Escherichia coli | 4D02 247
α8 β13 α9 β14 α10 β15 α11
280 290 300 310 320 330 340 350
Synechocystis sp. PCC 6803| Flv1 354
C Anabaena sp. PCC 7120| 4FEK
Anabaena sp. PCC 7120| 3FNI 77
Giardia intestinalis | 2Q9U 330
Desulfovibrio gigas | 1E5D 326
A Methanothermobacter marburgensis | 2OHI 330
Moorella thermoacetica | 1YCF 326
Thermotoga maritima | 1VME 326
B Escherichia coli | 4D02 327
α11 β16 α12 β17 β18 α13
360 370 380 390 400 410 420 430
Synechocystis sp. PCC 6803| Flv1 431
C Anabaena sp. PCC 7120| 4FEK
Anabaena sp. PCC 7120| 3FNI 153
Giardia intestinalis | 2Q9U 412
Desulfovibrio gigas | 1E5D 402
A Methanothermobacter marburgensis | 2OHI 403
Moorella thermoacetica | 1YCF 399
Thermotoga maritima | 1VME 398
B Escherichia coli | 4D02 400

Figure 4.2- Amino acid sequence alignment of flavodiiron proteins core domains. Alignment based on 3D structural superpositions of *Synechocystis* Flv1-ΔFlR and available FDPs structures (identified by organism name and PDB codes). Flv1-ΔFlR secondary structure is shown above the alignment, with α-helices and β-chains denominated according to Figure 1. Amino acid residues that coordinate the diiron site are highlighted with green background. Amino acid residues interacting with the FMN region are highlighted with yellow boxes. Strictly conserved amino acids are represented with black background, whereas the more conserved residues among the selected sequences are highlighted in grey background.

The flavodoxin-like domain (residues 279-431 for Flv1-ΔFlR and 279-428 for Flv1-ΔFlR_{soaked}) shows the typical αβα topology of short chain flavodoxins, with an inner β-sheet composed of six parallel strands, β_{13}-β_{18}, surrounded by five helices, α_9-α_{13} (Fig. 4.1A and B). In contrast with the β-lactamase-like domain, the Flv1-ΔFlR flavodoxin-like domain has higher structural similarity with Classes A and B FDPs (with exception of *T. maritima* FDP) than with that of Class C-Type 1 *Anabaena* FDP (PDB 3FNI, which also lacks the FMN cofactor) (Table 4.2).

In Flv1-ΔFlR, the spatial arrangement of the core domains differs remarkably from those of all available FDP structures. If one superimposes (Fig. 4.3B) the β-lactamase-like domains of *Synechocystis* Flv1-ΔFlR (Fig. 4.1A), and, *e.g., E. coli* FDP (Fig. 4.3A) (Romao et al., 2016b), their flavodoxin domains diverge visibly from each other, with a relative dislocation of about 15 Å translation and 97 degrees rotation between the two flavodoxin domains.

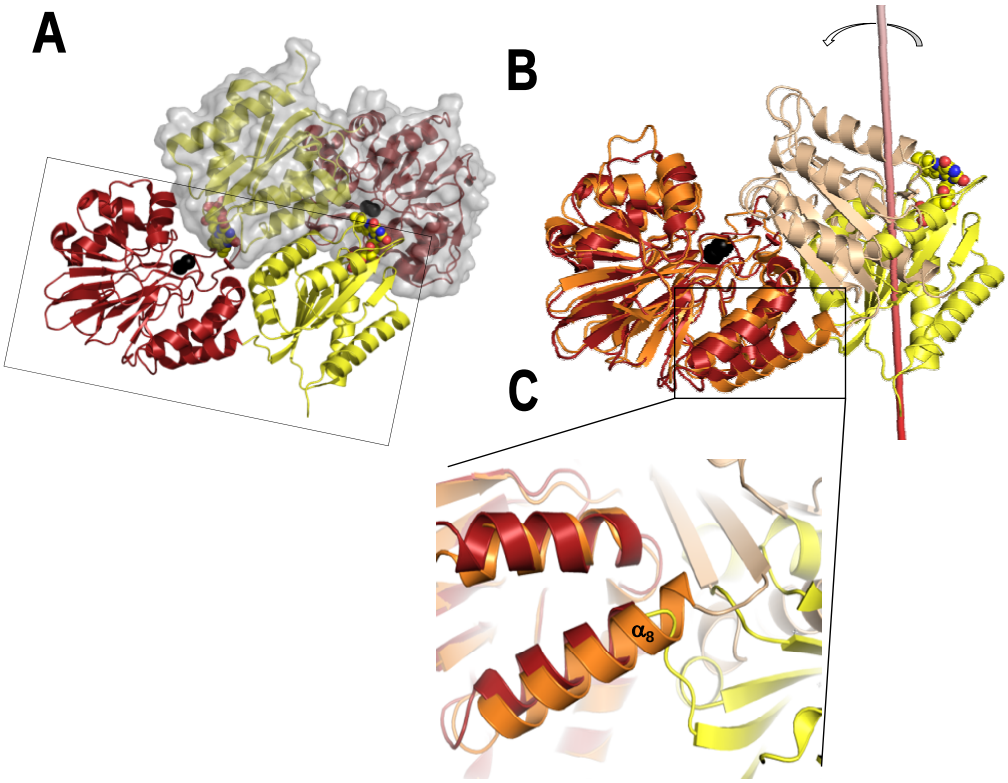

Figure 4.3- Structural comparison between the minimal functional units of *Synechocystis* Flv1-ΔFlR and *E. coli* FDP. **A.** Cartoon representation of *E. coli* FDP "head-to-tail" dimeric configuration. One of the monomers is also represented with a transparent grey surface. **B.** Cartoon representation of the structural superposition of Flv1-ΔFlR and *E. coli* FDP monomers, in the same orientation as in A. The β-lactamase and flavodoxin-like domains from Flv1-ΔFlR are colored as in Figure 1, while those from *E. coli* FDP are coloured as dark red and yellow, respectively. The red axis and rotation direction represent the movement of 15 Å translation and 97º rotation that displaced Flv1-ΔFlR flavodoxin domain from its superposition with *E. coli* FDP homologous domain. **C.** Zoomed view of Flv1-ΔFlR α_8 helix region. Iron ions are represented as black spheres and FMN is represented as spheres with carbon, nitrogen, oxygen and phosphorous atoms in yellow, blue, red and orange, respectively.

Flv1-ΔFlR structure is unique among FDP structures in both its domains arrangement and oligomeric state. Although one cannot discard a dependence of the domains arrangement from the oligomeric state, the observed domains dislocation might be related with the longer helix α_8 in *Synechocystis* Flv1-ΔFlR, when compared with other FDPs, which is located just before the short inter-domains linker, where Flv1-ΔFlR appears to "bend" over itself. The "bent" conformation in Flv1-ΔFlR is not due to the absence of the FMN cofactor, as the deflavinated *T. maritima* FDP (PDB 1VME) has the same conformation as the fully FMN loaded FDPs. Although the β-lactamase-like

domain structure from *Anabaena* FDP (PDB 4FEK) (a structure missing the iron ions) also shows a long helix equivalent to Flv1-ΔFlR helix α_8, the lack of a crystallographic structure of its flavodoxin-like domain prevents to know whether it also adopts a "bent" conformation or retains the typical FDPs conformation.

Pseudo catalytic region

The overexpressed Flv1-ΔFlR was isolated without iron ions, and reconstitution experiments either in solution or upon soaking of the crystals with iron were unsuccessful in leading to iron incorporation. This could be a result of the lack of suitable iron ligands. Nevertheless, at present we also cannot exclude that the amino acids present in the pseudo diiron site may act as iron ligands. In fact, there are already several examples in the literature of some of those amino acids as ligands to iron ions (see Discussion Section and (Berkovitch et al., 2004; Clarke et al., 2008; Pozzi et al., 2015)). Moreover, and as an example in the field of FDPs, it was shown that it is possible to substitute one ligand of the diiron site, H90 in the *T. maritima* FDP, by an asparagine or an alanine without significant effects on the O_2 reductase activities; the asparagine is bound to the metal through the side chain amide carbonyl, while the alanine substitution leads to a water bound species (Fang et al., 2012). Furthermore, the recent studies by Mustila et al (Mustila et al., 2016) revealed that Flv1 alone also improves photosynthesis and CO_2 uptake, being involved in alternative electron transfer pathways, which strongly argues in favour of a protein that in its native state contains redox cofactors.

The pseudo iron binding motif in Flv1 was proposed to be H108-x-N110-x-N112-R113-x_{64}-R178-x_{18}-K197-x_{56}-H254 based on the alignment of its amino acid sequence with those of the canonical FDPs (Gonçalves et al., 2011b) (Fig. 4.2). This contrasts with the iron binding motif in Type 1 FDPs, *e.g. E. coli* FDP shows H79-x-E81-x-D83-H84-x_{62}-H147-x_{18}-D166-x_{60}-H227 (Fig. 4.2). Globally, the Type 1 acidic glutamate and aspartates ligands are replaced in Flv1 by neutral asparagines and a basic lysine, and some histidines are replaced by basic arginines. Therefore, one observes a global substitution of three acidic metal ligands from Type 1 FDPs active site by three basic residues in the pseudo active site region of Type 2 Flv1, which suggests a significant alteration of its electrostatics relative to Type 1 FDPs. A 3D inspection of the predicted iron binding motif in Flv1-ΔFlR allowed concluding that its non-canonical residues occur in a cavity similar to that harbouring the diiron site in the canonical FDPs (Fig.

4.4A, B and C). Moreover, this analysis also pin pointed K51 and Y179 side chains as possible ligands, where the Y179 tyrosyl ring assumes a position similar to that of *E. coli* FDP H147 imidazole ring (Fig. 4.4C).

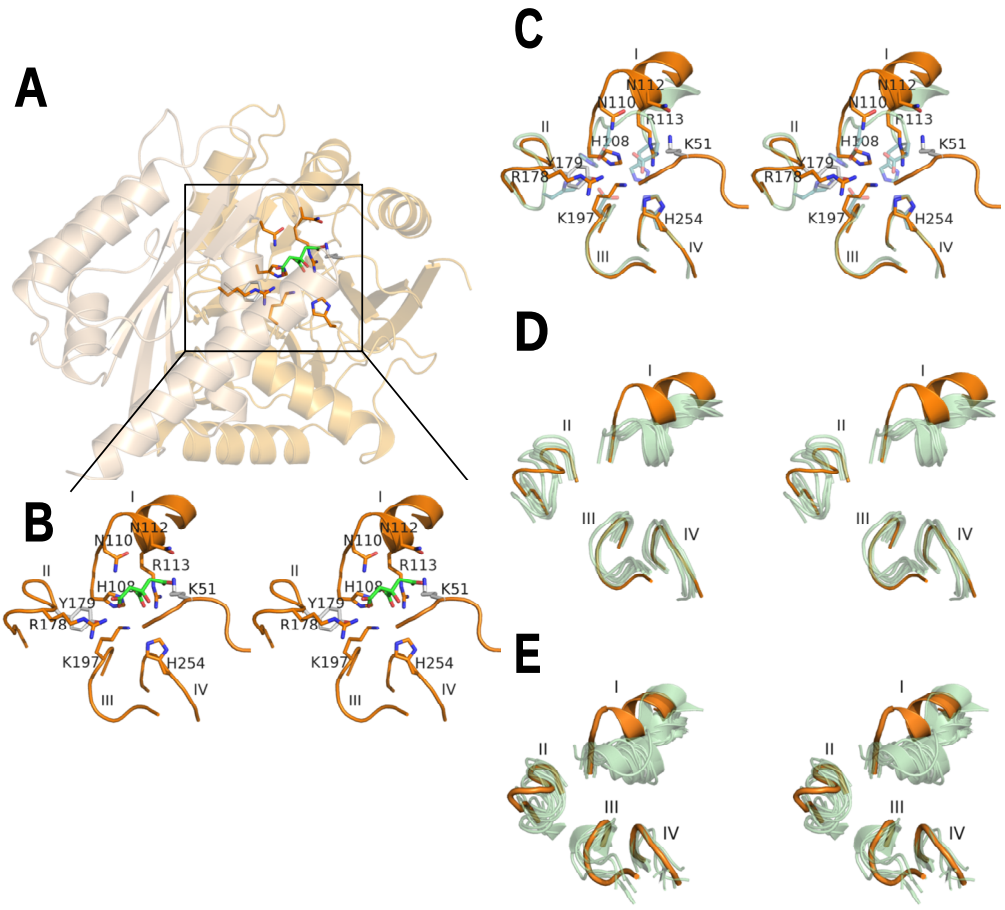

Figure 4.4- *Synechocystis* Flv1-ΔFlR pseudo diiron site. **A.** Cartoon representation of the pseudo catalytic region, with non-canonical residues and citrate anion highlighted as sticks, with carbon atoms coloured in orange and green, respectively. **B.** Zoomed stereo view of the four polypeptide segments (I, II, III and IV). The residues K51 and Y179 are represented as sticks with carbon in grey. **C.** Stereo view of the structural superposition of the four polypeptide segments from Flv1-ΔFlR (orange) and *E. coli* FDP (light green). The residues K51 and Y179 are represented as sticks with carbon in grey. The Flv1-ΔFlR non-canonical residues and *E. coli* FDP metal ligands are represented as sticks with carbon in orange and light green, respectively. Nitrogen and oxygen atoms are colored in blue and red, respectively. **D.** Stereo view of the structural superposition of the four polypeptide segments from Flv1-ΔFlR (orange) and from FDPs (*G. intestinalis*, PDB 2Q9U, *D. gigas*, PDB 1E5D, *M. thermoacetica*, PDB 1YCF, *M. marburgensis*, PDB 2OHH, *T. maritima*, PDB 1VME and *E. coli*, PDB 4D02) represented in light green cartoon. **E.** Stereo view of the structural superposition of the four polypeptide segments from Flv1-ΔFlR colored as orange cartoon and from β-lactamase-like structures (*Pseudomonas*

sp. WBC-3, PDB 1P9E, *H. sapiens*, PDB 1QH5, *S. maltophilia*, PDB 1SML, *S. pneumoniae* PDB 1WRA, *T. maritima*, PDB 1WW1, *P. putida*, PDB 1XTO, *B. thuringiensis*, PDB 2A7M, *P. aeruginosa*, PDB 2CFU, *H. sapiens*, PDB 2I7T, *P. aeruginosa*, PDB 2Q0J, *E. coli*, PDB 2WYM, *T. thermophiles*, PDB 3IEK, *H. sapiens*, PDB 4CHL, *S. venezuelae*, PDB 4JO0, *H. sapiens*, PDB 4QN9 and *E. coli*, PDB 4D02) colored as light green cartoon.

A 3D superposition of the structures of FDPs´ active sites (Di Matteo et al., 2008; Frazao et al., 2000; Romao et al., 2016b; Seedorf et al., 2007; Silaghi-Dumitrescu et al., 2005a) (Fig. 4.4D) drew attention to the four conserved peptide segments that include the canonical diiron binding motif, which C-alpha atoms positions overlaid within 1.3-2.2 Å *r.m.s.d.*s. In *E. coli* FDP these correspond to peptide segments H79-L88 (I), T143-S151 (II), S164-Q170 (III) and A224-V229 (IV). When the four corresponding Flv1-ΔFlR peptide segments were also included in the superposition, the segments III and IV overlaid nicely with their FDPs homologous, in contrast with the segments I and II that clearly diverged in space (Fig. 4.4D). Furthermore, a superposition of these peptide segments of the Flv1-ΔFlR pseudo diiron site with all available β-lactamase-like structures confirmed that segments I and II of the *Synechocystis* protein stand out of the ensemble showing their unique arrangement (Fig. 4.4E) (Cameron et al., 1999; Garau et al., 2005; Garces et al., 2010; Hagelueken et al., 2006; Ishii et al., 2005; Liu et al., 2005; Magotti et al., 2015; Makris et al., 2013; Mandel et al., 2006; Pettinati et al., 2015; Romao et al., 2016b; Ullah et al., 1998; Yu et al., 2009).

Flv1-ΔFlR crystals were soaked with iron, FMN, iron and FMN or zinc solutions, but none of the respective structures showed any metal or FMN cofactors. Nevertheless, while a sulfate anion was found at the pseudo diiron site of the crystals soaked with iron sulfate (Flv1-ΔFlR$_{soaked}$), all other Flv1-ΔFlR crystals contained a citrate anion at that site, probably from the crystallization solution (Fig. 4.4B). The presence of anions at the Flv1-ΔFlR pseudo diiron site prompted us to compare the distribution of basic and acidic residues in its vicinity. Within 10 Å distance, canonical FDPs show a difference between the number of basic and acidic residues of -7 to -4, while Flv1-ΔFlR presents an equal number of bases and acids (Fig. 4.5A and B). Noteworthy, in Flv1-ΔFlR most of the bases are within 5 Å of the pseudo diiron site, while most of the acids are at longer distances, which certainly contributed for the observed anions at the pseudo diiron site.

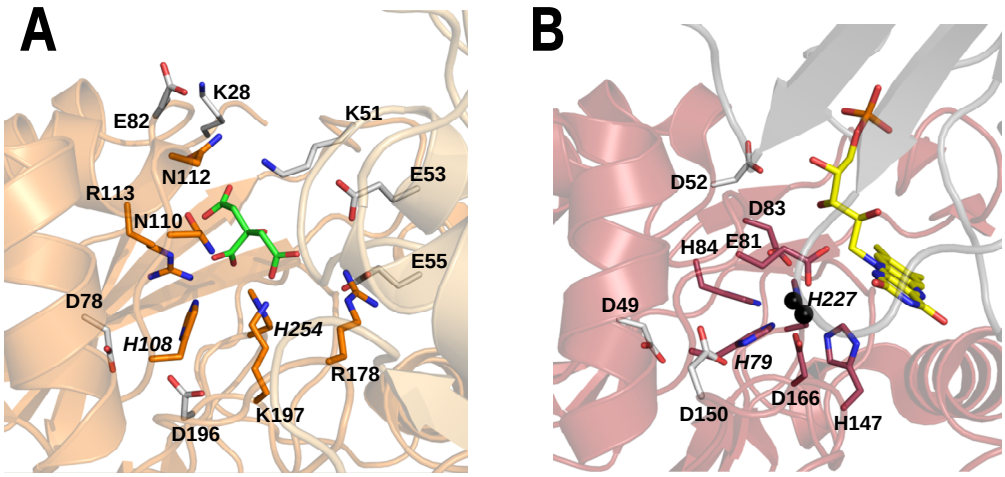

Figure 4.5- Acidic and basic residues of *Synechocystis* Flv1-ΔFlR and *E. coli* FDP in the pseudo diiron site neighbourhood. **A.** Pseudo catalytic site in Flv1-ΔFlR, in which the non-canonical residues and citrate anion are represented as sticks with carbon in orange and green, respectively. The acidic and basic residues within 10 Å of the pseudo diiron site are represented as sticks with carbon in grey. **B.** Diiron site in *E. coli* FDP showing the canonical metal ligands represented as sticks with carbon in dark red. In both panels italic labels correspond to residues that show the same structural position in both organisms. Iron ions are represented as black spheres. FMN is represented as sticks with carbon, nitrogen, oxygen and phosphorous atoms in yellow, blue, red and orange, respectively.

Flv1-ΔFlR and Flv1-ΔFlR$_{soaked}$ structures only differ in loop 288-292, which links β_{13} to α_9 in the flavodoxin-like domain (Fig. 4.2 and 4.6).

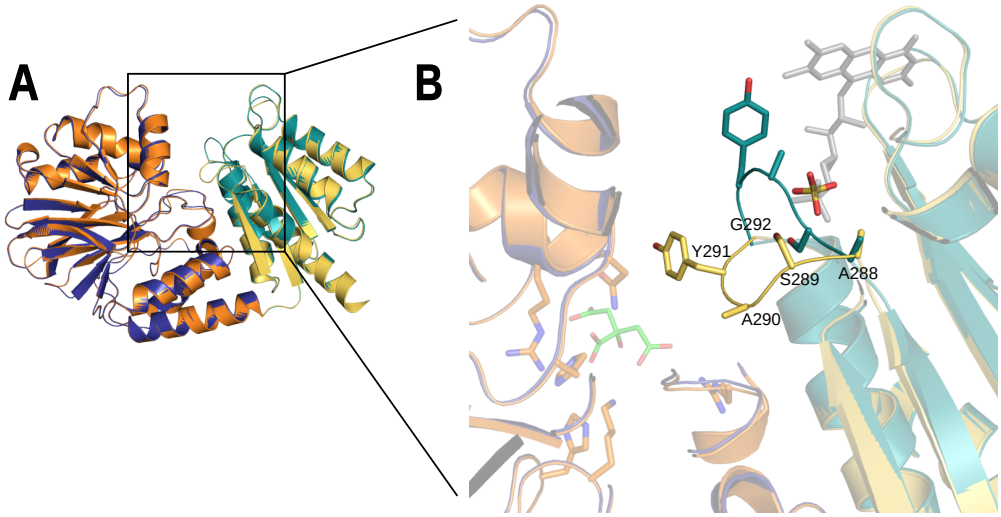

Figure 4.6- Structural differences between *Synechocystis* Flv1-ΔFlR and Flv1-ΔFlR$_{soaked}$ monomers. **A.** Monomer cartoon representation of Flv1-ΔFlR with β-lactamase- and flavodoxin-

like domains in orange and yellow, respectively, and Flv1-ΔFlR$_{soaked}$ with β-lactamase- and flavodoxin-like domains in dark and light blues, respectively. **B.** Zoomed view of loop 288-292 in Flv1-ΔFlR and Flv1-ΔFlR$_{soaked}$ flavodoxin-like domains. Superposed FMN from *E. coli* FDP is represented as grey sticks. The non-canonical residues and citrate anion are represented as sticks with carbon atoms in orange and green, respectively. Sulfate anion is represented as sticks with the sulfur atom in yellow. Nitrogen and oxygen atoms are coloured in blue and red, respectively.

Flv1-ΔFlR$_{soaked}$ shows the FDPs usual loop conformation around the putative FMN position, with residues 289-292 interacting with a mother liquor sulfate anion replacing the otherwise FMN phosphate group in flavin-loaded FDPs (Fig. 4.6A and B). This interaction bears similarities with the chloride anion found in deflavinated *T. maritima* FDP structure (PDB 1VME). In contrast, the Flv1-ΔFlR loop neighbours the pseudo diiron center and displays a conformation only found in deflavinated *Anabaena* FDP flavodoxin-like domain (PDB 3FNI).

A docking of *E. coli* FDP FMN cofactor into the corresponding cavities of Flv1-ΔFlR and Flv1-ΔFlR$_{soaked}$, showed steric clashes between protein residues and the putative FMN cofactor. Bigger clashes occurred on T294 (0.63 Å) and S376 (0.81 Å), and minor clashes on P340 (0.47 Å) and W375 (0.42 Å). In the presence of FMN such clashes might vanish through small configurational changes. A comparable analysis in native deflavinated *T. maritima* FDP (PDB 1VME) showed even larger steric clashes, namely with W152 (1.50 Å), V267 (1.22 Å), Y318 (1.18 Å), G350 (0.99 Å) and W351 (1.35 Å).

Molecular tunnels

The molecular surface of Flv1-ΔFlR, as defined using a 1.4 Å rolling probe, allowed identifying a tunnel lined by atoms with a slightly hydrophobic preponderance (57% of apolar atoms). The tunnel crosses the monomer through a major fraction of the β-lactamase domain and a small part of the flavodoxin-like domain, including the pseudo diiron site. This is accessible from two opposite tunnel apertures, at 24 and 26 Å distances (Fig. 4.7A), with undifferentiated hydrophobic *versus* hydrophilic properties, *e.g.* the crystal structure shows seven and nine water molecules in the shorter and longer tunnel sections, respectively (Fig. 4.7B).

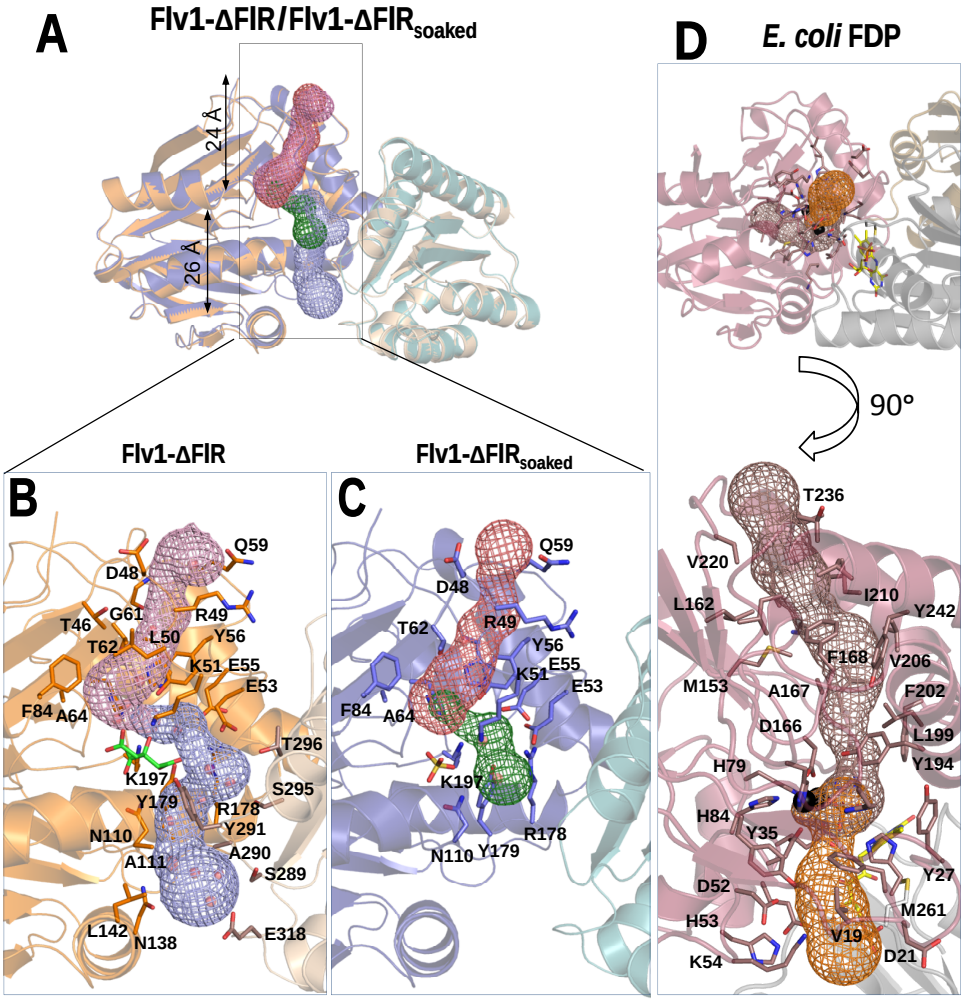

Figure 4.7- *Synechocystis* Flv1-ΔFlR and Flv1-ΔFlR$_{soaked}$ molecular tunnels. **A.** Cartoon representation of Flv1-ΔFlR and Flv1-ΔFlR$_{soaked}$ monomers superposition, with their molecular tunnels, as defined by MOLE (Sehnal et al., 2013) connecting the external protein surface to the pseudo diiron site cavity. These tunnels can be divided in two sections, one with 24 Å length represented in pink or red mesh for Flv1-ΔFlR or Flv1-ΔFlR$_{soaked}$, respectively, and the other section extending up to 26 Å or 10 Å lengths, and represented in blue or green mesh, for Flv1-ΔFlR or Flv1-ΔFlR$_{soaked}$, respectively. **B.** Zoomed view of Flv1-ΔFlR monomer tunnel, with its lining residues represented as sticks, with carbon atoms in orange or light orange, for residues belonging to the β-lactamase-like or the flavodoxin-like domains, respectively. The citrate anion is represented as sticks with carbon atoms in green. **C.** Zoomed view of Flv1-ΔFlR$_{soaked}$ monomer tunnel, with its lining residues represented as sticks with carbon atoms in blue. The sulfate anion is represented as sticks with carbon atoms in yellow. **D.** Cartoon representation of *E. coli* FDP dimer's tunnel. View (top) of the β-lactamase-like domain oriented similarly to panel A, and a zoomed view upon 90°rotation (bottom). The tunnel in *E. coli* FDP dimer can also be divided into a longer and a shorter sections, represented in pink and orange mesh, respectively. The residues lining the tunnel within the β-lactamase-like domain are represented as sticks with

carbon atoms in pink, and those in the “head-to-tail” flavodoxin-like domain of the opposing monomer in grey. FMN is represented as sticks with carbon, nitrogen, oxygen and phosphorous atoms in yellow, blue, red and orange, respectively.

The Flv1-ΔFlR$_{soaked}$ structure shows a different positioning of loop 288-292, which by widening the Flv1-ΔFlR longer tunnel section shortens to approximately 10 Å (Fig. 4.7A and C). The Flv1-ΔFlR tunnel does not relate with that described for *E. coli* FDP, which involves a β-lactamase-like domain of one monomer and the “head-to-tail” flavodoxin-like domain of the opposing monomer, and presents a tunnel with two distinct sections: a longer and more hydrophobic section and a shorter and less hydrophobic one, which are separated by the active site cavity (Fig. 4.7D) (Romao et al., 2016b).

4.5 Discussion

The present work describes for the first time, the crystal structure of the flavodiiron core from a Class C FDP, Flv1-ΔFlR from *Synechocystis* sp. PCC6803, which lacks the canonical ligands of the pseudo diiron site metal ions.

Until now, all known FDP structures presented a “head-to-tail” dimerization as minimal functional unit essential for an efficient electron transfer between the diiron center and FMN (from the opposing monomer) (Fig. 4.3A). In solution, FDPs oligomerize as dimers or as dimers of dimers (Romao et al., 2016a; Romao et al., 2016b; Vicente et al., 2012). Surprisingly, Flv1-ΔFlR in solution shows predominantly the monomeric state, although *in vivo*, in wild type *Synechocystis*, it appears to exist as a homodimer or as a heterodimer together with Flv3 (Allahverdiyeva et al., 2011; Helman et al., 2003; Mustila et al., 2016). Also, when overexpressed in a Δ*flv3* background, Flv1 forms a homodimer *in vivo* (Mustila et al., 2016).

As previously mentioned, Flv1 belongs to Class C FDPs, and thus it has an extra C-terminal domain, which is similar to NAD(P)H:flavin oxidoreductases (FlR). This domain is most probably the entry point for electrons directly from NAD(P)H that will be transferred to the catalytic core (Vicente et al., 2002). At present, it cannot be excluded that the FlR missing domain, would contribute to the stabilization of the homodimer. Nevertheless, the absence of the homodimer is probably not due to the lack of the flavin cofactor, since the deflavinated *T. maritima* FDP also exists as a homodimer (PDB 1VME). The crystal structure shows a single monomer in the

asymmetric unit (Fig. 4.1A), and the crystal packing did not hint for any particular oligomerization as well.

The unique "bent" conformation of the Flv1-ΔFlR flavodoxin-like domain appears to result from the longer helix α_8, relative to canonical FDPs (Fig. 4.3B and C). In fact, if the diiron site and the FMN were present in Flv1-ΔFlR, they would be located ~16 Å apart, thus impairing electron transfer. Nevertheless, we cannot exclude the presence of an induced conformational flexibility that would bring the two redox centers closer and thus allowing the electron transfer between them.

In contrast to the strictly conserved 3D arrangement of all available metallated β-lactamase-like crystal structures of the FDPs diiron binding motif, Flv1-ΔFlR shows only two (III and IV) of the four conserved 3D segments, and the other two (I and II) are unique within this protein's super-family (Fig. 4.4D and E). Similarly, these four polypeptide segments in *Synechocystis* Flv1-ΔFlR are identical to those of Class C-Type 3 *Anabaena* FDP (PDB 4FEK).

The canonical diiron binding sites of Classes A and B FDPs (Di Matteo et al., 2008; Frazao et al., 2000; Romao et al., 2016b; Silaghi-Dumitrescu et al., 2005a) are replaced in Class C- Type 2 *Synechocystis* Flv1 by a segment of neutral and basic residues, H108-x-N110-x-N112-R113-x_{64}-R178-x_{18}-K197-x_{56}-H254. Although Flv1-ΔFlR crystal soakings were tested with iron and zinc, no metal incorporation was detected. Instead, citrate and sulfate anions were observed at the pseudo diiron site of Flv1-ΔFlR and Flv1-ΔFlR$_{soaked}$, respectively (Fig. 4.4B). This might have resulted from the substitution of the canonical acidic metal ligands by basic and neutral amino acids, such as arginine, lysine and asparagine (Fig. 4.4C). Moreover, the neighbourhood of the Flv1-ΔFlR pseudo diiron site shows a prevalence of basic residues relative to acidic ones, in contrast to what has been found in FDP structures, which may impair metal coordination (Fig. 4.5A). However, as already mentioned, at the Protein Data Bank one finds proteins with neutral and basic metal ligands, although in rather small percentages (0.14-0.64%), including as ligands, for example, the main chain carbonyl group of the peptide bonds, or the side chains of glutamine and arginine residues (Berkovitch et al., 2004; Clarke et al., 2008; Fang et al., 2012; Lindqvist et al., 1999; Pozzi et al., 2015; Rajavel et al., 2009; Romero et al., 1993; Strater et al., 2005; Xiao et al., 1998).

The PDB includes a β-lactamase-like domain structure from a Class C-Type 3 *Anabaena* FDP (PDB 4FEK), which shows high structural similarity with Flv1-ΔFlR

(1.2 Å *r.m.s.d.)*. The two structures have almost identical non-canonical residues in the pseudo diiron site, with exception of N110 that is replaced by a serine residue in *Anabaena* FDP. The structure of this last enzyme also has a metal depleted site, and contains a phosphate anion; it should be noted that a serine can also act as a metal ligand, through its hydroxyl group (e.g., (Xiao et al., 1998)).

Unlike the majority of known FDP structures, Flv1-ΔFlR is deflavinated, similarly to Class C-Type 1 *Anabaena* flavodoxin-like domain (PDB 3FNI), and to *T. maritima* FDP (PDB 1VME). The overlay of the FMN cofactor from *E. coli* FDP with *Synechocystis* Flv1-ΔFlR and Flv1-ΔFlR$_{soaked}$ putative FMN binding region, suggests that a few interatomic clashes should arise upon docking of a FMN moiety. The present data does not allow predicting whether these clashes impair FMN binding, or whether the structural relaxation of the cavity allows successful FMN docking. A comparable situation occurred in *T. maritima* FDP, where although the protein in solution was successfully reconstituted with FMN (Hayashi et al., 2010), its crystal structure was obtained for the as-purified flavin lacking enzyme.

The major structural difference between Flv1-ΔFlR and Flv1-ΔFlR$_{soaked}$ was found in a new loop conformation of Flv1-ΔFlR, in residues 288-292 of the flavodoxin-like domain. This contrasts with the usual FDPs loop conformation also present in Flv1-ΔFlR$_{soaked}$. Interestingly, this last structure shows an additional sulfate anion at the presumed phosphate group position of the missing FMN (Fig. 4.6B).

The existence in FDPs dimers of diffusion pathways, for substrates or reaction products, was previously identified by molecular dynamics simulations and structure analyses (Romao et al., 2016b; Victor et al., 2009). A long hydrophobic pathway was suggested as the main entry for substrates (O_2 and/or NO), and a small less hydrophobic pathway was assigned as a possible exit route for the reaction products (H_2O and/or N_2O) (Romao et al., 2016b). Although in Flv1-ΔFlR monomer a tunnel including the pseudo diiron site is also detected, it is not comparable with those of other FDPs, because it involves a single monomer and it does not differentiate sections of higher or lower hydrophobic character (Fig. 4.7B and C).

The presence of a functional iron center in *Synechocystis* Flv1 remains to be demonstrated, and work is under progress towards this goal. Remarkably, both Flv1 and Flv3 are required for photoreduction of O_2 in the Mehler-like reaction that protects PSI under fluctuating light conditions (Allahverdiyeva et al., 2013; Helman et al., 2003). Moreover, the expression of Flv3 is strongly down-regulated in Δ*flv1* mutants

(Allahverdiyeva et al., 2011), whereas Flv1 expression is abolished in Δ*flv3* mutants (Mustila et al., 2016). Since Flv1 does not harbour the canonical metal ligands, it was proposed that Flv1 and Flv3 could form a functional heterodimer, taking profit of the canonical ligands present in Flv3 (Allahverdiyeva et al., 2011; Mustila et al., 2016). However, it was shown that Flv1 by itself is involved in alternative electron transfer pathways, as it improves photosynthesis and CO_2 uptake (Mustila et al., 2016). This strongly suggests that Flv1 contains redox cofactors, in its native state, and that so far the conditions for the incorporation of the iron ions and FMN in the recombinant protein could not be established.

4.6 Conclusions

FDPs are enzymes widespread in Bacteria, Archaea and Eukarya (anaerobic protozoa and oxygenic phototrophs). These proteins are responsible for the reduction of oxygen and/or nitric oxide into non-toxic compounds (H_2O and/or N_2O). Flv1 is one of the four FDPs encoded by the cyanobacterium *Synechocystis* sp. PCC6803 and it is classified in Class C- Type 2. This is the second most representative type of Class C FDPs containing non-canonical residues at the pseudo diiron catalytic site. Here, it is reported for the first time the crystal structure of a Class C-Type 2 FDP truncated to its flavodiiron core in the native form (Flv1-ΔFlR) and also after crystal soaking with iron sulfate (Flv1-ΔFlR$_{soaked}$). In contrast to FDPs minimal functional “head-to-tail” dimers, Flv1-ΔFlR reveals a monomeric form with a “bent” conformation. Additionally, it shows a unique 3D arrangement of the pseudo diiron site, which only retains about half of the conserved 3D arrangement. Instead of the canonical acidic and neutral metal ligands, it contains basic and neutral residues, together with a predominance of further basic residues in their close neighbourhood, which promoted the substitution of metal ions by anionic species. These structural differences relative to typical FDPs structures are expected to be relevant for their function, and the present data constitute the basis for further studies aiming to clarify the structure/function relationship of these elusive enzymes.

4.7 Acknowledgments

This work was financed by the Portuguese Fundação para a Ciência e a Tecnologia (FCT) through grant PTDC/BBB-BQB/3135/2014 (MT). CVR and PB acknowledge the FCT grants SFRH/BPD/94050/2013 and SFRH/BD/85106/2012, respectively. This work was further financially supported by MOSTMICRO (LISBOA-01-0145-FEDER-007660) and by iNOVA4Health (LISBOA-01-0145-FEDER-007344) Research Units cofunded by FCT, through national funds, and by FEDER under the PT2020 Partnership Agreement. We thank the beamline staff at ESRF (Grenoble, France) for the support during the synchrotron data collections.

Part III

General discussion and concluding remarks

Chapter V

General discussion and concluding remarks

FDPs, previously named as A-type flavoproteins, form a large family of enzymes widespread in three life Domains (Bacteria, Archaea and Eukarya), with a key function in oxygen and/or nitric oxide detoxification.

The present work was focused on studies of the flavodiiron core belonging to FDPs from two different classes: a Class B *E. coli* FDP-ΔRd and a Class C *Synechocystis* Flv1-ΔFlR. Moreover, these proteins have different substrate selectivities, being the *E. coli* FDP an NO reductase while the *Synechocystis* Flv1 is proposed to be an O_2 reductase involved in the protection of PSI.

The results obtained in this work led to a structural comparison between the different proteins studied, in which specific topics were addressed that impact on the general knowledge of flavodiiron proteins. The purpose of this chapter is to do an overview of the most relevant results obtained in this thesis related with these two FDPs, the canonical *E. coli* FDP-ΔRd and the non-canonical *Synechocystis* sp. PCC 6803 Flv1-ΔFlR.

5.1 Distinct three dimensional arrangements of the flavodiiron core

The determination of the first FDP crystallographic structure in 2000, *D. gigas* ROO (PDB 1E5D), was an important landmark in the elucidation of structural features in this family of proteins (Frazao et al., 2000). Until today, a total of 23 FDPs crystal structures from different organisms in different oxidation states, including some with point mutations, were determined (Table 1.3 and Chapters II, III and IV). These proteins are composed of a metallo-β-lactamase-like domain, containing the diiron center where the substrates reduction occurs, and a flavodoxin-like domain harbouring the non-covalently bound FMN cofactor. The two domains constitute the flavodiiron core, which is the fingerprint of this family of enzymes.

In each monomer, the diiron and FMN cofactors are located *ca.* 40 Å apart, hindering electron transfer between each other. FDPs structure revealed a minimal functional unit composed of a dimeric “head-to-tail” arrangement. This feature allows the diiron site of one monomer to be in close contact (~6 Å) with the FMN cofactor of the opposing monomer, ensuring an efficient electron transfer between the two redox centers.

In this work, FDPs from two different organisms were structurally studied, namely the Class B *E. coli* FDP truncated at the C-terminal Rd domain (FDP-ΔRd) and the Class C *Synechocystis* sp. PCC 6803 Flv1, that lacks the NAD(P)H:flavin oxidoreductase-like domain (Flv1-ΔFlR). *E. coli* FDP-ΔRd D52K, S262Y, D52K/S262Y mutants and *Synechocystis* Flv1-ΔFlR and Flv1-ΔFlR$_{soaked}$, were crystallized and their crystal structures determined and analyzed (Chapters II, III and IV). The *E. coli* FDP-ΔRd mutants crystal structures include two monomers in the *a.u*. However, they did not form the typical FDP "head-to-tail" dimer (Chapter II and III), which was produced by the crystal symmetry, instead (Fig. 5.1A). The crystal symmetry also reproduces the tetrameric arrangement (dimer of dimers) as observed in size-exclusion chromatography, with pseudo *222* point group symmetry.

Synechocystis Flv1-ΔFlR is so far the only known structure of a Class C-Type 2 FDP. It contains both β-lactamase and flavodoxin-like domains, but the minimal "head-to-tail" structural arrangement is not observed (Chapter IV). Its crystal structure shows a single monomer in the *a.u.*, as present in solution (Fig. 5.1B). For the first time, a distinct structural arrangement within this family of proteins was revealed. Still, it can not be discarded that the here truncated FlR domain could be involved in the full length molecule oligomerization (Chapter IV).

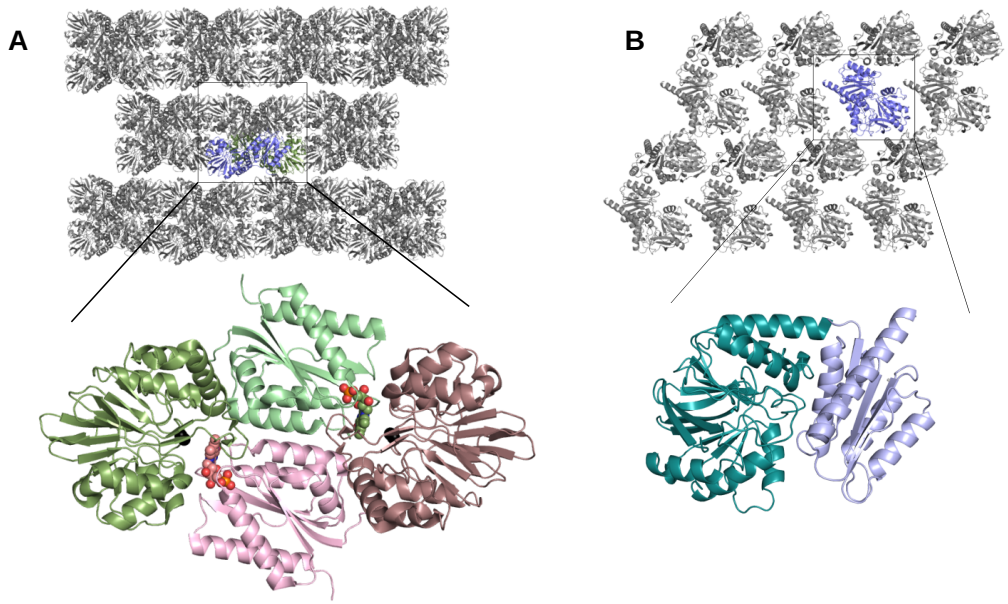

Figure 5.1- Overall structure of FDPs. **A)** Top view: *E. coli* FDP-ΔRd D52K crystal packing highlighting the two molecules (green and blue) in the asymmetric unit. Bottom view: cartoon representation of the *E. coli* FDP-ΔRd D52K dimeric "head-to-tail" configuration. One monomer is colored in green and the opposing one in pink. The metallo-β-lactamase and flavodoxin-like domains are shown with darker and lighter colors, respectively. Iron atoms are represented as black spheres. The FMN is shown as spheres with carbon in green or pink, nitrogen in blue, oxygen in red and phosphorous in orange. **B)** Top view: *Synechocystis* sp. PCC 6803 Flv1-ΔFlR crystal packing highlighting one molecule (blue) in the asymmetric unit. Bottom view: cartoon representation of the *Synechocystis* sp. PCC 6803 Flv1-ΔFlR monomeric configuration colored in blue. The metallo-β-lactamase and flavodoxin-like domains are shown with darker and lighter colors, respectively.

An analysis of the oligomerization of FDP-ΔRd mutants and others FDPs with PISA (Krissinel and Henrick, 2007) showed that the "head-to-tail" dimerization occurs with occlusion of approximately 12 % of the solvent accessible area (Fig. 5.2). All the residues involved in FDPs dimerization are listed in Table 5.1.

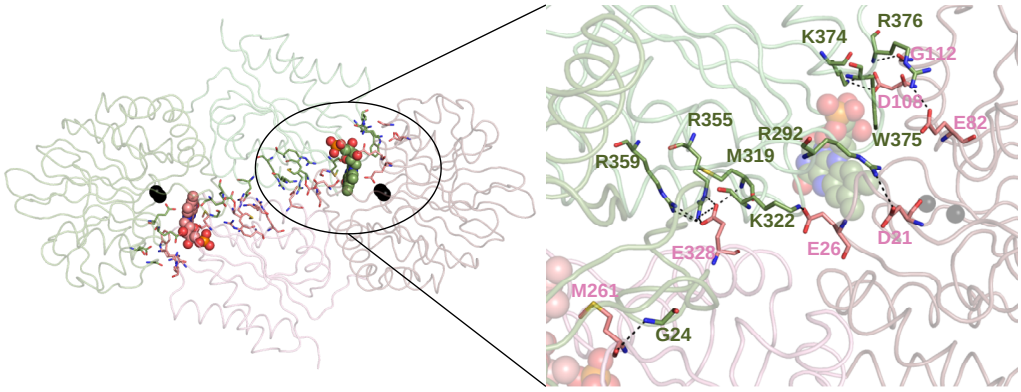

Figure 5.2- Dimerization interface of *E. coli* FDP. Several residues involved in the dimerization of *E. coli* FDP are labeled, establishing hydrogen bonds and salt bridges (black dash line) between each monomer. Iron atoms are represented as black spheres. The FMN is shown as spheres with carbon in green or pink, nitrogen in blue, oxygen in red and phosphorous in orange.

In order to find the conserved interactions involved in FDPs dimerization, an alignment based on 3D structural superposition was performed (Fig. 5.3A). These interactions are mainly located at the diiron-FMN interface, and involve three mainly conserved regions, *S1*, *S2* and *S3*. Region *S1* includes residues D21 to Y27 (*E. coli* FDP numbering), in the β-lactamase-like domain, which are covering the diiron site

(Fig. 5.3 A, B). Region *S2* contains residues E81 to H84. This region contains the metal ligands E81, D83 and H84, conserved among all FDPs with exception of those from Class C, Types 2-17 (see section 5.2). Region *S3* comprises Y258-N263 residues in the flavodoxin-like domain (Fig. 5.3 A, B). These residues are in the vicinity of the FMN phosphate group.

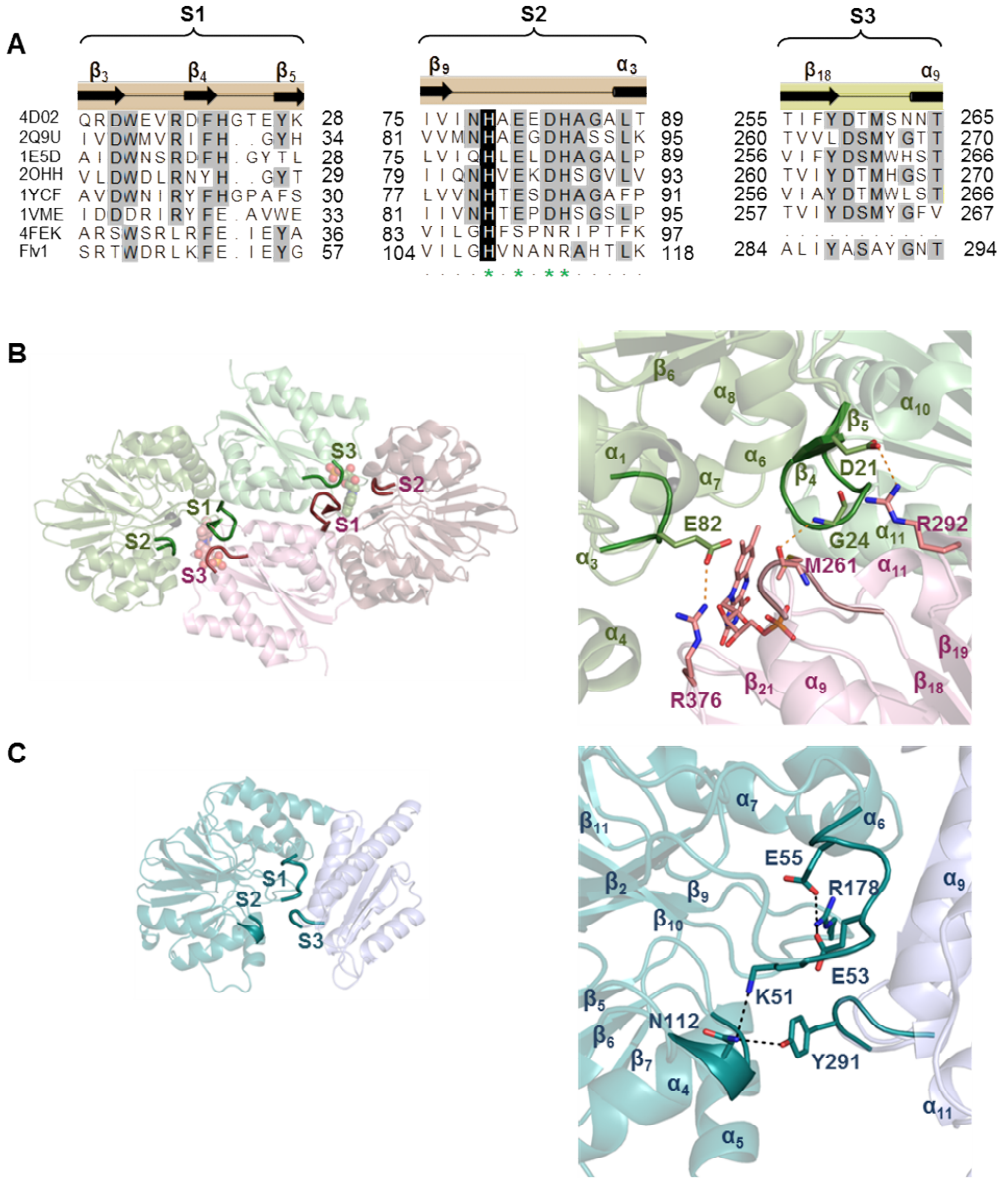

Figure 5.3- Regions involved in the dimerization interface. **A)** Amino acid sequence alignment based on 3D structural superposition of *E. coli* FDP and available FDPs structures, identified by PDB codes, namely, *E. coli* (4D02), *G. intestinalis* (2Q9U), *D. gigas* (1E5D), *M. marburgensis*

(2OHH), *M. thermoacetica* (1YCF), *T. maritima* (1VME), *Anabaena* sp. PCC 7120 metallo-β-lactamase-like domain (4FEK) and *Synechocystis* sp. PCC 6803 Flv1-ΔFlR (Flv1). The green asterisk below the alignment represent the diiron ligands conserved in Classes A and B FDPs.The orange and yellow bar (containing the secondary structure of *E. coli* FDP) above the alignment, represents the metallo-β-lactamase and flavodoxin-like domains, respectively. **B)** Cartoon representation of the *E. coli* FDP "head-to-tail" dimer, where each monomer is colored in green or pink. The FMN is shown as spheres with carbon in green or pink, nitrogen in blue, oxygen in red and phosphorous in orange The right panel is a zoomed view of S1, S2 and S3 regions. **C)** Cartoon representation of the *Synechocystis* Flv1-ΔFlR monomer colored in blue. The right panel is a zoomed view of S1, S2 and S3 regions.

In all FDPs presenting as minimal functional unit the "head-to-tail" dimer, the *S1* and *S2* regions are in the β-lactamase-like domain while *S3* belongs to the flavodoxin-like domain of the opposing monomer (Fig. 5.3 B). The dimerization interface reveals that *S3* region interacts with either *S1* or *S2* (except in *M. marburgensis* FDP that interacts with both *S1* and *S2*). In *E. coli* and *M. thermoacetica* FDPs, the *S3* region is interacting with *S1* (Table 5.1 and Fig. 5.3 B), while in *D. gigas*, *T. maritima* and *G. intestinalis* FDPs, the same region is interacting with *S2*. Since region *S3* is localized in the opposing monomer to that of *S1* and *S2* regions, these interactions mainly contribute for the "head-to-tail" dimer formation.

A superposition of *Synechocystis* Flv1-ΔFlR β-lactamase-like domain with available FDPs structure shows a relative 15 Å translation and 97 degrees rotation of the neighboring flavodoxin-like domain when compared with the other FDP structures (Fig. 4.3). This re-arrangement promotes interactions between *S2* and *S1* and S2 and S3 within the same monomer (Fig. 5.3 C). Therefore, the three regions involved in FDPs dimerization are still present in *Synechocystis* Flv1-ΔFlR.

Table 5.1- FDPs residue contacts in the “head-to-tail” dimer interface.

E. coli			*D. gigas*			*M. marburgensis*			*M. thermoacetica*			*G. intestinalis*		
Atom (Chain)	**Atom (Chain)**	**Distance (Å)**	**Atom (Chain)**	**Atom (Chain)**	**Distance (Å)**	**Atom (Chain)**	**Atom (Chain)**	**Distance (Å)**	**Atom (Chain)**	**Atom (Chain)**	**Distance (Å)**	**Atom (Chain)**	**Atom (Chain)**	**Distance (Å)**
$G24^{N}$ (B)	$M261^{O}$ (A)	3.4	$G25^{O}$ (B)	$K290^{NZ}$ (A)	3.0	$Y25^{OH}$ (E)	$H267^{NE2}$ (D)	3.2	$W19^{NE1}$ (C)	$M274^{SD}$ (A)	3.4	$Y267^{OH}$ (B)	$E87^{OE2}$ (A)	2.6
$R292^{NH1}$ (B)	$D21^{OD2}$ (A)	3.4	$E81^{OE2}$ (B)	$W263^{NE1}$ (A)	3.2	$E85^{OE2}$ (E)	$H267^{NE2}$ (D)	3.4	$N20^{ND2}$ (C)	$Y259^{OH}$ (A)	3.1	$Y267^{OH}$ (B)	$D89^{OD1}$ (A)	3.3
$M319^{N}$ (B)	$E328^{OE2}$ (A)	3.1	$S112^{OG}$ (B)	$N375^{OD1}$ (A)	2.7	$K86^{NZ}$ (E)	$H267^{O}$ (D)	3.2	$N20^{ND2}$ (C)	$E267^{OE1}$ (A)	3.4	$N331^{ND2}$ (B)	$M322^{O}$ (A)	3.1
$K322^{NZ}$ (B)	$E26^{OE2}$ (A)	2.6	$S112^{O}$ (B)	$V376^{N}$ (A)	3.2	$K116^{NZ}$ (E)	$Y380^{O}$ (D)	2.6	$R22^{NE}$ (C)	$V291^{O}$ (A)	3.1	$R334^{NH2}$ (B)	$T321^{OG1}$ (A)	3.1
$R355^{NH2}$ (B)	$E328^{OE1}$ (A)	2.9	$H115^{NE2}$ (B)	$V376^{O}$ (A)	2.5	$K116^{NZ}$ (E)	$V382^{O}$ (D)	2.8	$E83^{OE2}$ (C)	$H271^{NE2}$ (A)	3.3	$N383^{ND2}$ (B)	$I118^{O}$ (A)	3.0
$R355^{NE}$ (B)	$E328^{OE2}$ (A)	2.8	$W263^{NE1}$ (B)	$E81^{OE2}$ (A)	3.2	$K116^{NZ}$ (E)	$E387^{OE1}$ (D)	2.8	$S176^{OG}$ (C)	$V284^{N}$ (A)	3.2	$N383^{ND2}$ (B)	$L119^{O}$ (A)	3.4
$R355^{NH2}$ (B)	$E328^{OE2}$ (A)	3.4	$K290^{NZ}$ (B)	$G25^{O}$ (A)	2.8	$D154^{OD1}$ (E)	$Y381^{OH}$ (D)	3.4	$Y259^{OH}$ (C)	$N20^{ND2}$ (A)	3.2	$R28^{NH2}$ (B)	$S295^{O}$ (A)	2.9
$R359^{NH1}$ (B)	$E328^{OE1}$ (A)	3.2	$N316^{OD1}$ (B)	$R333^{NH2}$ (A)	3.1	$L202^{O}$ (E)	$Y319^{OH}$ (D)	2.4	$V291^{O}$ (C)	$R22^{NE}$ (A)	3.0	$R282^{NE}$ (B)	$S180^{O}$ (A)	2.7
$R359^{NH2}$ (B)	$E328^{OE1}$ (A)	3.3	$R333^{NH2}$ (B)	$N316^{OD1}$ (A)	3.3	$H267^{NE2}$ (E)	$E85^{OE2}$ (D)	3.4	$V291^{O}$ (C)	$R22^{NH2}$ (A)	3.3	$R282^{NH2}$ (B)	$S180^{O}$ (A)	2.9
$K374^{NZ}$ (B)	$D108^{OD1}$ (A)	3.0	$N375^{OD1}$ (B)	$S112^{OG}$ (A)	2.8	$H267^{O}$ (E)	$K86^{NZ}$ (D)	3.1	$S292^{OG}$ (C)	$R22^{NH2}$ (A)	3.4			
$K374^{NZ}$ (B)	$D108^{OD2}$ (A)	3.0	$V376^{N}$ (B)	$S112^{O}$ (A)	3.1	$H267^{NE2}$ (E)	$Y25^{OH}$ (D)	3.1						
$W375^{NE1}$ (B)	$D108^{OD2}$ (A)	2.9	$V376^{O}$ (B)	$H115^{NE2}$ (A)	2.6	$R298^{NH1}$ (E)	$Y323^{OH}$ (D)	3.4						

E. coli			*D. gigas*			*M. marburgensis*			*M. thermoacetica*			*G. intestinalis*		
Atom (Chain)	**Atom (Chain)**	**Distance (Å)**	**Atom (Chain)**	**Atom (Chain)**	**Distance (Å)**	**Atom (Chain)**	**Atom (Chain)**	**Distance (Å)**	**Atom (Chain)**	**Atom (Chain)**	**Distance (Å)**	**Atom (Chain)**	**Atom (Chain)**	**Distance (Å)**
$R376^{NH2}$ (B)	$E82^{OE1}$ (A)	3.0				$Y319^{OH}$ (E)	$L202^{O}$ (D)	2.4						
$R376^{N}$ (B)	$G112^{O}$ (A)	3.0				$Y319^{O}$ (E)	$K337^{NZ}$ (D)	3.1						
						$Y319^{OH}$ (E)	$H151^{ND1}$ (D)	2.7						
						$E321^{OE1}$ (E)	$R334^{NE}$ (D)	3.2						
						$E321^{OE2}$ (E)	$R334^{NE}$ (D)	2.7						
						$E321^{OE2}$ (E)	$R334^{NH2}$ (D)	2.9						
						$R334^{NE}$ (E)	$E321^{OE1}$ (D)	3.3						
						$R334^{NE}$ (E)	$E321^{OE2}$ (D)	3.0						
						$Y380^{O}$ (E)	$K116^{NZ}$ (D)	2.5						
						$E387^{OE1}$ (E)	$K116^{NZ}$ (D)	3.1						
						$E387^{OE2}$ (E)	$K116^{NZ}$ (D)	3.1						

5.2 Canonical and non-canonical FDPs

The diiron center present in FDPs is the active site where NO and/or O_2 reduction occurs. The proximal iron (Fe_p) is coordinated by residues H79, H147, and E81 (*E. coli* FDP numbering), while the distal iron (Fe_d) is coordinated by H84, H227, and D83, with D166 acting as a bridging ligand between both irons (Fig. 5.4 A). Additionally, a μ-hydroxo bridge coordinates both irons atoms as observed for all the *E. coli* FDP-ΔRd mutants crystal structures. These canonical ligands (Type 1) are almost strictly conserved in this protein family. Exceptions are observed in Class C FDPs, in some cyanobacteria and oxygenic photosynthetic eukaryotes. These organisms, beyond Type 1 FDPs, also encode other FDPs copies within the same genome, with 16 different combinations of non canonical ligands (Types 2-17) (Table 5.2). For instance, the cyanobacterium *Synechocystis* sp. PCC 6803, encodes four FDPs, the non canonical Class C Type 2 Flv1 and Flv2, and the canonical Class C Type 1 Flv3 and Flv4 (Section 1.8).

The identification of the distinct arrangements of Types 1-17 was achieved using a BLAST search only for the flavodiiron core, which allowed to gather approximately 500 putative sequences of Class C FDPs. This analysis revealed that approximately 50% of Class C FDPs sequences contain canonical iron ligands (Type 1) (H92-x-E94-x-D96-H97-x_{61}-H159-x_{18}-D178-x_{57}-H236, *Synechocystis* Flv3 numbering) (Table 5.2). These sequences comprise Flv3 and Flv4 from *Synechocystis* sp. PCC 6803. The remaining 50% of Class C FDPs sequences show a high number of possible ligand combinations, namely aliphatic, neutral or basic residues (Table 5.2). The second most predominant combination (~42%) is Type 2 (H108-x-N110-x-N112-R113-x_{64}-H178-x_{18}-K197-x_{56}-H254, *Synechocystis* Flv1 numbering). These sequences contain Flv1 and Flv2 from *Synechocystis* sp. PCC 6803. Moreover, analyses of almost all cyanobacteria and oxygenic photosynthetic eukaryotes genomes, revealed the presence of at least two genes encoding distinct FDPs within the same organism, one canonical Class C Type 1 and a second non canonical encoding for one of the multiple types of residues combinations (Gonçalves et al., 2011b). So far, the Types 9-12 and 16-17 are limited to only oxygenic photosynthetic eukaryotes, while the other types, are found in oxygenic photosynthetic eukaryotes and in cyanobacteria.

Table 5.2- Class C canonical FDPs diiron ligands (Type 1) and corresponding amino acids substitutions in Class C non-canonical FDPs (Types 2-17). Additionally, is represented the distribution of Class C FDPs (%). Organisms containing the different types of putative ligands: 1- *Synechocystis* sp. PCC 6803 Flv3 (BAA10483.1), 2- *Synechocystis* sp. PCC 6803 Flv1 (BAA18468.1), 3- *Hassallia byssoidea* VB512170 (KIF36639.1), 4- *Prochlorococcus marinus* (WP_075486811.1), 5- *Prochlorococcus marinus* (WP_011819375.1), 6- *Planktothricoides* sp. SR001 (WP_054469106.1), 7- *Prochlorococcus marinus* str. P0902-H212 (AJW30545.1), 8- *Synechococcus* sp. RCC307 (WP_011936799.1), 9- *Chlorella variabilis* (EFN57640.1), 10- *Coccomyxa subellipsoidea* C-169 (EIE18907.1), 11- *Micromonas pusilla* CCMP1545 (XP_003057013.1), 12- *Ostreococcus lucimarinus* CCE9901 (XP_001416100), 13- *Scytonema hofmannii* (WP_017742742.1), 14- *Cylindrospermum* sp. NIES-4074 (BAZ30624.1), 15- *Cyanobium* sp. NIES-981 (WP_087068256.1), 16- *Chlamydomonas reinhardtii* (XP_001692916.1), 17- *Ostreococcus tauri* (XP_003075211.2).

Type	(%)	Putative ligands												
1	50.0	**H**^{92}	x	**E**^{94}	X	**D**^{96}	**H**^{97}	x$_{61}$	**H**^{159}	x$_{18}$	**D**^{178}	x$_{57}$	**H**^{236}
2	41.8	**H**^{108}	x	**N**^{110}	X	**N**^{112}	**R**^{113}	x$_{64}$	**R**^{178}	x$_{18}$	**K**^{197}	x$_{56}$	**H**^{254}
3	4.0	**H**^{87}	x	**S**^{89}	X	**N**^{91}	**R**^{92}	x$_{62}$	**R**^{155}	x$_{18}$	**K**^{174}	x$_{56}$	**H**^{231}
4	1.0	**H**^{96}	x	**N**^{98}	X	**Q**^{100}	**I**^{101}	x$_{72}$	**R**^{174}	x$_{18}$	**K**^{193}	x$_{56}$	**H**^{250}
5	0.5	**H**^{96}	x	**N**^{98}	X	**K**^{100}	**I**^{101}	x$_{72}$	**R**^{174}	x$_{18}$	**K**^{193}	x$_{56}$	**H**^{250}
6	0.5	**H**^{88}	x	**N**^{90}	X	**N**^{92}	**R**^{93}	x$_{62}$	**K**^{156}	x$_{18}$	**K**^{175}	x$_{57}$	**H**^{233}
7	0.2	**H**^{105}	x	**N**^{107}	X	**N**^{109}	**K**^{110}	x$_{79}$	**R**^{190}	x$_{18}$	**K**^{209}	x$_{56}$	**H**^{266}
8	0.2	**N**^{89}	x	**N**^{91}	X	**D**^{93}	**R**^{94}	x$_{73}$	**R**^{168}	x$_{18}$	**R**^{187}	x$_{56}$	**Y**^{244}
9	0.2	**R**^{99}	x	**T**^{101}	X	**E**^{103}	**R**^{104}	x$_{73}$	**R**^{178}	x$_{18}$	**N**^{197}	x$_{100}$	**H**^{298}
10	0.2	**H**^{131}	x	**T**^{133}	X	**K**^{135}	**R**^{136}	x$_{74}$	**R**^{211}	x$_{18}$	**K**^{230}	x$_{111}$	**H**^{342}
11	0.2	**H**^{147}	x	**S**^{149}	X	**K**^{151}	**R**^{152}	x$_{83}$	**R**^{236}	x$_{18}$	**K**^{255}	x$_{122}$	**H**^{378}
12	0.2	**H**^{70}	x	**S**^{72}	X	**R**^{74}	**R**^{75}	x$_{84}$	**R**^{160}	x$_{18}$	**K**^{179}	x$_{57}$	**H**^{237}
13	0.2	**H**^{87}	x	**N**^{89}	X	**N**^{91}	**R**^{92}	x$_{62}$	**H**^{155}	x$_{18}$	**K**^{174}	x$_{56}$	**H**^{231}
14	0.2	**H**^{87}	x	**N**^{89}	X	**T**^{91}	**R**^{92}	x$_{62}$	**R**^{155}	x$_{18}$	**K**^{174}	x$_{56}$	**H**^{231}
15	0.2	**V**^{106}	x	**N**^{108}	X	**N**^{110}	**R**^{111}	x$_{77}$	**R**^{189}	x$_{18}$	**K**^{208}	x$_{56}$	**H**^{265}
16	0.2	**I**^{56}	x	**L**^{58}	X	**H**^{60}	**L**^{61}	x$_{66}$	**R**^{128}	x$_{18}$	**K**^{147}	x$_{57}$	**H**^{205}
17	0.2	**V**^{143}	x	**P**^{145}	X	**R**^{147}	**L**^{148}	x$_{83}$	**R**^{232}	x$_{18}$	**K**^{251}	x$_{99}$	**H**^{351}

Until today, only three crystal structures of cyanobacterial Class C FDPs were determined (Table 1.3). The first structures to be reported were from two truncated domains, the *Anabaena* sp. PCC 7120 metallo-β-lactamase-like domain (PDB 4FEK) that belongs to Class C Type 3 and the *Anabaena* sp. PCC7120 flavodoxin-like domain (PDB 3FNI) from Class C Type 1. Under the scope of this thesis, for the first time it is reported the flavodiiron core crystal structure of a Class C Type 2 FDP (Flv1-

ΔFlR) from *Synechocystis* sp. PCC 6803 (Chapter IV and Fig. 5.4 B). Flv1-ΔFlR revealed a new structural arrangement of the FDP core in the monomeric form with a "bent" conformation, in contrast to the typical minimal functional "head-to-tail" dimer. Additionally, the 3D arrangement of the pseudo diiron site in Flv1-ΔFlR is also significantly different from canonical FDPs. Therefore, while all previous FDPs and metallated β-lactamase-like crystal structures showed a strictly conserved 3D arrangement of the metal binding motif, the Flv1-ΔFlR only retained two of the four conserved 3D segments. The pseudo catalytic site in Flv1-ΔFlR did not reveal the presence of any metal in spite of several crystal soaking or co-crystallization attempts with iron- or zinc-containing solutions (Fig. 5.4 B). Instead, a sulfate anion was found at the pseudo diiron site of Flv1-ΔFlR$_{soaked}$, while Flv1-ΔFlR showed a citrate anion. Flv1-ΔFlR was also found deflavinated, in spite of various FMN crystal soakings or co-crystallization attempts. Flv1-ΔFlR putative metal ligands are neutral or basic (H108-x-N110-x-N112-R113-x_{64}-H178-x_{18}-K197-x_{56}-H254, *Synechocystis* Flv1 numbering) and incorporation of anions in the pseudo diiron site could be due to a prevalence of basic residues in its neighborhood (Fig. 5.4 B). Interestingly, the crystal structure of *Anabaena* sp. PCC 7120 β-lactamase-like domain (PDB 4FEK) belonging to Class C Type 3, also revealed a demetallated pseudo diiron site harboring a phosphate anion in the same region (Fig. 5.4 C). The Class C Types 2 and 3 FDPs differ only in the second residue of the pseudo iron binding motif: in Type 2 is an asparagine while in Type 3 is a serine residue (Table 5.2).

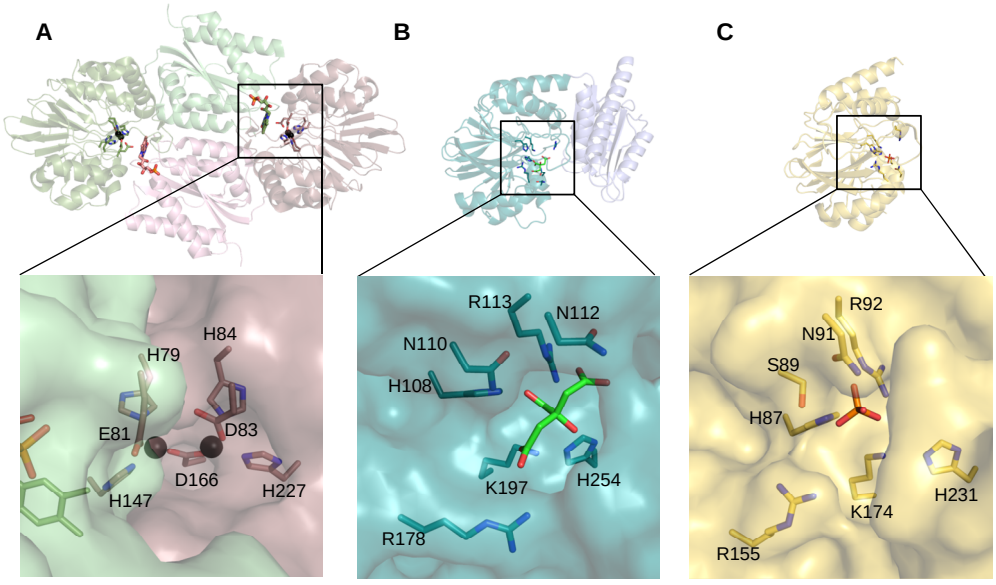

Figure 5.4- Catalytic cavity in FDPs from different classes. **A)** Cartoon representation of the *E. coli* FDP "head-to-tail" dimer (PDB 4D02). One monomer is colored in green and the opposing one in pink. The metallo-β-lactamase and flavodoxin-like domains are shown with darker and lighter colors, respectively. At the bottom it is shown a zoomed view of the metal catalytic center. **B)** Cartoon representation of the *Synechocystis* sp. PCC 6803 Flv1-ΔFlR monomer colored in blue. The metallo-β-lactamase and flavodoxin-like domains are shown with darker and lighter colors, respectively. At the bottom it is shown a zoomed view of the pseudo metal catalytic center. **C)** Cartoon representation of the *Anabaena* sp. PCC 7120 metallo-β-lactamase-like domain colored in yellow (PDB 4FEK). At the bottom it is shown a zoomed view of the pseudo metal catalytic center. Iron atoms are represented as black spheres. The FMN is shown as sticks with carbon in green or pink, nitrogen in blue, oxygen in red and phosphorous in orange. The residues are shown as sticks with carbon colored accordingly the monomer colour, nitrogen in blue and oxygen in red. Below the panel A is shown the canonical iron binding motif (Type 1), while below panel B and C is shown the corresponding amino acids residues substitutions for non canonical Class C FDPs, Type 2 and 3, respectively.

The high number of different combinations of putative ligands in oxygenic phototrophic organisms is intriguing. Nevertheless, although several attempts of metals incorporation in Flv1-ΔFlR pseudo catalytic site were not successful, there are reports of basic or neutral residues coordinating metals (Berkovitch et al., 2004; Fang et al., 2012; Owens et al., 2016; Sundheim et al., 2006) (Fig. 5.5). Moreover, as previously reported (Mustila et al., 2016), Flv1 by itself is involved in alternative electron transfer pathways, as it improves photosynthesis and CO_2 uptake suggesting that this protein

in its native state contains redox cofactors (Chapter IV).

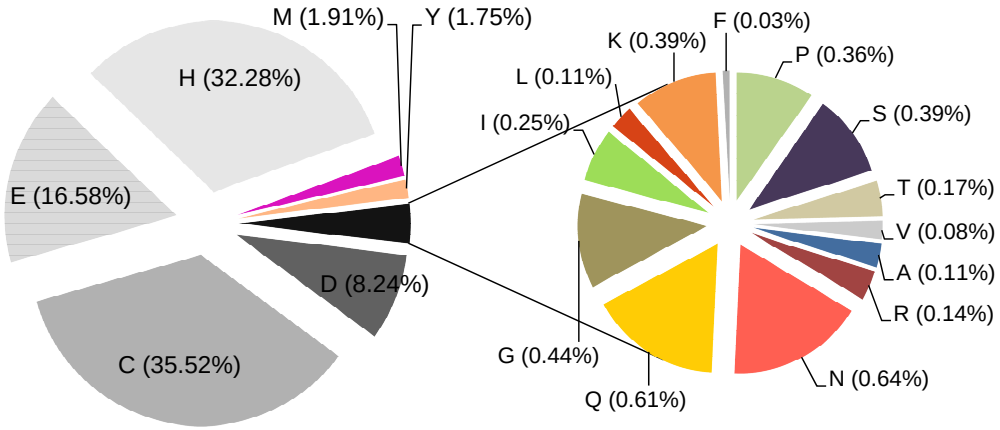

Figure 5.5- Schematic representation of metal ligands from proteins structures deposited in the PDB.

5.3 The family of flavodiiron proteins and their substrate selectivity

The genes encoding FDPs were originally believed to be restricted to prokaryotes but they were subsequently identified in the genomes of some anaerobic protozoa (Loftus et al., 2005; Sarti et al., 2004). Moreover, flavodiiron protein genes were also identified in the genomes of oxygenic photosynthetic prokaryotes and eukaryotes (Chaux et al., 2017; Gerotto et al., 2016; Helman et al., 2003; Shimakawa et al., 2017; Wasserfallen et al., 1998).

The molecular determinants that affect substrate selectivity were addressed in the oxygen-selective *E. histolytica* FDP, where K53 and Y271 residues were replaced by the corresponding residues in the nitric oxide-selective *E. coli* FDP, D52 and S262, respectively (Gonçalves et al., 2014). Thus, this was an attempt to try to convert a O_2 reductase into a NO reductase (Section 1.5). The reported results showed the relevance of Y271 residue, in modulating FDP substrate selectivity. In order to unravel at atomic level possible roles for the residues at these positions, sequences of biochemically and kinetically characterized FDPs were aligned against a FDPs 3D sequence profile, obtained upon superposition of all available FDP structures (Table

1.9, Fig. 5.6). The O_2 reductases are present in eukaryotic pathogenic *G. intestinalis*, *E. histolytica* and *T. vaginalis* organisms, and in prokaryotic *T. denticola*, *C. acetobutylicum* and *T. maritima* organisms. These FDPs show in the diiron second coordination sphere, conserved K and Y residues at the first and second positions, respectively (Di Matteo et al., 2008; Folgosa et al., 2018b; Frederick et al., 2015; Hayashi et al., 2010; Hillmann et al., 2009; Smutna et al., 2009; Vicente et al., 2012). Although there are no kinetic studies on the *R. capsulatus* FDP, the presence of K71 and Y284 residues at the referred positions, suggests that it might also be selective for oxygen. Additionally, the Class F FDP from *C. difficile* 630 presents both oxygen and hydrogen peroxide reductase activities, and includes K55 and H267 residues (Folgosa et al., 2018b).

The FDPs from *Desulfovibrio* species, *D. gigas* and *D. vulgaris*, show bifunctional activitiy and have K and W residues at the two positions (Rodrigues et al., 2006; Silaghi-Dumitrescu et al., 2005b). *M. thermoacetica* FDP also has bifunctional activity with Y54 and W263 residues at the two positions (Silaghi-Dumitrescu et al., 2003). With the same type of bifunctional activity there is *C. acetobutylicum* FDP_2 with H52 and Y265 residues at homologous positions.

The methanogenic archaeal FDPs from *M. marburgensis* and *M. arboriphilus*, have been shown to reduce only oxygen, and contain Y and H residues in both positions (Seedorf et al., 2004; Seedorf et al., 2007).

O_2 reductases	
T. vaginalis	$K_{65}Y_{267}$
G .intestinalis	$K_{58}Y_{267}$
T. maritima	$K_{58}Y_{264}$
T. denticola	$K_{53}Y_{273}$
E. histolytica	$K_{53}Y_{271}$
C. acetobutylicum FDP_1	$K_{52}Y_{259}$
R. capsulatus[1]	$K_{71}Y_{284}$
C. difficile[2]	$K_{55}H_{267}$

Methanogenic O_2 reductases	
M. arboriphilus	$Y_{53}H_{271}$
M. marburgensis	$Y_{53}H_{267}$
M. thermautotrophicus[1]	$Y_{53}H_{267}$

Cyanobacteria O_2 reductases	
Synechocystis Flv1[1]	$G_{81}Y_{291}$
Synechocystis Flv2[1]	$G_{79}Y_{287}$
Synechocystis Flv3	$H_{63}Y_{273}$
Synechocystis Flv4[1]	$H_{70}Y_{277}$

O_2/NO reductases	
D. vulgaris	$K_{52}W_{263}$
D. gigas	$K_{52}W_{263}$
M. thermoacetica	$Y_{54}W_{263}$
C. acetobutylicum FDP_2	$H_{52}Y_{265}$

NO reductases	
E. coli	$D_{52}S_{262}$

Figure 5.6- Analysis of characterized flavodiiron proteins. Amino acid sequences of FDPs were obtained from NCBI (http://www.ncbi.nlm.nih.gov/). *M. thermoacetica* (Q9FDN7.1), *M. marburgensis* (AAB88013.1), *M. thermautotrophicus* (AAB53659.1), *R. capsulatus* (BAA02789.2), *M. arboriphilus* (ACA13278.1), *D. vulgaris* (AAS97655.1), *G. intestinalis* (AAM94641.1), *T. maritima* (NP_228564.1), *D. gigas* (Q9F0J6.1), *E. histolytica* (XP_656946.1), *C. acetobutylicum* (FDP1; Q97K92.1, FDP2; Q97GC0.1), *T. vaginalis* (EAY22576.1), *T. denticola* (NP_971686.1), *E. coli* (NP_417190.1), *Synechocystis* sp. PCC 6803 (Flv1; BAA18468.1, Flv2; BAA16728.1, Flv3; BAA10483.1; Flv4; BAA16730.1). [1] FDPs with no activities reported. [2] FDP with peroxidase activity.

It is reported that *Synechocystis* Flv2 and Flv4 function in photoprotection of photosystem II (Zhang et al., 2009; Zhang et al., 2012), while Flv1 and Flv3 provide protection for photosystem I under fluctuating growth light (Allahverdiyeva et al., 2011; Helman et al., 2003). Additionally, Flv3 is the only protein from *Synechocystis* sp. PCC 6803 characterized *in vitro* with oxygen reductase activity (Vicente et al., 2002). The non canonical Flv1 and Flv2 and canonical Flv3 and Flv4 have G and Y or H and Y residues at the corresponding homologous positions, respectively.

Overall, it appears that FDPs with only oxygen selectivity contain K and Y residues at the two positions. Moreover, methanogenic oxygen reductases have Y and H residues, and cyanobacteria oxygen reductases have H/G and Y residues. The bifunctional FDPs show at the referred positions, K/Y/H and W/Y residues. Therefore, the common denominator of FDPs showing oxygen reductase activity is the presence of a tyrosine or a tryptophan residue located at one or both positions. Thus, the NO-selective *E. coli* FDP is unique, since it has neither tyrosine nor tryptophan residues at the mentioned positions.

An analysis of tyrosines and tryptophans chains bridging the diiron site with the protein external surface (Fig. 2.7 and 5.7) showed that, FDPs selective only for oxygen have four radicals exit routes, the bifunctional enzymes have three routes while the exclusive NO-selective *E. coli* FDP only has two exit routes.

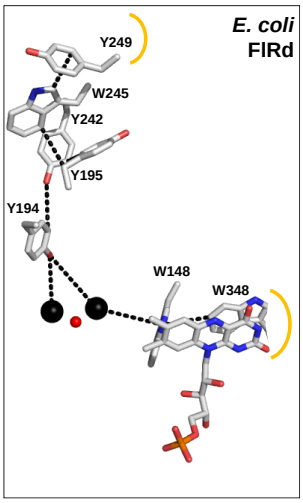

Figure 5.7- Distribution of tyrosine and tryptophan residues, from *E. coli* FDP (4D02) with the shortest edge-to-edge distance (dash line) between residues, from the active site to the protein solvent accessible surface. The tyrosine/tryptophan chains are represented as sticks with carbons colored in grey, nitrogen in blue and oxygen in red. The residues that contact with the external surface of the protein are highlighted with a yellow line. The iron atoms and μ-hydroxo bridge are represented as black and red spheres, respectively. FMN is shown as sticks with carbon atoms in green, nitrogen in blue, oxygen in red and phosphorous in orange.

Based on the previous *E. histolytica* FDP studies, and in order to understand the role of D52 and S262 residues from *E. coli* FDP in substrate selectivity, single mutants D52K, S262Y and double mutant D52K/S262Y were designed, in an attempt to convert a NO reductase into an O_2 reductase. The S262Y mutant structure differs from the wild-type or the other two mutants structures in the diiron catalytic site (Chapters II and III), in particular it shows longer iron coordination distances, negative Fourier difference densities and lack of electron density at side chains of some metal ligands. These structural differences were attributed to a higher sensitivity of S262Y crystal to X-ray radiation. Noteworthy, in these experiments the S262Y mutant crystal had a lower absorbed dose than the other crystals. Its higher X-ray sensitivity may be related to a lower solvent exposed area from Y262 residue, when compared with the double mutant, since it decreases the efficiency for harmful radicals escape. On the other hand, the K52 residue present in the double mutant, induced a conformation change of E82 residue in the neighborhood of Y262, allowing a higher exposed accessible surface area of this aromatic residue.

The analysis of the tyrosine and tryptophan chains in the *E. coli* FDP-ΔRd mutants, shows two exit routes in the *E. coli* FDP-ΔRd D52K as it does in the native protein, while the S262Y and D52K/S262Y mutants display three escape routes, suggesting that these mutants may have more affinity towards oxygen.

Overall, we suggest that an aromatic residue, such as tyrosine and tryptophan, located in the diiron second coordination sphere and a higher number of escape routes may facilitate the selectivity towards oxygen.

5.4 Concluding remarks

The present thesis focuses on the crystal structures analyses of two truncated FDPs from *E. coli* and *Synechocystis* sp. PCC 6803, belonging to Classes B and C, respectively. Thus, it is reported the crystal structure of the flavodiiron core (metallo-β-lactamase and flavodoxin-like domains) of *E. coli* FDP-ΔRd single and double mutants (D52K, S262Y, D52K/S262Y), as well as the corresponding domains in *Synechocystis* Flv1-ΔFlR.

E. coli FDP-ΔRd mutants include the minimal "head-to-tail" dimeric conformation (like in native *E. coli* FDP), which is maintained mainly by three conserved regions involved in the dimerization interface. These interactions are established between residues from the β-lactamase-like domain and the flavodoxin-like domain from the opposing monomer. *Synechocystis* Flv1 lacking the NAD(P)H:flavin oxidoreductase domain (Flv1-ΔFlR), retains only a monomeric form, but interestingly, the three regions present in the "head-to-tail" dimer from other FDPs are also conserved in Flv1-ΔFlR, although they are within the same monomer. Therefore, we report for the first time in this family of proteins, a minimal FDP monomeric structure, but it remains to be elucidate whether the presence of NAD(P)H:flavin oxidoreductase domain would affect the oligomeric state of the full length Flv1.

Additionally, FDP-ΔRd mutants and Flv1-ΔFlR structures reveal differences in the catalytic center regarding metal ligands, as previously proposed upon amino acid sequence comparisons. Thus, while *E. coli* FDP-ΔRd mutants contain the FDPs canonical diiron ligands (Type 1), *Synechocystis* sp. PCC 6803 Flv1-ΔFlR shows a non-canonical combination of putative metal ligands (Type 2). However, a functional diiron site in Flv1-ΔFlR remains to be determined since several attempts of metal soaking were not successful. Instead, anionic species were located in the demetallated cavity, which could have resulted from its predominantly basic neighbourhood. Although some *in vivo* studies point out for a functional protein with

intact redox cofactors, the role of all these structural differences in Flv1-ΔFlR catalytic activity are indeed intriguing.

The substrate selectivity among FDPs is one of the main issues in this area, since no significant differences were observed in the diiron first coordination sphere from FDPs exhibiting distinct substrate activities. However, some reported studies in *Entamoeba histolytica* FDP point out for a modulation of the substrate selectivity by residues surrounding the diiron first coordination sphere. In this work, we tried to unravel the molecular determinants that affect the substrate preference. Therefore, a structural analysis of single and double mutants from *E. coli* FDP-ΔRd, was performed in an attempt to convert this NOR into a O_2R. *E. coli* FDP-ΔRd S262Y crystals showed higher sensitivity to X-ray radiation, despite the calculated low absorbed dose, and structural inconsistencies were observed in this mutant diiron site region, thus contrasting with FDP native and others mutants (D52K and D52K/S262Y) structures. Since the oxygen selective FDPs contain in the diiron site second coordination sphere at least one tyrosine or a tryptophan residue, this may suggest that FDP-ΔRd S262Y and D52K/S262Y may have more affinity to oxygen than the native protein.

Overall, the present work allowed the comparison of the flavodiiron core from Classes B and C FDPs structures. Apart from the radiation damage effects observed only in FDP-ΔRd S262Y diiron site and its lower Y262 accessible surface area, no further structural differences were detected. Therefore, the structural determinants modulating substrate selectivity still need to be clarified and thus further kinetic and structural studies are required to elucidate this intriguing question.

Directed evolution would be a promising strategy to address the substrate selectivity in FDPs, in order to convert an NO- towards O_2 –selective, or the other way around.

Bibliographic References

Abreu, I.A., and D.E. Cabelli. 2010. Superoxide dismutases-a review of the metal-associated mechanistic variations. *Biochim Biophys Acta*. 1804:263-274.

Adam, V., A. Royant, V. Niviere, F.P. Molina-Heredia, and D. Bourgeois. 2004. Structure of superoxide reductase bound to ferrocyanide and active site expansion upon X-ray-induced photo-reduction. *Structure*. 12:1729-1740.

Adams, P.D., P.V. Afonine, G. Bunkoczi, V.B. Chen, I.W. Davis, N. Echols, J.J. Headd, L.W. Hung, G.J. Kapral, R.W. Grosse-Kunstleve, A.J. McCoy, N.W. Moriarty, R. Oeffner, R.J. Read, D.C. Richardson, J.S. Richardson, T.C. Terwilliger, and P.H. Zwart. 2010a. PHENIX: a comprehensive Python-based system for macromolecular structure solution. *Acta Crystallogr D*. 66:213-221.

Adams, P.D., P.V. Afonine, G. Bunkoczi, V.B. Chen, I.W. Davis, N. Echols, J.J. Headd, L.W. Hung, G.J. Kapral, R.W. Grosse-Kunstleve, A.J. McCoy, N.W. Moriarty, R. Oeffner, R.J. Read, D.C. Richardson, J.S. Richardson, T.C. Terwilliger, and P.H. Zwart. 2010b. PHENIX: a comprehensive Python-based system for macromolecular structure solution. *Acta crystallographica. Section D, Biological crystallography*. 66:213-221.

Afonine, P.V., R.W. Grosse-Kunstleve, N. Echols, J.J. Headd, N.W. Moriarty, M. Mustyakimov, T.C. Terwilliger, A. Urzhumtsev, P.H. Zwart, and P.D. Adams. 2012. Towards automated crystallographic structure refinement with phenix.refine. *Acta Crystallogr D*. 68:352-367.

Aliverti, A., V. Pandini, A. Pennati, M. de Rosa, and G. Zanetti. 2008. Structural and functional diversity of ferredoxin-NADP(+) reductases. *Archives of biochemistry and biophysics*. 474:283-291.

Allahverdiyeva, Y., M. Ermakova, M. Eisenhut, P. Zhang, P. Richaud, M. Hagemann, L. Cournac, and E.M. Aro. 2011. Interplay between flavodiiron proteins and photorespiration in Synechocystis sp. PCC 6803. *J Biol Chem*. 286:24007-24014.

Allahverdiyeva, Y., J. Isojarvi, P. Zhang, and E.M. Aro. 2015a. Cyanobacterial Oxygenic Photosynthesis is Protected by Flavodiiron Proteins. *Life (Basel)*. 5:716-743.

Allahverdiyeva, Y., H. Mustila, M. Ermakova, L. Bersanini, P. Richaud, G. Ajlani, N. Battchikova, L. Cournac, and E.M. Aro. 2013. Flavodiiron proteins Flv1 and Flv3 enable cyanobacterial growth and photosynthesis under fluctuating light. *Proceedings of the National Academy of Sciences of the United States of America*. 110:4111-4116.

Allahverdiyeva, Y., M. Suorsa, M. Tikkanen, and E.M. Aro. 2015b. Photoprotection of photosystems in fluctuating light intensities. *Journal of experimental botany*. 66:2427-2436.

Almeida, C.C., C.V. Romao, P.F. Lindley, M. Teixeira, and L.M. Saraiva. 2006. The role of the hybrid cluster protein in oxidative stress defense. *J Biol Chem*. 281:32445-32450.

Andersson, J.O., A.M. Sjogren, L.A. Davis, T.M. Embley, and A.J. Roger. 2003. Phylogenetic analyses of diplomonad genes reveal frequent lateral gene transfers affecting eukaryotes. *Curr Biol*. 13:94-104.

Arai, H., Y. Igarashi, and T. Kodama. 1995. The structural genes for nitric oxide reductase from Pseudomonas aeruginosa. *Biochim Biophys Acta*. 1261:279-284.

Arndt, U.W., R.A. Crowther, and J.F. Mallett. 1968. A computer-linked cathode-ray tube microdensitometer for x-ray crystallography. *J Sci Instrum*. 1:510-516.

Auchere, F., and F. Rusnak. 2002. What is the ultimate fate of superoxide anion in vivo? *J Biol Inorg Chem*. 7:664-667.

Baptista, J.M., M.C. Justino, A.M. Melo, M. Teixeira, and L.M. Saraiva. 2012. Oxidative stress modulates the nitric oxide defense promoted by Escherichia coli flavorubredoxin. *J Bacteriol*. 194:3611-3617.

Bebrone, C. 2007. Metallo-beta-lactamases (classification, activity, genetic organization, structure, zinc coordination) and their superfamily. *Biochem Pharmacol*. 74:1686-1701.

Beckman, J.S., T.W. Beckman, J. Chen, P.A. Marshall, and B.A. Freeman. 1990. Apparent hydroxyl radical production by peroxynitrite: implications for endothelial injury from nitric oxide and superoxide. *Proceedings of the National Academy of Sciences of the United States of America*. 87:1620-1624.

Berkovitch, F., Y. Nicolet, J.T. Wan, J.T. Jarrett, and C.L. Drennan. 2004. Crystal structure of biotin synthase, an S-adenosylmethionine-dependent radical enzyme. *Science*. 303:76-79.

Berman, H.M., J. Westbrook, Z. Feng, G. Gilliland, T.N. Bhat, H. Weissig, I.N. Shindyalov, and P.E. Bourne. 2000. The Protein Data Bank. *Nucleic acids research*. 28:235-242.

Bernroitner, M., M. Zamocky, P.G. Furtmuller, G.A. Peschek, and C. Obinger. 2009. Occurrence, phylogeny, structure, and function of catalases and peroxidases in cyanobacteria. *Journal of experimental botany*. 60:423-440.

Bersanini, L., N. Battchikova, M. Jokel, A. Rehman, I. Vass, Y. Allahverdiyeva, and E.M. Aro. 2014. Flavodiiron protein Flv2/Flv4-related photoprotective mechanism dissipates excitation pressure of PSII in cooperation with phycobilisomes in Cyanobacteria. *Plant physiology*. 164:805-818.

Blankenship, R.E. 2010. Early evolution of photosynthesis. *Plant physiology*. 154:434-438.

Borisov, V.B., E. Forte, S.A. Siletsky, P. Sarti, and A. Giuffre. 2015. Cytochrome bd from Escherichia coli catalyzes peroxynitrite decomposition. *Biochimica et biophysica acta*. 1847:182-188.

Borisov, V.B., R.B. Gennis, J. Hemp, and M.I. Verkhovsky. 2011. The cytochrome bd respiratory oxygen reductases. *Biochim Biophys Acta*. 1807:1398-1413.

Bothe, H., O. Schmitz, M.G. Yates, and W.E. Newton. 2010. Nitrogen fixation and hydrogen metabolism in cyanobacteria. *Microbiology and molecular biology reviews : MMBR*. 74:529-551.

Bredt, D.S., P.M. Hwang, C.E. Glatt, C. Lowenstein, R.R. Reed, and S.H. Snyder. 1991. Cloned and expressed nitric oxide synthase structurally resembles cytochrome P-450 reductase. *Nature*. 351:714-718.

Buick, R. 2008. When did oxygenic photosynthesis evolve? *Philosophical transactions of the Royal Society of London. Series B, Biological sciences*. 363:2731-2743.

Burmeister, W.P. 2000. Structural changes in a cryo-cooled protein crystal owing to radiation damage. *Acta Crystallogr D Biol Crystallogr*. 56:328-341.

Busch, A., B. Friedrich, and R. Cramm. 2002. Characterization of the norB gene, encoding nitric oxide reductase, in the nondenitrifying cyanobacterium Synechocystis sp. strain PCC6803. *Applied and environmental microbiology*. 68:668-672.

Cameron, A.D., M. Ridderstrom, B. Olin, and B. Mannervik. 1999. Crystal structure of human glyoxalase II and its complex with a glutathione thiolester substrate analogue. *Structure*. 7:1067-1078.

Carfi, A., S. Pares, E. Duee, M. Galleni, C. Duez, J.M. Frere, and O. Dideberg. 1995. The 3-D structure of a zinc metallo-beta-lactamase from Bacillus cereus reveals a new type of protein fold. *The EMBO journal*. 14:4914-4921.

Carlioz, A., M.L. Ludwig, W.C. Stallings, J.A. Fee, H.M. Steinman, and D. Touati. 1988. Iron superoxide dismutase. Nucleotide sequence of the gene from Escherichia coli K12 and correlations with crystal structures. *The Journal of biological chemistry*. 263:1555-1562.

Chaux, F., A. Burlacot, M. Mekhalfi, P. Auroy, S. Blangy, P. Richaud, and G. Peltier. 2017. Flavodiiron Proteins Promote Fast and Transient O2 Photoreduction in Chlamydomonas. *Plant physiology*. 174:1825-1836.

Chelikani, P., I. Fita, and P.C. Loewen. 2004. Diversity of structures and properties among catalases. *Cellular and molecular life sciences : CMLS*. 61:192-208.

Chen, L., M.Y. Liu, J. Legall, P. Fareleira, H. Santos, and A.V. Xavier. 1993a. Purification and characterization of an NADH-rubredoxin oxidoreductase involved in the utilization of oxygen by Desulfovibrio gigas. *European journal of biochemistry / FEBS*. 216:443-448.

Chen, L., M.Y. Liu, J. LeGall, P. Fareleira, H. Santos, and A.V. Xavier. 1993b. Rubredoxin oxidase, a new flavo-hemo-protein, is the site of oxygen reduction to water by the "strict anaerobe" Desulfovibrio gigas. *Biochemical and biophysical research communications*. 193:100-105.

Chen, L., Q.W. Xie, and C. Nathan. 1998. Alkyl hydroperoxide reductase subunit C (AhpC) protects bacterial and human cells against reactive nitrogen intermediates. *Molecular cell*. 1:795-805.

Chen, V.B., W.B. Arendall, 3rd, J.J. Headd, D.A. Keedy, R.M. Immormino, G.J. Kapral, L.W. Murray, J.S. Richardson, and D.C. Richardson. 2010. MolProbity: all-atom structure validation for macromolecular crystallography. *Acta Crystallogr D Biol Crystallogr*. 66:12-21.

Choong, Y.S., and V. Massey. 1980. Stabilization of lactate oxidase flavin anion radical by complex formation. *The Journal of biological chemistry*. 255:8672-8677.

Clarke, T.A., G.L. Kemp, J.H. Van Wonderen, R.M. Doyle, J.A. Cole, N. Tovell, M.R. Cheesman, J.N. Butt, D.J. Richardson, and A.M. Hemmings. 2008. Role of a conserved glutamine residue in tuning the catalytic activity of Escherichia coli cytochrome c nitrite reductase. *Biochemistry*. 47:3789-3799.

Corbett, M.C., M.J. Latimer, T.L. Poulos, I.F. Sevrioukova, K.O. Hodgson, and B. Hedman. 2007. Photoreduction of the active site of the metalloprotein putidaredoxin by synchrotron radiation. *Acta Crystallogr D Biol Crystallogr*. 63:951-960.

Cotter, P.A., S.B. Melville, J.A. Albrecht, and R.P. Gunsalus. 1997. Aerobic regulation of cytochrome d oxidase (cydAB) operon expression in Escherichia coli: roles of Fnr and ArcA in repression and activation. *Molecular microbiology*. 25:605-615.

Cramm, R., R.A. Siddiqui, and B. Friedrich. 1997. Two isofunctional nitric oxide reductases in Alcaligenes eutrophus H16. *J Bacteriol*. 179:6769-6777.

Culotta, V.C., and M.J. Daly. 2013. Manganese complexes: diverse metabolic routes to oxidative stress resistance in prokaryotes and yeast. *Antioxidants & redox signaling*. 19:933-944.

Culotta, V.C., M. Yang, and T.V. O'Halloran. 2006. Activation of superoxide dismutases: putting the metal to the pedal. *Biochim Biophys Acta*. 1763:747-758.

da Costa, P.N., M. Teixeira, and L.M. Saraiva. 2003. Regulation of the flavorubredoxin nitric oxide reductase gene in Escherichia coli: nitrate repression, nitrite induction, and possible post-transcription control. *FEMS microbiology letters*. 218:385-393.

Dang, K.V., J. Plet, D. Tolleter, M. Jokel, S. Cuine, P. Carrier, P. Auroy, P. Richaud, X. Johnson, J. Alric, Y. Allahverdiyeva, and G. Peltier. 2014. Combined increases in mitochondrial cooperation and oxygen photoreduction compensate for deficiency in cyclic electron flow in Chlamydomonas reinhardtii. *Plant Cell*. 26:3036-3050.

Darwin, A., H. Hussain, L. Griffiths, J. Grove, Y. Sambongi, S. Busby, and J. Cole. 1993. Regulation and sequence of the structural gene for cytochrome c552 from Escherichia coli: not a hexahaem but a 50 kDa tetrahaem nitrite reductase. *Molecular microbiology*. 9:1255-1265.

Dassa, J., H. Fsihi, C. Marck, M. Dion, M. Kieffer-Bontemps, and P.L. Boquet. 1991. A new oxygen-regulated operon in Escherichia coli comprises the genes for a putative third cytochrome oxidase and for pH 2.5 acid phosphatase (appA). *Molecular & general genetics : MGG*. 229:341-352.

de Boer, A.P., J. van der Oost, W.N. Reijnders, H.V. Westerhoff, A.H. Stouthamer, and R.J. van Spanning. 1996. Mutational analysis of the nor gene cluster which encodes nitric-oxide reductase from Paracoccus denitrificans. *European journal of biochemistry / FEBS*. 242:592-600.

DeLano, W.L. 2002. The PyMOL Molecular Graphics System.

Di Matteo, A., F.M. Scandurra, F. Testa, E. Forte, P. Sarti, M. Brunori, and A. Giuffre. 2008. The O2-scavenging flavodiiron protein in the human parasite Giardia intestinalis. *J Biol Chem*. 283:4061-4068.

Diaz, A., P.C. Loewen, I. Fita, and X. Carpena. 2012. Thirty years of heme catalases structural biology. *Arch Biochem Biophys*. 525:102-110.

Diederichs, K., and P.A. Karplus. 1997. Improved R-factors for diffraction data analysis in macromolecular crystallography. *Nat Struct Biol*. 4:269-275.

Dong, Y.J., M. Bartlam, L. Sun, Y.F. Zhou, Z.P. Zhang, C.G. Zhang, Z. Rao, and X.E. Zhang. 2005. Crystal structure of methyl parathion hydrolase from Pseudomonas sp. WBC-3. *J Mol Biol*. 353:655-663.

Dundas, J., Z. Ouyang, J. Tseng, A. Binkowski, Y. Turpaz, and J. Liang. 2006. CASTp: computed atlas of surface topography of proteins with structural and topographical mapping of functionally annotated residues. *Nucleic acids research*. 34:W116-118.

Dykhuizen, R.S., A. Fraser, H. McKenzie, M. Golden, C. Leifert, and N. Benjamin. 1998. Helicobacter pylori is killed by nitrite under acidic conditions. *Gut*. 42:334-337.

Eisenhut, M., J. Georg, S. Klahn, I. Sakurai, H. Mustila, P. Zhang, W.R. Hess, and E.M. Aro. 2012. The antisense RNA As1_flv4 in the Cyanobacterium Synechocystis sp. PCC 6803 prevents premature expression of the flv4-2 operon upon shift in inorganic carbon supply. *The Journal of biological chemistry*. 287:33153-33162.

Elvers, K.T., G. Wu, N.J. Gilberthorpe, R.K. Poole, and S.F. Park. 2004. Role of an inducible single-domain hemoglobin in mediating resistance to nitric oxide and nitrosative stress in Campylobacter jejuni and Campylobacter coli. *J Bacteriol*. 186:5332-5341.

Emsley, P., and K. Cowtan. 2004. Coot: model-building tools for molecular graphics. *Acta Crystallogr D Biol Crystallogr*. 60:2126-2132.

Emsley, P., B. Lohkamp, W.G. Scott, and K. Cowtan. 2010. Features and development of Coot. *Acta Crystallogr D*. 66:486-501.

Engh, R.A., and R. Huber. 1991. Accurate Bond and Angle Parameters for X-Ray Protein-Structure Refinement. *Acta Crystallographica Section A*. 47:392-400.

Ericsson, U.B., B.M. Hallberg, G.T. Detitta, N. Dekker, and P. Nordlund. 2006. Thermofluor-based high-throughput stability optimization of proteins for structural studies. *Anal Biochem*. 357:289-298.

Evans, P.R. 2011. An introduction to data reduction: space-group determination, scaling and intensity statistics. *Acta crystallographica. Section D, Biological crystallography*. 67:282-292.

Fang, F.C. 1997. Perspectives series: host/pathogen interactions. Mechanisms of nitric oxide-related antimicrobial activity. *The Journal of clinical investigation*. 99:2818-2825.

Fang, F.C. 2004. Antimicrobial reactive oxygen and nitrogen species: concepts and controversies. *Nature reviews. Microbiology*. 2:820-832.

Fang, H., J.D. Caranto, R. Mendoza, A.B. Taylor, P.J. Hart, and D.M. Kurtz, Jr. 2012. Histidine ligand variants of a flavo-diiron protein: effects on structure and activities. *J Biol Inorg Chem*. 17:1231-1239.

Fee, J.A. 1991. Regulation of sod genes in Escherichia coli: relevance to superoxide dismutase function. *Molecular microbiology*. 5:2599-2610.

Figueiredo, M.C., S.A. Lobo, S.H. Sousa, F.P. Pereira, J.D. Wall, L.S. Nobre, and L.M. Saraiva. 2013. Hybrid cluster proteins and flavodiiron proteins afford protection to Desulfovibrio vulgaris upon macrophage infection. *J Bacteriol*. 195:2684-2690.

Fischer, D.S., and D.C. Price. 1964. A Simple Serum Iron Method Using the New Sensitive Chromogen Tripyridyl-S-Triazine. *Clin Chem*. 10:21-31.

Folgosa, F., M.C. Martins, and M. Teixeira. 2018a. Diversity and complexity of flavodiiron NO/O2 reductases. *FEMS Microbiol Lett*. 365.

Folgosa, F., M.C. Martins, and M. Teixeira. 2018b. The multidomain flavodiiron protein from Clostridium difficile 630 is an NADH:oxygen oxidoreductase. *Scientific reports*. 8:10164.

Frazao, C., G. Silva, C.M. Gomes, P. Matias, R. Coelho, L. Sieker, S. Macedo, M.Y. Liu, S. Oliveira, M. Teixeira, A.V. Xavier, C. Rodrigues-Pousada, M.A. Carrondo, and J. Le Gall. 2000. Structure of a dioxygen reduction enzyme from Desulfovibrio gigas. *Nat Struct Biol*. 7:1041-1045.

Frederick, R.E., J.D. Caranto, C.A. Masitas, L.L. Gebhardt, C.E. MacGowan, R.J. Limberger, and D.M. Kurtz, Jr. 2015. Dioxygen and nitric oxide scavenging by Treponema denticola flavodiiron protein: a mechanistic paradigm for catalysis. *J Biol Inorg Chem*. 20:603-613.

Frei, B. 1994. Reactive oxygen species and antioxidant vitamins: mechanisms of action. *Am J Med*. 97:5S-13S; discussion 22S-28S.

Frey, A.D., and P.T. Kallio. 2003. Bacterial hemoglobins and flavohemoglobins: versatile proteins and their impact on microbiology and biotechnology. *FEMS Microbiol Rev*. 27:525-545.

Friedrich, M.J., L.C. de Veaux, and R.J. Kadner. 1986. Nucleotide sequence of the btuCED genes involved in vitamin B12 transport in Escherichia coli and homology with components of periplasmic-binding-protein-dependent transport systems. *Journal of bacteriology*. 167:928-934.

Gabdulkhakov, A., A. Guskov, M. Broser, J. Kern, F. Muh, W. Saenger, and A. Zouni. 2009. Probing the accessibility of the Mn(4)Ca cluster in photosystem II: channels calculation, noble gas derivatization, and cocrystallization with DMSO. *Structure*. 17:1223-1234.

Gaber, A., M. Tamoi, T. Takeda, Y. Nakano, and S. Shigeoka. 2001. NADPH-dependent glutathione peroxidase-like proteins (Gpx-1, Gpx-2) reduce unsaturated fatty acid hydroperoxides in Synechocystis PCC 6803. *FEBS letters*. 499:32-36.

Gantt, E. 2011. Oxygenic photosynthesis and the distribution of chloroplasts. *Photosynthesis research*. 107:1-6.

Garau, G., D. Lemaire, T. Vernet, O. Dideberg, and A.M. Di Guilmi. 2005. Crystal structure of phosphorylcholine esterase domain of the virulence factor choline-binding protein e from streptococcus pneumoniae: new structural features among the metallo-beta-lactamase superfamily. *J Biol Chem*. 280:28591-28600.

Garces, F., F.J. Fernandez, C. Montella, E. Penya-Soler, R. Prohens, J. Aguilar, L. Baldoma, M. Coll, J. Badia, and M.C. Vega. 2010. Molecular architecture of the Mn2+-dependent lactonase UlaG reveals an RNase-like metallo-beta-lactamase fold and a novel quaternary structure. *J Mol Biol*. 398:715-729.

Gardner, A.M., R.A. Helmick, and P.R. Gardner. 2002. Flavorubredoxin, an inducible catalyst for nitric oxide reduction and detoxification in Escherichia coli. *J Biol Chem*. 277:8172-8177.

Gardner, P.R. 2005. Nitric oxide dioxygenase function and mechanism of flavohemoglobin, hemoglobin, myoglobin and their associated reductases. *J Inorg Biochem*. 99:247-266.

Gardner, P.R., A.M. Gardner, L.A. Martin, and A.L. Salzman. 1998. Nitric oxide dioxygenase: an enzymic function for flavohemoglobin. *Proceedings of the National Academy of Sciences of the United States of America*. 95:10378-10383.

Garman, E. 2003. 'Cool' crystals: macromolecular cryocrystallography and radiation damage. *Curr Opin Struct Biol*. 13:545-551.

Garthwaite, J. 1991. Glutamate, nitric oxide and cell-cell signalling in the nervous system. *Trends Neurosci*. 14:60-67.

Gerotto, C., A. Alboresi, A. Meneghesso, M. Jokel, M. Suorsa, E.M. Aro, and T. Morosinotto. 2016. Flavodiiron proteins act as safety valve for electrons in Physcomitrella patens. *Proceedings of the National Academy of Sciences of the United States of America*. 113:12322-12327.

Giuffre, A., V.B. Borisov, M. Arese, P. Sarti, and E. Forte. 2014. Cytochrome bd oxidase and bacterial tolerance to oxidative and nitrosative stress. *Biochimica et biophysica acta*. 1837:1178-1187.

Gomes, C.M., C. Frazao, A.V. Xavier, J. Legall, and M. Teixeira. 2002a. Functional control of the binuclear metal site in the metallo-beta-lactamase-like fold by subtle amino acid replacements. *Protein Sci*. 11:707-712.

Gomes, C.M., A. Giuffre, E. Forte, J.B. Vicente, L.M. Saraiva, M. Brunori, and M. Teixeira. 2002b. A novel type of nitric-oxide reductase. Escherichia coli flavorubredoxin. *J Biol Chem*. 277:25273-25276.

Gomes, C.M., G. Silva, S. Oliveira, J. LeGall, M.Y. Liu, A.V. Xavier, C. Rodrigues-Pousada, and M. Teixeira. 1997. Studies on the redox centers of the terminal oxidase from Desulfovibrio gigas and evidence for its interaction with rubredoxin. *J Biol Chem*. 272:22502-22508.

Gomes, C.M., J.B. Vicente, A. Wasserfallen, and M. Teixeira. 2000. Spectroscopic studies and characterization of a novel electron-transfer chain from Escherichia coli involving a flavorubredoxin and its flavoprotein reductase partner. *Biochemistry*. 39:16230-16237.

Gomez, R., N. Carrillo, M.P. Morelli, S. Tula, F. Shahinnia, M.R. Hajirezaei, and A.F. Lodeyro. 2018. Faster photosynthetic induction in tobacco by expressing cyanobacterial flavodiiron proteins in chloroplasts. *Photosynth Res*. 136:129-138.

Gonçalves, V.L., L.M. Saraiva, and M. Teixeira. 2011a. Gene expression study of the flavodiiron proteins from the cyanobacterium Synechocystis sp. PCC6803. *Biochem Soc Trans*. 39:216-218.

Gonçalves, V.L., J.B. Vicente, L. Pinto, C.V. Romao, C. Frazao, P. Sarti, A. Giuffre, and M. Teixeira. 2014. Flavodiiron oxygen reductase from Entamoeba histolytica: modulation of substrate preference by tyrosine 271 and lysine 53. *J Biol Chem*. 289:28260-28270.

Gonçalves, V.L., J.B. Vicente, L.M. Saraiva, and M. Teixeira. 2011b. Flavodiiron Proteins and their role in cyanobacteria. *In* The Bioenergetic Processes of cyanobacteria- From Evolutionary Singularity to Ecological Diversity. C. Obinger and G.A. Peschek, editors. Springer Verlag, Springer Netherlands. 631-655.

Gray, H.B., and J.R. Winkler. 2015. Hole hopping through tyrosine/tryptophan chains protects proteins from oxidative damage. *Proceedings of the National Academy of Sciences of the United States of America*. 112:10920-10925.

Green, G.N., J.E. Kranz, and R.B. Gennis. 1984. Cloning the cyd gene locus coding for the cytochrome d complex of Escherichia coli. *Gene*. 32:99-106.

Griffith, O.W., and D.J. Stuehr. 1995. Nitric oxide synthases: properties and catalytic mechanism. *Annu Rev Physiol*. 57:707-736.

Hagelueken, G., T.M. Adams, L. Wiehlmann, U. Widow, H. Kolmar, B. Tummler, D.W. Heinz, and W.D. Schubert. 2006. The crystal structure of SdsA1, an alkylsulfatase from Pseudomonas aeruginosa, defines a third class of sulfatases. *Proceedings of the National Academy of Sciences of the United States of America*. 103:7631-7636.

Hakkila, K., T. Antal, L. Gunnelius, J. Kurkela, H.C. Matthijs, E. Tyystjarvi, and T. Tyystjarvi. 2013. Group 2 sigma factor mutant DeltasigCDE of the cyanobacterium Synechocystis sp. PCC 6803 reveals functionality of both carotenoids and flavodiiron proteins in photoprotection of photosystem II. *Plant & cell physiology*. 54:1780-1790.

Hancock, J.T., R. Desikan, and S.J. Neill. 2001. Role of reactive oxygen species in cell signalling pathways. *Biochem Soc Trans*. 29:345-350.

Harding, M. 1999. The geometry of metal-ligand interactions relevant to proteins. *Acta Crystallographica Section D*. 55:1432-1443.

Hausladen, A., A. Gow, and J.S. Stamler. 2001. Flavohemoglobin denitrosylase catalyzes the reaction of a nitroxyl equivalent with molecular oxygen. *Proceedings of the National Academy of Sciences of the United States of America*. 98:10108-10112.

Hayashi, T., J.D. Caranto, D.A. Wampler, D.M. Kurtz, and P. Moenne-Loccoz. 2010. Insights into the nitric oxide reductase mechanism of flavodiiron proteins from a flavin-free enzyme. *Biochemistry*. 49:7040-7049.

Hayward, S., and H.J. Berendsen. 1998. Systematic analysis of domain motions in proteins from conformational change: new results on citrate synthase and T4 lysozyme. *Proteins*. 30:144-154.

Hayward, S., A. Kitao, and H.J. Berendsen. 1997. Model-free methods of analyzing domain motions in proteins from simulation: a comparison of normal mode analysis and molecular dynamics simulation of lysozyme. *Proteins*. 27:425-437.

Helman, Y., E. Barkan, D. Eisenstadt, B. Luz, and A. Kaplan. 2005. Fractionation of the three stable oxygen isotopes by oxygen-producing and oxygen-consuming reactions in photosynthetic organisms. *Plant physiology*. 138:2292-2298.

Helman, Y., D. Tchernov, L. Reinhold, M. Shibata, T. Ogawa, R. Schwarz, I. Ohad, and A. Kaplan. 2003. Genes encoding A-type flavoproteins are essential for photoreduction of O2 in cyanobacteria. *Curr Biol*. 13:230-235.

Hendriks, J., A. Warne, U. Gohlke, T. Haltia, C. Ludovici, M. Lubben, and M. Saraste. 1998. The active site of the bacterial nitric oxide reductase is a dinuclear iron center. *Biochemistry*. 37:13102-13109.

Hernandez-Sanchez, I.E., I. Maruri-Lopez, A. Ferrando, J. Carbonell, S.P. Graether, and J.F. Jimenez-Bremont. 2015. Nuclear localization of the dehydrin OpsDHN1 is determined by histidine-rich motif. *Frontiers in plant science*. 6:702.

Hillmann, F., O. Riebe, R.J. Fischer, A. Mot, J.D. Caranto, D.M. Kurtz, Jr., and H. Bahl. 2009. Reductive dioxygen scavenging by flavo-diiron proteins of Clostridium acetobutylicum. *FEBS letters*. 583:241-245.

Hino, T., Y. Matsumoto, S. Nagano, H. Sugimoto, Y. Fukumori, T. Murata, S. Iwata, and Y. Shiro. 2010. Structural basis of biological N2O generation by bacterial nitric oxide reductase. *Science*. 330:1666-1670.

Hohmann-Marriott, M.F., and R.E. Blankenship. 2011. Evolution of photosynthesis. *Annual review of plant biology*. 62:515-548.

Holton, J.M. 2007. XANES measurements of the rate of radiation damage to selenomethionine side chains. *Journal of synchrotron radiation*. 14:51-72.

Hoover, D.M., C.L. Drennan, A.L. Metzger, C. Osborne, C.H. Weber, K.A. Pattridge, and M.L. Ludwig. 1999. Comparisons of wild-type and mutant flavodoxins from Anacystis nidulans. Structural determinants of the redox potentials. *J Mol Biol*. 294:725-743.

Hussain, H., J. Grove, L. Griffiths, S. Busby, and J. Cole. 1994. A seven-gene operon essential for formate-dependent nitrite reduction to ammonia by enteric bacteria. *Molecular microbiology*. 12:153-163.

Hutchings, M.I., N. Mandhana, and S. Spiro. 2002. The NorR protein of Escherichia coli activates expression of the flavorubredoxin gene norV in response to reactive nitrogen species. *J Bacteriol*. 184:4640-4643.

Ilari, A., A. Bonamore, A. Farina, K.A. Johnson, and A. Boffi. 2002. The X-ray structure of ferric Escherichia coli flavohemoglobin reveals an unexpected geometry of the distal heme pocket. *J Biol Chem*. 277:23725-23732.

Ilik, P., A. Pavlovic, R. Kouril, A. Alboresi, T. Morosinotto, Y. Allahverdiyeva, E.M. Aro, H. Yamamoto, and T. Shikanai. 2017. Alternative electron transport mediated by flavodiiron proteins is operational in organisms from cyanobacteria up to gymnosperms. *New Phytol*. 214:967-972.

Imlay, K.R., and J.A. Imlay. 1996. Cloning and analysis of sodC, encoding the copper-zinc superoxide dismutase of Escherichia coli. *Journal of bacteriology*. 178:2564-2571.

Ishii, R., A. Minagawa, H. Takaku, M. Takagi, M. Nashimoto, and S. Yokoyama. 2005. Crystal structure of the tRNA 3' processing endoribonuclease tRNase Z from Thermotoga maritima. *J Biol Chem*. 280:14138-14144.

Jin, S., D.M. Kurtz, Jr., Z.J. Liu, J. Rose, and B.C. Wang. 2002. X-ray crystal structures of reduced rubrerythrin and its azide adduct: a structure-based mechanism for a non-heme diiron peroxidase. *Journal of the American Chemical Society*. 124:9845-9855.

Jokel, M., S. Kosourov, N. Battchikova, A.A. Tsygankov, E.M. Aro, and Y. Allahverdiyeva. 2015. Chlamydomonas Flavodiiron Proteins Facilitate Acclimation to Anoxia During Sulfur Deprivation. *Plant & cell physiology*. 56:1598-1607.

Jokipii-Lukkari, S., A.D. Frey, P.T. Kallio, and H. Haggman. 2009. Intrinsic non-symbiotic and truncated haemoglobins and heterologous Vitreoscilla haemoglobin expression in plants. *Journal of experimental botany*. 60:409-422.

Jouanneau, Y., C. Meyer, M. Asso, B. Guigliarelli, and J.C. Willison. 2000. Characterization of a nif-regulated flavoprotein (FprA) from *Rhodobacter capsulatus*. Redox properties and molecular interaction with a [2Fe-2S] ferredoxin. *European journal of biochemistry / FEBS*. 267:780-787.

Justino, M.C., J.B. Vicente, M. Teixeira, and L.M. Saraiva. 2005. New genes implicated in the protection of anaerobically grown Escherichia coli against nitric oxide. *J Biol Chem*. 280:2636-2643.

Kabil, O., and R. Banerjee. 2012. Characterization of patient mutations in human persulfide dioxygenase (ETHE1) involved in H2S catabolism. *The Journal of biological chemistry*. 287:44561-44567.

Kabsch, W. 2010. Xds. *Acta Crystallogr D Biol Crystallogr*. 66:125-132.

Kantardjieff, K.A., and B. Rupp. 2003. Matthews coefficient probabilities: Improved estimates for unit cell contents of proteins, DNA, and protein-nucleic acid complex crystals. *Protein science : a publication of the Protein Society*. 12:1865-1871.

Karplus, P.A., and K. Diederichs. 2012. Linking crystallographic model and data quality. *Science*. 336:1030-1033.

Kawasaki, S., J. Ishikura, Y. Watamura, and Y. Niimura. 2004. Identification of O2-induced peptides in an obligatory anaerobe, Clostridium acetobutylicum. *FEBS letters*. 571:21-25.

Kawasaki, S., Y. Watamura, M. Ono, T. Watanabe, K. Takeda, and Y. Niimura. 2005. Adaptive responses to oxygen stress in obligatory anaerobes Clostridium acetobutylicum and Clostridium aminovalericum. *Applied and environmental microbiology*. 71:8442-8450.

Kim, S.O., Y. Orii, D. Lloyd, M.N. Hughes, and R.K. Poole. 1999. Anoxic function for the Escherichia coli flavohaemoglobin (Hmp): reversible binding of nitric oxide and reduction to nitrous oxide. *FEBS letters*. 445:389-394.

Krissinel, E., and K. Henrick. 2007. Inference of macromolecular assemblies from crystalline state. *J Mol Biol*. 372:774-797.

Kurtz, D.M. 2007. Flavo-diiron enzymes: nitric oxide or dioxygen reductases? *Dalton Transactions*:4115-4121.

Kurtz, D.M., Jr. 2004. Microbial detoxification of superoxide: the non-heme iron reductive paradigm for combating oxidative stress. *Acc Chem Res*. 37:902-908.

Langrehr, J.M., R.A. Hoffman, J.R. Lancaster, Jr., and R.L. Simmons. 1993. Nitric oxide--a new endogenous immunomodulator. *Transplantation*. 55:1205-1212.

Larkin, M.A., G. Blackshields, N.P. Brown, R. Chenna, P.A. McGettigan, H. McWilliam, F. Valentin, I.M. Wallace, A. Wilm, R. Lopez, J.D. Thompson, T.J. Gibson, and D.G. Higgins. 2007. Clustal W and Clustal X version 2.0. *Bioinformatics*. 23:2947-2948.

Le Fourn, C., M.L. Fardeau, B. Ollivier, E. Lojou, and A. Dolla. 2008. The hyperthermophilic anaerobe Thermotoga Maritima is able to cope with limited amount of oxygen: insights into its defence strategies. *Environ Microbiol*. 10:1877-1887.

Lee, I.M. 1999. Antioxidant vitamins in the prevention of cancer. *Proc Assoc Am Physicians*. 111:10-15.

Lindqvist, Y., E. Johansson, H. Kaija, P. Vihko, and G. Schneider. 1999. Three-dimensional structure of a mammalian purple acid phosphatase at 2.2 A resolution with a mu-(hydr)oxo bridged di-iron center. *J Mol Biol*. 291:135-147.

Liu, D., B.W. Lepore, G.A. Petsko, P.W. Thomas, E.M. Stone, W. Fast, and D. Ringe. 2005. Three-dimensional structure of the quorum-quenching N-acyl homoserine lactone hydrolase from Bacillus thuringiensis. *Proceedings of the National Academy of Sciences of the United States of America*. 102:11882-11887.

Loewen, P.C., B.L. Triggs, C.S. George, and B.E. Hrabarchuk. 1985. Genetic mapping of katG, a locus that affects synthesis of the bifunctional catalase-peroxidase hydroperoxidase I in Escherichia coli. *Journal of bacteriology*. 162:661-667.

Loftus, B., I. Anderson, R. Davies, U.C. Alsmark, J. Samuelson, P. Amedeo, P. Roncaglia, M. Berriman, R.P. Hirt, B.J. Mann, T. Nozaki, B. Suh, M. Pop, M. Duchene, J. Ackers, E. Tannich, M. Leippe, M. Hofer, I. Bruchhaus, U. Willhoeft, A. Bhattacharya, T. Chillingworth, C. Churcher, Z. Hance, B. Harris, D. Harris, K. Jagels, S. Moule, K. Mungall, D. Ormond, R. Squares, S. Whitehead, M.A. Quail, E. Rabbinowitsch, H. Norbertczak, C. Price, Z. Wang, N. Guillen, C. Gilchrist, S.E. Stroup, S. Bhattacharya, A. Lohia, P.G. Foster, T. Sicheritz-Ponten, C. Weber, U. Singh, C. Mukherjee, N.M. El-Sayed, W.A. Petri, Jr., C.G. Clark, T.M. Embley, B. Barrell, C.M. Fraser, and N. Hall. 2005. The genome of the protist parasite Entamoeba histolytica. *Nature*. 433:865-868.

Lu, C., T. Egawa, L.M. Wainwright, R.K. Poole, and S.R. Yeh. 2007a. Structural and functional properties of a truncated hemoglobin from a food-borne pathogen Campylobacter jejuni. *J Biol Chem*. 282:13627-13636.

Lu, C., M. Mukai, Y. Lin, G. Wu, R.K. Poole, and S.R. Yeh. 2007b. Structural and functional properties of a single domain hemoglobin from the food-borne pathogen Campylobactor jejuni. *J Biol Chem*. 282:25917-25928.

Lundberg, J.O., E. Weitzberg, J.A. Cole, and N. Benjamin. 2004. Nitrate, bacteria and human health. *Nature reviews. Microbiology*. 2:593-602.

Lundberg, J.O., E. Weitzberg, and M.T. Gladwin. 2008. The nitrate-nitrite-nitric oxide pathway in physiology and therapeutics. *Nat Rev Drug Discov*. 7:156-167.

Magotti, P., I. Bauer, M. Igarashi, M. Babagoli, R. Marotta, D. Piomelli, and G. Garau. 2015. Structure of human N-acylphosphatidylethanolamine-hydrolyzing phospholipase D: regulation of fatty acid ethanolamide biosynthesis by bile acids. *Structure*. 23:598-604.

Makris, T.M., C.J. Knoot, C.M. Wilmot, and J.D. Lipscomb. 2013. Structure of a dinuclear iron cluster-containing beta-hydroxylase active in antibiotic biosynthesis. *Biochemistry*. 52:6662-6671.

Mandel, C.R., S. Kaneko, H. Zhang, D. Gebauer, V. Vethantham, J.L. Manley, and L. Tong. 2006. Polyadenylation factor CPSF-73 is the pre-mRNA 3'-end-processing endonuclease. *Nature*. 444:953-956.

Marletta, M.A. 1994. Nitric oxide synthase: aspects concerning structure and catalysis. *Cell*. 78:927-930.

Marsden, P.A., K.T. Schappert, H.S. Chen, M. Flowers, C.L. Sundell, J.N. Wilcox, S. Lamas, and T. Michel. 1992. Molecular cloning and characterization of human endothelial nitric oxide synthase. *FEBS letters*. 307:287-293.

Martins, M.C., C.V. Romao, F. Folgosa, P.T. Borges, C. Frazao, and M. Teixeira. 2019. How superoxide reductases and flavodiiron proteins combat oxidative stress in anaerobes. *Free radical biology & medicine*.

Matthews, B.W. 1968. Solvent content of protein crystals. *J Mol Biol*. 33:491-497.

McCarthy, A.A., R. Barrett, A. Beteva, H. Caserotto, F. Dobias, F. Felisaz, T. Giraud, M. Guijarro, R. Janocha, A. Khadrouche, M. Lentini, G.A. Leonard, M. Lopez Marrero, S. Malbet-Monaco, S. McSweeney, D. Nurizzo, G. Papp, C. Rossi, J. Sinoir, C. Sorez, J. Surr, O. Svensson, U. Zander, F. Cipriani, P. Theveneau, and C. Mueller-Dieckmann. 2018. ID30B - a versatile beamline for macromolecular crystallography experiments at the ESRF. *Journal of synchrotron radiation*. 25:1249-1260.

McCoy, A.J., R.W. Grosse-Kunstleve, P.D. Adams, M.D. Winn, L.C. Storoni, and R.J. Read. 2007a. Phaser crystallographic software. *Journal of applied crystallography*. 40:658-674.

Mccoy, A.J., R.W. Grosse-Kunstleve, P.D. Adams, M.D. Winn, L.C. Storoni, and R.J. Read. 2007b. Phaser crystallographic software. *J Appl Crystallogr*. 40:658-674.

Medina, M. 2009. Structural and mechanistic aspects of flavoproteins: photosynthetic electron transfer from photosystem I to NADP+. *The FEBS journal*. 276:3942-3958.

Membrillo-Hernandez, J., M.D. Coopamah, M.F. Anjum, T.M. Stevanin, A. Kelly, M.N. Hughes, and R.K. Poole. 1999. The flavohemoglobin of Escherichia coli confers resistance to a nitrosating agent, a "Nitric oxide Releaser," and paraquat and is essential for transcriptional responses to oxidative stress. *J Biol Chem*. 274:748-754.

Membrillo-Hernandez, J., M.D. Coopamah, A. Channa, M.N. Hughes, and R.K. Poole. 1998. A novel mechanism for upregulation of the Escherichia coli K-12 hmp (flavohaemoglobin) gene by the 'NO releaser', S-nitrosoglutathione: nitrosation of homocysteine and modulation of MetR binding to the glyA-hmp intergenic region. *Molecular microbiology*. 29:1101-1112.

Meyer, D.J. 1973. Interaction of cytochrome oxidases aa3 and d with nitrite. *Nat New Biol*. 245:276-277.

Mighell, A.D. 2002. Conventional Cells-The Last Step Toward General Acceptance of Standard Conventional Cells for the Reporting of Crystallographic Data. *Journal of research of the National Institute of Standards and Technology*. 107:373-377.

Milani, M., A. Pesce, M. Nardini, H. Ouellet, Y. Ouellet, S. Dewilde, A. Bocedi, P. Ascenzi, M. Guertin, L. Moens, J.M. Friedman, J.B. Wittenberg, and M. Bolognesi. 2005. Structural bases for heme binding and diatomic ligand recognition in truncated hemoglobins. *J Inorg Biochem*. 99:97-109.

Miller, A.F. 2012. Superoxide dismutases: ancient enzymes and new insights. *FEBS letters*. 586:585-595.

Mills, P.C., G. Rowley, S. Spiro, J.C. Hinton, and D.J. Richardson. 2008. A combination of cytochrome c nitrite reductase (NrfA) and flavorubredoxin (NorV) protects Salmonella enterica serovar Typhimurium against killing by NO in anoxic environments. *Microbiology*. 154:1218-1228.

Moncada, S., R.M. Palmer, and E.A. Higgs. 1989. Biosynthesis of nitric oxide from L-arginine. A pathway for the regulation of cell function and communication. *Biochem Pharmacol*. 38:1709-1715.

Mukhopadhyay, P., M. Zheng, L.A. Bedzyk, R.A. LaRossa, and G. Storz. 2004. Prominent roles of the NorR and Fur regulators in the Escherichia coli transcriptional response to reactive nitrogen species. *Proceedings of the National Academy of Sciences of the United States of America*. 101:745-750.

Muller, F., M. Brustlein, P. Hemmerich, V. Massey, and W.H. Walker. 1972. Light-absorption studies on neutral flavin radicals. *European journal of biochemistry*. 25:573-580.

Murray, J.W., and J. Barber. 2007. Structural characteristics of channels and pathways in photosystem II including the identification of an oxygen channel. *J Struct Biol*. 159:228-237.

Murray, J.W., K. Maghlaoui, J. Kargul, M. Sugiura, and J. Barber. 2008. Analysis of xenon binding to photosystem II by X-ray crystallography. *Photosynth Res*. 98:523-527.

Mustila, H., P. Paananen, N. Battchikova, A. Santana-Sanchez, D. Muth-Pawlak, M. Hagemann, E.M. Aro, and Y. Allahverdiyeva. 2016. The Flavodiiron Protein Flv3 Functions as a Homo-Oligomer During Stress Acclimation and is Distinct from the Flv1/Flv3 Hetero-Oligomer Specific to the O2 Photoreduction Pathway. *Plant Cell Physiol*. 57:1468-1483.

Nathan, C., and M.U. Shiloh. 2000. Reactive oxygen and nitrogen intermediates in the relationship between mammalian hosts and microbial pathogens. *Proceedings of the National Academy of Sciences of the United States of America*. 97:8841-8848.

Nefedova, L.N., V.A. Mel'nik, and M.M. Babykin. 2003. [Mutants of cyanobacterium Synechocystis sp. PCC6803 with insertion of the sodB gene encoding Fe-superoxide dismutase]. *Genetika*. 39:478-482.

Neville, R.G. 1974. Steps leading to the discovery of oxygen, 1774. A bicentennial tribute to Joseph Priestley. *Journal of chemical education*. 51:428-431.

Niesen, F.H., H. Berglund, and M. Vedadi. 2007. The use of differential scanning fluorimetry to detect ligand interactions that promote protein stability. *Nat Protoc*. 2:2212-2221.

Niviere, V., and M. Fontecave. 2004. Discovery of superoxide reductase: an historical perspective. *J Biol Inorg Chem*. 9:119-123.

Nobre, L.S., V.L. Goncalves, and L.M. Saraiva. 2008. Flavohemoglobin of Staphylococcus aureus. *Methods in enzymology*. 436:203-216.

Nolling, J., M. Ishii, J. Koch, T.D. Pihl, J.N. Reeve, R.K. Thauer, and R. Hedderich. 1995. Characterization of a 45-kDa flavoprotein and evidence for a rubredoxin, two proteins that could participate in electron transport from H2 to CO2 in methanogenesis in Methanobacterium thermoautotrophicum. *European journal of biochemistry*. 231:628-638.

Nugent, J.H. 1996. Oxygenic photosynthesis. Electron transfer in photosystem I and photosystem II. *European journal of biochemistry*. 237:519-531.

Olieric, V., E. Ennifar, A. Meents, M. Fleurant, C. Besnard, P. Pattison, M. Schiltz, C. Schulze-Briese, and P. Dumas. 2007. Using X-ray absorption spectra to monitor specific

radiation damage to anomalously scattering atoms in macromolecular crystallography. *Acta Crystallogr D Biol Crystallogr*. 63:759-768.

Ouellet, H., Y. Ouellet, C. Richard, M. Labarre, B. Wittenberg, J. Wittenberg, and M. Guertin. 2002. Truncated hemoglobin HbN protects Mycobacterium bovis from nitric oxide. *Proceedings of the National Academy of Sciences of the United States of America*. 99:5902-5907.

Owen, R.L., E. Rudino-Pinera, and E.F. Garman. 2006. Experimental determination of the radiation dose limit for cryocooled protein crystals. *Proceedings of the National Academy of Sciences of the United States of America*. 103:4912-4917.

Owens, C.P., F.E. Katz, C.H. Carter, V.F. Oswald, and F.A. Tezcan. 2016. Tyrosine-Coordinated P-Cluster in G. diazotrophicus Nitrogenase: Evidence for the Importance of O-Based Ligands in Conformationally Gated Electron Transfer. *Journal of the American Chemical Society*. 138:10124-10127.

Painter, J., and E.A. Merritt. 2006. Optimal description of a protein structure in terms of multiple groups undergoing TLS motion. *Acta Crystallogr D*. 62:439-450.

Park, K.W., K.J. Kim, A.J. Howard, B.C. Stark, and D.A. Webster. 2002. Vitreoscilla hemoglobin binds to subunit I of cytochrome bo ubiquinol oxidases. *J Biol Chem*. 277:33334-33337.

Paul-Soto, R., M. Hernandez-Valladares, M. Galleni, R. Bauer, M. Zeppezauer, J.M. Frere, and H.W. Adolph. 1998. Mono- and binuclear Zn-beta-lactamase from Bacteroides fragilis: catalytic and structural roles of the zinc ions. *FEBS letters*. 438:137-140.

Paulsen, K.E., M.T. Stankovich, B.J. Stockman, and J.L. Markley. 1990. Redox and spectral properties of flavodoxin from Anabaena 7120. *Archives of biochemistry and biophysics*. 280:68-73.

Payne, W.J., M.Y. Liu, S.A. Bursakov, and J. Le Gall. 1997. Microbial and plant metabolism of NO. *Biofactors*. 6:47-52.

Peltier, G., D. Tolleter, E. Billon, and L. Cournac. 2010. Auxiliary electron transport pathways in chloroplasts of microalgae. *Photosynth Res*. 106:19-31.

Petoukhov, M.V., J.B. Vicente, P.B. Crowley, M.A. Carrondo, M. Teixeira, and D.I. Svergun. 2008. Quaternary structure of flavorubredoxin as revealed by synchrotron radiation small-angle X-ray scattering. *Structure*. 16:1428-1436.

Pettinati, I., J. Brem, M.A. McDonough, and C.J. Schofield. 2015. Crystal structure of human persulfide dioxygenase: structural basis of ethylmalonic encephalopathy. *Hum Mol Genet*. 24:2458-2469.

Pinto, A.F., J.V. Rodrigues, and M. Teixeira. 2010. Reductive elimination of superoxide: Structure and mechanism of superoxide reductases. *Biochim Biophys Acta*. 1804:285-297.

Poock, S.R., E.R. Leach, J.W. Moir, J.A. Cole, and D.J. Richardson. 2002. Respiratory detoxification of nitric oxide by the cytochrome c nitrite reductase of Escherichia coli. *J Biol Chem*. 277:23664-23669.

Poole, R.K., and M.N. Hughes. 2000. New functions for the ancient globin family: bacterial responses to nitric oxide and nitrosative stress. *Molecular microbiology*. 36:775-783.

Pozzi, C., F. Di Pisa, C. Bernacchioni, S. Ciambellotti, P. Turano, and S. Mangani. 2015. Iron binding to human heavy-chain ferritin. *Acta Crystallogr D Biol Crystallogr*. 71:1909-1920.

Rajavel, M., A. Mitra, and B. Gopal. 2009. Role of Bacillus subtilis BacB in the synthesis of bacilysin. *J Biol Chem*. 284:31882-31892.

Regelsberger, G., C. Jakopitsch, M. Engleder, F. Ruker, G.A. Peschek, and C. Obinger. 1999. Spectral and kinetic studies of the oxidation of monosubstituted phenols and anilines by recombinant Synechocystis catalase-peroxidase compound I. *Biochemistry*. 38:10480-10488.

Rhee, S.G. 1999. Redox signaling: hydrogen peroxide as intracellular messenger. *Exp Mol Med*. 31:53-59.

Rhee, S.G., K.S. Yang, S.W. Kang, H.A. Woo, and T.S. Chang. 2005. Controlled elimination of intracellular H(2)O(2): regulation of peroxiredoxin, catalase, and glutathione peroxidase via post-translational modification. *Antioxidants & redox signaling*. 7:619-626.

Rioux, C.R., and R.J. Kadner. 1989. Vitamin B12 transport in Escherichia coli K12 does not require the btuE gene of the btuCED operon. *Molecular & general genetics : MGG*. 217:301-308.

Robinett, N.G., R.L. Peterson, and V.C. Culotta. 2018. Eukaryotic copper-only superoxide dismutases (SODs): A new class of SOD enzymes and SOD-like protein domains. *J Biol Chem*. 293:4636-4643.

Rochaix, J.D. 2011. Regulation of photosynthetic electron transport. *Biochimica et biophysica acta*. 1807:375-383.

Rodrigues, R., J.B. Vicente, R. Felix, S. Oliveira, M. Teixeira, and C. Rodrigues-Pousada. 2006. Desulfovibrio gigas flavodiiron protein affords protection against nitrosative stress in vivo. *J Bacteriol*. 188:2745-2751.

Romao, C.V., J.B. Vicente, P.T. Borges, C. Frazao, and M. Teixeira. 2016a. The dual function of flavodiiron proteins: oxygen and/or nitric oxide reductases. *J Biol Inorg Chem*. 21:39-52.

Romao, C.V., J.B. Vicente, P.T. Borges, B.L. Victor, P. Lamosa, E. Silva, L. Pereira, T.M. Bandeiras, C.M. Soares, M.A. Carrondo, D. Turner, M. Teixeira, and C. Frazao. 2016b. Structure of Escherichia coli Flavodiiron Nitric Oxide Reductase. *J Mol Biol*. 428:4686-4707.

Romero, A., C.W. Hoitink, H. Nar, R. Huber, A. Messerschmidt, and G.W. Canters. 1993. X-ray analysis and spectroscopic characterization of M121Q azurin. A copper site model for stellacyanin. *J Mol Biol*. 229:1007-1021.

Royant, A., P. Carpentier, J. Ohana, J. McGeehan, B. Paetzold, M. Noirclerc-Savoye, X. Vernede, V. Adam, and D. Bourgeois. 2007. Advances in spectroscopic methods for biological crystals. 1. Fluorescence lifetime measurements. *J Appl Crystallogr*. 40:1105-1112.

Santos, S.P., T.M. Bandeiras, A.F. Pinto, M. Teixeira, M.A. Carrondo, and C.V. Romao. 2012. Thermofluor-based optimization strategy for the stabilization and crystallization of Campylobacter jejuni desulforubrerythrin. *Protein Expr Purif*. 81:193-200.

Saraiva, L.M., J.B. Vicente, and M. Teixeira. 2004. The role of the flavodiiron proteins in microbial nitric oxide detoxification. *Adv Microb Physiol*. 49:77-129.

Sarti, P., P.L. Fiori, E. Forte, P. Rappelli, M. Teixeira, D. Mastronicola, G. Sanciu, A. Giuffre, and M. Brunori. 2004. Trichomonas vaginalis degrades nitric oxide and expresses a flavorubredoxin-like protein: a new pathogenic mechanism? *Cell Mol Life Sci*. 61:618-623.

Schellhorn, H.E. 1995. Regulation of hydroperoxidase (catalase) expression in Escherichia coli. *FEMS microbiology letters*. 131:113-119.

Schilling, O., A. Vogel, B. Kostelecky, H. Natal da Luz, D. Spemann, B. Spath, A. Marchfelder, W. Troger, and W. Meyer-Klaucke. 2005. Zinc- and iron-dependent cytosolic metallo-beta-lactamase domain proteins exhibit similar zinc-binding affinities, independent of an atypical glutamate at the metal-binding site. *The Biochemical journal*. 385:145-153.

Schiltz, M., R. Fourme, and T. Prange. 2003. Use of noble gases xenon and krypton as heavy atoms in protein structure determination. *Methods in enzymology*. 374:83-119.

Schrodinger, L.L.C. 2010. The PyMOL Molecular Graphics System, Version 1.3r1.

Seedorf, H., A. Dreisbach, R. Hedderich, S. Shima, and R.K. Thauer. 2004. F420H2 oxidase (FprA) from Methanobrevibacter arboriphilus, a coenzyme F420-dependent enzyme involved in O2 detoxification. *Arch Microbiol*. 182:126-137.

Seedorf, H., C.H. Hagemeier, S. Shima, R.K. Thauer, E. Warkentin, and U. Ermler. 2007. Structure of coenzyme F420H2 oxidase (FprA), a di-iron flavoprotein from methanogenic Archaea catalyzing the reduction of O2 to H2O. *The FEBS journal*. 274:1588-1599.

Sehnal, D., R. Svobodova Varekova, K. Berka, L. Pravda, V. Navratilova, P. Banas, C.M. Ionescu, M. Otyepka, and J. Koca. 2013. MOLE 2.0: advanced approach for analysis of biomacromolecular channels. *J Cheminform*. 5:39.

Severinghaus, J.W. 2003. Fire-air and dephlogistication. Revisionisms of oxygen's discovery. *Advances in experimental medicine and biology*. 543:7-19.

Sharma, N.P., C. Hajdin, S. Chandrasekar, B. Bennett, K.W. Yang, and M.W. Crowder. 2006. Mechanistic studies on the mononuclear ZnII-containing metallo-beta-lactamase ImiS from Aeromonas sobria. *Biochemistry*. 45:10729-10738.

Sheng, Y., I.A. Abreu, D.E. Cabelli, M.J. Maroney, A.F. Miller, M. Teixeira, and J.S. Valentine. 2014. Superoxide dismutases and superoxide reductases. *Chemical reviews*. 114:3854-3918.

Shimakawa, G., K. Ishizaki, S. Tsukamoto, M. Tanaka, T. Sejima, and C. Miyake. 2017. The Liverwort, Marchantia, Drives Alternative Electron Flow Using a Flavodiiron Protein to Protect PSI. *Plant physiology*. 173:1636-1647.

Silaghi-Dumitrescu, R., E.D. Coulter, A. Das, L.G. Ljungdahl, G.N. Jameson, B.H. Huynh, and D.M. Kurtz, Jr. 2003. A flavodiiron protein and high molecular weight rubredoxin from Moorella thermoacetica with nitric oxide reductase activity. *Biochemistry*. 42:2806-2815.

Silaghi-Dumitrescu, R., D.M. Kurtz, Jr., L.G. Ljungdahl, and W.N. Lanzilotta. 2005a. X-ray crystal structures of Moorella thermoacetica FprA. Novel diiron site structure and mechanistic insights into a scavenging nitric oxide reductase. *Biochemistry*. 44:6492-6501.

Silaghi-Dumitrescu, R., K.Y. Ng, R. Viswanathan, and D.M. Kurtz, Jr. 2005b. A flavo-diiron protein from Desulfovibrio vulgaris with oxidase and nitric oxide reductase activities. Evidence for an in vivo nitric oxide scavenging function. *Biochemistry*. 44:3572-3579.

Smillie, D.A., R.S. Hayward, T. Suzuki, N. Fujita, and A. Ishihama. 1992. Locations of genes encoding alkyl hydroperoxide reductase on the physical map of the Escherichia coli K-12 genome. *Journal of bacteriology*. 174:3826-3827.

Smith, W.D. 1972. A history of nitrous oxide and oxygen anaesthesia. IA. The discovery of nitrous oxide and of oxygen. *British journal of anaesthesia*. 44:297-304.

Smutna, T., V.L. Goncalves, L.M. Saraiva, J. Tachezy, M. Teixeira, and I. Hrdy. 2009. Flavodiiron protein from Trichomonas vaginalis hydrogenosomes: the terminal oxygen reductase. *Eukaryot Cell*. 8:47-55.

Solomon, E.I., T.C. Brunold, M.I. Davis, J.N. Kemsley, S.K. Lee, N. Lehnert, F. Neese, A.J. Skulan, Y.S. Yang, and J. Zhou. 2000. Geometric and electronic structure/function correlations in non-heme iron enzymes. *Chemical reviews*. 100:235-350.

Southworth-Davies, R.J., and E.F. Garman. 2007. Radioprotectant screening for cryocrystallography. *Journal of synchrotron radiation*. 14:73-83.

Stanier, R.Y., and G. Cohen-Bazire. 1977. Phototrophic prokaryotes: the cyanobacteria. *Annual review of microbiology*. 31:225-274.

Storz, G., F.S. Jacobson, L.A. Tartaglia, R.W. Morgan, L.A. Silveira, and B.N. Ames. 1989. An alkyl hydroperoxide reductase induced by oxidative stress in Salmonella typhimurium and Escherichia coli: genetic characterization and cloning of ahp. *Journal of bacteriology*. 171:2049-2055.

Strater, N., B. Jasper, M. Scholte, B. Krebs, A.P. Duff, D.B. Langley, R. Han, B.A. Averill, H.C. Freeman, and J.M. Guss. 2005. Crystal structures of recombinant human purple Acid phosphatase with and without an inhibitory conformation of the repression loop. *J Mol Biol*. 351:233-246.

Sundheim, O., C.B. Vagbo, M. Bjoras, M.M. Sousa, V. Talstad, P.A. Aas, F. Drablos, H.E. Krokan, J.A. Tainer, and G. Slupphaug. 2006. Human ABH3 structure and key residues for oxidative demethylation to reverse DNA/RNA damage. *The EMBO journal*. 25:3389-3397.

Susin, S., J. Abian, F. Sanchez-Baeza, M.L. Peleato, A. Abadia, E. Gelpi, and J. Abadia. 1993. Riboflavin 3'- and 5'-sulfate, two novel flavins accumulating in the roots of iron-deficient sugar beet (Beta vulgaris). *The Journal of biological chemistry*. 268:20958-20965.

Svensson, O., S. Malbet-Monaco, A. Popov, D. Nurizzo, and M.W. Bowler. 2015. Fully automatic characterization and data collection from crystals of biological macromolecules. *Acta crystallographica. Section D, Biological crystallography*. 71:1757-1767.

Szori-Doroghazi, E., G. Maroti, M. Szori, A. Nyilasi, G. Rakhely, and K.L. Kovacs. 2012. Analyses of the large subunit histidine-rich motif expose an alternative proton transfer pathway in [NiFe] hydrogenases. *PLoS One*. 7:e34666.

Takeda, Y., and H. Avila. 1986. Structure and gene expression of the E. coli Mn-superoxide dismutase gene. *Nucleic acids research*. 14:4577-4589.

Tarricone, C., A. Galizzi, A. Coda, P. Ascenzi, and M. Bolognesi. 1997. Unusual structure of the oxygen-binding site in the dimeric bacterial hemoglobin from Vitreoscilla sp. *Structure*. 5:497-507.

Terwilliger, T.C., R.W. Grosse-Kunstleve, P.V. Afonine, N.W. Moriarty, P.H. Zwart, L.W. Hung, R.J. Read, and P.D. Adams. 2008. Iterative model building, structure refinement and density modification with the PHENIX AutoBuild wizard. *Acta Crystallogr D*. 64:61-69.

Theveneau, P., R. Baker, R. Barrett, A. Beteva, M.W. Bowler, P. Carpentier, H. Caserotto, D.d. Sanctis, F. Dobias, D. Flot, M. Guijarro, T. Giraud, M. Lentini, G.A. Leonard, M. Mattenet, A.A. McCarthy, S.M. McSweeney, C. Morawe, M. Nanao, D. Nurizzo, S. Ohlsson, P. Pernot, A.N. Popov, A. Round, A. Royant, W. Schmid, A. Snigirev, J. Surr, and C. Mueller-Dieckmann. 2013. The Upgrade Programme for the Structural Biology beamlines at the European Synchrotron Radiation Facility – High throughput sample evaluation and automation. *Journal of Physics: Conference Series*. 425:012001.

Thompson, J.D., T.J. Gibson, F. Plewniak, F. Jeanmougin, and D.G. Higgins. 1997. The CLUSTAL_X windows interface: flexible strategies for multiple sequence alignment aided by quality analysis tools. *Nucleic acids research*. 25:4876-4882.

Thorndycroft, F.H., G. Butland, D.J. Richardson, and N.J. Watmough. 2007. A new assay for nitric oxide reductase reveals two conserved glutamate residues form the entrance to a proton-conducting channel in the bacterial enzyme. *The Biochemical journal*. 401:111-119.

Tichy, M., and W. Vermaas. 1999. In vivo role of catalase-peroxidase in synechocystis sp. strain PCC 6803. *Journal of bacteriology*. 181:1875-1882.

Touati, D. 1983. Cloning and mapping of the manganese superoxide dismutase gene (sodA) of Escherichia coli K-12. *Journal of bacteriology*. 155:1078-1087.

Triggs-Raine, B.L., B.W. Doble, M.R. Mulvey, P.A. Sorby, and P.C. Loewen. 1988. Nucleotide sequence of katG, encoding catalase HPI of Escherichia coli. *Journal of bacteriology*. 170:4415-4419.

Ullah, J.H., T.R. Walsh, I.A. Taylor, D.C. Emery, C.S. Verma, S.J. Gamblin, and J. Spencer. 1998. The crystal structure of the L1 metallo-beta-lactamase from Stenotrophomonas maltophilia at 1.7 A resolution. *J Mol Biol*. 284:125-136.

Valentine, J.S., D.L. Wertz, T.J. Lyons, L.L. Liou, J.J. Goto, and E.B. Gralla. 1998. The dark side of dioxygen biochemistry. *Curr Opin Chem Biol*. 2:253-262.

van der Linden, P., F. Dobias, H. Vitoux, U. Kapp, J. Jacobs, S. Mc Sweeney, C. Mueller-Dieckmann, and P. Carpentier. 2014. Towards a high-throughput system for high-pressure cooling of cryoprotectant-free biological crystals. *J Appl Crystallogr*. 47:584-592.

Vasudevan, S.G., W.L. Armarego, D.C. Shaw, P.E. Lilley, N.E. Dixon, and R.K. Poole. 1991. Isolation and nucleotide sequence of the hmp gene that encodes a haemoglobin-like protein in Escherichia coli K-12. *Molecular & general genetics : MGG*. 226:49-58.

Veal, E.A., A.M. Day, and B.A. Morgan. 2007. Hydrogen peroxide sensing and signaling. *Mol Cell*. 26:1-14.

Vicente, J.B., M.A. Carrondo, M. Teixeira, and C. Frazao. 2008a. Structural studies on flavodiiron proteins. *Methods in enzymology*. 437:3-19.

Vicente, J.B., M.A. Carrondo, M. Teixeira, and C. Frazão. 2007a. Flavodiiron Proteins: Nitric Oxide and/or Oxygen Reductases. *In* Handbook of Metalloproteins. Vol. 1. John Wiley & Sons, Ltd.

Vicente, J.B., C.M. Gomes, A. Wasserfallen, and M. Teixeira. 2002. Module fusion in an A-type flavoprotein from the cyanobacterium Synechocystis condenses a multiple-component pathway in a single polypeptide chain. *Biochemical and biophysical research communications*. 294:82-87.

Vicente, J.B., M.C. Justino, V.L. Goncalves, L.M. Saraiva, and M. Teixeira. 2008b. Biochemical, spectroscopic, and thermodynamic properties of flavodiiron proteins. *Methods in enzymology*. 437:21-45.

Vicente, J.B., F.M. Scandurra, E. Forte, M. Brunori, P. Sarti, M. Teixeira, and A. Giuffre. 2008c. Kinetic characterization of the Escherichia coli nitric oxide reductase flavorubredoxin. *Methods in enzymology*. 437:47-62.

Vicente, J.B., F.M. Scandurra, J.V. Rodrigues, M. Brunori, P. Sarti, M. Teixeira, and A. Giuffre. 2007b. Kinetics of electron transfer from NADH to the Escherichia coli nitric oxide reductase flavorubredoxin. *The FEBS journal*. 274:677-686.

Vicente, J.B., and M. Teixeira. 2005. Redox and spectroscopic properties of the Escherichia coli nitric oxide-detoxifying system involving flavorubredoxin and its NADH-oxidizing redox partner. *J Biol Chem*. 280:34599-34608.

Vicente, J.B., F. Testa, D. Mastronicola, E. Forte, P. Sarti, M. Teixeira, and A. Giuffre. 2009. Redox properties of the oxygen-detoxifying flavodiiron protein from the human parasite Giardia intestinalis. *Arch Biochem Biophys*. 488:9-13.

Vicente, J.B., V. Tran, L. Pinto, M. Teixeira, and U. Singh. 2012. A detoxifying oxygen reductase in the anaerobic protozoan Entamoeba histolytica. *Eukaryot Cell*. 11:1112-1118.

Victor, B.L., A.M. Baptista, and C.M. Soares. 2009. Dioxygen and nitric oxide pathways and affinity to the catalytic site of rubredoxin:oxygen oxidoreductase from Desulfovibrio gigas. *J Biol Inorg Chem*. 14:853-862.

Voegtli, W.C., M. Sommerhalter, L. Saleh, J. Baldwin, J.M. Bollinger, Jr., and A.C. Rosenzweig. 2003. Variable coordination geometries at the diiron(II) active site of ribonucleotide reductase R2. *Journal of the American Chemical Society*. 125:15822-15830.

von Ossowski, I., M.R. Mulvey, P.A. Leco, A. Borys, and P.C. Loewen. 1991. Nucleotide sequence of Escherichia coli katE, which encodes catalase HPII. *Journal of bacteriology*. 173:514-520.

von Stetten, D., T. Giraud, P. Carpentier, F. Sever, M. Terrien, F. Dobias, D.H. Juers, D. Flot, C. Mueller-Dieckmann, G.A. Leonard, D. de Sanctis, and A. Royant. 2015. In crystallo optical spectroscopy (icOS) as a complementary tool on the macromolecular crystallography beamlines of the ESRF. *Acta Crystallographica Section D*. 71:15-26.

Vothknecht, U.C., and P. Westhoff. 2001. Biogenesis and origin of thylakoid membranes. *Biochimica et biophysica acta*. 1541:91-101.

Vuletich, D.A., and J.T. Lecomte. 2006. A phylogenetic and structural analysis of truncated hemoglobins. *J Mol Evol*. 62:196-210.

Wada, S., H. Yamamoto, Y. Suzuki, W. Yamori, T. Shikanai, and A. Makino. 2018. Flavodiiron Protein Substitutes for Cyclic Electron Flow without Competing CO2 Assimilation in Rice. *Plant physiology*. 176:1509-1518.

Wakabayashi, S., H. Matsubara, and D.A. Webster. 1986. Primary sequence of a dimeric bacterial haemoglobin from Vitreoscilla. *Nature*. 322:481-483.

Walker, J.M. 1994. The bicinchoninic acid (BCA) assay for protein quantitation. *Methods Mol Biol*. 32:5-8.

Walters, C.L., and A.M. Taylor. 1965. The Reduction of Nitrite by Skeletal-Muscle Mitochondria. *Biochim Biophys Acta*. 96:522-524.

Wang, J., C.E. Vine, B.K. Balasiny, J. Rizk, C.L. Bradley, M.T. Trejo, R.K. Poole, L.L. Bergaust, L.R. Bakken, and J.A. Cole. 2016. The roles of the hybrid cluster protein, Hcp, and its reductase, Hcr, in high affinity nitric oxide reduction that protects anaerobic cultures of Escherichia coli against nitrosative stress. *Molecular microbiology*. 100:877-892.

Wasserfallen, A., K. Huber, and T. Leisinger. 1995. Purification and structural characterization of a flavoprotein induced by iron limitation in Methanobacterium thermoautotrophicum Marburg. *J Bacteriol*. 177:2436-2441.

Wasserfallen, A., S. Ragettli, Y. Jouanneau, and T. Leisinger. 1998. A family of flavoproteins in the domains Archaea and Bacteria. *European journal of biochemistry / FEBS*. 254:325-332.

Webb, B., and A. Sali. 2014. Protein structure modeling with MODELLER. *Methods Mol Biol*. 1137:1-15.

Webster, D.A., and D.P. Hackett. 1966. The purification and properties of cytochrome o from Vitreoscilla. *J Biol Chem*. 241:3308-3315.

Weiss, M. 2001. Global indicators of X-ray data quality. *J Appl Crystallogr*. 34:130-135.

Weitz, A.C., N. Giri, J.D. Caranto, D.M. Kurtz, Jr., E.L. Bominaar, and M.P. Hendrich. 2017. Spectroscopy and DFT Calculations of a Flavo-diiron Enzyme Implicate New Diiron Site Structures. *Journal of the American Chemical Society*. 139:12009-12019.

Wenzel, N.F., A.L. Carenbauer, M.P. Pfiester, O. Schilling, W. Meyer-Klaucke, C.A. Makaroff, and M.W. Crowder. 2004. The binding of iron and zinc to glyoxalase II occurs exclusively as di-metal centers and is unique within the metallo-beta-lactamase family. *J Biol Inorg Chem*. 9:429-438.

White, K.A., and M.A. Marletta. 1992. Nitric oxide synthase is a cytochrome P-450 type hemoprotein. *Biochemistry*. 31:6627-6631.

Wink, D.A., M.B. Grisham, J.B. Mitchell, and P.C. Ford. 1996. Direct and indirect effects of nitric oxide in chemical reactions relevant to biology. *Methods in enzymology*. 268:12-31.

Wink, D.A., and J.B. Mitchell. 1998. Chemical biology of nitric oxide: Insights into regulatory, cytotoxic, and cytoprotective mechanisms of nitric oxide. *Free radical biology & medicine*. 25:434-456.

Winkler, J.R., and H.B. Gray. 2015. Electron flow through biological molecules: does hole hopping protect proteins from oxidative damage? *Q Rev Biophys*. 48:411-420.

Wittenberg, J.B., M. Bolognesi, B.A. Wittenberg, and M. Guertin. 2002. Truncated hemoglobins: a new family of hemoglobins widely distributed in bacteria, unicellular eukaryotes, and plants. *J Biol Chem*. 277:871-874.

Wu, G., L.M. Wainwright, and R.K. Poole. 2003. Microbial globins. *Adv Microb Physiol*. 47:255-310.

Xiao, Z., M.J. Lavery, M. Ayhan, S.D.B. Scrofani, M.C.J. Wilce, J.M. Guss, P.A. Tregloan, G.N. George, and A.G. Wedd. 1998. The Rubredoxin from Clostridium pasteurianum: Mutation of the Iron Cysteinyl Ligands to Serine. Crystal and Molecular Structures of Oxidized and Dithionite-Treated Forms of the Cys42Ser Mutant. *Journal of the American Chemical Society*. 120:4135-4150.

Yamamoto, H., S. Takahashi, M.R. Badger, and T. Shikanai. 2016. Artificial remodelling of alternative electron flow by flavodiiron proteins in Arabidopsis. *Nature Plants*. 2:16012.

Yu, S., V. Jensen, J. Seeliger, I. Feldmann, S. Weber, E. Schleicher, S. Haussler, and W. Blankenfeldt. 2009. Structure elucidation and preliminary assessment of hydrolase activity of PqsE, the Pseudomonas quinolone signal (PQS) response protein. *Biochemistry*. 48:10298-10307.

Zamocky, M., P.G. Furtmuller, and C. Obinger. 2008. Evolution of catalases from bacteria to humans. *Antioxidants & redox signaling*. 10:1527-1548.

Zamocky, M., S. Jaxecek, and F. Koller. 1997. The area of the main substrate channel is highly conserved among all true catalases. 723-730 pp.

Zamocky, M., and F. Koller. 1999. Understanding the structure and function of catalases: clues from molecular evolution and in vitro mutagenesis. *Prog Biophys Mol Biol*. 72:19-66.

Zang, T.M., D.A. Hollman, P.A. Crawford, M.W. Crowder, and C.A. Makaroff. 2001. Arabidopsis glyoxalase II contains a zinc/iron binuclear metal center that is essential for substrate binding and catalysis. *The Journal of biological chemistry*. 276:4788-4795.

Zehr, J.P. 2011. Nitrogen fixation by marine cyanobacteria. *Trends in microbiology*. 19:162-173.

Zeldin, O.B., M. Gerstel, and E.F. Garman. 2013. RADDOSE-3D: time- and space-resolved modelling of dose in macromolecular crystallography. *J Appl Crystallogr*. 46:1225-1230.

Zhang, P., Y. Allahverdiyeva, M. Eisenhut, and E.M. Aro. 2009. Flavodiiron proteins in oxygenic photosynthetic organisms: photoprotection of photosystem II by Flv2 and Flv4 in Synechocystis sp. PCC 6803. *PLoS One*. 4:e5331.

Zhang, P., M. Eisenhut, A.M. Brandt, D. Carmel, H.M. Silen, I. Vass, Y. Allahverdiyeva, T.A. Salminen, and E.M. Aro. 2012. Operon flv4-flv2 provides cyanobacterial photosystem II with flexibility of electron transfer. *Plant Cell*. 24:1952-1971.

Zumft, W.G. 2005. Nitric oxide reductases of prokaryotes with emphasis on the respiratory, heme-copper oxidase type. *J Inorg Biochem*. 99:194-215.

Zumft, W.G., C. Braun, and H. Cuypers. 1994. Nitric oxide reductase from Pseudomonas stutzeri. Primary structure and gene organization of a novel bacterial cytochrome bc complex. *European journal of biochemistry / FEBS*. 219:481-490.

Zweier, J.L., A. Samouilov, and P. Kuppusamy. 1999. Non-enzymatic nitric oxide synthesis in biological systems. *Biochim Biophys Acta*. 1411:250-262.